COMBINED EFFECT OF ELECTRIC FIELD AND SURFACE MODIFICATION ON POOL BOILING OF R-123

A thesis is submitted for the degree of Doctor of Philosophy by

Syed Waqas Ahmad

School of Engineering and Design

Brunel University

May 2012

Dedicated to

My parents

Mr. & Mrs. Syed Ejaz Ahmad Shah

Abstract

The effect of surface modification and high intensity electric field (uniform and non – uniform) acting separately or in combination on pool boiling of R-123 is presented in this thesis. The effect of surface modification was investigated on saturated pool boiling of R-123 for five horizontal copper surfaces modified by different treatments, namely: an emery polished surface, a fine sandblasted surface, a rough sandblasted surface, an electron beam (EB) enhanced surface and a sintered surface. Each 40 mm diameter heating surface formed the upper face of an oxygen-free copper block, electrically heated by embedded cartridge heaters. The experiments were performed from the convective heat transfer regime to the critical heat flux, with both increasing and decreasing heat flux, at 1.01 bar, and additionally at 2 bar and 4 bar for the emery polished surface. Significant enhancement of heat transfer with increasing surface modification was demonstrated, particularly for the EB enhanced and sintered surfaces. The emery polished and sandblasted surface results are compared with nucleate boiling correlations and other published data.

The effect of uniform and non-uniform electric fields on saturated pool boiling of R-123 at 1.01 bar pressure was also examined. This method of heat transfer enhancement is known as electrohydrodynamic abbreviated as EHD-enhancement. A high voltage potential was applied at the electrode located above the heating surface, which was earthed. The voltage was varied from 0 to 30 kV. The uniform electric field was provided through a 40 mm diameter circular electrode of stainless steel 304 wire mesh having an aperture of 5.1 mm, while the non-uniform electric field was obtained by using a 40 mm diameter circular rod electrode with rods 5 and 8 mm apart. The effect of uniform electric field was investigated using all five modified surfaces, i.e. emery polished, fine sandblasted, rough sandblasted, EB enhanced and sintered surfaces, while non – uniform electric field was tested using the emery polished, fine sandblasted, EB enhanced and sintered surfaces.

The effect of pressure on EHD enhancement was also examined using emery polished surface at saturation pressure of 2 and 4 bars while the electric field was fix at 20 kV corresponding to 2 MV/m. Further, the bubble dynamics is presented for the emery polished surface obtained using a high-speed high – resolution camera.

Declaration of Originality

The research presented in this thesis is the original work of the author except where otherwise specified, or where acknowledgements are made by references. This project was carried out under the supervision of Prof. D.B.R. Kenning, Prof. T.G. Karayiannis and Dr. J.S. Lewis.

The work has not been submitted for another degree or award to any other institution.

Syed Waqas Ahmad

Acknowledgement

All the praises are attributed to the Sole Creator of the whole universe ALMIGHTY ALLAH, The Most Beneficent, The Most Merciful and The Most Compassionate, Who bestowed on me the power of vision and wisdom to unravel the mysteries of the universe in a more systematic way. And only by the grace of ALLAH ALMIGHTY I am able to make this material contribution to already existing ocean of knowledge.

I invoke Allah's blessings and peace for my beloved PROPHET HAZRAT MUHAMMAD (Peace Be upon Him), who is forever torch of guidance and knowledge for humanity as a whole and whose moral and spiritual teachings enlightened my heart and mind.

I wish to extend most sincere thanks and deep sense of obligations to my supervisor, Professor. T.G. Karayiannis. This manuscript has found its way to a significant completion due to his dynamic supervision, generous guidance, great cooperation and masterly advice. He was only the source of inspiration for me during this programme of study and looking forward to work with him in future endeavours.

I feel much pleasure to express the heartiest gratitude and sincere appreciation to my other supervisors; Professor D.B.R. Kenning and Dr. J.S. Lewis for their kind guidance and help in completing this manuscript.

I also want to express my sincerest thanks and appreciation to Beatriz Alcala Lopez for helping me in paper work and dealing with bureaucracy.

I am grateful to the technician, Mr. C. Xanthos for his support and help in the preparation of the test facility.

I would like to acknowledge the Government of Pakistan for granting me a full time and fully funded scholarship.

I wish to extend my gratitude to my best friend Mr. Hafiz Manzoor Ahmad for encouragement and support throughout this work. In the end, I want to acknowledge my family back home, who stood firm behind me and support me both morally and socially.

Table of contents

Contents

Table of Figures

Table of Tables

Nomenclature

A		Constant in equations (5.15, 5.16, 5.18)
A_c	[m^2]	Cross sectional area of boiling chamber
A_s	[m^2]	Cross sectional area of boiling surface
a	[-]	Constants in equations (2.27, 2.30, 3.9,5.15,5.18)
B	[-]	Defined by equations (2.25, 3.19)
B_i		Bias error of i^{th} component
b	[-]	Constants in equations (2.27, 2.30, 5.15,5.18), exponent in equation (3.9)
C	[-]	Constant in equations (2.8,2.27, 5.16, 5.19)
c	[-]	Constant in equation (2.27)
c_1	[-]	Defined by equation (2.19, 5.14, 5.1)
c_p	[kJ/kg K]	Specific heat capacity

C_{sf}	[-]	Constant in equation (2.26)
D_b	[m]	Bubble departure diameter
d	[-]	Constant in equation (2.27)
$\mathrm{d_s}$	[mm]	Diameter of boiling surface
E	[kV/m]	Electric field strength
El	[-]	Electric number
F	[N]	Force
F_f	[-]	Function of fluid properties, equation (2.10)
F_{Pr}	[-]	Function of reduced pressure, equations (2.10,2.13)
F_q	[-]	Function of heat flux, equations (2.10,2.14)
F_W	[-]	Function of heater wall, equations (2.10,2.14)
F_{WR}	[-]	Function of wall roughness, equations (2.14,2.15)
F_{WM}	[-]	Function of wall material, equations (2.15,2.16)

f_e	[N/m]	Volume force
f_1		Defined by the equation (3.17)
g	[m/s^2]	Acceleration due to gravity
h	[kW/m^{2}K]	Heat transfer coefficient
h_{lg}	[kJ/kg]	Specific enthalpy of vaporization
K	[-]	Variable in equations (2.21,2.22)
k	[kW/m^{2}K]	Thermal conductivity
l_p	[µm]	Sample length of primary profile
l_r	[µm]	Sample length of roughness profile
M	[kg/kmol]	Molecular mass
M_e	[Cm]	Electric moment
M_g	[kg]	Mass of residual gas
m	[K/m]	Temperature gradient

N		Number of samples
Ne	[-]	Electrical influence number
Nu	[-]	Nusselt number
n	[-]	Exponent in equations (2.8,2.11, 3.9)
P	[bar]	Pressure
P_a	[µm]	Primary profile parameter
P_f	[1/µm K]	Defined by equation (13)
P_i		Precision error of i^{th} component
Pr	[-]	Prandtl number
Q	[W]	heat
Q_e	[Coulomb]	Electrical charge
q	[kW/m^2]	Heat flux
R	[kJ/kg K]	Specific gas constant

R_a	[µm]	Roughness profile parameter, average surface roughness
Ra_{EL}	[-]	Electrical Rayleigh number
$R_{p,\mathrm{old}}$	[µm]	Surface roughness defined by DIN 4272:1960
Re_s	[-]	Modified Reynolds number, defined in equation (2.23)
Re_o	[-]	Modified Reynolds number, defined in equation (3.11)
r	[m]	Radius of the vapour
r_f	[-]	Roughness factor
r_o	[m]	Average cavity radius
S_i		Standard deviation of i^{th} component
T	[K]	Temperature
T_e	[N/m]	Electric stress
T_i	[K]	Temperature of i^{th} component

$\bar{T}$	[K]	Average temperature
U_i		Uncertainty of ith component
V	[V]	Voltage
V_{fg}	[m^3/kg]	Specific volume change on vaporization
X,x	[m]	Distance below the boiling surface
x_1	[°C]	Thermocouple reading
x_2	[V]	Transducer output voltage
y_1	[°C]	Reading of precision thermometer
y_2	[psi]	Absolute pressure
z	[μm]	Profile deviation from mean line

Greek Symbols

α	[m^2/s]	Thermal diffusivity
β,θ	[deg]	Contact angle

θ_W	[deg]	Wenzel contact angle
φ	[deg]	Wedge angle
ε	[F/m]	Electric permittivity
ε_o	[F/m]	Vacuum electric permittivity
μ	[N s/m^2]	Dynamic viscosity
ν	[m^2/s]	Kinematic viscosity
ρ	[kg/m^3]	Density
ρ_e	[C/m^3]	Electric charge density
λ_m	[H/m]	Magnetic permeability
σ	[N/m]	Surface tension
σ_e	[N/m]	Apparent change in surface tension
σ_{elec}	[S]	Electric conductivity
τ_c	[s]	Bubble departure period

τ_e	[s]	Charge relaxation time
τ_m	[s]	Magnetic diffusion time

Subscripts

cond	conduction
cric	Critical
CHF	Critical heat flux
g	Residual gas
gw	Vapour and wall
l	Liquid
lg	Liquid and vapour
sat,meas	Measured at saturation
Sat,p	Saturation property corresponding to given pressure
o	Reference condition

r	Reduced property
ref	Reference fluid
s,sat	Saturation
tr	Transition
v	Vapour
w	Wall
wl	Liquid and wall
0	No electric field

Chapter 1 Introduction

Boiling heat transfer is an effective and efficient process for transferring heat at low values of the wall superheat, i.e. the temperature difference between the boiling fluid and the heater surface. It is a widely used phenomenon in chemical industries; especially in the power sector where large amount of heat is produced due to the burning of fossil and nuclear fuels. The complexity of the boiling process makes it difficult to fully understand the mechanism and improve the heat transfer facility. In other words, the enhancement in the efficiency of the boiling equipment is still a big challenge for the researchers. Many efforts have been made to improve the boiling heat transfer during the last fifty years. The boiling heat transfer enhancement leads to decrease the equipment size, which results in low capital investment. Furthermore, it makes the process more efficient thermodynamically and this leads to higher cycle efficiency, reduced running and maintenance cost of the equipment. Past researchers employed many techniques for the enhancement of boiling heat transfer, which can be divided into three categories namely; active technique, passive technique and compound technique as will be discussed in Section 2.3.

A number of different modified surfaces were used by the researchers in the past namely; emery polished, sanded, finned and porous surfaces. It was observed that the surface modification can provide a plateform for bubble generation, i.e. potential nucleation sites or cavities, which can play an important role in the heat transfer process. But the relationship of surface characterization and the heat transfer coefficient during the two-phase process has not yet been completely understood.

The second important point in this discussion was the fluid – heater surface combination. In the past, work has been carried out to develop correlations, based on the properties of the boiling liquid. Some of the nucleate boiling correlations included the surface characteristics, which were based on the average height and depth of the cavity, i.e. average surface roughness. Due to the assumptions and lack of information in surface characteristics involved in the correlations, the predicted data may deviate from the experimental results.

During the heat transfer augmentation, the delaying of the onset of nucleate boiling (ONB) and critical heat flux (CHF) was an area of special interest. This will lead to smaller equipment size and also abate concerns on the safety. In the past, a lot of accidents occurred at CHF. Based on the mechanism and understanding of CHF published in the literature, there are two schools of thought; the first that believe that CHF is independent of surface characteristics (i.e. hydrodynamic theory see section 2.10) and second that oppose this view. The proposed mechanisms, for CHF, based on the hydrodynamic theory can be further divided into the following categories; i.e. the instability of the vapour – liquid interface, Taylor wavelength instability and dry spots on the boiling surface.

Pool boiling hysteresis, explained later in section 2.7, was believed to be dependent on the properties of the boiling liquid and the conditions of the heater surface. In general, the interaction between liquid contact angle and the wedge angle of the surface cavity located on the boiling surface plays an important role in boiling hysteresis. Furthermore, the wetting properties of the liquid contribute towards the size of the contact angle, i.e. the more wetting the liquid is the smaller the contact angle and vice versa. If the liquid contact angle is smaller than the wedge angle, the cavity becomes flooded by the liquid and can’t act as potential nucleate site. A large superheat is required to active a flooded cavity for boiling. This leads to low heat flux at higher values of wall superheat and delay in the ONB, discussed in Section 2.7.

EHD was employed by researchers for last four decades. It was reported that the application of high intensity electric field can improve the heat transfer coefficient during pool boiling up to a factor of 1.5 (Hristov et al. (2009)). It was further reported in the review by Allen and Karayiannis (1995) that the application of electric field on a dielectric fluid can alter the liquid properties by acting on the vapour – liquid interface, changing the bubble dynamics and altering the liquid contact angle and the surface tension, discussed in section 3.5. The dielectric liquids were defined by Yabe et al. (1996), i.e. if a liquid has higher charge relaxation time, τ_e, than the bubble departure period, τ_c, then it is considered dielectric. This will be discussed further in Section 3.1. Only dielectric fluids exhibit enhancement during boiling heat transfer under the application of an electric field. Moreover, Pohl (1978) explained the resultant force, which was induced due to application of intense non – uniform electric field on a dielectric molecule. He further elaborated that the dielectric molecule first become polarized and then moves under the action of dielectrophoretic and electristrictive forces.

The motion of the dielectric molecule is independent of the electrode polarity and depends on the electric permittivity of the dielectric molecule. He argued that the molecule with higher electric permittivity moves towards the region of high electric intensity, this is discussed in Section 3.2.

The electrohydrodynamics technique can be employed by fixing an electrode at a specific distance from the boiling surface. A high voltage supply (either positive or negative) was connected with the electrode. On the other hand, the boiling surface is earthed and serves as a second electrode, see in Figure 1.1.

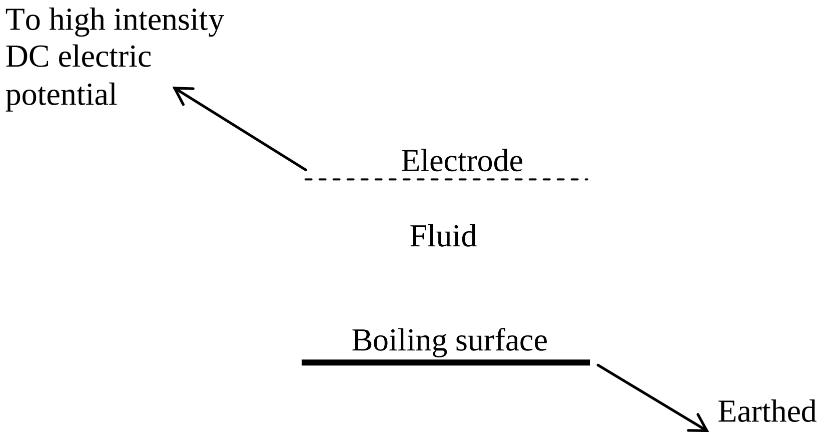

Figure 1.1 Schematic description of electric field arrangements

This arrangement produced high intensity electric field (uniform or non – uniform depending on the electrode design) between the boiling surface and the electrode. During the present experiments, a mesh electrode was used to provide uniform electric field and two rod electrodes were employed for non – uniform electric field, as discussed in Chapter 4. The EHD technique has negligible power consumption and it can act as a replacement of gravity force in space application, i.e. due to the absence of gravity force in the space the bubbles gather around the heating surface. These bubbles act as an insulator on the heating surface. In this situation high intensity electric field provides an additional force, which help to remove the bubbles from the heating surface. Due to application of electric field, the bubble dynamics alters. The mathematical analysis showed that the distortion in the value of electric field due to presence of the bubble (Karayiannis and Xu (1998)), see in Section 3.6. Furthermore, the augmentation in the value of heat transfer due to application of non – uniform electric field is comparatively better than uniform electric field, see in Section 3.5.

The application of high intensity electric field can significantly increase the value of critical heat flux. At high heat flux, the vapours coalescence to make the bubble columns. But with the application of electric field, the bubble columns become destabilize and result in the increase in the magnitude of critical heat flux (Berghmans (1976)), see section 3.7.

1.1 Aims of the project

The present study involved an assessment of the effect of surface modification and high intensity electric field on pool boiling of R-123. These enhancement techniques were tested both separately and in combination. R-123 was selected as a working fluid due to its dielectric properties, i.e. $\tau_e / \tau_c > 1$. The particular objectives of the research project were.

- Up-grade the existing pool boiling facility.
- Performing pool boiling experiments using five different modified surfaces namely; emery polished, fine sandblasted, rough sandblasted, EB enhanced and sintered surfaces at 1.01 bar saturation pressure. Examine the complete range of the boiling curve for both increasing and decreasing heat flux.
- Examine and report in the effect of pressure on pool boiling Assess and report on the effect of uniform and non – uniform electric fields on pool boiling for all five modified surfaces and conclude on compound enhancement.
- Examine the combined effect of saturation pressure and EHD using the emery polished surface. The pressure was at 1.01, 2 and 4 bar saturation pressure.
- Compare the experimental data for emery polished and fine and rough sandblasted surfaces with published nucleate boiling correlations and make recommendations.

Published work on surface modification and electrohydrodynamics was reviewed in Chapter 2 and Chapter 3, respectively. The detailed construction and design of the experimental rig is discussed in Chapter 4. The data reduction, error analysis and data validation is presented in Chapter 5. Finally, the combined and individual effects of surface modification and electrohydrodynamics are presented in the Chapter 6. Chapter 7 gives the conclusion and recommendations of this study.

Chapter 2 Pool Boiling

Pool boiling is an important heat transferring phenomenon used in the process industries. Efforts had been made since last fifty years to enhance the heat transfer in order to improve the efficiency and performance of the heat transfer facility. The published literature on pool boiling mechanism and enhancement using surface modification has been reviewed in this chapter. Furthermore, nucleate boiling correlations, boiling hysteresis and critical heat flux have also been discussed.

2.1 Boiling

Verplaetsen (1999) explained the term boiling, i.e. the process of evaporation from the liquid – vapour interface. Boiling can be divided into two groups (i) Pool boiling (ii) Forced convection boiling.

During pool boiling the heating element is submerged into the stagnant liquid and the motion of the fluid molecules near the heating surface is due to free convection. While in case of forced convection boiling, an external force is induced to carry out fluid motion. Furthermore, on the basis of fluid temperature – pressure conditions, boiling can also be categorized into subcooled boiling and saturated boiling. In saturated boiling the temperature of bulk liquid is slightly above the saturation temperature, the bubbles produced from the heating surface detached under the action of resultant force. On the other hand, during sub – cooled boiling the bulk liquid temperature is less than the saturation temperature. The bubbles produced from the boiling surface tend to diminish before departure or immediately after departure as described by Tong and Tang (1997).

2.2 Explanation of boiling curve

Nukiyama (1966) reported an experiment on pool boiling of water at saturation pressure of 1 atm. Electrically heated Nichorome wire was horizontally placed in a pool of water and the temperature of the wire was calculated using its resistance value. As shown in Figure 2.1, he reported that there was hardly any boiling up to 5 K wall superheat. Furthermore, increase in the power input to the heater wire resulted in increasing wall superheat.

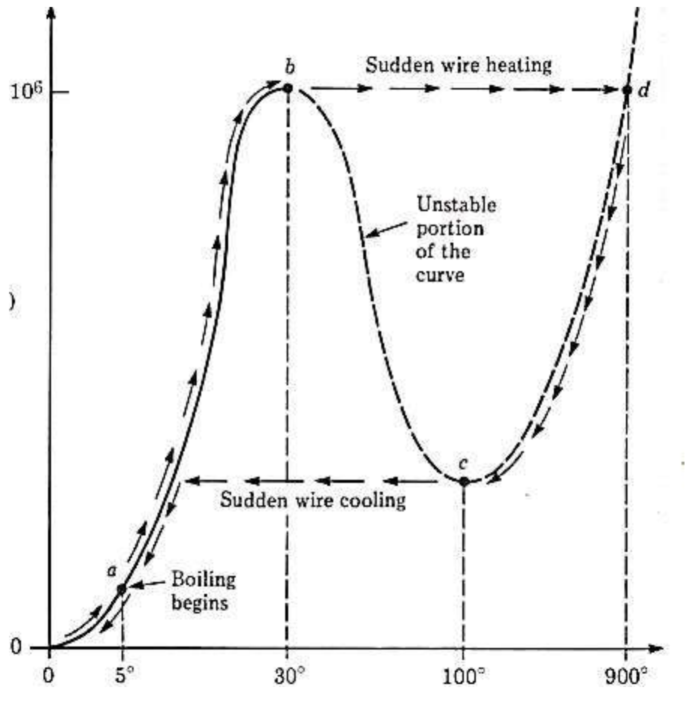

Figure 2.1 Typical Boiling Curve (Nukiyama (1934) cited in reference White (1988))

At q = 10^6 W/m^2, there was a sudden temperature overshoot and the wire melted. Then the experiments were repeated using platinum wire. The results followed almost the same curve as obtained in the previous experiments up to q = 10^6 W/m^2. Beyond this heat flux value , Nukiyama (1966) reported that the platinum wire suddenly glowed up but didn't melt and the boiling curve suddenly shifted from point 'b' to point 'd'. During decreasing heat flux, the boiling curve followed the path 'b' to 'c', as shown in Figure 2.1. Further cooling resulted in a sudden decrease in wall superheat, i.e. along the 'ab' curve, see Figure 2.1.

The boiling curve as reported by Nukiyama (1966) can be categorized in different physical regimes. Tong and Tang (1997) discussed the boiling regimes in detail. As shown in Figure 2.2, the portion of the curve between points 'A' and 'B' is identified as the natural convection region. During this regime, the heat flux is proportional to 5/4th the power of wall superheat. Along the part B-C, the liquid in contact with the heating surface becomes superheated and bubbles can be observed from the scratches or cavities on the boiling surface, which are called nucleation sites. The bubbles are responsible for the latent heat transfer and also agitating the liquid in the vicinity of heating surface. This regime is known as nucleate boiling and according to Tong and Tang (1997) can be subdivided into two categories, i.e.

(1) Local boiling
(2) Bulk boiling

Local boiling occurs within the subcooled liquid, where bubbles tend to collapse after departing from heating surface. On the other hand, bulk boiling takes place during saturated boiling conditions and the bubbles do not collapse after leaving the boiling surface. During nucleate boiling regime, the heat flux is proportional to 2 to 5th power of the wall superheat (Tong and Tang (1997)). As the heat flux increases, the number of bubbles also increases around the heating surface. At point 'C', the bubbles hinder cold liquid from reaching the boiling surface. Then the bubbles act as the blanket around the heating surface. This vapour blanket hinders the heat transfer from the boiling surface to the bulk of liquid. This situation leads to ‘burn out’ or ‘boiling crisis’. The heat flux at this point is at its maximum value and is called as Critical Heat Flux. The dotted line C-D represents the transition boiling or unstable film boiling. Along this region, the heating surface is alternatively exposed to vapor or liquid layers. If the heater input is constant, the heat flux decreases to point ‘D’, while the wall superheat increases. The segment of the curve D-E represents the stable film boiling region. Along this region, there is a stable vapour film on the boiling surface. Furthermore, any increase in heater input results increasing heat flux and wall superheat. During stable film boiling, thermal radiation is responsible for increase in the rate of heat transfer.

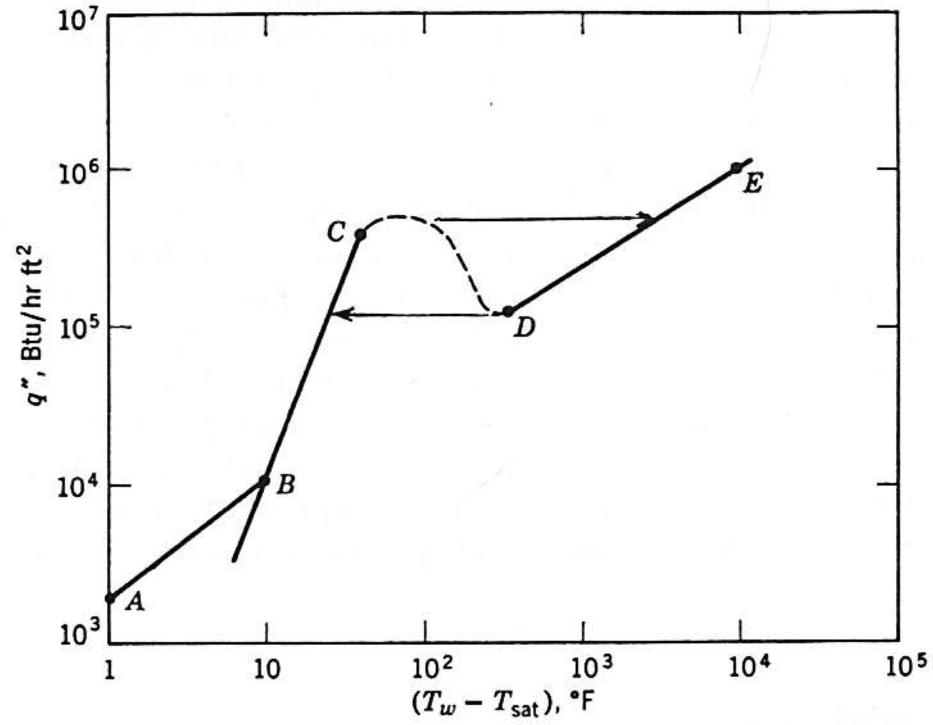

Figure 2.2 Boiling regimes (Tong and Tang (1997))

2.3 Heat transfer enhancement techniques

Webb (1994) classified the heat transfer enhancement techniques into the following three categories:

1. Passive Techniques
2. Active Techniques
3. Compound Enhancement

Passive techniques do not require any external power for enhancement, while in the case of active techniques, an external power is supplied to get the heat transfer augmentation. Moreover, any combination of two or more active or passive techniques is termed as compound enhancement. The enhancement techniques are summarized in Table 2.1 Webb and Bergles (1983).

Table 2.1 Enhancement Techniques Webb and Bergles (1983).

Passive Techniques	Active Techniques	Compound Enhancement
Treat surfaces	Mechanical aids	Any combination of two or more of the above techniques
Roughness surfaces	Surface vibration	
Extended surfaces	Fluid vibration	
Displaced enhancement devices	Electrostatic fields	
Swirl flow devices	Suction or injection	
Coiled tubes	Jet impingement	
Additives for fluids		

2.4 Mechanisms involved in heat transfer

Stephan (1977) reviewed the hypotheses which are involved in the heat transfer mechanism see Figure 2.3: firstly, the microconvection proposes that the liquid layer near the heating surface remains in constant motion. As a result of bubble production, cold liquid moves towards the heating surface and replacing the growing bubble around the boiling surface. This continuous pulsation of liquid and vapour is responsible for the heat transferring process Stephan (1977). A second hypothesis relates to transient heat conduction and states that heat transfer occurs due to conduction between the metal and adjacent liquid layer, which results in superheating the liquid layer.

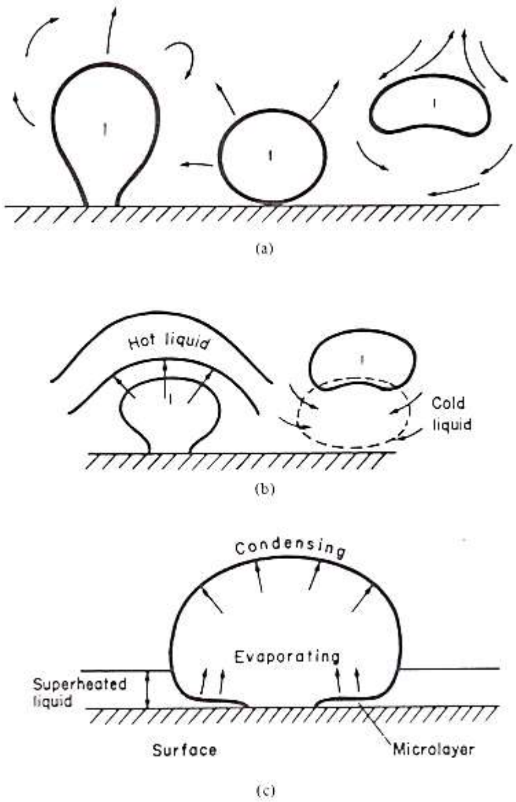

Figure 2.3 Heat transfer mechanisms during boiling (a) Microconvection model (b) Transient heat conduction model (c) Microlayer model Tong and Tang (1997).

During the boiling process, the vapour bubble growth closely sticks with the wall without any liquid layer underneath. Bubble growth is due to evaporation of the superheated boundary layer. This hypothesis does not state any convection process (Jakob (1935) and Jakob (1933) cited in reference by Stephan (1977). Thirdly the "mircolayer theory" states that the bubbles produced from the thin liquid layer between the bubble and the heating surface. As the bubble detaches from the heating surface, the temperature of the surface decreases due to transfer of heat from the liquid layer to the bubbles. It is difficult to find out the thickness of the boundary layer underneath the bubble, which limits the application of boundary layer theory (Moore and Mesler cited in reference Cooper and Lloyd (1969)). Han and Griffith (1965) explained “the bulk convection of transient thermal boundary layer theory”. They proposed that the pool boiling process from a heating surface was divided into two parts, i.e. (i) bulk convection region (ii) natural convection region. It is assumed that the heat transfer process in the bulk convection region is governed by a transient conduction phenomenon. In this phenomenon, small amount of superheated liquid was lifted by the departing bubbles, which moved through the bulk of liquid.

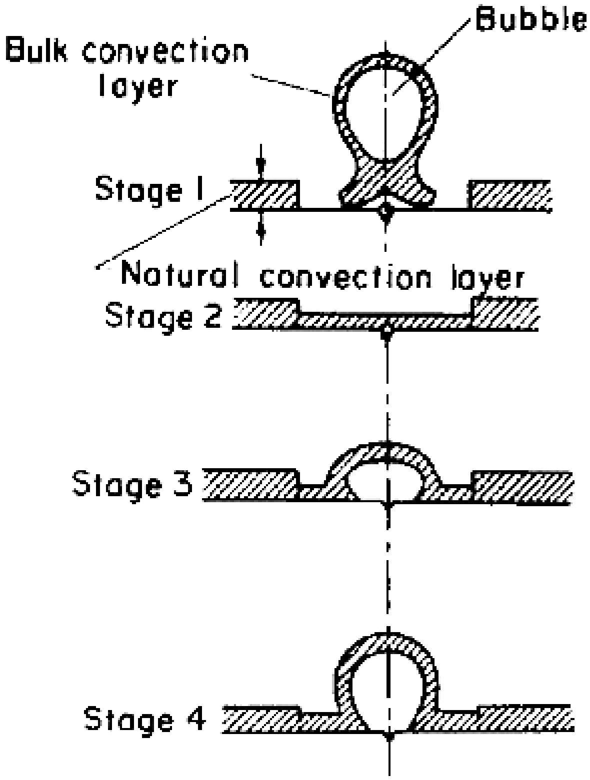

Figure 2.4 Bubble growing Han and Griffith (1965)

The repetition of this process is responsible for heat transfer from boiling surface to bulk of liquid. In natural convection region, the usual convection process is responsible for heat transfer from the boiling surface to the bulk fluid. The mechanism of this process is shown in Figure 2.4 and can be explained as follows: During stage 1, the detaching bubble destroys the superheated transient thermal boundary layer and the cold liquid gathers against the heating surface. After a specific period of time the cold liquid becomes superheat in the form of tiny bubbles within the cavity, which is represented by stage see Figure 2.4. During stage 3, the bubbles grow rapidly and lift up a large piece of thermal boundary layer within a short span of time. At stage 4, the bubble is going to leave the boiling surface, which is similar to stage 1. This repetitive process is responsible for transfer of heat from the boiling surface to the bulk of the liquid.

2.5 Bubble growth during pool boiling

Stephan (1977) hypothetically demonstrated that how the bubbles grow on the heating surface see in Figure 2.5. When the bubble departs from the heating surface, it transfers its internal energy to the surroundings, i.e. the cold liquid. A drift flow in the wake is produced behind this bubble which induces a suction effect within the thermal boundary layer.

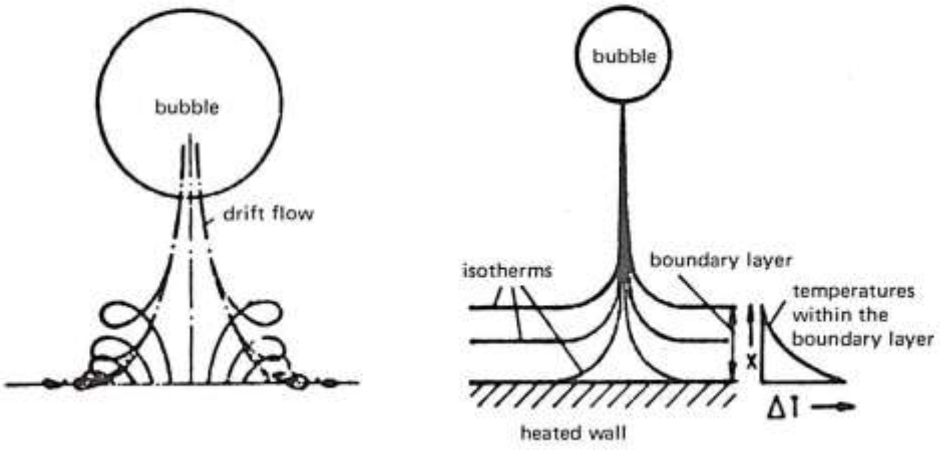

Figure 2.5 The bubble rise up during pool boiling Stephan (1977).

Under this suction effect, a specific volume of the boundary layer is separated and mixed with the bulk of the liquid. The volume of separated liquid is approximately equal to half the volume of the vapour. This drift flow is also responsible for the deformation of the temperature profile within the thermal boundary layer as demonstrated at the right of Figure 2.5.

2.6 Contact angle and surface tension

In two phase heat transfer, contact angle and surface tension are important factors. Yan et al. (2011) reviewed Young's equation in order to define the contact angle as a function of surface tension as follows:

$$\cos\theta = \frac{\sigma_{gw} - \sigma_{wl}}{\sigma_{lg}} \tag{2.1}$$

where σ represents the surface tension and θ denotes the contact angle. The equation (2.1) was derived for the flat surface which showed the effect of liquid properties on contact angle but did not include surface conditions. Yan et al. (2011) further reviewed the Wenzel's equation which is the modified form of young's equation as follows:

$$r_f(\sigma_{sv} - \sigma_{sl}) = \sigma_{lv}\cos\theta_W \tag{2.2}$$

where θ_W is the Wenzel's contact angle and r_f shows the roughness factor which is the ratio of the area of the actual rough surface to the area of corresponding flat surface. Wenzel's equation relates both the fluid properties and the surface conditions with contact angle. Further, Zu et al. (2010) argued that the rough surface increases the wetting properties of the fluid. It can be deduced that as the surface roughness increasers the contact angle decreases. In other words, the fluid wettability increases with the decreasing the contact angle. So, the wettability is the function of both surface tension and surface conditions. Furthermore, increasing the surface roughness can improve the liquid wetting properties which can attribute to the heat transfer enhancement.

2.7 Role of Surface roughness on pool boiling incitation

The role of the heating surface was discussed by Winterton (1977) and mathematically explained that the small bubble can't grow within the bulk of pure liquid, which is at saturation temperature. He argued that the vapour must grow from a small radius according to Thomson's equation:

$$P_v = P + \frac{2\sigma}{r} \tag{2.3}$$

where

P_v = pressure within the vapour

P = external pressure of the liquid.

σ = surface tension.

r = radius of the vapour.

The bubble will grow if the following condition is satisfied, i.e.

$$P_v > P + \frac{2\sigma}{r} \tag{2.4}$$

This condition is impossible by definition (within the pure liquid) because $P_v = P$. So, the embryonic vapour bubbles can't grow within the bulk of pure liquid. This is the mathematical explanation that nucleation requires some solid surface. Furthermore, Griffith (1965) summarized that nucleation is a heterogeneous process. He proved his point by arguing that during boiling the bubbles can be only observed on stationery points. These points located on the solid surface because the liquid was observed in constant motion during the boiling process and the bubble growing points can’t remain stationery if they were in the liquid.

Winterton (1977) further discussed that nucleation sites are required for the initiation of bubble growth, which are filled with a preexisting region of inert and non – condensable gases and vapours. At the moment of nucleation, these sites provide platforms for bubble growth. In the case of boiling, the pressure inside the bubble, i.e. ‘P_v’ must be greater than the external pressure ‘P’. The cracks on the boiling surface or cavities can act as the sites for nucleation, if these are already filled with the vapour or inert gas. On the other hand, if the cracks or cavities on the heating surface are filled by the liquid they became inactive or flooded.

Bankoff (1958) explained the active and deactive surface cavities during the boiling process on the basis of ‘contact angle’ and ‘cone angle’. The contact angle ‘θ’ is the angle between the liquid bubble interface and the solid, while the cone angle ‘φ’ is the angle of the cavity as shown in the Figure 2.6 (a). According to Bankoff (1958), the surface cavities having a contact angle greater than the cone angle are considered as vapour trapping cavities, i.e. liquid can’t fully displace the vapour and non – condensable gases from the cavity. On the other hand, the cavities for which the contact angle is smaller than the cone angle can’t trap vapours, i.e. the cavity will become flooded with the liquid.

Furthermore, Lorenz et al. (1972) explained the vapour trapping mechanism by supposing a conical cavity with cone angle ‘θ’ and radius of the cavity ‘R’ as shown in Figure 2.6. The contact angle ‘θ’ advanced into the favorable direction as shown in Figure 2.6 (b). As the pressure inside the bubble increase the vapour liquid interface moved up in the cavity, i.e. the volume with the vapour increases .Trapping is completed when the vapour liquid interface crosses point ‘A’ as shown in Figure 2.6 (b).

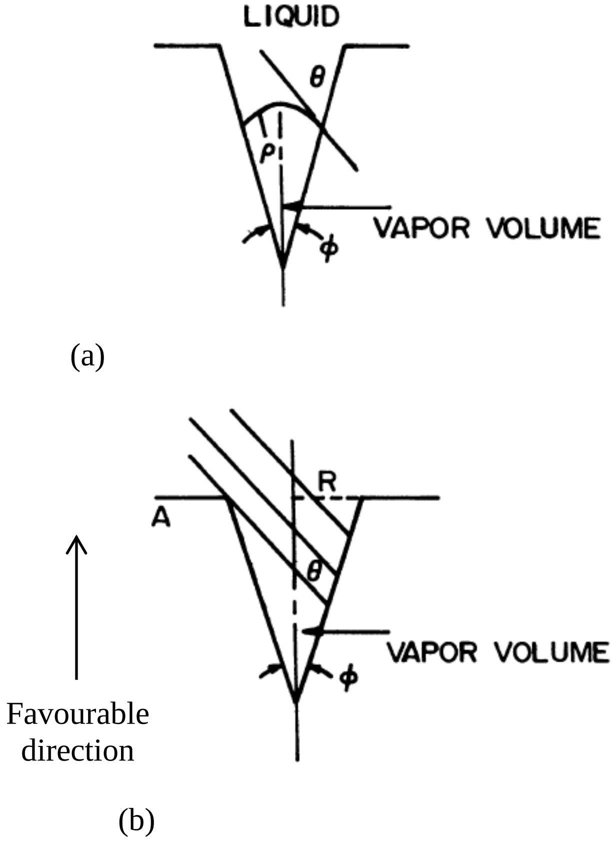

Figure 2.6 Bubble (a) Radius of curvature within the cavity (b) Trapping process within the cavity Lorenz et al. (1972)

Griffith and Wallis (1958) related the wall superheat to the cavity on the boiling surface. They defined a critical radius by supposing a conical cavity, which has already trapped vapour while in Figure 2.7 the bubble volume is plotted against the reciprocal of bubble radius. It can be observed from the Figure 2.7, the unusual shape of the curve lies between the maximum and minimum values. This happens when the vapour liquid interface lies on the mouth of the cavity, at this point the volume of the vapour start to increase as the radius of curvature of bubble increases. The minimum radius of curvature at this stage is termed as critical radius. Moreover, they explained the minimum superheat requires initiating the boiling within the vapour trapping cavity as follows:

$$r_{crit} = \frac{2\sigma T_w V_{fg}}{h_{fg}(T_w - T_{sat})} \tag{2.5}$$

The expression proposed by Griffith and Wallis (1958) revealed that during boiling the radius of the cavity is one of the factors which affect the superheat required for the boiling inception. As the critical radius of the cavity increases the superheat required decreases, this is experimentally observed by the authors.

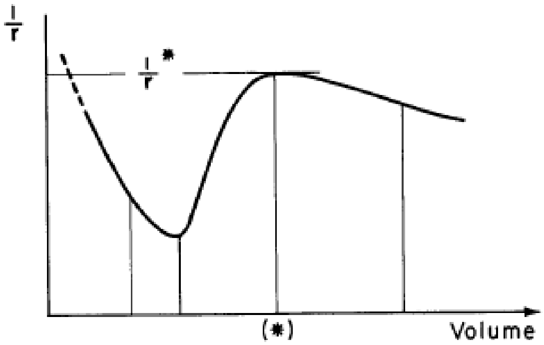

Figure 2.7 The graph between vapour volume and reciprocal of radius of curvature of vapour liquid interface Griffith and Wallis (1958).

2.8 Boiling hysteresis

Corty and Foust (1955) experimentally observed boiling hysteresis. They reported that at 3.4 kW/m^{2}K and 14 K wall superheat, the boiling surface was covered with thousands of vapour columns, which decreases with decreasing heat flux. On the other hand, for increasing heat flux, it was reported that the convective heat transfer remained for 28 K (wall superheat). This value of wall superheat was higher than the value of wall superheat that corresponds to vigorous boiling for decreasing heat flux. As the first bubble appeared on the boiling surface, the wall superheat decreased to normal value, i.e. the boiling curve for increasing heat flux superimpose the curve obtained from decreasing heat flux, as shown in Figure 2.8. Then the boiling spread over the boiling surface randomly. This continuation of convective regime over high value of wall superheat is termed as boiling hysteresis.

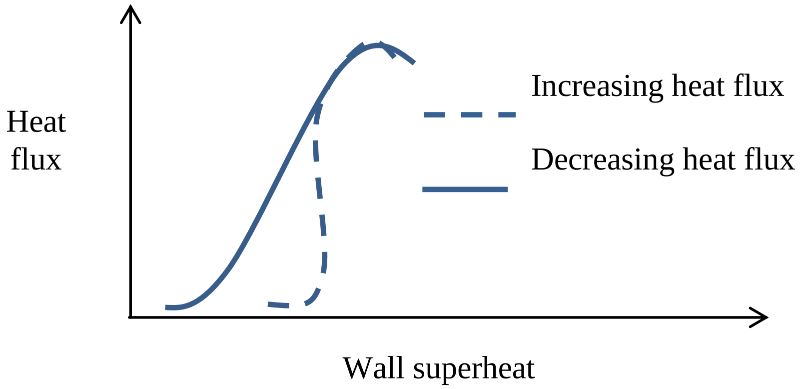

Figure 2.8 boiling hysteresis

Zhou et al. (2004) reported that during pool boiling of R-113, the boiling curve for increasing heat flux did not follow the path of decreasing heat flux up to the inception of nucleate boiling. Once boiling initiated, the wall superheat decreased and the plot between heat flux and wall superheat agreed with the typical path of convectional boiling curve. Moreover, if the heat flux decreased, the plot for decreasing heat flux and wall superheat remained in agreement with the typical boiling curve. Zhou et al. (2004) explained the hysteresis phenomenon on the basis of active nucleation sites. They argued that the cavities which have preexisting vapour or non – condensable gas phase can be the centers of bubbles when boiling first initiated. If the preexisting vapour is removed from the cavity by the boiling liquid, then the cavity becomes inactive for bubble nucleation. The activation of nucleation sites depends upon the nature of boiling liquid and the finish of the heating surface. Moreover, if the liquid wetting angle is smaller than the cone angle of the cavity resulted in the flooding of the surface cavity and can't act as potential nucleation site for bubble generation. Hsu (1962) explained earlier that a higher value of wall superheat was required for activating the larger cavities or in other words a thicker boundary layer was necessary to initiate boiling. The highly wetting liquid results in deactivation of a large number of cavities, i.e. depleting the vapour or non – condensable gases from the potential nucleation sites, except of the smaller cavities.

Chu and Morgan (1977) reported that surface roughness also acts as a crucial factor in determining the value of superheat required to initiate boiling. They argued that the smooth surface required low value of wall superheat to start boiling as compared to the rough surface. The smooth surface contains large number of small cavities, which can trap the vapours or non-condensable gases and become potential nucleation sites for generation. This observation is similar to the arguments of Zhou et al. (2004), i.e. deactivation of large cavities in the presence of highly wetting liquid, which leads to hysteresis problem. In other words, as the surface roughness increases the wall superheat required for boiling initiation also increases.

The effect of liquid properties on boiling hysteresis was experimentally observed and reported by Joudi and James (1977). They performed boiling experiments using R-113, menthol and water as working fluids. They reported that R-113 and menthol exhibit hysteresis during increasing heat flux. Furthermore, they visually observed that after boiling inception the bubbles clouds appeared at random locations on the heating surface. This sudden bubble formation produced a quenching effect on the heating surface, which appeared in the form of decreasing heating wall temperature. On the contrary, no hysteresis was observed during pool boiling experiments on water before boiling inception when the heat flux was increased. This is due to the difference in physical properties, i.e. R-113 and menthol are more wetting than water, which leads to small contact angle between solid and liquid. Due to the small contact angle the cavities on the heating surface become inactive which leads to higher wall temperature required to initiate boiling. Similar to above observations, Bankoff et al. (1958) explained that as the wetting angle increases the nucleation centres on the boiling surfaces become inactive and require higher wall superheat for bubble initiation. The sudden increase in the number of bubbles after boiling inception was explained by Corty and Foust (1955). They proposed that bubbles grow with larger curvature as compared to the cavity radius and hence covers the neighboring cavities before they break into the liquid. This departing vapour leaves their residues in the neighboring cavities and makes them active, which results in the sudden bubble growth at random locations on the heating surface. Furthermore, before bubble initiation the heat transfer was due to convection and conduction. The bubble generation leads to latent heat transfer and turbulence effect within the liquid body which results in increasing heat transfer and heating wall temperature decreases.

Shi et al. (1993) proposed that hysteresis can be categories into two groups (i) TOS (temperature overshoot) hysteresis (ii) TD (temperature deviation) hysteresis as shown in Figure 2.9.

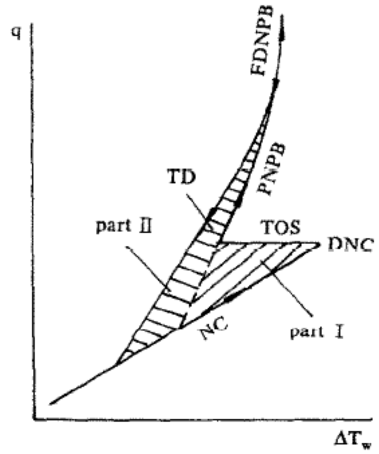

Figure 2.9 Boiling showing hysteresis, where NC: natural convection, DNC : departure of natural convection, TOS: temperature overshoot, PNPB: partial nucleate pool boiling, FDNPB: fully developed nucleate pool boiling and TD: temperature deviation Shi et al. (1993).

They further elaborated that the TOS hysteresis related to rough and porous surface. They explained TOS hysteresis on the basis of liquid trapping and vapour propagation phenomenon. As discussed earlier, vapour trapping cavities act as potential sites for boiling initiation Zhou et al. (2004). Shi et al. (1993) predicted mathematically the wall superheat required for boiling initiation as follows:

$$\Delta T = \frac{T_s}{\rho_v h_{fg}}\left[\frac{2\sigma}{r} - \frac{3M_g R T_v}{4\pi r^3}\right] \qquad (2.6)$$

It can be deduced from equation (2.6) that the required wall superheat required for boiling initiation depends upon the mass of vapour trapped in the cavity. They explained two mechanisms of vapour generation. During the vapour propagation phenomenon, the growing bubble removes the liquid in the neighboring cavity when the contact angle larger than the cavity cone angle as depicted in the Figure 2.10(a). This liquid removing process makes the cavity active for bubble generation. In the liquid trapment mechanism the growing bubble will cover the mouth of the neighboring cavity, which results in the liquid trapment between growing bubble and embryonic bubble, which already exist within the cavity, as shown in Figure 2.10 (b).

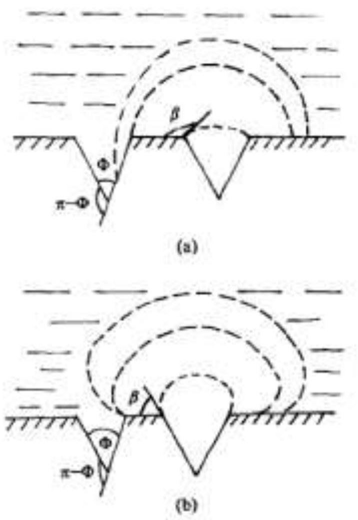

Figure 2.10 Cavity activation mechanism (a) vapour propagation (b) liquid trapment in neighboring cavity Shi et al. (1993).

This process leads to increase in temperature of trapped liquid due to the insulation effect of vapour phase above and below and results in cavity activation. On the other hand, TD hysteresis usually observed on the smooth surface and it occurred during the transition of partial and developed nucleate boiling. Only the vapour propagation mechanism is responsible for TD hysteresis.

2.9 Heat transfer enhancement

2.9.1 Due to surface roughness

Nucleate pool boiling at low to moderate heat flux and critical heat flux were examined using different heating surface topographies combined with different geometries: tube and horizontal flat surface. It was also observed that the degree of enhancement differs from fluid to fluid and depends on the material of the surface. Surface topography is mostly characterized by average surface roughness, R_a (average surface roughness and roughness profile parameter are identical and will be discussed in Section 4.2). Physical surface enhancement or roughness can be produced by applying sand blasting, emery paper treatment or chemical etching Reay (1991).

The important reality is that cavities on the heating surface serve as nucleation sites. They are responsible for initiating bubble formation at low superheat. With the increase in the number of nucleation sites, the heat flux at a particular value of wall superheat is increased. Moreover, physical surface treatment increases the average value of surface roughness which increases the nucleation site density Pioro and Rohsenow (2004). Das and Das (2007) examined topographically different surfaces by drilling holes of 600 μm in diameter and 2 mm in depth (see
Figure 2.11) using distilled water as the working fluid and reported enhancement by up to 100% when comparing their results with the values for a plain surface, see Figure 2.12. Based on the results from the microdrilled surface Das and Das (2007) modified the Yamgate’s correlation [cited in reference Das and Das (2007)] and proposed the following equation in which the heat flux is a function of nucleation site density and wall superheat.

$$q = a(\Delta T)^b \left(\frac{N}{A}\right)^c \tag{2.7}$$

where a= 7.7655, b= 2.0307 and c= 0.523141 are empirical constants calculated for distilled water.

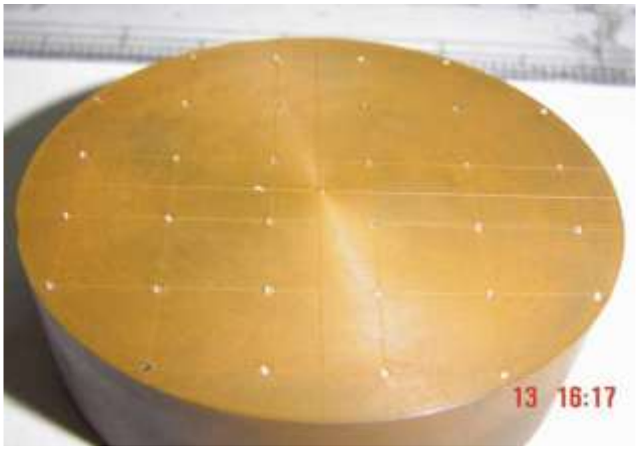

Figure 2.11 View of micro drilled surface Das and Das (2007)

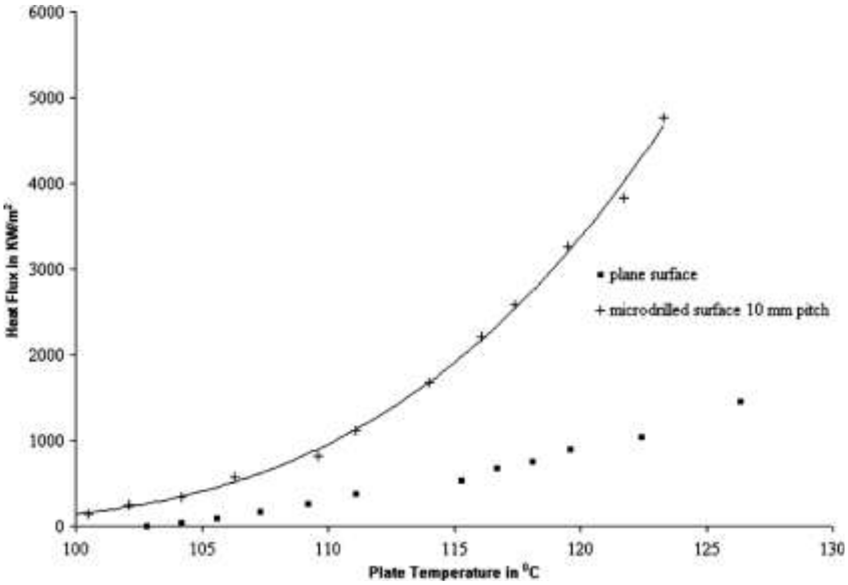

Figure 2.12 Boiling curves for microdrilled and plain surfaces Das and Das (2007)

A similar increasing trend was observed by Benjamin and Balakrishnan (1997) during experiments, which involved boiling at low to moderate heat flux of four different liquids namely: water, acetone, carbon tetrachloride and n-hexane on an aluminum surface (R_a = 1.17 μm). The heat flux increased by up to 25% in water, 90% in carbon tetrachloride, 122% in acetone and 60% in n-hexane compared to a similar experiment on an aluminum surface of R_a = 0.089 μm at a specific value of wall superheat. Similar to the above results, the experiments with refrigerants R-134a and R-407c reported by Hsieh and Weng (1997) revealed that as the surface roughness was increased, pool boiling was enhanced. They used 19 mm (OD) copper tubes and used emery paper # 20, 50, 100 and 150 to treat the surface. The surface roughness R_a was reported as 4.57, 3.95, 2.12 and 1.82 μm respectively. They gave no further details on how they actually used the paper on the tubes (e.g. pressure applied and direction). The enhancement in the heat transfer coefficient ratio of the emery treated tubes over a polished tube (surface roughness 0.03 μm) was reported to be upto 2.36 for R-134a and 1.55 for R-407c at the heat flux value of 10 kW/m^2. Kang (2000) observed a 71.4 % rise in pool boiling heat flux of water when there was an increase of 300 % in surface roughness with horizontal tubes.

Gorenflo et al. (2004) reported that the surface treatment methods play a vital role in the heat transfer rates during pool boiling. They performed experiments on horizontal copper tubes (8 mm OD). The outer surfaces of the tubes were treated in three different ways namely: fine sandblasting, fine + medium sandblasting and emery grinding. During the fine sandblasting procedure, corundum grains F320 (d_p = 20-30 μm) were used at 3 bar pressure (the detailed sandblasting procedure is described in Luke (2006)). For fine + medium sandblasting method, the fine sand blasting was performed as mentioned above and for the medium sandblasting corundum grains C220 (d_p = 50-80 μm) were utilized at 1.5 bar pressure. The third tube was grinded with emery paper grade # 400. The surfaces were characterized by primary profile parameter P_a (according to DIN EN ISO 4287) (by definition standardized surface is same as average surface roughness, R_a) and reported as 0.58 μm, 0.27 μm and 0.56 μm for emery grounded, fine sandblasted and fine + medium sandblasted copper tubes respectively. The results obtained from the pool boiling tests of normal propane at a saturated pressure of 4.247 bar revealed that at a given value of heat flux the heat transfer coefficient was greater for both sandblasted tubes than the emery treated in the nucleate boiling regime. Luke et al. (2000) provided a possible explanation by analysing the surface roughness profiles of the tubes as shown in Figure 2.13.

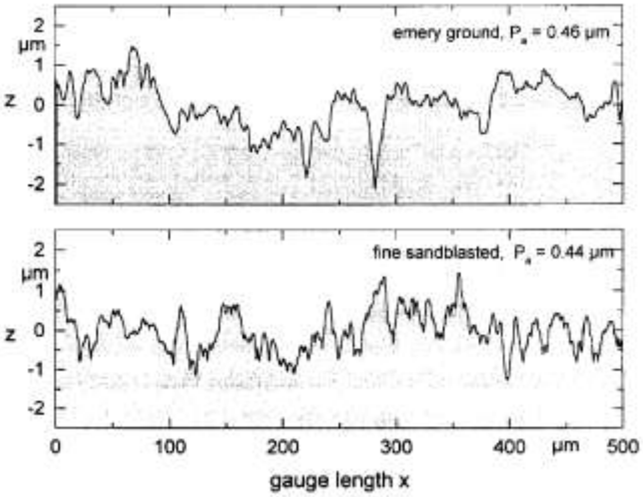

Figure 2.13 Roughness profile of emery grounded and fine sandblasted copper surfaces Luke et al. (2000).

The primary profile parameter P_a is almost the same for both sandblasted and emery treated tubes. From the overview analysis of the surface profile, it can be observed clearly that on the emery ground surface there were deeper valleys and higher peaks than the sandblasted surface. On the other hand, there was a more homogenous cavity distribution on the sandblasted surface (Luke et al. (2000) and Luke (2009)). Furthermore, the surface microstructure was explained by Luke (2006) by analysing the surface roughness profile using a ball rolling procedure (R_B = 25, 250 and 2500 μm discussed Luke (2006)in detail) and statistical techniques Luke found that the density of cavities was higher on the sandblasted surface than on the emery grounded surface. Moreover, the analysis of fine sandblasted and fine + medium sandblasted revealed that the cavities on the fine + medium sandblasted surface were bigger than on the fine sandblasted surface Luke (2006,a). Similar to these observations, Kottof et al. (2006) analysed a new modified surface which was prepared by fine + medium sandblasting and then was rolled to create re-entrant cavities. After a detailed surface profile and statistical analysis, it was reported by and Kottof et al. (2006) that before rolling there were sharp edges in the bottom of the cavities and the surface between two cavities. But after the rolling process the surface in the bottom and between the cavities flattened and the mouth of the cavity became narrow. The vapour could be trapped more effectively in narrow mouth cavities which resulted in augmentation in heat transfer rates. From the above discussion it can be concluded that the method of surface preparation should be considered and careful surface finish may lead to more effective and smaller equipment design for given thermal loads. Jones et al. (2009) examined the effect of surface modification on pool boiling of FC-77 and water at 100 ^{0}C saturation temperature. They modified aluminum surfaces to carry out boiling tests. The surface modification was performed using a ram – type electric discharge machine (EDM). By controlling the machine parameters four different surface textures were obtained. The surfaces were characterized in terms of average surface roughness (R_a) values, which were reported as 1.08 µm, 2.22 µm, 5.89 µm and 10 µm, see Figure 2.14.

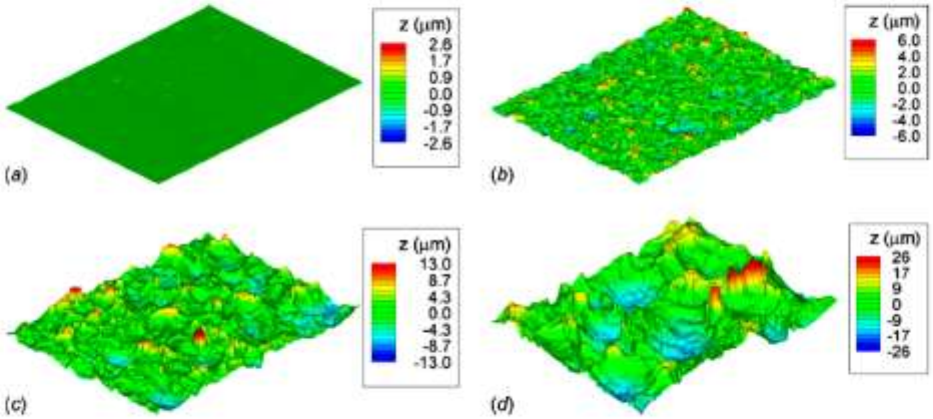

Figure 2.14 Topography of the surfaces (a) R_a = 0.038 µm (plain surface) (b) R_a = 1.08 µm (c) R_a = 2.22 µm (d) R_a = 5.89 µm Jones et al. (2009).

Due to the modification of the surface texture the heat transfer coefficient for water was found to increase by a factor of between 1.3 and 2 (at 100 kW/m^2) compared to that for a smooth surface with R_a = 0.038 µm. The corresponding enhancement with

FC-77 was between 2 and 2.5 (at 100 kW/m^2) when the average surface roughness of the smooth surface was 0.027 µm, see Figure 2.15. The difference in the values of enhancement for water and FC- 77 was attributed to the difference in the physical properties of the liquids.

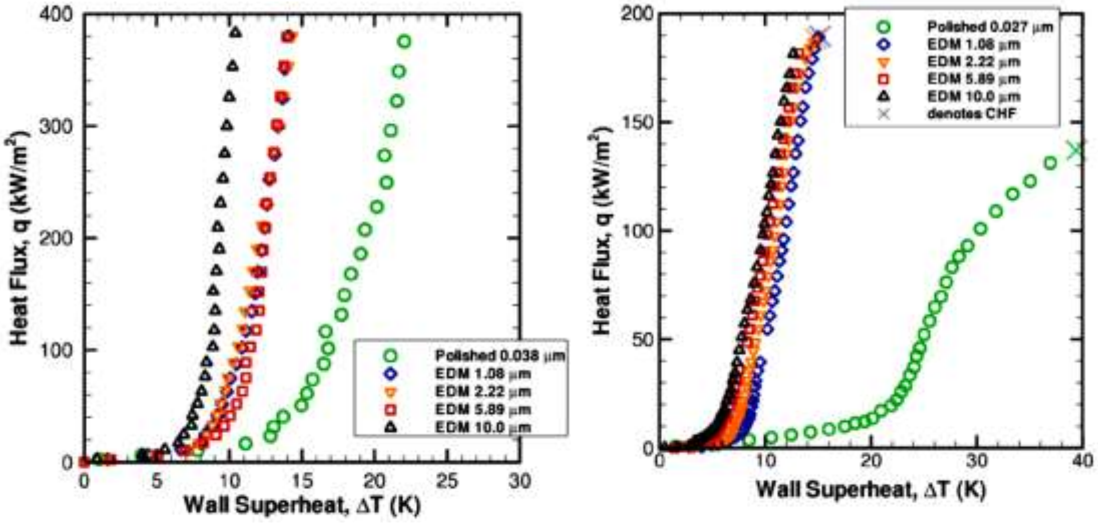

(a) (b)

Figure 2.15 Boiling curves (a) water (b) FC 77 Jones et al. (2009)

During the early sixties, Berenson (1962) reported the effect of surface roughness using three different liquid – heating surface combinations namely: copper – n-pentane, Inconel – n-pentane and nickel – n-pentane. Four copper surfaces were prepared for performing the tests. First copper surface was mirror finished, second surface was lapped circularly with grit E no. 120, third and fourth surfaces were grinded with emery paper no. 320 and 60 respectively. It was observed from the tests results that the boiling curve moved towards the left as the boiling surface became rougher, i.e. at specific value of wall superheat, the rate of heat transfer increased as the roughness of boiling surface increased. Similar results were reported for Inconel – n-pentane and nickel – n-pentane combinations. This indicates that the surface roughness of heating surface can cause direct effect on pool boiling.

Table 2.2 Heat transfer enhancement due to surface roughness

Sr no.	Boiling fluid	Boiling surface	% enhancement	Reference surface	Reference
1	Distilled water	Copper, microdrilled surface	100	Plain copper surface.	Das and Das (2007)
2	Water	Aluminum tube, R_a = 1.17 µm	25	Aluminum tube, R_a = 0.089 µm	Benjamin and Balakrishnan (1997)
	Acetone		122		
	CCl_4		90		
	n-hexane		60		
3	R-134a	Copper tube	236 (max)	Copper tube R_a= 0.03 µm, at 10 kW/m^2	Hsieh and Weng (1997)
	R-407c		155(max)		
4	Water	Copper surfaces (R_a= 1.08 µm, 2.22 µm, 5.89 µm and 10 µm)	130 to 200	Copper surface, R_a = 0.038 µm, at 100 kW/m^2	Jones et al. (2009)
	FC-77		200 to 250	Copper surface, R_a = 0.027 µm, at 100	

2.9.2 Due to finned structure

Earlier, Saidi et al. (1999) performed pool boiling experiments at 26.5 ^oC saturation temperature for R-123. They used two finned copper tubes. The dimensions of the first tube were OD = 17.1 mm, fins/m = 1923, fin height = 0.909 mm, fin pitch = 0.52 mm and fin thickness = 0.4 mm. The second tube had an OD = 17.1 mm, fins/m =

752, fin height = 1.050 mm and fin thickness = 0.9 mm. They reported that the enhancement ratio (defined as the ratio of the heat transfer coefficient to the heat transfer coefficient for a smooth tube at the same heat flux) was between 2.4 and 2.2 and between 2.4 and 1.3 for the first tube and the second tube respectively. No information about the surface of smooth tube was given by the authors. Similar experiments were executed earlier by Ayub and Bergles (1987) to observe the effect of enhanced surfaces on saturated pool boiling of R – 113 and water at 1 bar pressure. They tested electrically heated commercially available GEWA-T, GEWA-K (see Figure 2.16) and smooth copper tubes. At 80 kW/m^2, enhancement ratios (defined as above) of 1.11 and 1.56 were reported for water and R-113 respectively for the GEWA-K tube. On the other hand for the GEWA-T tube, the enhancement ratio was 160% for water and 200% for R-113, at the same heat flux of 80 kW/m^2.

a b

Figure 2.16 Profiles of (a) GEWA – K (b) GEWA – T Ayub and Bergles (1987)

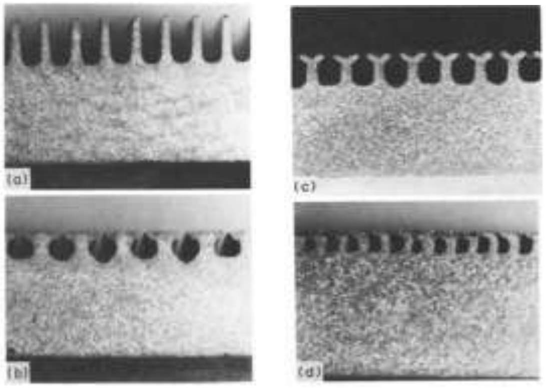

Figure 2.17 Profile of (a) GEWA K 26 (b) GEWA TX 19 (c) GEWA SE (d) Turbo B Webb and Pais (1992)

Pool boiling tests were performed by Webb and Pais (1992) to measure the performance of enhanced copper tubes, namely: GEWA-K26, GEWA-TX19, GEWA-SE, Turbo-B (see Figure 2.17) and a plain tube, for five different refrigerants.

Their results show enhancement ratios of heat transfer coefficient of between 2 and 4.67 for R-123 at a saturation temperature of 26.7 ^{o}C and a heat flux of10 kW/m^2. Memory et al. (1995) carried out the saturated pool boiling experiments at 2.2 ^{o}C using R-114 as a working fluid. Four enhanced surface copper tubes, namely: GEWA-K, GEWA-T, GEWA-YX and Thermoexcel-HE, were evaluated as electrically heated boiling surfaces. It was reported that the enhancement ratios achieved with these tubes ranged from 4 to 20, and from 1.8 to 2.8 for heat fluxes of 5kW/m^2 and 80 kW/m^2 respectively. Kim and Choi (2001) performed pool boiling experiments using enhanced tubes. The enhancement process was carried out by rolling low integral fin tubes having 1654 fin/m and 1.33 mm fin height. The resultant surface of tubes leaded to triangular pores with connecting tunnels. The heat transfer results of enhanced surface were compared to the emery treated smooth surface. The surface of smooth tube was characterized using Kosaka lab. SE 3300 profiler and average surface roughness, R_a, was reported as 0.29 µm. The saturated boiling tests were performed using R-11, R-123 and R-134a as the working fluids. It was reported that at saturation temperature of 4.4 ^{o}C, the heat transfer enhancement (defined as the ratio of heat transfer coefficient of enhanced tube to the heat transfer coefficient of smooth tube) was 6.0, 6.5 and 5.0 for R-11, R-123 and R-134a respectively, at 40 kW/m^2. Kim et al. (2008) studied the pool boiling characteristics of treated surfaces, including the effects of sub-cooling and surface orientation, using the dielectric liquid PF5060 and 20 mm x 20 mm copper test surfaces. Four different surfaces were tested: a plain surface, a sanded surface, a micro-finned surface and a micro-porous coated surface. The sanded surface was prepared using grade #80 sandpaper and had an average roughness height of 1.546 µm. The micro-finned surface tested by Kim et al. (2008) was fabricated by etching a copper test block to produce micro-fins of 100 µm x 100 µm square cross-section with a height of 50 µm, see Figure 2.18 Figure 2.19. The spacing between the fins was 200 µm and the increase in heat transfer area was 43.6% compared to the original plain surface. Their PF5060 pool boiling curves show that for a heat flux of 120 kW/m^2 the wall superheat for the micro-finned surface was 47% lower than for a plain surface. For saturated conditions and horizontal orientation, the sanded surface achieved a wall superheat reduction of 43% at 120 kW/m^2 compared to that measured for the plain surface.

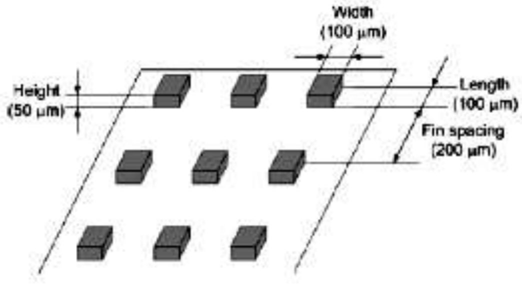

Figure 2.18 Photograph of microfinned surface Kim et al. (2008)

McGillis et al. (1991) obtained experimental data showing the effect of surface finish on pool boiling of water at a sub atmospheric pressure of 9 kPa on three flat copper surfaces. For a constant wall superheat of 25 K, the heat flux increased by about 100% when the root mean square (rms) surface roughness increased from 0.16 μm to 5.72 μm. McGillis et al. (1991) conducted parametric experiments to determine the effects of fin geometry for low-pressure pool boiling of water on rectangular fin arrays at 9 kPa. The fin arrays were machined on 12.7 mm square copper test sections, with fin lengths from 0 to 10.2 mm, fin gaps from 0.3 mm to 3.58 mm and nominal fin widths of 1.8 mm and 3.6 mm. All the finned surfaces reduced wall superheat and extended the nucleate boiling range compared to smooth surface. However, based on the evidence for fins of 1.8 mm nominal width, additional increase in the base heat flux was fairly marginal for fin lengths greater than 2.54 mm. Smaller fin gaps were found to lead to greater heat transfer enhancement. For example, at 60 kW/m^2, a fin gap of 0.3 mm resulted in the wall superheat decreasing by 72 % compared to a flat surface, whereas for a fin gap of 3.58 mm the decrease in wall superheat was only 28 %. No significant influence of fin width on heat transfer rates was reported.

Yu and Lu (2007) investigated the heat transfer performance of rectangular fin arrays for saturated pool boiling of FC-72 at 1 atm. The EDM process was used to manufacture 7 x 7, 5 x 5 and 4 x4 fin array test surfaces from copper blocks of 10 mm x 10 mm base area, with fin spacings of 0.5 mm, 1 mm and 2 mm respectively (see Figure 2.19). Four different fin lengths (0.5 mm, 1 mm, 2 mm and 4 mm) were investigated and the thickness of the fins was fixed as 1 mm. In general, the heat transfer rate increased as the fin length increased and the fin spacing decreased, the maximum value being achieved with the fin array having the narrowest fin gaps (0.5 mm) and the highest fins (4 mm) was over five times that for the reference plain surface. Note that the boiling heat transfer coefficient (based on the total finned surface area) was found to be approximately independent of fin length at low heat flux. However, at moderate and high heat flux values, the heat transfer coefficient decreased as the fin length was increased at constant wall superheat.

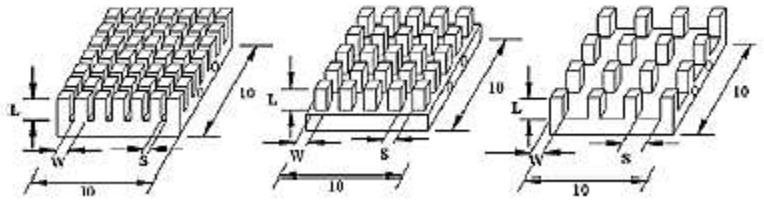

Figure 2.19 array fin structure on boiling surface Yu and Lu (2007)

Hübber and Künstler (1997) investigated the effect of surface roughness and fin shape on pool boiling of n-pentane. Three types of structured finned tubes were used to carry out the experiments, i.e. trapezoid – shaped, T- shaped and Y – shaped as shown in Figure 2.20 The dimensions of the tubes are given in Table 2.3.

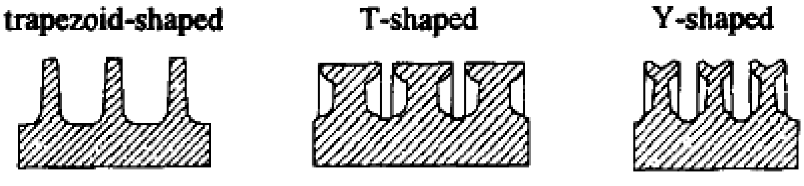

Figure 2.20 structure of enhanced finned surface Hübber and Künstler (1997).

It was reported that the heat transfer increased significantly for above mentioned finned tubes. Moreover, the augmentation in heat transfer was better at T – shaped and Y – shaped finned tubes as compared to plain tube having average surface roughness 0.34 µm. It was proposed that the augmentation may be due to two effects, firstly the surface roughness and secondly the shape of fin, which leads to high heat transfer area. It was also reported that for saturation pressure of 3 bars, the heat transfer coefficient during pool boiling of propane increased by the factor of 4.0, 3.0, 2.4 and 1.6 for YX19, TX19, T19 and K36 (see Table 2.3) type finned tubes as compared to smooth tubes.

Table 2.3 dimensions of finned surface Hübber and Künstler (1997)

Fin type	Fin per inch	Gap at fin tops (mm)	Fin height (mm)	Heated length (mm)	Diameter at fin base (mm)	Outer diameter (mm)
K19	19	1.05	1.40	200	13.01	15.81
K36	36	0.5	0.95	200	13.01	14.91
T19	19	0.35	1.00	200	12.88	14.88
TX19	19	0.23	1.04	200	12.48	14.55
YX26	26	0.34	1.10	200	12.76	14.96

Recently, Cooke and Kandlikar (2011) carried out pool boiling tests on silicon micro-channels. The silicon chip was 20 mm × 20 mm rectangular test surface which was 725 µm thick. Six different silicon chips were used in pool boiling experiments using distilled water at saturated atmospheric conditions. The dimensions of the micro-channels are mentioned in Table 2.4. The average surface roughness R_a for plain silicon chip was reported as 0.030 µm. It was reported that the heat transfer coefficient enhanced by the factor of 2.5, 2.4, 3.4, 2.2 and 1.6 for chip #2, chip #3, chip #4, chip #5 and chip #6 respectively, when the wall superheat was 19.5 °C. Cooke and Kandlikar (2011) argued that the enhancement in the value of heat transfer coefficient was attributed to the increase in the heat transfer area of the silicon chip.

Table 2.4 dimensions of micro-channels Cooke and Kandlikar (2011)

Chip	Type	Channel (μm)	Fin (μm)	Depth (μm)
1	Plain	-	-	-
2	Micro-channel	200	200	208
3	Micro-channel	200	200	192
4	Micro-channel	100	100	275
5	Micro-channel	100	100	182
6	Offset strip fin	40	60	180

Table 2.5 Enhancement due to finned surfaces

Sr. no	Boiling fluid	Boiling surface	Enhancement (%)	Remarks	Reference
1	R-123	Finned tube, fin/m = 1923, OD = 17.1 mm, fin height = 0.909 mm, fin thickness = 0.4 mm.	240 to 220	At saturation temperature 26.5 ºC	Saidi et al. (1999)
		Finned tube, fin/m = 752, OD = 17.1 mm, fin height = 1.05 mm, fin thickness = 0.9 mm	240 to 130		
2	R-113	GEWA-K (tube)	156	80 kW/m^2	Ayub and Bergles (1987)
		GEWA-T (tube)	160		
	Water	GEWA-K (tube)	111		
		GEWA-T (tube)	200		
3	R-123	GEWA-K26 (tube) GEWA-TX19 (tube)	200 to 467	26.7 ºC saturation	Webb and Pais (1992)

		GEWA-SE (tube) Turbo-B (tube)		temperature	
4	R-114	GEWA-K(tube) GEWA-T(tube) GEWA-YX Thermoexcel-HE	180 to 280	At 80 kW/m^2	Memory et al. (1995)
5	R-11	Tube, fin/m = 1654, fin height = 1.33 mm	600	40 kW/m^2	Kim and Choi (2001)
	R-123		650		
	R-134a		500		
6	PF5060	Microfinned horizontal copper surface, fin dimensions = 100 μm × 100 μm × 50 μm	47 % reduction of wall superheat	1 bar saturation pressure	Kim et al. (2008)

2.9.3 Due to porous structure

Surface enhancement techniques for pool boiling include porous microstructures formed by sintered metallic layers and porous coatings. Scurlock (1995) presented experimental results for saturated pool boiling of liquid nitrogen and refrigerant R-12 on surfaces with porous aluminium/silicon coatings. The surfaces were manufactured by plasma spraying a mixture of aluminium powder with 10 % silicon and polyester on to 50 mm x 50 mm aluminium plates, which were subsequently heated in air at 500°C for 2 hours to evaporate the polyester. Six surfaces were prepared with coating thicknesses between 0.13 mm and 1.32 mm. For the 0.13 mm thick coating and a heat flux of 13 kW/m^2, the wall superheat was found to decrease compared to that for a smooth surface, by approximately 90% for LN_2 and 85% for R-12. The optimum coating thickness for maximum heat transfer coefficient was found to be 0.38 mm for LN_2 and 0.25 mm for R-12. Rainey and You (2001) investigated the effect of micro-porous coated surfaces on pool boiling of saturated FC-72 at atmospheric pressure. Copper test surfaces, 20 mm x 20 mm and 50 mm x 50 mm, were coated using a mixture of Diamond particles, Omegabond 101 and Methyl-Ethyl-Ketone (MEK), known as DOM, by drip-coating onto the 20 mm square surface and spray-coating onto the 50 mm square surface. Evaporation of the MEK produced a micro-porous layer on the surface, approximately 50 μm thick and containing 8-12 μm diamond particles. Heat transfer coefficients for nucleate boiling on the micro-porous coated surfaces were always augmented by more than 300% compared to those for plain polished surfaces. As previously mentioned, Kim et al. (2008) also tested a micro-porous coated surface for pool boiling of PF5060. The DOM coating applied to the 20 mm square copper test surface contained 4-8 μm diamond particles and was around 45 μm thick, see Figure 2.21. At a heat flux of 120 kW/m^2, the wall superheat decreased by 66% compared to that for a plain horizontal surface.

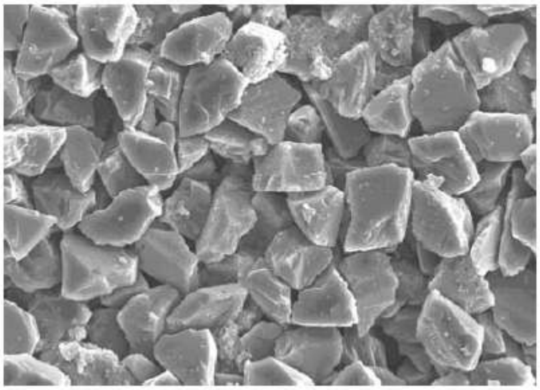

Figure 2.21 Photograph of porous structure Kim et al. (2008)

Tang et al. (2012) performed pool boiling experiments using nanoporous metallic copper surface. Boiling tests were carried out using deionized water as a working fluid under saturated atmospheric conditions. Hot-dip galvanizing/dealloying process was employed to modify the boiling surface, which was a copper rod having 19.1 mm OD. The pore size of the resultant modified surface was reported as 50-200 nm. The heat transfer coefficient enhanced by 172.7 % as compared to flat surface at 15 kW/m^2 (no information about the flat surface was reported by the authors). Lee et al.

(2010) performed pool boiling experiments using deionized water under saturated atmospheric conditions. Cylindrical aluminum alloy (6061) was used as a test section with 19.1 mm OD. Nano porous structure was fabricated on the Al rod by employing two-step process; electro-polishing and anodizing. The resulted nanostructure is shown in Figure 2.22.

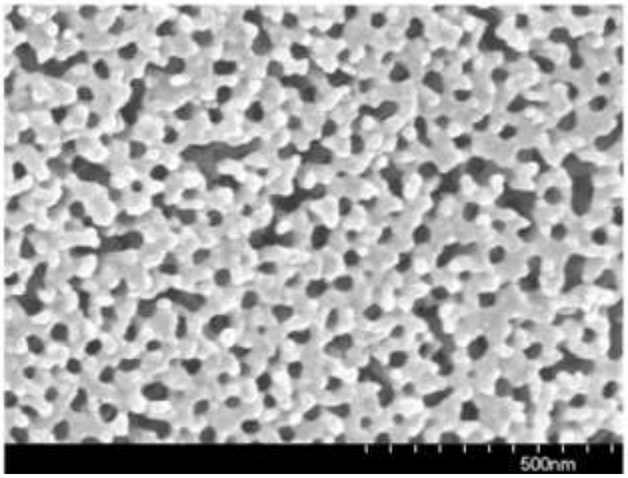

Figure 2.22 SEM image of nanostructured surface Lee et al. (2010)

Pool boiling was carried out in a transparent acrylic chamber which was 178 mm in length, 100 mm in width and 130 mm in height. It was reported that the heat transfer coefficient increased 12.07 % at 40 kW/m^2, when the results of nano-porous surface was compared with non-porous surface (no information about the non-porous surface was reported by the authors).

2.10 Correlations for nucleate boiling heat transfer

Details of some of the correlations proposed to predict heat transfer coefficients in nucleate boiling are set out below. Stephan and Abdelsalam (1980) proposed correlations to predict the heat transfer coefficient for water, hydrocarbons, cryogenics and refrigerants in the nucleate boiling regime. The correlations were based on a regression analysis representing approximately 2800 experimental data points obtained for pool boiling on horizontal surfaces with fully established nucleate boiling under the influence of the gravity field. The pressure range for these data points was $0.0001 \leq P/P_c \leq 0.97$. The following correlation developed specifically for refrigerants with $0.003 \leq P/P_c \leq 0.78$ gave a mean absolute error of 10.6 %:

$$h = 207\frac{k_l}{D_b}\left(\frac{qD_b}{k_l T_s}\right)^{0.745}\left(\frac{\rho_g}{\rho_l}\right)^{0.581}\left(\frac{\nu_l}{\alpha_l}\right)^{0.533} \tag{2.8}$$

where the bubble departure diameter D_b is expressed as

$$D_b = 0.0146\beta\left(\frac{2\sigma}{g(\rho_l-\rho_g}\right)^{0.5} \tag{2.9}$$

and the bubble contact angle β was taken as 35^o for refrigerants. A mean surface roughness $R_{p,\mathrm{old}}$ = 1 µm was assumed, where $R_{p,\mathrm{old}}$ is an older roughness measure defined by the superseded standard DIN 4272:1960 and equal to $R_a/0.4$ according to Gorenflo et al. (2004). Stephan and Abdelsalam recommended that, to a first approximation, surface roughness may be accounted for by multiplying equation (2.8) by a factor $R_{p,\mathrm{old}}^{0.133}$, for $0.1 \leq R_{p,\mathrm{old}} \leq 10$ µm.

Cooper (1984) developed the following simple correlation for predicting the heat transfer coefficient for nucleate boiling (in W/m^{2}K) based on the reduced pressure, the heat flux (in W/m^2) and the surface roughness (in µm):

$$h = \mathrm{C}(q)^{0.67} M^{-0.5} P_r^n(-\log_{10} P_r)^{-0.55} \tag{2.10}$$

and the constant was given as C = 55, but with the suggestion that this value should be replaced by C = 95 for horizontal copper cylinders. The exponent n is given by

$$n = 0.12 - 0.2\log_{10} R_{p,old} \tag{2.11}$$

A comprehensive correlation for predicting pool boiling heat transfer coefficients was suggested by Gorenflo and Kenning (2009) in the form

$$\frac{h}{h_{o,ref}} = F_q F_{P_r} F_W F_f \tag{2.12}$$

The four factors on the right-hand side of equation (2.12) are functions of the heat flux, the reduced pressure, the heating surface and the fluid properties respectively, defined as

$$F_q = \left(\frac{q}{q_o}\right)^n \tag{2.13}$$

where $q_o = 20$ kW/m^2 and n is given by

$$n = 0.95 - 0.3P_r^{0.3} \tag{2.14}$$

$$F_{P_r} = 0.7P_r^{\ 0.2} + 4P_r + \frac{1.4P_r}{1-P_r} \tag{2.15}$$

$$F_W = F_{WR} F_{WM} \tag{2.16}$$

where

$$F_{WR} = \left(\frac{R_a}{R_{ao}}\right)^{\frac{2}{15}} \tag{2.17}$$

with the reference surface roughness $R_{ao} = 0.4$ µm

$$F_{WM} = \left(\frac{k c_p \rho}{(k c_p \rho)_{copper}}\right)^{0.25} \tag{2.18}$$

and

$$F_f = \left(\frac{P_f}{P_{f,ref}}\right)^{0.6} \tag{2.19}$$

The fluid parameter P_f in equation (2.20) is defined as

$$P_f = \frac{\left(\frac{dP}{dT}\right)_s}{\sigma} \tag{2.20}$$

where $(dP/dT)_s$, the slope of vapour pressure curve, and σ are both at a reference pressure $P_r = 0.1$. Values of P_f, in $(\mu m\ K)^{-1}$, are tabulated by Gorenflo and Kenning (2009) for a large number of fluids. The reference fluid values are $h_{0,ref} = 3.58$ kW/m^{2}K and $P_{f,ref} = 1.0\ (\mu m\ K)^{-1}$.

Jung et al. (2003) developed a correlation to predict pool boiling heat transfer coefficients for pure halogenated refrigerants by modifying the correlation of Stephan and Abdelsalam (1980). Based on a regression analysis of their experimental data for halogenated refrigerants, they suggested that the power on the heat flux term in equation (2.8) is a function of fluid properties and therefore has a unique value for each refrigerant. The new correlation is as follows:

$$h = 10\frac{k_l}{D_b}\left(\frac{qD_b}{k_l T_s}\right)^{c_1} P_r^{0.1}(1 - T_r)^{-1.4}\left(\frac{\nu_l}{\alpha_l}\right)^{-0.25} \tag{2.21}$$

where

$$c_1 = 0.855\left(\frac{\rho_g}{\rho_l}\right)^{0.309} P_r^{-0.437} \tag{2.22}$$

and D_b is given by equation (2.9). Equation (2.21) fitted the data of Jung et al. with a mean deviation of less than 7%.

Shekriladze (2008) presented a correlation for predicting the Nusselt number in developed nucleate boiling. The effective radius of nucleation cavities was assumed to be the characteristic linear dimension, denoted here as r_o. For commercial heating surfaces it was suggested that r_o can be represented by an average value of 5 µm. The Shekriladze (2008) correlation is as follows:

$$\mathrm{Nu} = \frac{hr_o}{k_l} = 0.88 \times 10^{-2} K^{0.7} \mathrm{Re}_s^{0.25} \tag{2.23}$$

where

$$K = \frac{q r_o^2 \rho_g h_{lg}}{\sigma k_l T_s} \tag{2.24}$$

and

$$\mathrm{Re}_s = \frac{c_p T_s \sigma \rho_l}{h_{lg}^{\frac{3}{2}} \rho_g^2 \nu} \tag{2.25}$$

Yagov (2009) proposed a correlation on the basis of boiling fluid properties as follows:

$$q = 3.43 \times 10^{-4} \frac{k_l^2 \Delta T^3}{v_l \sigma T_s} \left[1 + \frac{h_{lg} \Delta T}{2R T_s^2}\right]$$

$$. \left(1 + \sqrt{1 + 800B} + 400B\right) \tag{2.26}$$

Where

$$B = \frac{h_{lg} (v_l \rho_g)^{3/2}}{\sigma (k_l T_s)^{1/2}} \tag{2.27}$$

Rohsenow (1952) developed the following correlation for nucleate boiling of liquids other than water:

$$\frac{c_{pl} \Delta T}{h_{lg}} = C_{sf} \left[\frac{q}{h_{lg} \mu_l} \left(\frac{\sigma}{g(\rho_l - \rho_g)}\right)^{1/2}\right]^{0.33} \left[\frac{c_{pl} \mu_l}{k_l}\right]^{1.7} \tag{2.28}$$

Jabardo et al. (2004) reevaluated the exponents and the leading coefficient C_{sf} in the Rohsenow correlation using experimental data for refrigerants. Modified exponents were determined as 0.21 and 1.03, replacing the values 0.33 and 1.7, respectively, in equation (2.29). C_{sf} was expressed as a function of average surface roughness, fluid/surface material combination and reduced pressure as follows:

$$C_{sf} = \mathrm{C}[(\mathrm{a} \ln R_a - \mathrm{b})P_r - \mathrm{c} \ln R_a + \mathrm{d}] \tag{2.29}$$

For R-123 and copper the following values were found: C = 1, a = 0.0077, b = 0.0258, c = 0.0036 and d = 0.0138.

2.11 Critical heat flux mechanisms

Tong and Tang (1997) explained the phenomenon of the critical heat flux that as follows: As the heat flux increases the bubble generation from the boiling surface increases. The bubbles eventually coalescence to form big bubble columns or jets. At this stage more increase in heat flux hinders the cold liquid from reaching the heating surface. This is the beginning of Departure of Nucleate Boiling (DNB). The heat flux corresponding to this point is the maximum heat flux possible and called critical heat flux (CHF). This situation is also called equipment ‘burn out’.

There are two basic phenomena for the explanation of boiling crisis (cited in Tong and Tang (1997)) (i) The Helmholtz instability phenomenon (ii) The Taylor instability phenomenon.

The Helmholtz instability is based on relative motion of two immiscible fluids, which are separated by an interface, as shown in Figure 2.23. According to this phenomenon, when two immiscible fluids are in relative motion there is a maximum value of the relative velocity that exists between them. Above that maximum value of the velocity, a small disturbance on the interface leads to high impact and results in flow distortion.

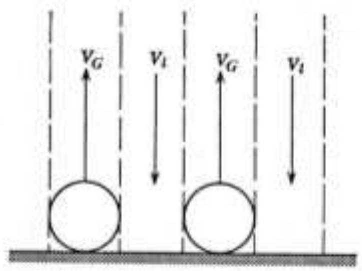

Figure 2.23 Vapour liquid interface Tong and Tang (1997)

The Taylor instability relates to vapour liquid interface on the horizontal surface, which is facing upward direction, see Figure 2.23. It postulates that the stability of interface of a wave which is produced between two fluids having different densities, as shown in Figure 2.24 , depends upon the balance of the surface tension energy and the summation of kinetic and potential energies.

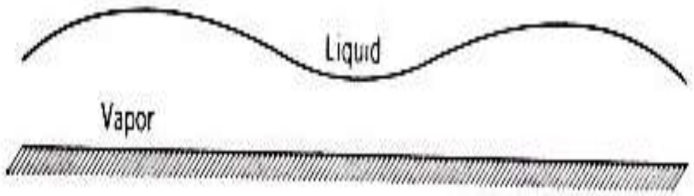

Figure 2.24 Vapour-liquid interface in horizontal direaction Tong and Tang (1997)

Furthermore, if the surface tension energy is greater than the sum of kinetic and potential energy, the fluid having less density can remain under the fluid of high density. This is the criterion of stable film on the boiling surface.

According to Haramura and Katto (1983) when the wave length is greater than the diameter of the heating surface, fresh liquid can’t reach the boiling surface and the situation leads to critical heat flux. The wavelength is called Taylor instability wavelength.

Moissis and Berenson (1963) explained the burn out on the basis of the Helmholtz instability phenomenon. They divided the process into two transition phases. During the first transition phase, they explained the conversion of single bubble growth from the heating surface into the vapour bubble columns. As shown in Figure 2.25 (a), the individual bubbles are separated by a significantly high distance so that there is no coalescence between them vertically. But as the heat flux increases, the distance between them becomes small. At a specific value of heat flux, vertical coalescence can be seen in the Figure 2.25 (c) and (d).

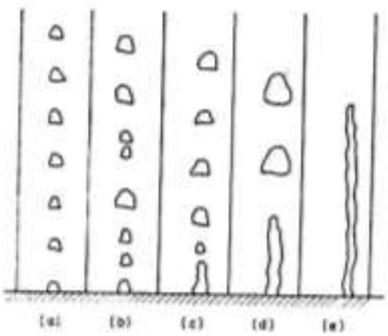

Figure 2.25 Vapour generation (a), (b) at low heat flux (c) moderate heat flux (d) and (e) at high heat flux Moissis and Berenson (1963)

This stage is termed as first transition stage. Furthermore, Moissis and Berenson (1963) also proposed the expression for predicting heat flux at the first transition stage as follows:

$$\left(\frac{Q}{A}\right)_{tr} = 0.11\rho_v h_{fg} \beta^{1/2} \left[\frac{g_0 g \sigma}{\rho_l - \rho_v}\right]^{1/4} \tag{2.30}$$

Moreover, they explained that the first transition was based on the assumption that individual bubbles interact with each other in the direction normal to the heating surface and heat flux at this stage is dependent on the conditions of boiling surface. In the second transition stage, due to further increment in the heat flux, the bubble columns interact in the direction parallel to the boiling surface. This situation leads to decrease in the vapour removal rate from the boiling surface and eventually results in equipment burnout. According to Moissis and Berenson (1963), the second transition stage is independent of surface conditions. They also proposed the mathematical expression to predict the value of critical heat flux as follows:

$$\left(\frac{Q}{A}\right)_{CHF} = 0.18\,\frac{\rho_v h_{fg}\left[\frac{\rho_l+\rho_v}{\rho_l\rho_v}\right]^{1/2}\left[g_o g\sigma(\rho_l-\rho_v)\right]^{1/4}}{1+2\left(\frac{\rho_v}{\rho_l}\right)^{1/2}+\left(\frac{\rho_v}{\rho_l}\right)} \tag{2.31}$$

Gaertner (1965) visually observed the boiling process using a high speed camera (3000 frames per second). He reported that near critical heat flux, the heating surface was covered with mushrooms of bubbles. He tried to explain this situation hypothetically and proposed that the stems of the vapour mushrooms become unstable hydrodynamically near the burn out situation. Due to this instability, the vapour mushrooms collapse leaving small vapor patches on the boiling surface. These vapour patches were also termed as local vapour film on the heating surface. These patches eliminate the active boiling sites on the heating surface, which results in decreasing the heat transfer rate. As surface temperature increases, the local vapour patches also increases on the boiling surface and leads to the maximum possible heat flux or equipment burn out.

Chung and No (2003) observed the mechanism of critical heat flux experimentally. They performed pool boiling tests using R-113 as a working fluid. They reported that a large fraction of boiling surface (more than 70 %) dried out at critical heat flux. They also reported that just before critical heat flux, a large vapour film covered the boiling surface. If the large vapour blanket collapse liquid rewetting takes place and due to high rate of heat flux the liquid film converts into vapour quickly, which coalescences and large vapour film formed again. Furthermore, the authors did not observe any vapour stem and microlayer dryout, which is contrary to the dryout model proposed by the same group in Ha and No (1997). It was further reported by Chung and No (2003) that the nucleate boiling occurred both at the edge of the large mushroom and also beneath it on a very few locations. After critical heat flux, the nucleate boiling takes place only at the edges of big vapour mushroom.

A majority of well known models describing the CHF were based on two different principles, i.e. (i) the instability of the vapour-liquid interface on the heating surface is responsible for boiling crisis (ii) the vapour cloud, at high heat flux, on the boiling surface hinders the cold liquid flow to the boiling surface. Haramura and Katto (1983) proposed a model to explain the burnout situation, which was based on a compromise of both principles, i.e. vapour – liquid instability and blockage of liquid inflow. They proposed that the interference region, on which the Helmholtz instability acts, remains during nucleate boiling and it serves as prodrome of CHF. Moreover, despite of the interference region the boiling surface is covered by vapour bubbles which hinder the cold liquid inflow from the bulk to the boiling surface.

Ha and No (1997) presented a dryout model (on a hypothetical basis) to elucidate the critical heat flux condition. They proposed that as the heat flux increases the number of bubbles on the heating surface increases. Moreover, the number of bubbles surrounding the growing bubbles (i.e. bubble before detachment from the boiling surface) increases. When the number of surrounding bubbles reaches a critical value, the supply of fresh liquid to the liquid microlayer which is under the growing bubble stops. The remaining liquid microlayer evaporates leaving an insulating dryspot on the boiling surface. As heat flux increase, the number of bubbles nucleation sites also increases. This situation leads to increase the bubbles, which results in an increasing the number of dryspots on the boiling surface. Due to the accumulation of a large number of dryspots, the heat transferring locations on the heating surface “die out”. This situation leads to boiling crisis. Furthermore, Theofanous et al. (2002) practically observed the dryspot on the boiling surface. They also introduced the concept of reversible and irreversible dryspots on the basis of observations obtained from IR images. At moderate heat flux, they observed that the reversible dryspot on the heating surface disappeared due to liquid rewetting after short span of time. As the heat flux increases, the life span of dryspot increases. They further reported that near the critical heat flux the liquid rewetting process stops, which results in irreversible dryspots. The emergence of a large number of irreversible dryspots leads to equipment burnout.

Zhao et al. (2002) presented a more detailed model for explaining the critical heat flux situation. They proposed model was based on microlayer on the boiling surface and behaviour of bubbles growing underneath the big vapour mushrooms under high heat flux. They explained that at high heat flux, bubble coalescence resulting into big bubble mushroom structures, which cover the boiling surface. Under these conditions, new bubbles grow under the vapour film. Furthermore, they divided the heating surface into three parts (i) dryout region (ii) microlayer region (microlayer is defined by the authors that thin liquid layer formed underneath the bubble during initial growth, i.e. upto the semispherical shape) (iii) Macrolayer region (Macrolayer is the liquid layer which forms underneath and between semispherical and the spherical shape) as shown in the Figure 2.26 (a) and (b).

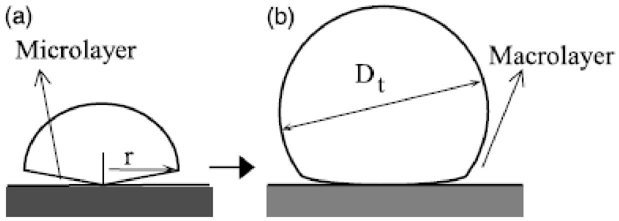

Figure 2.26 Explanation of (a) Microlayer region (b) Macrolayer region Zhao et al. (2002)

They further explained that in these regions initially the dryout area is negligible and most part of the evaporation takes place in the microlayer only a small portion of the macrolayer is involved in bubble growth. They argued that no rewetting of microlayer takes place during bubble growth. After the vapour departure, the microlayer is rewetted by cold liquid from the surroundings. As the heat flux increases the microlayer region decreases. In other words, as the microlayer becomes thinner the wall superheat increases. The thin microlayer results into dryout at high heat flux and an increase of the dryout region results into the critical heat flux.

Sefiane et al. (1998) proposed a mechanism for the CHF. They explained that vapour recoil effect was observed on the initiation of boiling. The vapour recoil is a non-uniform pressure, which acts in the downward direction, as shown in Figure 2.27, at the vapour liquid interface. The magnitude of pressure is strongest at the contact line. This effect contracts the vapour film and reduces the evaporation rate. Moreover, the effect of vapour recoil can change the meniscus of vapour liquid interface and contact angle increases which results in reducing the evaporation rate. According to Sefiane et al. (1998) the vapour recoil effect causes instability of the vapour liquid interface and small disturbances to the interface lead to equipment burnout. They further elaborated that the small change in the surface temperature increases the evaporation, which gives rise to the vapour recoil effect. This increase in vapour recoil effect can increase the contact angle and then the evaporation rate decreases. This situation leads to the CHF.

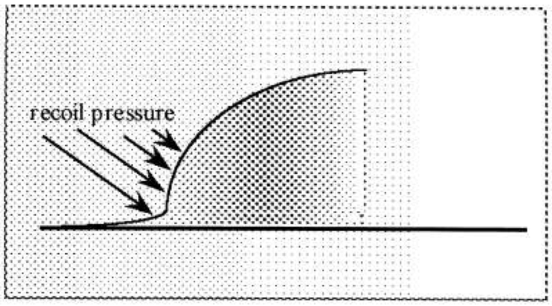

Figure 2.27 Vapour recoil mechanism Sefiane et al. (1998).

Katto and Yokoya (1968) proposed boiling crisis mechanism on the basis of the average life of vapour and liquid masses on the boiling surface. According to this mechanism, at peak heat flux, the life time of liquid film adjacent to the heating surface is equal to the bubble detachment period. They further elaborated that the rate of the depletion of liquid film from the boiling surface is directly proportional to heat flux. But the vapour detachment period is nearly independent of heat flux.

Lienhard and Hasan (1979) proposed the critical heat flux on the basis of mechanical energy. They termed the path of vapour as a wake, which is adjacent to boiling surface. It was also postulated that the vapour wake is isothermal and the dominant energy interactions are mechanical and isentropic. The authors proposed that at critical heat flux, the vapour escaping wake becomes unstable. Furthermore, if the net mechanical energy transfer to the system is positive and vapour escaping wake becomes unstable, this situation leads to boiling crisis.

2.12 Effect of surface roughness on CHF characteristics

As discussed earlier in section 2.7, Yu et al. (2006) performed pool boiling experiments on the microcavity surface made of silicon, while the working fluid was FC-72. They observed that critical heat flux on 33×33 mm, 25×25 mm and 16×16 mm array surfaces. It was reported that the CHF improved by a factor of 2.5 for 33×33 mm array surface as compared to plain surface. Similar observations were reported by Abuaf et al. (1985) performed pool boiling experiments on horizontal finned surface having fin dimensions as 0.16 cm fin width, 0.16 cm fin spacing and 0.32 cm fin height. They reported that the CHF value for finned surface was increased by a factor of 2.4 as compared to the smooth surface (no information of smooth surface was reported by the authors). This fact was hypothetically explained by Abuaf et al. (1985) on the basis of hydrodynamic theory. They argued that vapour liquid counter flow is closely spaced in the fin geometry as compared to a smooth surface. This decrease in the width makes the vapour liquid counter flow stable for larger value of heat flux, which results in increasing critical heat flux.

On the other hand, as discussed earlier in section 2.7, Berenson (1962) performed pool boiling experiments with different surface – fluid combinations. They reported that there was no effect of boiling surface conditions on the critical heat flux.

On the contrary, the influence of surface characteristics on the critical heat flux was examined by Ferjancic and Golobic (2002) in experiments with saturated boiling of water at atmospheric pressure on steel. Topographically different surfaces of steel – 1010 were investigated by treating the surface with sand paper of different grade numbers, i.e. 600, 400, 320, 150, 80 and 50 to obtain the average roughness R_a= 0.1, 0.2, 0.3, 0.6, 1.0 and 1.5 µm respectively. The results were presented in the form of the equation below:

$$q_{CHF} = a \ln R_a + b \tag{2.32}$$

where a and b are empirical constants dependent on the properties of the boiling liquid and heating surface. From this work it can be concluded that the q_{CHF} increases with increasing the surface roughness.

2.13 Summary

It can be concluded from the literature review that

- Surface modification is an effective technique for two phase heat transfer augmentation.
- The relationship between the microstructure of boiling surface and heat transfer coefficient is complex and unclear. Luke et al. (2000) and Luke (2009) tried to explain the two phase heat transfer on the basis of primary profile parameter, *Pa* (will be discussed in section 4.2). But the size of the cavities may alter with the alteration of surface modification method.
- The augmentation in the value of heat transfer from nucleate boiling to critical heat flux was well documented and attributed to the shape of surface cavity and the physical properties of boiling liquid (Lorenz et al. (1972) and Cooper (1984)).
- It was also reported that the boiling hysteresis was dependent on the shape of surface cavity and the surface tension of the boiling liquid.

- The researchers described the critical heat flux on the basis of two criterions: firstly vapour – liquid interface and secondly the formation of vapour cloud on the boiling surface (Moissis and Berenson (1963) and Gaertner (1965)). But there is consensus among the most of the researchers that the critical heat flux during pool boiling is independent of boiling surface conditions, i.e. on the hydrodynamic theory (Zuber (1958)). On the other hand, Ferjancic and Golobic (2002) proposed, on the basis experimental results, that the critical heat flux is directly proportional to surface roughness for a specific fluid.

Chapter 3 Pool Boiling with EHD

Application of high intensity electric field (abbreviated as EHD) is an important and effective active technique for enhancing two phase heat transfer especially in space applications (i.e. at zero gravity). Researchers have been analyzing EHD technique on heat transfer from last seven decades and their work was briefly reviewed by Allen and Karayiannis (1995). In this chapter, the basic theories and experimental work, which was presented in the literature, has been reviewed from the nucleate boiling regime to critical heat flux. Furthermore, alteration in the bubble dynamics due to the application of high intensity electric field has also been presented in section 3.6.

According to Germant (1934), there is a motion induced within the molecules of a fluid, when it is subjected to high intensity electric field. This motion can be divided into two categories.

1. Direct or electric displacement
2. Indirect or mechanical displacement

Direct or electric displacement

During direct or electrical displacement, the electric force is applied directly to the liquid. Depending on the nature of the liquid, the direct or electrical displacement can be subdivided into three groups

i. Dielectric displacement
ii. Displacement of the double layer
iii. Motion of space charges

Dielectric displacement

This displacement arises when neutral liquid is subjected to a high intensity electric field. Germant (1934) further elaborated that the molecules of the dielectric become polarized and move towards the region of high intensity electric field.

Double layer displacement

This kind of displacement takes place when the liquid, which is neutral overall but internally has positive and negative charges, is subjected to a high intensity electric field. The carriers of these charges are moved in the opposite direction. This motion is termed as double layer displacement.

Motion due to space charges

This displacement is due to excessive charges within the liquid, which then moves under the application of electric field.

Indirect or mechanical displacement

During indirect or mechanical displacement, the electric field is first converted into the mechanical motion and then applied to the molecules of the liquid.

3.1 Charge relaxation time

There are two possibilities whenever a fluid is subjected to a high intensity electric filed, i.e. electric storage or magnetic storage. According to Pohl (1978) during electrohydrodynamics abbreviated as EHD, electric storage is important. He explained the situation mathematically on the basis of electric the relaxation time 'τ_e' and magnetic diffusion time 'τ_m':

$$\tau_e = \frac{\varepsilon}{\sigma_{elec}} \tag{3.1}$$

where ε is electrical permittivity and σ_{elec} is electrical conductivity of the material.

And

$$\tau_m = \lambda_m \sigma_{elec} l^2 \tag{3.2}$$

where λ_m is the electrical permeability and *l* is characterized by a single important dimension.

If $\tau_m >> \tau_e$, the magnetic induction phenomenon dominates and the movement of charges due to application of electric field is negligible. On the other hand, if $\tau_e >> \tau_m$ electrohydrodynamics dominates and magnetic induction is negligible. In case of perfect dielectric, the electrical conductivity is zero and $\tau_m = 0$. Practically, there is no perfect dielectric but most of the refrigerants are poor conductors of electricity and so is R-123 (the refrigerant under observation during present studies). We assume that magnetic induction phenomenon is negligible, when R-123 is subjected to an applied electric field and only electrohydrodynamic phenomena dominate.

Moreover, Yabe et al. (1996) explained the significance of charge relaxation time and bubble detachment period within a two phase heat transfer system under the application of electric field. They noted that the charge relaxation time is the rate at which the charges are relax from the bulk liquid to the vapour liquid interface. This measure does not include the free charges. During the boiling process, they defined an insulator on the basis of charge relaxation time and bubble detachment period 'τ_c'. Furthermore, if $\tau_e/\tau_c < 1$ the fluid is considered as a conductor, while if $\tau_e/\tau_c > 1$ the heating liquid acts as an insulator. This fact was further elaborated by Zaghdoudi and Lallemand (2005) that if the boiling liquid is an insulator, i.e. $\tau_e >> \tau_c$, the electric field is distributed in both phases (liquid and vapour) during pool boiling. On the other hand, if $\tau_c >> \tau_e$, there was hardly an electric field distribution within the liquid and free charges appeared on the vapour – liquid interface. These free charges were then responsible for potential difference.

3.2 Polarization

Edminister (1993) explained the polarization process as shown in Figure 3.1. He proposed that the molecules of dielectric fluid arranged themselves in a way that positive and negative regions superimposed on each other. By the application of an electric field, the positively charged part of the molecules moves in the direction of the electric field, while the negatively charged part moves opposite to the direction of electric field, see Figure 3.1. The motion is termed as the dipole moment.

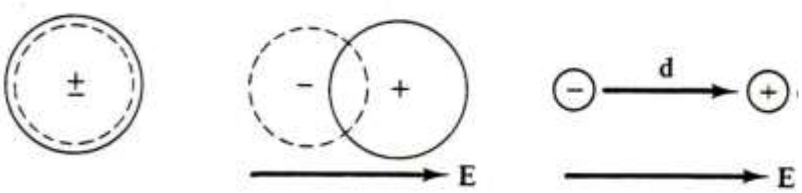

Figure 3.1 Dipole moment within the dielectric molecule Edminister (1993)

Hippel (1954) provided a mathematically analysis of the dipole moment due to the application of an electric field as follows:

$$M_e = Q_e d \tag{3.3}$$

$\pm Q_e$ are two opposite charges, which are separated by the distance ‘d’, see Figure 3.1. The electrical dipole moment is represented by the vector ‘M_e’ having direction from the negative to the positive charge. While the force is given by

$$F = M_e . \nabla E \tag{3.4}$$

and the torque is

$$T_e = M_e \times \nabla E \tag{3.5}$$

Hippel (1954) further explained the polarization on macroscopic basis. He proposed that initially the dielectric particles are neutral. After the application of the electric field positive and negative portions of dielectric particles align themselves according to external electric field. This alignment results in bound charges appearing on the surface of dielectric, as shown in Figure 3.2. On the other hand the bulk of the dielectric is neutral.

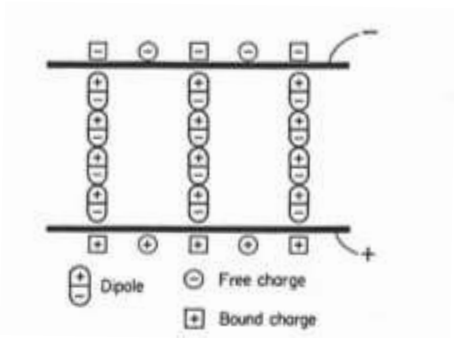

Figure 3.2 Schematic diagram of the alignment of dielectric molecule under applied electric field Hippel (1954).

Furthermore, the effect of uniform and non – uniform electric field on the polarization was explained by Pohl (1978), as shown in Figure 3.3. He explained that during the application of a uniform electric field the neutral particles of the dielectric become polarized. This action may result in a torque but no net force is induced on the dielectric particles. It means that the body does not move towards any of the electrodes, see in Figure 3.3 (a). On the other hand, with the application of a non – uniform electric field, the neutral particles of dielectric become polarized and experience a translational force due to the non – uniformity of external electric field. The particle moves towards the region of high electric field intensity regardless of the charge of the electrode, see in Figure 3.3 (b) and Figure 3.3 (c).

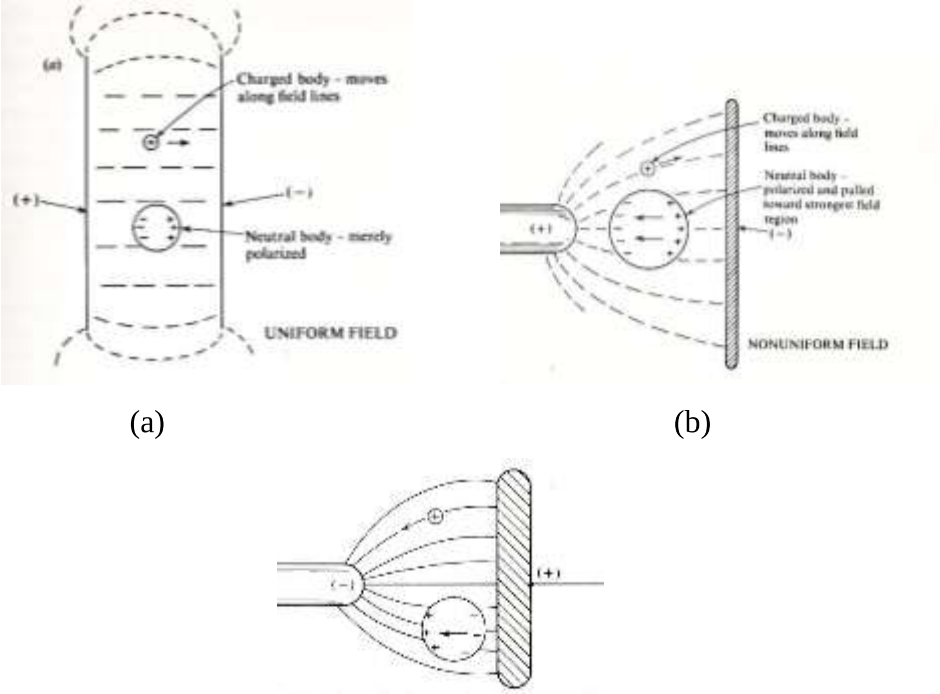

(a) (b)

(c)

Figure 3.3 Action of EHD (a) on dielectric molecule within uniform electric field (b) on dielectric molecule within non – uniform electric field (c) on dielectric due to different electrode polarity Pohl (1978).

3.3 Electric force

The body force due the application of electric field is given by Pohl (1978) as follows:

$$F_e = \rho_e \bar{E} - \frac{1}{2} E^2 \nabla \varepsilon + \frac{1}{2} \nabla \left[E^2 \rho \left(\frac{\partial \varepsilon}{\partial \rho} \right)_T \right] \qquad (3.6)$$

There is a consensus between the researchers about the first term in right hand side of equation (3.6). According to Pohl (1978), Mardarskii and Bologa (2009), Jones (1978) and Yabe et al. (1985) the first term on the right hand side of equation (3.6) represents the force acting on a charged particle of fluid, i.e. the Coulomb force and termed as electrophoretic force. Pohl (1978) discussed further the electrophoretic force, i.e. this force represents the motion of charged particles due to the application of an external electric field and the direction of motion depends on the direction of applied electric field.

The second term indicates the force due to the change of electric permittivity within the dielectric fluid, while the third term represents the force arises due to inhomogeneity of electic field. There is a contradiction between the researchers, i.e. Yabe et al. (1985) and Jones (1978) explained that the second term is due to the dielectrophoretic force and third term is due electrostriction force. On the other hand, Pohl (1978) and Mardarskii and Bologa (2009) left the second as unmanned and believed that the third term is the combination of both dielectrophoretic and electrostriction forces, which appear due to the non-uniform electric field and spatial changes of electric permittivity.

Furthermore, Pascual et al. (2000) explained that first term on the right hand side of equation (3.6) was due to the Coulomb force. The second was termed as the electroconvection force, which was induced due to the gradient in electric permittivity within the liquid resulting from the temperature change. Third term on the right hand side was named as the dielectrophoretic force and it was dependent on the non – uniformity of electric field. According to Pascual et al. (2000) this induced force was due to the translational motion of dielectric molecules caused by polarization. Moreover, due to square of the electric field, the dielectrophoretic force is independent of electric polarity and also independent of temperature gradient Pascual et al. (2000).

The dielectrophoretic phenomenon was explained by Pohl (1978), i.e. when a strong electric field is applied to a finite volume of dielectric fluid, the molecules of the fluid initially become polarized and then experience a force if the applied electric field is non-uniform (under the action of uniform electric field the force experienced by the dielectric molecule is negligible). This concept is true only if the dielectric fluid is homogeneous in nature. On the other hand, in the case of heat transfer applications, the value of electric permittivity changes through the fluid (due to temperature gradients), which may then give rise to an electric force even if the field is uniform. Pohl (1978) also defined the electrostriction force that arises due to the distortion response of dielectric molecule under high intensity electric field. This distortion response is independent of nature of the electric field, i.e. homogenous or non – homogenous.

Pohl (1978) modified equation (3.6) for a specific situation, i.e. when a dielectric sphere is introduced into a fluid of different permittivity and exposed to a non-uniform electric field, a force is generated acting on the sphere given by the expression below, where the volume refers to the sphere:

$$f_e = \frac{3}{2}(\text{volume})\varepsilon_l\left(\frac{\varepsilon_v-\varepsilon_l}{\varepsilon_v+\varepsilon_l}\right)\nabla E^2 \tag{3.7}$$

It can be deduced from the equation (3.7) that since the electric permittivity of vapour is always less than the electric permittivity of the liquid, the equation results in a negative value, which shows that the direction of force acting on the bubble is opposite to the direction of applied electric field. It means that the vapour is attracted towards the region of low electric field intensity. So we can also conclude that under the influence of the electric field the material with higher permittivity, is attracted towards the region of higher electric field strength.

3.4 Effect of EHD on boiling hysteresis

Wang et al. (2009) performed pool boiling experiments using a highly wetting liquid, i.e. liquid nitrogen, as discussed in earlier in section 2.7. They reported large hysteresis in inception of nucleate boiling due to the high wetting properties of the boiling liquid, i.e. onset of boiling was observed at a large value of wall superheat as discussed in section 2.8. Due to application of uniform electric field, the boiling hysteresis become less, i.e. the onset of nucleate boiling occurs at lower value of wall superheat. It was further reported that the onset of nucleate boiling occurs at 16 K wall superheat when there was no electric field applied. On the other hand, with the application of 40 kV, electric potential, the onset of nucleate boiling was reported at 5 K wall superheat Wang et al. (2009).

Cooper (1990) also reported the elimination of hysteresis during increasing heat flux with the application of electric field. He performed pool boiling tests on R-114 using a low – fin evaporator. Similar observation were reported by Zaghdoudi and Lallemand (2005) when they performed pool boiling experiments using R-113, R-123 and n – pentane. They reported that with the application of uniform electric field of 2.5 MV/m the hysteresis was eliminated when they performed pool boiling tests using n-pentane, see Figure 3.4.

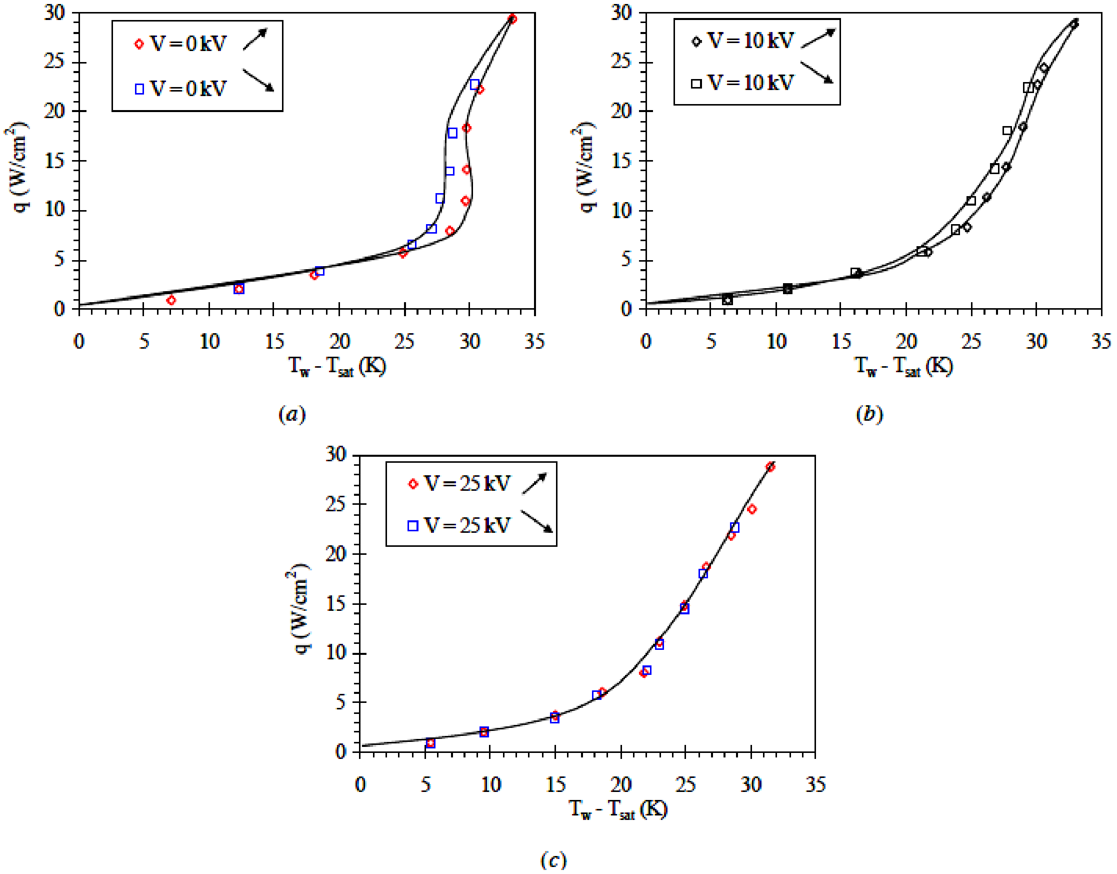

Figure 3.4 Hysteresis of n – pentane at (a) 0 kV/m (b) 1 MV/m (c) 2.5 MV/m Zaghdoudi and Lallemand (2005).

Similar observation were reported by Wang et al. (2009), when they tested pool boiling experiments of liquid nitrogen under high intensity uniform electric conditions. They observed that as the electric potential increases from 0 to 40 kV, there was a successive decrease in hysteresis, see Figure 3.5.

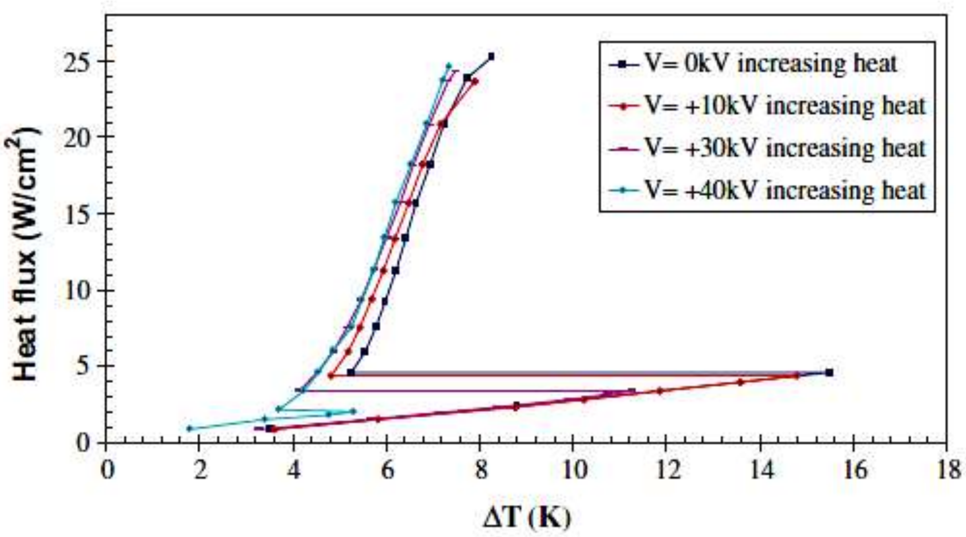

Figure 3.5 Hysteresis under high intensity uniform electric potential Wang et al. (2009).

Earlier, Basu (1973) performed pool boiling experiments to observe the effect of electric field on onset of nucleate boiling, with carbon tetrachloride as the working fluid. He carried out the experiments using both a.c. and d.c. electric field. It was observed from the results that boiling hysteresis was eliminated due to application of the electric field. He proposed that this elimination was due to the agitation within the thermal boundary layer, which was induced due the application of electric field.

Moreover, Zaghdoudi and Lallemand (2005) mathematically explained the elimination of boiling hysteresis due to the application of electric field as follows:

$$P_v - P_l = \frac{2}{r}\left[\sigma + \frac{\varepsilon_0\varepsilon_l(\varepsilon_l-\varepsilon_v)E^2}{4(2\varepsilon_l+\varepsilon_v)}\right] \tag{3.8}$$

Equation (3.8) shows that the pressure difference within the cavity can be characterized by the surface tension of boiling liquid. Furthermore, the pressure gradient is proportional to the square of the electric field. It means that the electric field modified the surface tension of the boiling fluid, which leads to activation of nucleation site at lower heat flux. Moreover, Cooper (1990) reported that this activation of nucleation sites was due to the application of electric field was similar to thermal activation of nucleation sites , i.e. activation at high heat flux. It was further reported that the sites remain active even if the electric field was removed, which is identical to the thermal activation of nucleation sites.

3.5 Heat Transfer enhancement due to EHD

The mechanism of pool boiling enhancement under the application of high intensity electric field was discussed in details by Allen and Karayiannis (1995). They proposed that the augmentation in the value of the heat transfer coefficient was due to three factors, which can act either in combination or individually.

i. Action of EHD on vapour – liquid interface
ii. Action of EHD on vapour
iii. Change in the contact angle and surface tension

The action of EHD on vapour – liquid interface and vapour bubble can destabilize the thermal boundary layer, which can revert the film boiling into the nucleate boiling. Moreover, with the application of high intensity electric field, the change in the contact angle and surface tension can result in elimination of hysteresis or initiation of nucleate boiling at low wall superheat as discussed earlier in section 3.5.

3.5.1 EHD on boiling surfaces

A report on the enhancement of pool boiling heat transfer under the influence of high intensity electric field was presented by Yokoyama et al. (1986). They performed an experiment under EHD pool boiling conditions using R-11 as a working fluid, where the test surface was a smooth copper plate. At very low heat flux, about 2.8 kW/m^2, there was no boiling from the heating surface but tiny bubbles were observed from the edges of the surface. As the heat flux increased, but still at low values and in the absence of an electric field, they noted that the bubble production from the heating surface was uniform. When the electric field was applied the bubble generation was suppressed. This bubble suppression effect increased as the applied voltage was increased up to 26 kV. However, at high heat flux values the bubble generation became more vigorous upon the application of high intensity electric field.

Recently, Wang et al. (2009) performed pool boiling experiments to observe the effect of uniform electric field on highly wetting liquid, i.e. liquid nitrogen. The uniform electric field was provided using a brass mesh electrode (dimensions: 2.36 mm mesh width, 1 mm wire diameter and 0.47 void fraction) which was mounted 10 mm above the boiling surface. The boiling surface was grounded and served as the second electrode. The copper heating surface was carefully polished and experiments were performed at saturation pressure of 1 bar (no information about the surface characterization was provided by the authors).

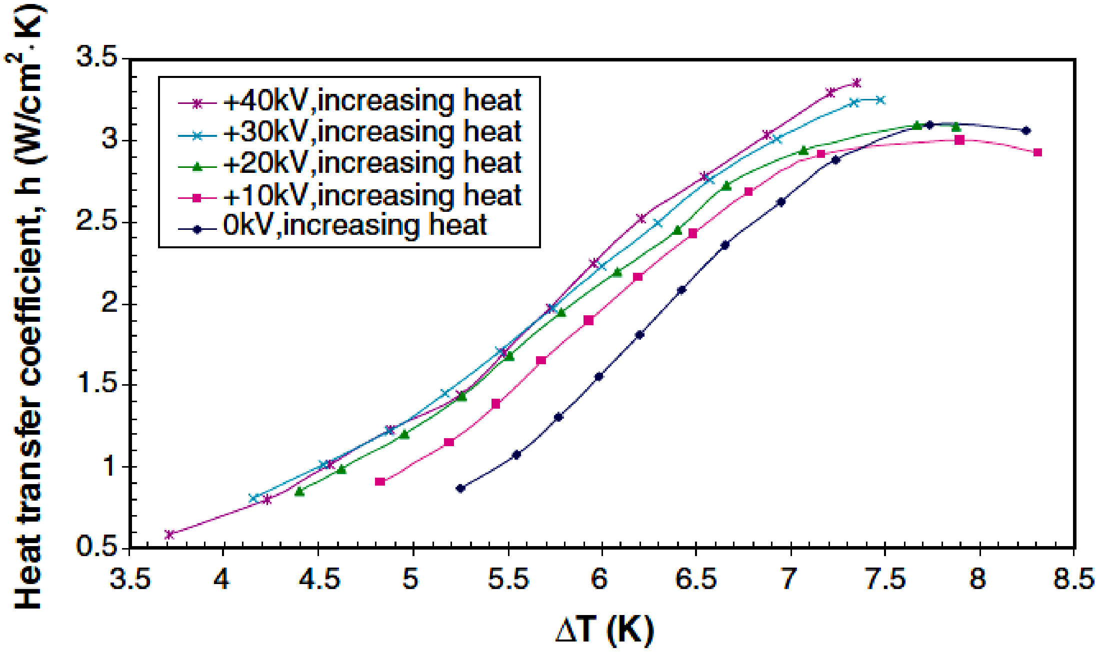

Figure 3.6 Effect of uniform electric field on pool boiling of liquid nitrogenWang et al. (2009).

It was reported that with the application of 4000 kV/m, electric field, the heat transfer coefficient was increased by a factor of 1.5 at the specific value of wall superheat when compared to the no field condition. It can be further deduced from the data given by Wang et al. (2009) that the heat transfer augmentation was significant with the application of electric field up to 2000 kV/m. But any further increase in the value of the electric field resulted only in marginal heat transfer augmentation, see Figure 3.6.

Snyder et al. (1996) mathematically calculated the existence of the dielectric force. The calculation geometry consisted of two electrodes, i.e. a ball electrode 1.27 mm in diameter and a rod electrode 0.025 mm in diameter. They reported that the value of dielectrophoretic force increased rapidly in the vicinity of rod electrode, which was reported that 90,000 times greater than buoyancy force. These analyses showed that both the electric field and electric field gradient become intense near the rod electrode.

Earlier, Rutkowski (1977) observed the effect of AC electric field on pool boiling of liquid nitrogen. Boiling was carried out on 0.1 mm in diameter and 70 mm long horizontal platinum wire. The electric field was provided using a wire electrode 3 mm in diameter and 75 mm long, which was placed 5 mm away from the heating wire, which was earthed. It was reported that with the application of E = 470 kV/m, the heat transfer increased by a factor of 5 as compared to no field condition at the wall superheat of 4 K. It was further reported that the application of electric field can cause an increase in convection around the heating wire, which resulted in delay of the onset of nucleate boiling. At higher heat flux, it was also reported that the application of the electric field reduced the nucleation sites and also the bubble diameter.

Kawahira et al. (1990) investigated the electrohydrodynamic effects on pool boiling of R-11. Two types of test sections were employed to carry out boiling experiments, i.e. a horizontal flat plate and a single tube. The horizontal flat plate test section consisted of a rectangular copper plate 300 mm long, 30 mm wide and 10 mm in depth. Several steel wires were mounted 3 mm above the horizontal copper plate and 7 mm apart from each other, which served as positive electrodes to provide high intensity electric field. The heating surface was grounded which acted as a second electrode. In the case of single tube experiments, a smooth copper tube having 22.4 mm outer diameter was used while the electrode system was the same as mentioned for the flat plate system. It was reported that with the application of 20 kV electric potential the heat transfer coefficient increased by the factor of 1.88 and 1.78 as compared to no field conditions, for flat plate and tube respectively.

Oh and Kwak (2000) performed pool boiling tests to observe the effect of non – uniform electric field using R-11 and R-113 as working fluids. At 10 kV electric potential, the heat transfer enhancement was reported as 130 % and 180 % for R-11 and R-113 respectively, while the wall superheat was 10 K. Chen et al. (2007 b) investigated the effect of non – uniform electric field on nucleate boiling of R-11. It was reported that with the increase in electric potential the augmentation in the value of heat transfer coefficient was nearly exponential, i.e. at 63.4 ºC the augmentation in heat transfer coefficient was 33 % with the application of 14 kV.

Earlier, Hristov et al. (2009) examined the effect of both uniform and non – uniform electric fields on saturated pool boiling of R-123 at 1 bar pressure. The uniform electric field was generated by using a 77 × 77 mm rectangular mesh electrode with a 2.8 mm square aperture size. The non-uniform electric field was generated with a rectangular rod electrode, with the same overall dimensions and open area, constructed with the parallel rods of diameter 1.56 mm. The distance between the electrode and the heating surface was kept at 5 mm. The boiling surface was polished with emery paper P 1200. Enhancement factors for the heat transfer coefficient approached 1.5 and 1.8 for the mesh and rod electrodes respectively, at a heat flux of 68 kW/m^2 and an applied voltage of 20 kV, see Figure 3.7. EHD enhancement during pool boiling of R-113 on a 0.37 mm diameter platinum wire was examined by Kweon and Kim (2000). The electric field was generated using a copper plate electrode

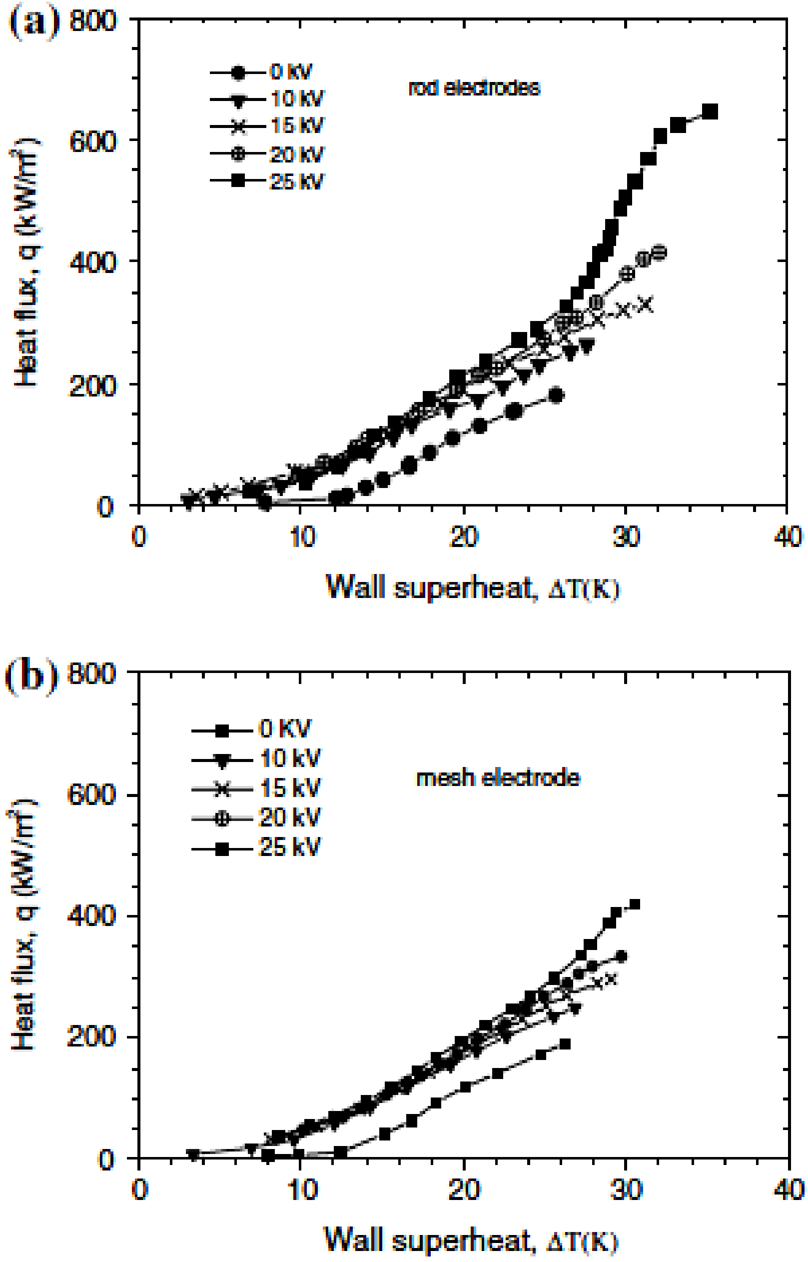

Figure 3.7 Pool boiling of R-123 under (a) uniform electric field (b) non – uniform electric field Hristov et al. (2009).

located 16 mm above the wire. EHD enhancement during pool boiling of R-113 on a 0.37 mm diameter platinum wire was examined by Kweon and Kim (2000). The electric field was generated using a copper plate electrode located 16 mm above the wire. At an applied voltage of 15 kV, the heat transfer coefficient increased by 215

%, 127 %, 81 %, 54 % and 32 % at heat fluxes of 29 kW/m^2, 69 kW/m^2, 115 kW/m^2, 189 kW/m^2 and 265 kW/m^2 respectively.

3.5.2 EHD effect on finned surfaces

Cooper (1990) performed pool boiling experiments on an enhanced boiling surface under the effect of electric field. The boiling surface was lo – fin brass tube having dimensions 0.5 mm in fin height, 7.6 mm and 1136 fin per meter, see Figure 3.8.

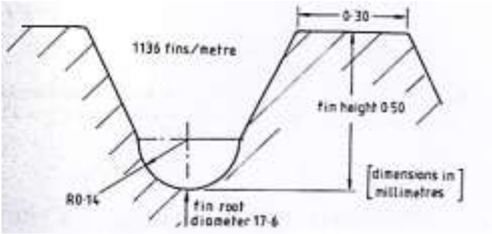

Figure 3.8 Cross section of lo-fin tube Cooper (1990)

Up to 30 kV electric potential was provided using cylindrical copper mesh electrode having 38 mm in diameter. It was reported that with the application of 10 kV electric potential, the heat transfer increased by a factor of 10. It was further reported that there was little effect of electrode polarity on the heat transfer augmentation. Moreover, Cooper (1990) explained the augmentation in the heat transfer on the basis of visual observations. He proposed that the application of the electric field altered the bubble dynamics. It was also reported that under that application of the electric field, the bubbles were trapped between the fins as shown in Figure 3.9. In other words, due to the application of dielectrophoretic forces the bubbles were pushed against the heating surface, i.e. trapped in the lo – fins. The bubble entrapment causes an increase in mixing and turbulence, which lead to heat transfer augmentation. According to Cooper (1990) the heat transfer augmentation due to electric field was analogous to the enhancement due to enhanced surfaces like GEWA surfaces, which can trap the vapours more effectively. He further reported that the application of the electric field, resulted in increasing in bubble diameter.

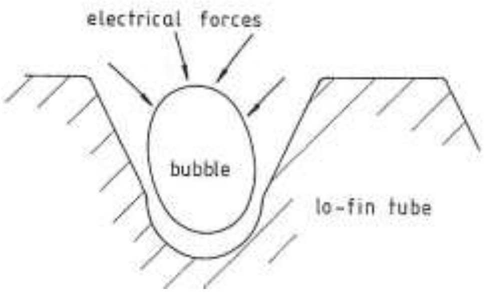

Figure 3.9 Bubble within the lo – fin tube under high intensity electric field Cooper (1990).

Moreover, Cooper (1990) proposed a mathematical relation to predict the heat transfer enhancement within the nucleate boiling regime. This was given as the function of modified Reynolds number and electrical number as follow:

$$\frac{h_E}{h_{zero}} = aNe^{\left(\frac{n}{2}\right)}(Re_o)^b \tag{3.9}$$

$$Ne = \left[1 + \left(\frac{1.5\varepsilon_l(\varepsilon_v - \varepsilon_l)}{(\varepsilon_v + 2\varepsilon_l)g(\rho_l - \rho_v)}\right)\nabla E^2\right]^{-0.5} \tag{3.10}$$

$$Re_o = \frac{q}{h_{fg}\mu_l}\sqrt{\frac{\sigma_l}{g(\rho_l - \rho_v)}} \tag{3.11}$$

where a = 0.3, b = - 0.16 and n = 0.33.

Yan et al. (1996) performed pool boiling experiments to observe the effect of high intensity uniform electric field on enhanced surface. Boiling was carried out in a single tube experimental rig. Thermoexcel – HE and Gewa – T tubes were used as test tubes, while a uniform electric field was provided using a cylindrical copper mesh having 0.038 m in diameter placed coaxially with the test tube. R-114 was the working fluid, while boiling was carried out of 21.5 ^{o}C saturation temperature. It was reported that the value of heat transfer coefficient augmented by a factor of 3 at 7 kW/m^2 for Thermoexcel – HE tube when 30 kV electric potential was applied. On the other hand, in the case of Gewa – T tube, the heat transfer coefficient was increased by the factor of 1.8 at 30 kV electric potential while the heat flux was 6 kW/m^2.

3.5.3 EHD effect on fluid properties

The effect of fluid properties under the influence of EHD was examined by Zaghdoudi and Lallemand (2005). They performed pool boiling experiments under saturated atmospheric conditions using R-123, R-113 and n-pentane on a copper surface polished with emery paper N 600. The electric field was provided by using a 2 mm mesh as one electrode while grounding the heating surface, which served as the second electrode. The electric potential was varied from 0-25 kV. They observed that the heat transfer coefficient increased by 160%, 170% and 600% for n- pentane, R113 and R-123 respectively. The values of charge relaxation time of n-pentane, R-113 and R-123 are 3.40×10^{-3} s, 2.76×10^{-3} s and 0.9×10^{-3} s respectively. The different in the enhancement may be due to the difference in the charge relaxation time. . The rise in the heat transfer coefficient at low heat flux was explained by Zaghdoudi and Lallemand (2005) as follows: at low heat flux, natural convection is responsible for heat transfer. A thermal boundary layer forms over the heating surface while the bulk fluid is under saturation temperature at a specific pressure. When a high intensity electric field is applied, dielectrophoretic and electrostrictive forces appear within the thermal boundary layer. This is due to the thermal gradient within the boundary layer, i.e. electric conductivity and permittivity vary and this produces dielectrophoretic and electrostrictive forces. Note that these forces are negligible within the bulk fluid due to the uniform temperature. According to Zaghdoudi and Lallemand (2005) this difference in the forces gives rise to electroconvective movement (i.e. the motion induced in the boiling liquid due to application of electric field) and the thickness of the thermal boundary decreases the wall temperature also decreases, see Figure 3.10. Of course one could argue that this drop in the wall temperature (wall superheat) results in the suppression of boiling while at the same time it provides improved heat transfer rates.

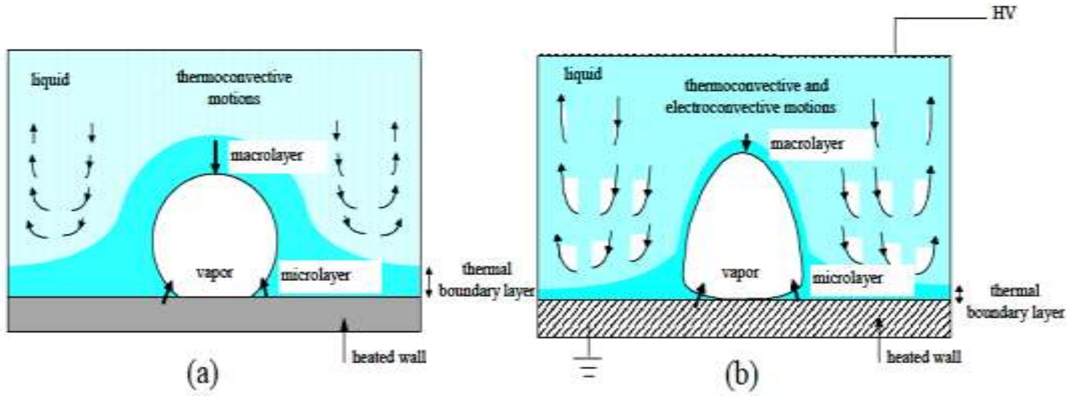

Figure 3.10 Nucleate boiling (a) without EHD (b) with EHD Zaghdoudi and Lallemand (2005).

Earlier, Karayiannis (1998) reported tests with R-11 and R-123 in a (five-tube) shell and tube heat exchanger. The high intensity electric potential was provided by using fourteen mild steel rods and was varied from 0-25 kV. He noticed that, in case of R-123, augmentation using EHD was significant especially at low heat flux values and was about 9.3 at 5 kW/m^2, see Figure 3.11.

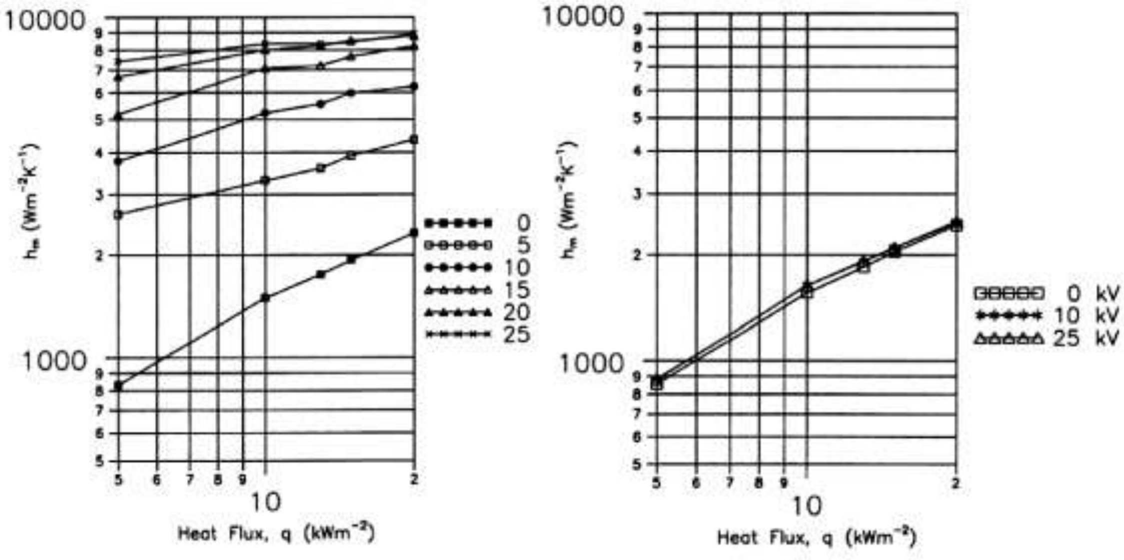

(a) (b)

Figure 3.11 Effect of EHD for (a) R-123 (b) R-11 Karayiannis (1998)

In case of R-11, the augmentation was marginal which indicates that EHD is strongly dependent upon the properties of the fluid; the charge relaxation time of R-123 and R-11 is estimated to be 0.9×10^{-3} s and 1.3s respectively (reported by Hristov et al. (2009)).

Furthermore, Ohadi and Paper (1992) investigated the EHD effect on pool boiling of R-123 and R-11 with oil concentration (0, 2%, and 5% by weight) on the shell side of a shell and tube heat exchanger. It was observed that R-123 exhibited a high EHD augmentation as compared to R-113 in pure form. The authors stated that this was due to the difference in permittivity of the two fluids, which of course relates to differences in the charge relaxation time. The maximum enhancement was 450% and 170% for R-123 and R-11 respectively. It was also noticed that with the oil addition the enhancement factor decreases. Contradicting the above three studies, which noted significant enhancement with R-123 (Zaghdoudi and Lallemand (2005), Karayiannis (1998) and Ohadi and Paper (1992)) and smaller or marginal enhancement with R-11, Yokoyama et al. (1986) noticed that the heat transfer augmentation at low heat flux with R11 was 3 to 7 times under the influence of EHD at an electric potential of 26 kV on a smooth copper heating surface. However, they did not compare directly (experimentally) with other fluids. It can be concluded from the above review that fluid properties play a significant role in the heat transfer augmentation when high intensity electric field is employed. It can be further stated that it is difficult to measure and control the effect of accidental contamination of water, dissolved gases and the decomposition of the fluid, which results in poor reproducibility and repeatability of experimental data between different laboratories.

Table 3.1 Enhancement due to the application of electric field.

Sr No.	Fluid	Electric field/Electric potential	h_E/h_o (%)	Reference
1	Liquid nitrogen	4000 kV/m	150	Wang et al. (2009)
2	R-123	25 kV	600	Zaghdoudi and Lallemand (2005)
	R-11		170	
	n-pentane		160	
3	R-123	25 kV	930 at 5 kW/m^2	Karayiannis (1998)
4	Liquid nitrogen	470 kV/m	500	Rutkowski (1977)
5	Perfluoromethylcyclohexane	20 kV	250	Schnurmann and Lardge (1973)
6	R-123	20 kV	700	Ogata et al. (1992)

7	R-113	10 kV	180	Oh and Kwak (2000)
	R-11		130	
8	R-123	20kV	150 / mesh electrode	Hristov et al. (2009)
			180 / rod electrode	
9	R-114	15 kV	215	Kweon and Kim (2000)
10	R-11	26 kV	700 (max)	Ohadi and Paper (1992)
12	R-114	30 kV	300 (Thermoexcel HE tube)	Yan et al. (1996)
		30 kV	180 (GEWA – T)	

3.5.4 EHD enhancement mechanism

The effect of electric field was experimentally observed by Babaoi et al. (1968). Boiling was carried out using 0.05 – 0.5 mm in diameter stretched platinum wire, which was 60 mm long. High intensity electric field was provided using a 6 mm diameter rod electrode. After careful examination of the videos, it was reported by Babaoi et al. (1968) that with the application of the electric field at low heat flux, the bubble generating centers diminished. They postulated that the electric field induced an additional force, which resulted in effective mixing within the dielectric fluid near the boiling wire. This electric convection was responsible for diminishing the bubble generating centers on the boiling surface even at higher heat flux. It was also reported that with the application of electric field the bubble detachment diameter decreases. They further explained this situation theoretically that in the absence of electric field bubbles grow in the heating wire and coalescence to make big bubbles, which resulted in large detachment diameters. On the other hand, due to application of electric field the bubble generating nuclei act individually. In other words, the electric force hinders the bubble coalescence which leads to smaller bubble detachment diameter.

Madadnia and Koosha (2003) performed pool boiling experiments to observe the effect of electrohydrodynamics on bubble dynamics within the nucleate boiling region. Boiling was carried out on an electrically heated Cr80Ni20 wire 1 mm in diameter and 85 mm in length. High intensity electric field was provided using 1.6 mm in diameter and 85 mm long copper rod, which was mounted 5 mm above the heating wire, which was earthed. Similar to the observations of Babaoi et al. (1968), it was reported by Madadnia and Koosha (2003) that at low heat flux, the application of electric field resulted in the elimination of nucleation centers. Moreover, at high heat flux it was described that the bubble diameter slightly increased when high intensity electric field was applied. They explained the first situation, i.e. at low heat flux electroconvection (motion induced within the fluid due to application of electric field) was responsible for the elimination of bubbles. They explained the second situation, at high heat flux, on the basis of coulomb and polarization forces. They reported that bubbles had negative polarity due to the attachment to heating wire, which was connected with the negative polarity. The positive electrode exerted a pull on the bubble but due to dielectric medium the Coulomb force is very weak. On the other hand, polarization forces (dielectrophoretic force) pushed the bubble against the heating surface. Furthermore, Coulomb force within a dielectric is weaker than the polarization force and net force pushed the bubbles against the heating surface and this leads to the slightly increase in the bubble diameter.

Schnurmann and Lardge (1973) performed pool boiling tests to observe the effect of non – uniform electric field on a dielectric liquid, i.e. perfluoromethylcyclohexane. Boiling was carried out using 0.0127 cm in diameter and 26 cm in length platinum wire, which was electrically heated. The non – uniform electric field was provided by placing a rectangular plate electrode (25.4 cm × 5.08 cm) at 1.27 cm apart from the heating wire. The platinum heating wire was earthed, which served as the second electrode. The electric potential was varied from 0 to 25 kV. It was reported that due to application of 20 kV electric potential, the value of heat flux increased by a factor of 2.5. Furthermore, it was reported by Schnurmann and Lardge (1973) that the size of the bubbles reduced due to application of non – uniform electric field. They further elaborated that the electric force help to detach the bubble form the heating surface before the force remove them during no field conditions. They also postulated that the increase in the value of heat transfer due to application of electric field was a result of the existence of region of different electric susceptibility (defined as the degree of polarization within the dielectric fluid under the action of applied electric field). They further argued that due to existence of these regions, the dielectrophoretic force was induced. The effect of dielectric force superimposed on the temperature gradient. They further discussed that the temperature gradient that there was a thin thermal boundary layer formed on the heating surface. The value of the temperature is greater within the thermal boundary layer as compared to bulk of the liquid. So, electric susceptibility is more within the bulk of liquid rather than the thermal boundary layer.

The gradient in the electric and temperature fields superimpose with each other and induce a flow of cold liquid towards the boiling surface. According to Schnurmann and Lardge (1973), this process was responsible for the heat transfer augmentation.

Ogata et al. (1992) explained the mechanism of boiling enhancement due to the application of electric field. They argued that the dielectrophoretic force pressed the boiling bubble against the heating surface. They further explained that the electric field strength was less within the thermal boundary layer, which is formed around the boiling surface, as compared to bulk of the liquid. The electric field gradient pushes the bubbles against the heat transfer surface. Moreover, they performed pool boiling tests using R-123 as the working fluid. The electric potential was provided up to 20 kV. It was reported that heat transfer coefficient increased by a factor of 7 as compared to the no field conditions.

Similar to Schnurmann and Lardge (1973), Pascual et al. (2000) commented on the heat transfer augmentation process. They proposed that the additional force induced by the application of the electric field supported the force, which resulted in early departure of the bubble from the boiling surface. Moreover, at constant heat flux, the augmentation in the value of the heat transfer coefficient is due to the decrease in wall superheat, i.e. the temperature difference between the heating surface and the bulk of the liquid. The reduction of wall superheat was due to the increase in the convection, i.e. the thermal convection superimposed on electric convection. This effect leads to augmentation in the value of heat transfer coefficient at constant heat flux. On the basis of regression analysis Pascual et al. (2000) proposed an empirical correlation to predict the augmentation in the value of heat transfer coefficient within the natural convection region no boiling due to the application of electric field.

$$\Delta Nu = 0.0895 Ra_{El}^{0.365} \tag{3.12}$$

$$Ra_{El} = El \times Pr \tag{3.13}$$

$$El = \frac{\rho \frac{d\varepsilon}{dT} d_s^2 \Delta T \varepsilon_0 E^2}{\mu^2} \tag{3.14}$$

The above expression is applicable for $4\times10^3 \leq Ra_{El} \leq 8\times10^8$.

Pascual et al. (2001) later commented on the effect of EHD during nucleate boiling. They explained that the total heat flux was a summation of the latent heat transfer, natural convection heat transfer and forced convection heat transfer. As shown in Figure 3.12 (a), at low heat flux, i.e. 8 W/cm^2 all three modes of heat transfer contribute towards the total heat flux. As the power to the heater increases, the fraction of latent heat transfer and forced convection heat transfer increases while the fraction of natural heat transfer diminishes. It is believed that further increase in heater power results in boosting up latent heat transfer. At critical heat flux, forced convection heat transfer diminished completely.

On the other hand, with the application of high intensity electric field, electroconvection superimposed with the thermal convection (it means that the motion induced by the application of electric field adds with the motion induced due to the temperature difference, see Figure 3.10). This effect results in delaying the onset of nucleate boiling and natural convection is the only mode of heat transfer up to 10 W/cm^2 as shown in Figure 3.12 (b). Furthermore, increasing the heater power resulted in squeezing the natural convection contribution towards the total heat flux. In other words, the contribution of force convection heat transfer and latent heat transfer increases in the total heat transfer (total heat transfer was defined by Pascual et al. (2001) as the summation of natural convection heat transfer, latent heat transfer and forced convection heat transfer). It can be deduced from this discussion that according to Pascual et al. (2001) high intensity electric field increases the natural convection which remain active for longer period of time resulting in augmentation in the value of the heat transfer coefficient.

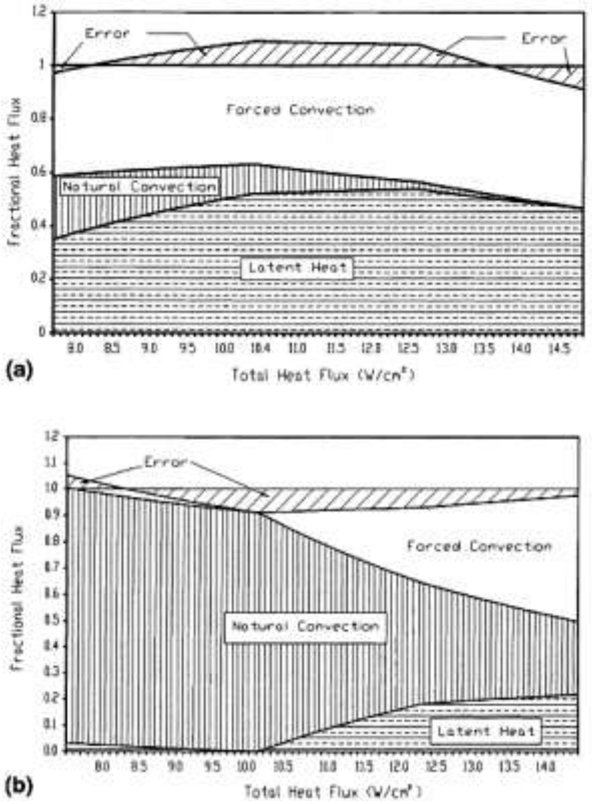

Figure 3.12 Contribution of different modes of heat transfer in the total heat flux during pool boiling (a) no EHD (b) with EHD Pascual et al. (2001).

Bonjour et al. (1962) performed boiling tests on ethylene to observe the effect of EHD. They reported that heat transfer enhanced by a factor of 4 to 10 (depending on the magnitude of electric field) with the application of the high electric field. They reported that at q = 2 Watt / cm^2 , the application of electric field resulted in increasing the cooling of the heating wire. Moreover, in the nucleate boiling region, application of electric field reduced the amount of vapour nuclei and tended to shift the system into natural the convection region. In other words, natural convection region was prolonged due to the application of the electric field. Similar observations were reported for the film boiling region, i.e. with the application of electric field the system returned to nucleate boiling region. They supported this argument by reporting their observation that with the application of electric field the wall superheat decreased from 500 ^{o}C to 20 ^{o}C.

It can be observed from the discussion that two different bubble behaviours were reported under the application of high intensity electric field, firstly the bubble diameter decreased (Babaoi et al. (1968)) and secondly the diameter of the bubble increased (Madadnia and Koosha (2003) and Wang et al. (2008), see Figure 3.15). It was due to the electrode arrangements shown in the Figure 3.13.

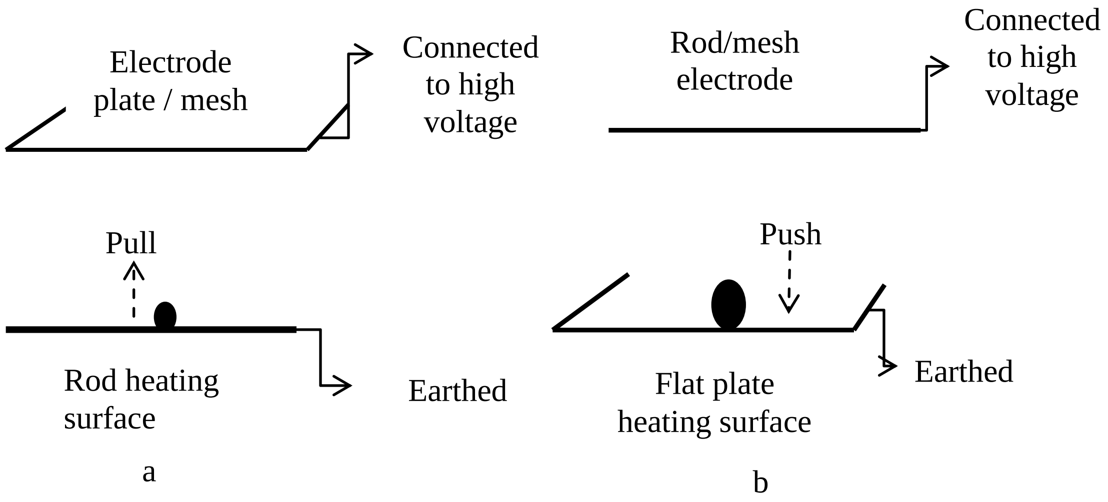

Figure 3.13 Bubble behaviour under electric field (a) on rod heating surface (b) on flat plate heating surface.

In case of Babaoi et al. (1968), the heating surface was a rod as mentioned in Figure 3.13 (a) and, as discussed earlier, according to Pohl (1978) the when a dielectric fluid is subjected to a high intensity electric field, the component having higher electric permittivity is attracted towards the region of higher electric field intensity. It means that the liquid (which has higher electric permittivity) is attracted towards the heating rod, see Figure 3.13 (a). This will increase the liquid motion towards the heating rod and the bubble (which has low electric permittivity) is attracted towards the mesh or plate electrode. This situation leads to smaller bubble departure diameter (the diameter of the bubble just before breaking into the fluid is called the bubble departure diameter) as mentioned by Babaoi et al. (1968). On the other hand, when the heating surface is a flat plate and the electrode is a mesh or a rod, see Figure 3.13

(b), the high intensity electric field lies at rod or mesh as compared to the flat surface. So, the bubble is pushed against the heating surface, which results in increasing the bubble departure diameter.

3.6 Bubble behaviour

During the application of electric field, the alteration in the bubble dynamics was reported by the researchers. They observed the bubble behaiour during two situations, i.e. the bubble were introduced within a dielectric liquid using fixed orifice and in second case bubbles were thermally induced using the heating surface, i.e. pool boiling. In both cases, high intensity electric was applied and the effect on the bubbles was monitored using high speed camera.

The bubble behaviour in a uniform electric field was visualized by Dong et al. (2006). They introduced air bubbles, through an orifice plate, into a dielectric fluid, i.e. carbon tetrachloride. The tests were conducted in a rectangular glass chamber of dimensions 540 mm (height), 400 mm (width) 300 (length). The electric potential was provided by placing a copper plate electrode 8 mm apart from the orifice plate, which was used as the second electrode. It was observed that the bubble growth time (defined by Dong et al. (2006) as the time from the first appearance of the bubble to departure) increased by 550 % with the application of an electric field strength, E = 4.4 MV/m as compared to field free conditions, when the bubble injection pressure was identical (no information about the magnitude of the pressure was given by the authors). Furthermore, the bubbles were found to elongate in the direction of the electric field, i.e. the bubble size increases vertically but decreased horizontally. Similar experiments were carried out by Chen et al. (2007 a); they introduced nitrogen bubbles in 25 # transformer oil under a uniform electric field of 50 kV. The nitrogen bubbles were injected, at a pressure of 0.21 MPa, through an orifice of 1.5 mm, which was drilled in a brass plate (the orifice brass plate also served as the negative electrode). The positive electrode was a brass mesh to allow the bubble to pass through it. The observations showed that with the application of 3 MV/m, the bubble growth time increased by 565 %. Further, Dong et al. (2006) reported that the bubbles were found to elongate along the electric field, see Figure 3.14.

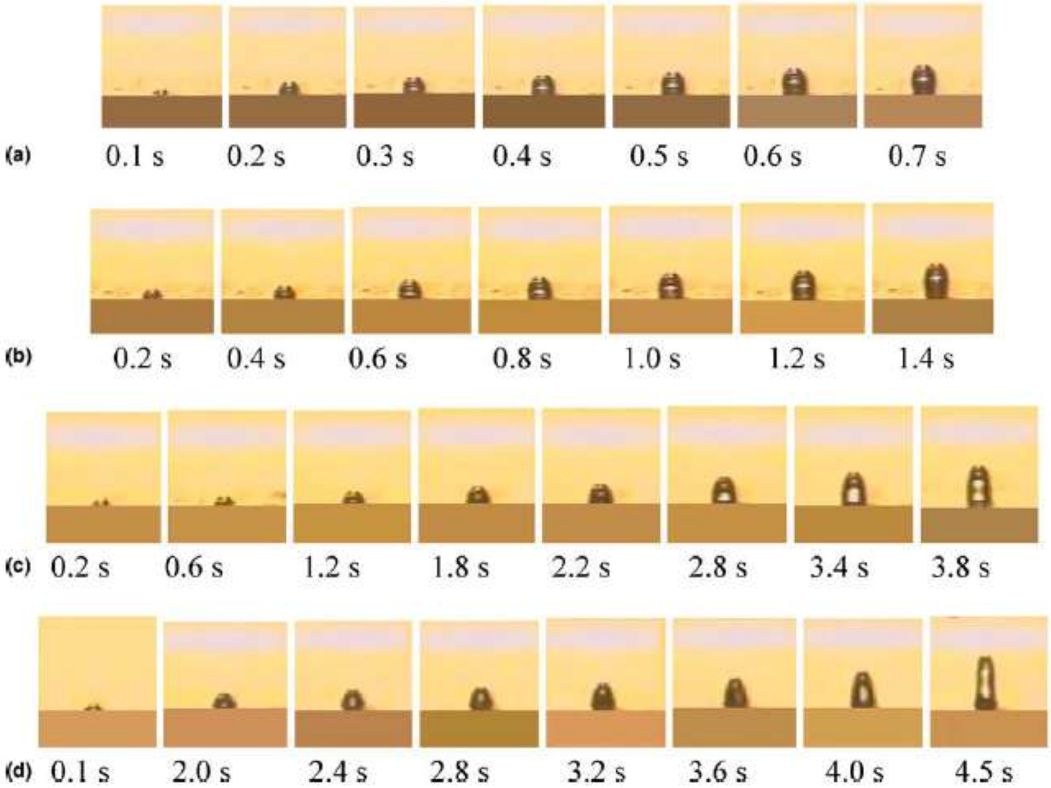

Figure 3.14 Bubble growth (a) at 0 kV (b) at 15 kV (c) at 25 kV (d) at 35 kV Dong et al. (2006)

Moreover, Dong et al. (2006) explained the bubble elongation and increase in the bubble detachment time. They argued that in the absence of the electric field the bubble growth was under the effect of inertial and surface tension forces, i.e. the bubble grow like a sphere and broke into the liquid in 0.7 sec, see Figure 3.14 (a). The application of high intensity uniform electric field results into an additional force, which results in altering the bubble growth, i.e. as prolate spheroid (mentioned by Dong et al. (2006)). Due to the application of electric force, the bubble detachment time also increased as 4.5 sec. Further, the elongation behaviour was also mathematically explained by Chen et al. (2007 a) by calculating the stresses on the bubble under the application of the electric field. They found that the value of the compressive stresses was higher than the expanding stresses, which leads to bubble elongation. Dong et al. (2006) and Chen et al. (2007 a) considered the electric field effects on gas bubbles introduced in a liquid of different permittivity.

On the other hand, Siedel et al. (2011) performed their experiments to observe bubble dynamics under a high intensity uniform electric field and pool boiling conditions. They soldered a mirror polished copper heating surface 18 mm in diameter and 40 µm thin on a copper rod, which was embedded with cartridge heaters. Then they drilled an artificial cavity, 500 µm deep and 180 µm in diameter in the heating surface. High electric potential - up to 30 kV - was generated by placing a brass mesh electrode 7 mm above the heating surface (the dimensions of the mesh were not given). The tests were carried out using n–pentane. The visualization analysis indicated the elongation in the bubble size with the application of the electric field, as shown in Figure 3.15. It can be deduced from the visual observations that, in the absence of electric field, the bubble grows nearly like a sphere. On the other hand, with the application of the electric field, strength E = 3.4 MV/m, the bubble is found to elongate in the direction of electric field. Similar observations were reported by Wang et al. (2008). They performed pool boiling experiments to evaluate the behaviour of thermally induced bubbles under uniform electric field. The uniform electric field was applied by placing a steel mesh electrode having 1.8 mm aperture. Boiling was performed using stainless steel cylinder, which was grounded and served as a second electrode. The distance between the electrodes was kept at 6 mm. An artificial cavity of 100 µm in diameter and 30 mm in depth was made on the top surface of boiling cylinder. The electric potential was applied up to 50 kV, while liquid nitrogen was the working fluid. During this growth the shape of the bubble was nearly spherical before detachment from the boiling surface. With the application of electric field, the bubble elongated in the direction of electric field and according to the authors the shape of the bubble was nearly prolate spheroid on detachment, see Figure 3.15. Furthermore, the bubble detachment time also increased by 690 % at 8.33 MV/m when compared with no field conditions. The increment in the bubble detachment time is summarized in Table 3.2. It can be observed from the Figure 3.15, at 3.4 MV/m, that the bubble dynamics of the n- pentane was altered as reported by Siedel et al. (2011). But the increment in the bubble detachment time was marginal. On the other hand, Wang et al. (2008) reported that with the application of electric field both the bubble dynamics and the bubble detachment was changed when they performed the experiment using liquid nitrogen, see Figure 3.16. This contradiction may be due to the difference of electrical and thermal properties of both fluids, i.e. electric permittivity and surface tension.

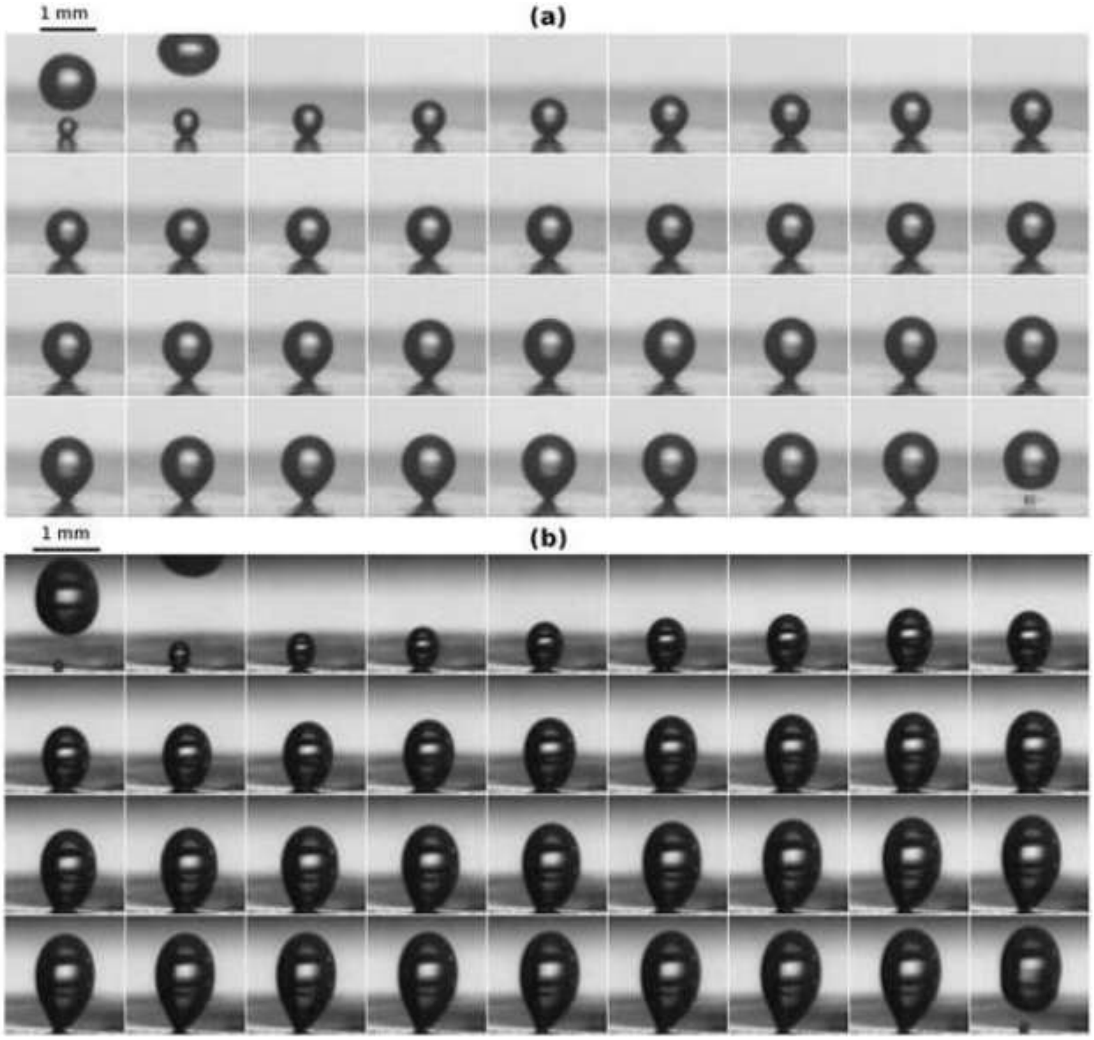

Figure 3.15 Bubble growth (a) at E = 0 (b) at E = 3.4 MV/m. Time between two frams is 5.7 msec Siedel et al. (2011).

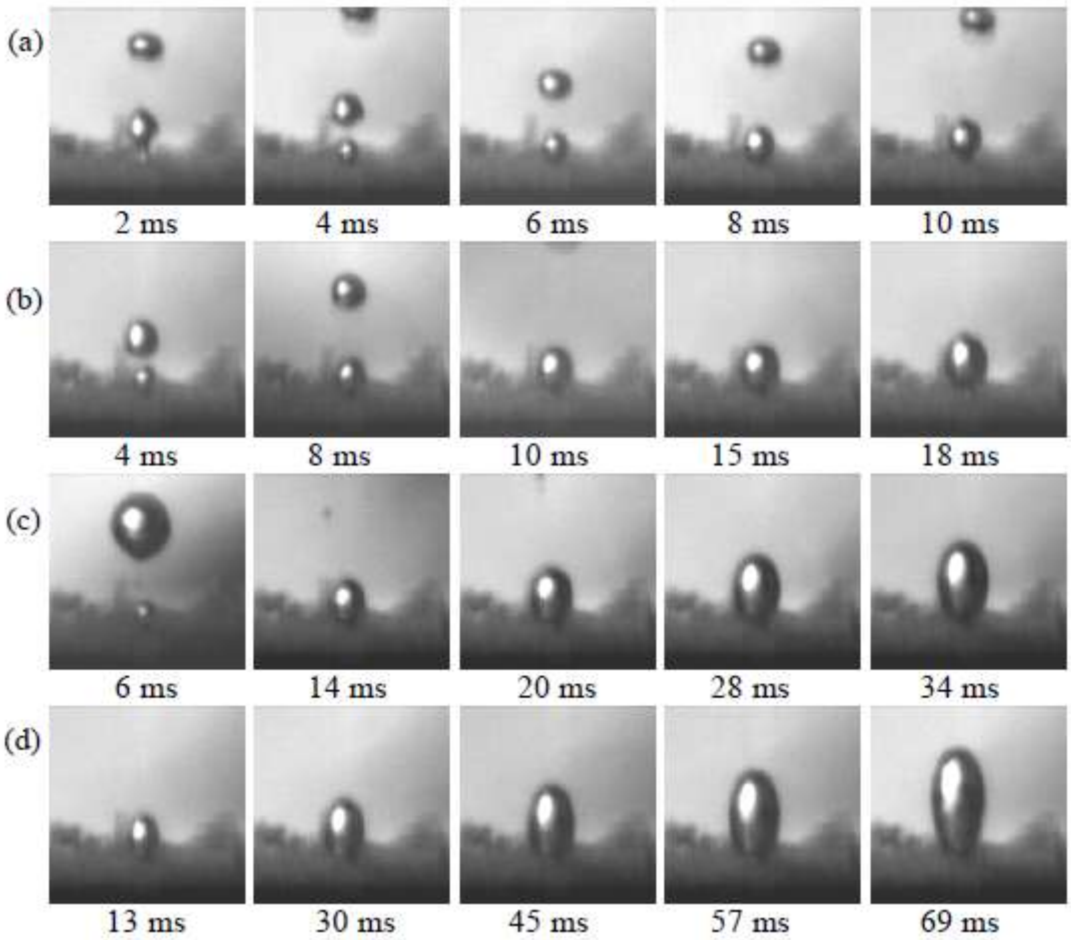

Figure 3.16 Bubble growth E = (a) 0 (b) 5 MV/m (c) 6.67 MV/m (d) 8.33 MV/m
Wang et al. (2008)

Wang et al. (2008) also explained this situation mathematically. In the absence of bubbles, they reported that electric field is homogeneous. As bubble appeared, the electric field was distorted. It was further reported that the value of the electric field decreased at the top and bottom of the bubble, while increased at the sides of the bubbles. These findings were similar to the mathematical modeling results of Karayiannis and Xu (1998). They reported that the uniform electric field distorted with the presence of bubble. The magnitude of the electric field increased at the sides of the bubble by 30 %, while decreased slightly at the top and bottom of the bubble.

Zhang et al. (2010) performed a detailed mathematical study to simulate the electrical forces around a single bubble of R134a. The results of the simulation showed that, due to the application of electric field, the vortex of fluid motion which is attached both with the bubble and heating wall changes. The size of these vortices decreases with increase in the applied electric field which results in thinner shear flow layer around the bubble. Thus temperature gradient around the interface becomes steeper which enhances the heat transfer. Moreover, the simulation results indicate that the bubble elongate in the axial direction while squeeze inwards at the middle when electric field is applied. Dong et al. (2011) experimentally observed the behaviour of both thermally induced and injected bubbles under the application of uniform electric field. For bubble injection, the nitrogen bubbles were injected into the medium of R-123 through orifices. The electric field was provided using the plate electrodes having 190 mm × 150 mm, which were placed 10 mm apart. For thermally induced bubbles, R-123 was heated at 27.8 °C saturation temperature. It was reported that the bubble produced like a sphere in the absence of electric field. As the electric field is applied the bubble changed from the sphere to prolate spheroid. It was further reported that the deformation was more prominent in the thermally induced bubbles as compared to injected bubbles. This fact can be explained that there was a temperature gradient around the thermally induced bubbles. This thermal gradient alters the electric permittivity. Due to this fact the effect of electric field was more as compared to injected bubbles. Moreover, similar to the mathematical studies reported by Zhang et al. (2010), the bubbles found to elongate in the direction of electric field, while compressed at the center of the bubble when the electric field was applied.

Liu et al. (2006) investigated the effect of a non–uniform electric field on air bubbles, which were injected in a dielectric fluid, i.e. FC-72. The experiments were carried out in a rectangular chamber made of polycarbonate (90 mm × 90 mm × 100 mm). The air bubbles were injected through an orifice plate, which was also used as one of the electrodes. In order to generate a non–uniform electric field, a 5 mm spherical copper electrode was placed 11.6 mm apart from the orifice plate. It was observed that the air bubbles tend to deform towards the electrode under the influence of 25 kV electric potential. They also reported the effect of 25 kV electric potential on the bubble detachment time (same as growth time mentioned in Dong et al. (2006)), when the volumetric flow rate of air bubble injection was changed from 2.58×10^{-7} to 8.61×10^{-7} m^3/s. At low volumetric flow rate the detachment time was decrease up to 40 % with the application of electric field as compared to field free conditions. At 8×10^{-7} m^3/s, the bubble detachment time increased with the application of the electric field Liu et al. (2006). Similar observations were reported by Kweon and Kim (2000) during the investigation of pool boiling under the influence of non – uniform electric field. The apparatus consisted of glass vessel and R113 was used as a working fluid. The electric potential applied was up to 30 kV. A plate–wire electrode system was used in order to generate a non–uniform electric field. The copper plate electrode was used, which was 100 mm long and 85 mm wide. The wire electrode was made of Platinum, 110 mm long and 0.37 mm in diameter. The gap between the plate–wire electrodes was 16 mm. The visual observations showed that at high heat flux, in the absence of the electric field, the bubble columns were extremely disordered. In the presence of the electric field, there was a change observed in the bubble dynamics, i.e. the bubbles organized in more ordered columns having large departure frequencies and small detachment diameter. Bubble coalescence was also observed to reduce with the application of the electric field.

Table 3.2 Enhancement in the bubble detachment time

Sr No.	Fluid	Percentage increase in bubble detachment time	Electric force/ electric potential	Remarks	Reference
1	Air	550	4.4 MV/m	Air bubbles introduced into carbon tetrachloride	Dong et al. (2006)

2	Nitrogen	565	3 MV/m	Nitrogen bubble were injected into 25 # transformer oil	Chen et al. (2007 a)
3	n-pentane	marginal	3.4 MV/m	Thermally induced during pool boiling	Siedel et al. (2011)
4	Liquid nitrogen	620	8.33 MV/m	Thermally induced during pool boiling	Wang et al. (2008)
5	Air	40	2.2 MV/m	Air bubbles were introduced in the FC -72.	Liu et al. (2006)

3.7 Effect of EHD on critical heat flux

As discussed earlier in section 2.10, the CHF is an important phenomenon especially in thermal and nuclear power industries. The enhancement in the CHF value can help to design more efficient equipment (i.e. heat exchangers, boilers) and control the system more effectively in the process industry. In the following section, the effect of EHD on CHF, which was reported by the researchers, will be reviewed.

Earlier, Berghmans (1976) mathematically examined the effect of EHD on the CHF and suggested that vapour columns formed on the heating surface near the critical heat flux are destabilized by applying DC electric field. This destabilization is responsible for the increase in the CHF. He derived a mathematical expression to predict maximum heat flux based on the hydrodynamic theory presented by Zuber (1958) as follows:

$$(q_{CHF})_E = \frac{1}{8}\left(\frac{\pi}{3}\right)\left(\varepsilon_g \rho_g\right)^{\frac{1}{2}} \frac{\Delta V}{d} h_{lg} \tag{3.15}$$

Equation 3.15 was found to be in good agreement with the experimental work of Markels and Durfee (1964) who used isopropyl alcohol and distilled water as working fluids, who performed pool boiling experiments using horizontal copper tubes .They reported that the value of critical heat flux was increased . Earlier Johnson (1968) derived an expression to estimate the CHF under the influence of the electric field. He considered the electric field effect on hydrodynamic stability and the analysis resulted to the following expression:

$$\frac{(q_{CHF})_E}{(q_{CHF})_0} = \left[\frac{f_1\left[1+\sqrt{1+\frac{3(\rho_l-\rho_g)g\sigma}{f_1^2}}\right]}{\sqrt{3(\rho_l-\rho_g)g\sigma}}\right] \tag{3.16}$$

$$f_1 = \left(\frac{\varepsilon_g}{\varepsilon_l}\right)\frac{[\varepsilon_l-\varepsilon_g]^2}{\varepsilon_l+\varepsilon_g}E^2 \tag{3.17}$$

Johnson (1968) also experimentally tested the effect of electric field on critical heat flux using Freon 114. He reported that the enhancement in the value of critical heat flux was 167 % at 4 MV/m, when it was compared to no field conditions.

Lovenguth and Hanesian (1971) noted that the critical heat flux increases with the increase in the DC non – uniform electric field using four different dielectric fluids namely: Freon 113, Carbon tetrachloride, Chloroform and Freon 21 (the enhancement value is given in Table 3.3).Furthermore, they derived an expression based on the Kelvin – Helmholtz instability to predict the effect of DC non – uniform electric field on the critical heat flux, as follows:

$$\frac{(q_{CHF})_E}{(q_{CHF})_0} = \left[\frac{BE^2}{\sqrt{3(\rho_l-\rho_g)\sigma g}} + \left[\left[\frac{BE^2}{\sqrt{3(\rho_l-\rho_g)\sigma g}}\right]^2\right]^{\frac{1}{2}}\right]^{\frac{1}{2}} \tag{3.18}$$

$$B = \frac{\varepsilon_g\varepsilon_l(\varepsilon_l-\varepsilon_g)^2}{\varepsilon_g(\varepsilon_l+\varepsilon_g)} \tag{3.19}$$

Babaoi et al. (1968) suggested that at the CHF point the bubble coalescence becomes higher in volume, which covers the entire heating surface. It results in stopping the colder liquid from reaching the surface. Due to this process equipment burnout happens. But with the application of electric field the size of bubble detachment diameter decreases and colder liquid remains available even at higher heat fluxes. This decrease in bubble detachment diameter may result in increasing the CHF to higher wall superheat value when electric field is applied.

Moreover, Zaghdoudi and Lallemand (2005) experimentally observed the effect of high intensity electric field on CHF of R-123, R-113 and n-pentane. During pool boiling tests with EHD, a uniform electric potential was provided using a mesh electrode (56 % free area), which was placed 10 mm above the boiling surface. It can be observed from the Figure 3.17 that the increase in the critical heat flux value with the application of electric potential was marginal for n-pentane and R-113. While for R-123, the critical heat flux increased almost three times at 25 kV electric potential. As discussed earlier, this difference in the increase was due to the difference in the electrical properties of the fluid, i.e. the charge relaxation time, $\tau_{e,}$ were 3.4×10^{-3} s, 2.76×10^{-3} s and 0.9×10^{-3}s (reported by Zaghdoudi and Lallemand (2005)) for n-pentane, R-113 and R-123 respectively. Later on, similar experiments were performed by Hristov et al. (2009) when they tested pool boiling of R-123. The uniform and non – uniform electric fields were applied using mesh and rod electrodes respectively (see section 3.5 for details). Both the electrodes were placed 5 mm from the heating surface, while the boiling surface was earthed. They reported that the enhancement in the value of critical heat flux was 220 % and 345 % when using mesh and rod electrode respectively at 5 MV/m.

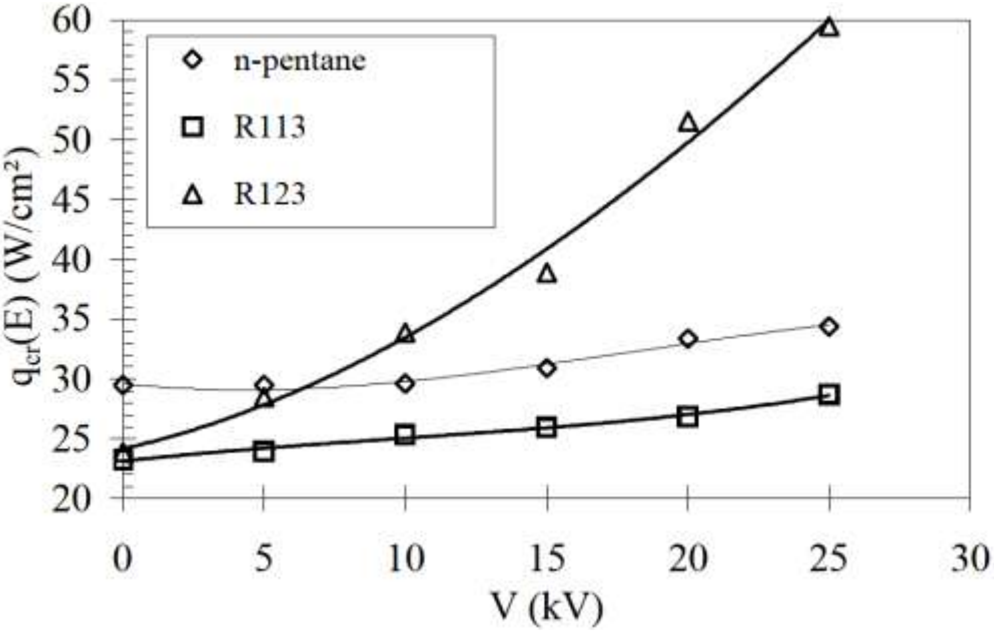

Figure 3.17 Graph between CHF and applied electric potential Zaghdoudi and Lallemand (2005)

Wang et al. (2009) performed pool boiling experiments using liquid nitrogen (LN_2) as a working fluid. The uniform electric field was employed by using a mesh electrode place 10 mm from the copper heating surface. They reported that the enhancement in the value of critical heat flux was 14 %, when 40 kV electric potential was applied. They further observed that the effect of electrode polarity on the critical heat flux enhancement was marginal, see Figure 3.18. Moreover, as discussed earlier in section 3.5, Kweon and Kim (2000) performed pool boiling experiments under non – uniform electric field using R-113 a as working fluid. They reported that the value of the critical heat flux was found to increase by 80 % as the applied voltage was increased from zero to 7.5 kV.

Wang et al. (2009) also observed the critical heat flux situation visually and reported that at critical heat flux big vapour mushroom covered the boiling surface, which hinder the cold liquid from reaching the heating surface. With the application of electric field, the size of mushroom bubble becomes.

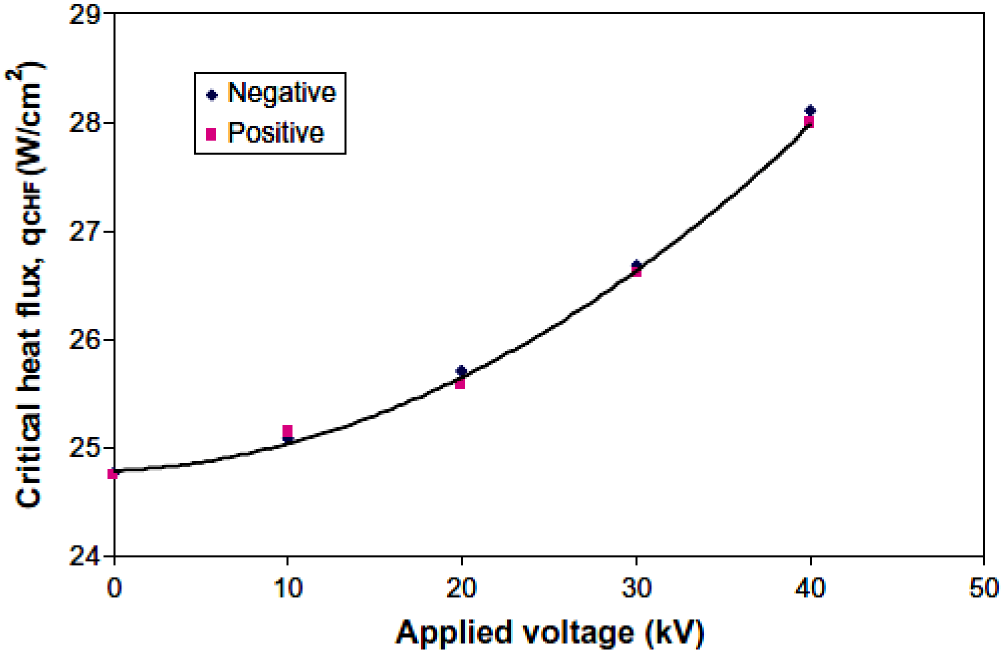

Figure 3.18 Effect of polarity on critical heat flux enhancement under uniform electric field Wang et al. (2009)

Table 3.3 Enhancement in the value of critical heat flux

Sr. No	Fluid	Electric field / electric potential	Percentage enhancement (max)	Remarks	Reference
1	Isopropanol	8 kV	455	Pressure was close to ambient.	Markels and Durfee (1964)
	Distilled water	10 kV	14.3		
2	Freon 113	13.63 MV/m	292.13		Lovenguth and Hanesian (1971)
	Freon 21	4.6 MV/m	144		
	Carbon tetrachloride	13.8 MV/m	200		

	Chloroform	8.2 MV/m	72.95		
3	Freon 114	4.2 MV/m	167	P = 2 atm	Johnson (1968)
4	n-pentane	2.5 MV/m	120	P = 1 bar, mesh electrode	Zaghdoudi and Lallemand (2005)
	R-113	2.5 MV/m	120		
	R-123	2.5 MV/m	300		
5	R-123	5 MV/m	220	P = 1 bar, mesh electrode	Hristov et al. (2009)
		5 MV/m	345	P = 1bar, Rod electrode	
6	LN_2	4 MV/m	14	P = 1 bar, mesh electride	Wang et al. (2009)
7	R-113	7.5 kV	80	P = 1 bar, plate and rod electrode system.	Kweon and Kim (2000)

3.8 Summary

It can be summarized from this review that

- Electrohydrodynamics is an effective heat transfer enhancement technique, which require negligible amount of power.
- Due to the application of electric field the dielectric fluid was first polarized and then subjected to an electrically induced force. The magnitude of the electric force was mathematically defined by Pohl (1978).
- During two phase heat transfer, the electric properties of the liquid are very important to account for the enhancement under high intensity electric field, especially charge relaxation time. Allen and Karayiannis (1995) explained

that the magnitude of charge relaxation time and bubble detachment time contributes towards the amount of heat transfer enhancement, i.e. if charge relaxation time for dielectric is very large then there is no effect of high intensity electric field on pool boiling enhancement.

- It was reported both experimentally (Wang et al. (2008), Siedel et al. (2011) and Dong et al. (2006)) and mathematically (Karayiannis and Xu (1998)) that due to application of high intensity electric field the bubble dynamics alter.
- The bubble diameter and bubble detachment time increase due to the application of electric field, either vapours were injected in the inert liquid (Dong et al. (2006)) or bubbles were thermally induced as a result of boiling (Wang et al. (2008)) .
- Critical heat flux is one of the decisive parameters in equipment design and the enhancement in the value of critical heat flux can lead to efficient and effective design. Due to the application of electric field, the enhancement in the value of critical heat flux was experimentally observed (Hristov et al. (2009) and Zaghdoudi and Lallemand (2005)).

Chapter 4 Experimental Facility

This chapter provides a full description of the experimental facility used in this study of pool boiling on upward facing, horizontal surfaces with and without electrohydrodynamic (EHD) enhancement. The current pool boiling facility at Brunel university is similar to that used by Hristov et al. (2009). However, during this work a new boiling chamber was designed and installed allowing visualization of the bubble dynamics. Furthermore, a moveable electrode arrangement was introduced and three types of circular electrode were fabricated and tested to observe the effects of uniform and non – uniform electric fields on the pool boiling process. In addition, five different boiling surfaces were prepared and characterized to investigate the effects of surface modification on pool boiling.

4.1 Description of experimental rig

The experimental rig, shown schematically diagram in Figure 4.1, consisted of the following main components: (a) the boiling chamber, (b) the heater block incorporating the boiling surface, (c) the EHD electrode arrangement, (d) a water-cooled R-123 condenser, (e) the cooling water heat exchange loop, and (f) a R-134a cooling unit. The experimental setup also included a high-voltage DC supply and equipment for AC electrical power measurement and control, high-speed video imaging, temperature and pressure measurements and a computer-based data acquisition system.

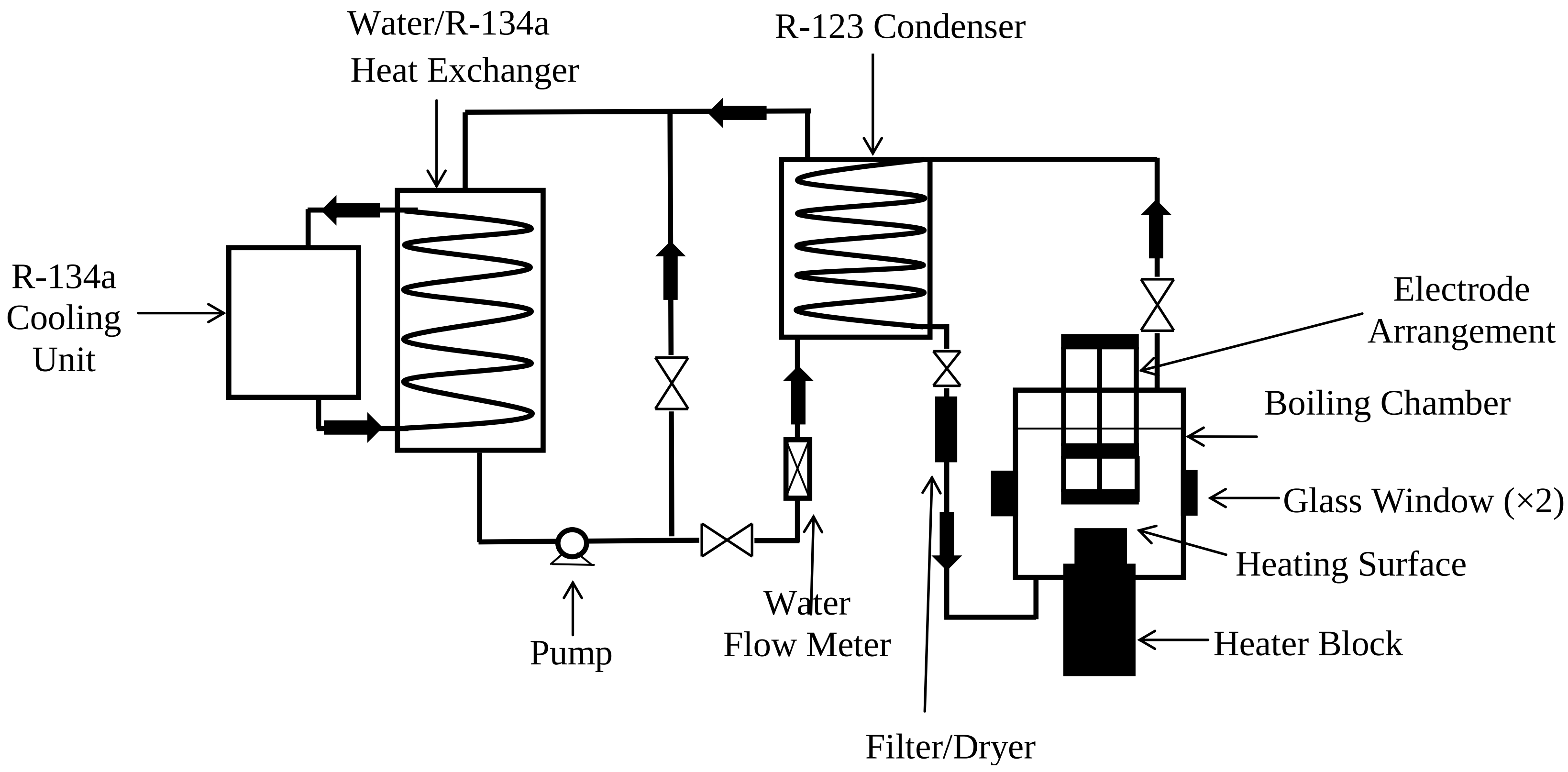

Figure 4.1 Schematic diagram of experimental rig.

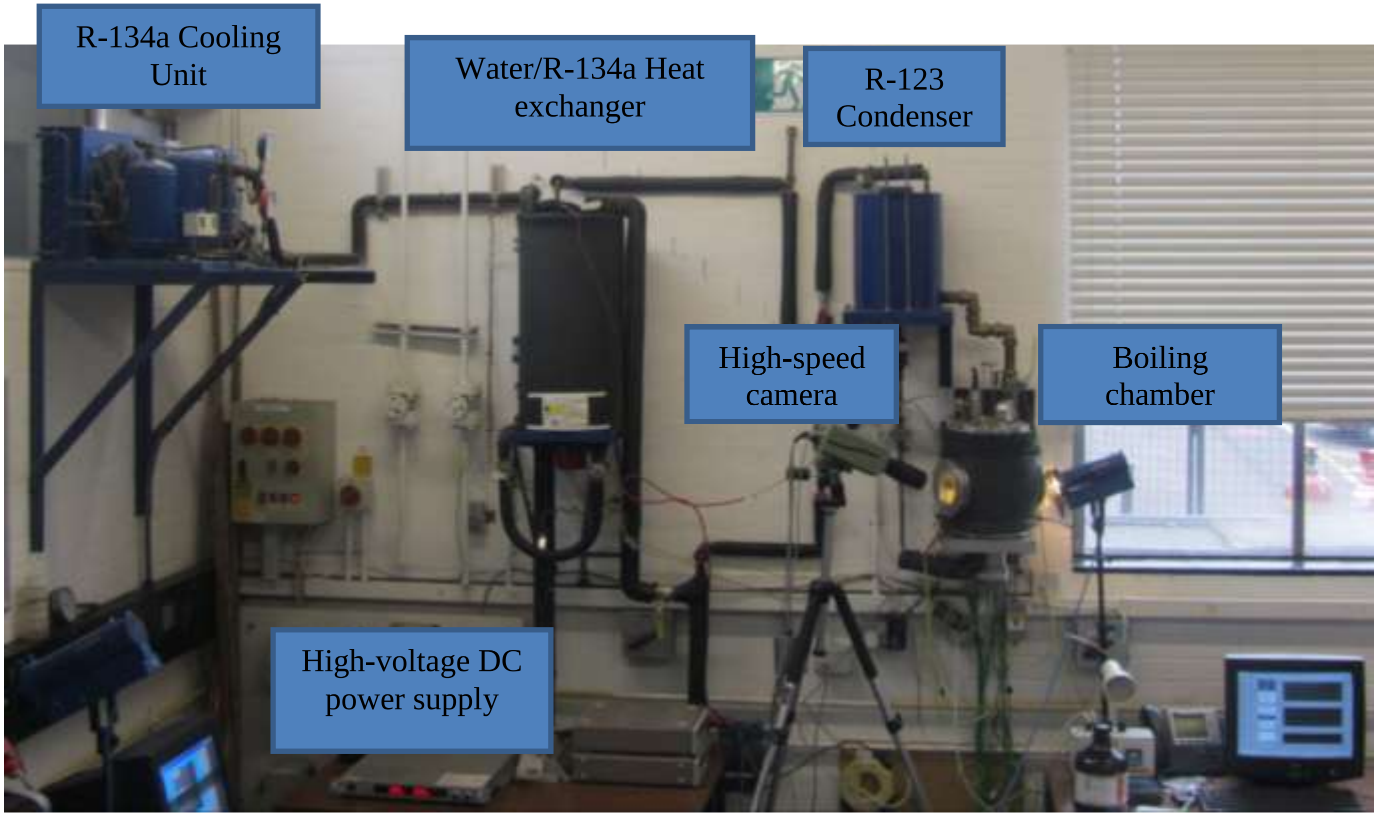

Figure 4.2 Photograph of the experimental rig.

A general view of the experimental rig is shown in Figure 4.2 Saturated pool boiling experiments with R-123 were carried out in the boiling chamber at pressures of 1 bar, 2 and 4 bar. The apparatus operated as a two-phase thermosyphon. The R-123 vapour produced in the boiling chamber was condensed in the external water-cooled condenser and the condensate was returned to the chamber via a filter/dryer. The cooling water used in the condenser was recirculated by a pump and chilled in a heat exchanger using a R-134a vapour compression refrigeration unit.

The boiling chamber was a vertical stainless steel (grade 304) cylinder, 220 mm in diameter and 300 mm in height and is discussed in more detail in Section 4.1.1. Two circular glass windows, 140 mm in diameter, were mounted on diametrically opposite sides of the chamber in order to visualize the boiling process. A Phantom V6 digital high-speed video camera (800 pictures per second) and an illumination source were used when recording bubble dynamics. Each of the boiling surfaces tested was formed by the 40 mm diameter upper face of a cylindrical copper heater block located in a housing connected to the base of the boiling chamber. The heater block was electrically heated and was discussed in Section 4.1.3.

4.1.1 The Boiling Chamber

A new boiling chamber was designed for this study and fabricated in stainless steel (grade 304) as shown in Figure 4.3. The dimensions of the boiling chamber can play a very important role in the pool boiling process. The height and diameter of the chamber may influence the bubble formation process and convection currents in the chamber. In order to design a chamber suitable for pool boiling experiments with and without the effect of EHD a review was carried out of the dimensions of boiling chambers and boiling surfaces used by previous researchers.

Yu and Lu (2007) used a stainless steel cylindrical chamber of 154 mm diameter and 304 mm height. Their test heating surfaces had a square base area 10 mm × 10 mm. Madadnia and Koosha (2003) carried out pool boiling experiments under high intensity electric field using R-123 as the working fluid. The boiling facility consisted of a cylindrical glass vessel 250 mm in height and 250 mm in diameter. The test surface was a nichrome wire (Cr80Ni20) 85 mm long and 1 mm in diameter. Das and Das (2007) used distilled water as a working fluid and performed pool boiling experiments in a cylindrical borosilicate glass vessel of 150 mm diameter and 300 mm height. The test surface was a 60.5 mm diameter circular horizontal copper plate facing upward. Benjamin and Balakrishnan (1997) used a cylindrical glass vessel, 250 mm in height and 93 mm in diameter, to carry out pool boiling experiments. The test surface was a 25 mm diameter circular plate. Stutz et al. (2007) used a cylindrical boiling vessel of 160 mm diameter and 150 mm height. The test surface was a circular copper plate of 30 mm diameter and the working fluid was n-pentane. Zaghdoudi and Lallemand (2005) carried out EHD pool boiling experiments using R-113, R-123 and n-pentane. Their boiling chamber was a cylindrical glass vessel 160 mm in diameter and 160 mm in height. The test surface was a horizontal circular copper plate of 30mm diameter. Hahne (1983) carried out pool boiling experiments to investigate the effect of test surface and boiling chamber dimensions on the heat transfer coefficient. R-113 was used as a working fluid. The experiments were performed using two types of boiling chamber; cylindrical and rectangular. It was found that boiling chamber geometry affects the heat transfer coefficient for values of the chamber to surface diameter ratio up to D/d = 6.6 for cylindrical chambers and D/d=19.6 for rectangular chambers. The dimensions of the boiling chambers and heating surfaces used in the studies reviewed above are summarized in Table 4.1

It can be concluded from the work of Hahne (1983) that the heat transfer coefficient in pool boiling may be was affected by boiling chamber diameter for values up to D/d = 6.6 when R-113 is the working fluid. The approach of Zaghdoudi and Lallemand (2005) was adopted to design the boiling chamber used in this work. In their pool boiling experiments using R-123, R-113 and n-pentane, Zaghdoudi and Lallemand (2005) used a boiling chamber-to-heating surface diameter ratio equal to 5.5.

Table 4.1 Dimensions of heating surfaces and boiling chambers used by previous researchers.

Boiling chamber dimensions		Test surface dimensions			H/D	D/d_s	A_c/A_s	Working Fluid	Reference
Height	Diameter	Form	Diameter	Orientation					
H (mm)	D (mm)		d_s (mm)						
304	154	Rectangular		Horizontal	1.97	15.4	186.3	FC-72	Yu and Lu (2007)
250	250	Cylindrical	1	Horizontal	1	2.9	183.3	R-123	Madadnia and Koosha (2003)
300	150	Circular	60.5	Horizontal	2	2.47	6.147	Distilled water	Das and Das (2007)
250	93	Circular	25	Horizontal	2.67	3.72	13.83	Distilled water, CCl_4, acetone, n-hexane	Benjamin and Balakrishnan (1997)
160	160	Circular	30	Horizontal	1	5.33	28.44	R-113, R-123, n-pentane	Zaghdoudi and Lallemand (2005)
680	370	Rectangular	18	Horizontal	1.84	19.6	370	R-113	Hahne (1983)
800	125	Circular	18.9	Horizontal	6.4	6.6	36	R-113	

Note: A_c =cross sectional area of the chamber, A_s = area of the boiling surface, D = diameter of boiling chamber and d_s = diameter of heating surface.

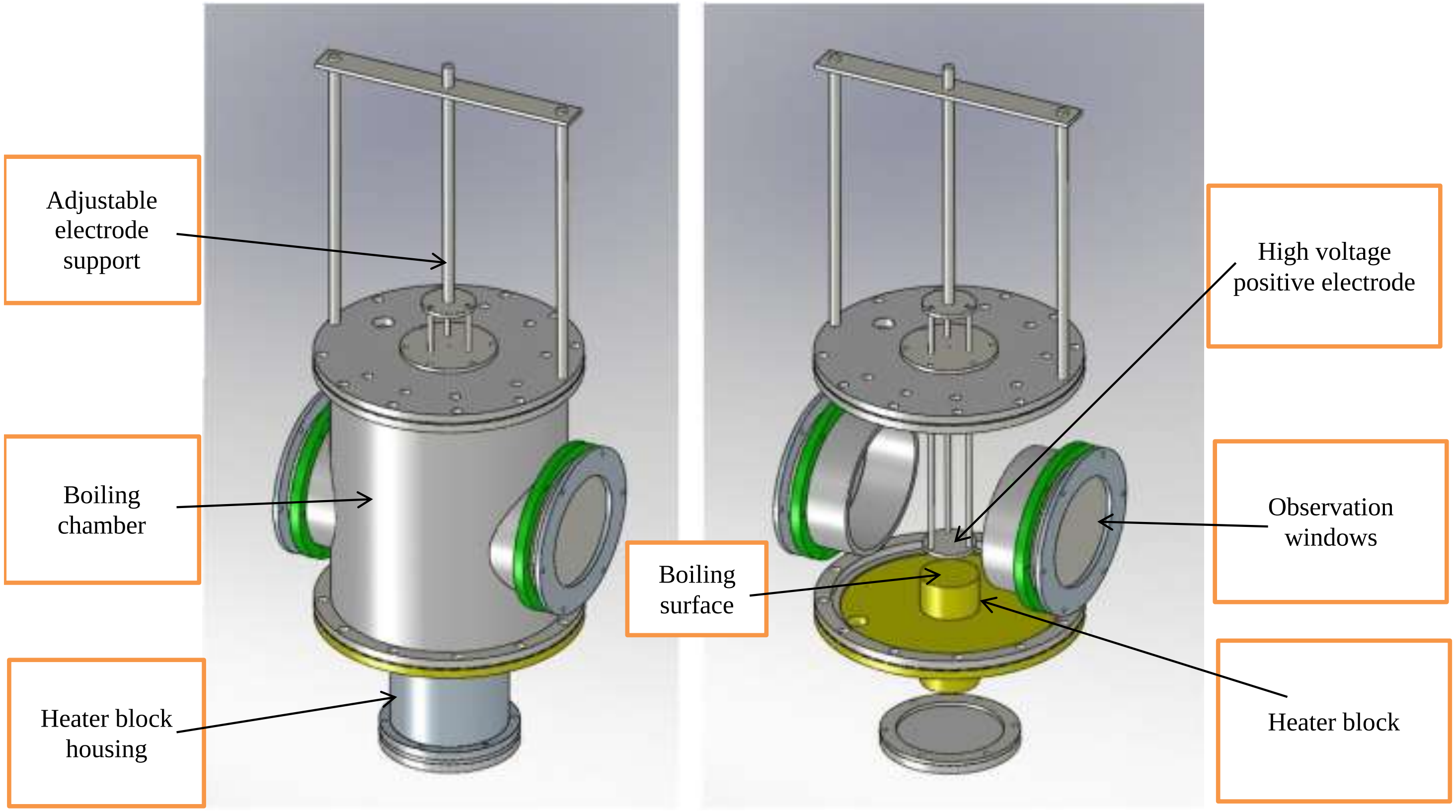

Figure 4.3 3-dimensional drawing of boiling chamber.

In this study, the D/d was also taken as 5.5 and the height of the chamber was chosen to be slightly higher than the diameter to accommodate the installation of an adjustable electrode support system.

The boiling surface and boiling chamber dimensions used in this work can be summarized as follows:

Diameter of the boiling surface, $d = 40\ \text{mm}$

Assuming $\frac{D}{d} = 5.5$

Diameter of the boiling chamber, $D = 220\ \text{mm}$

Height of the boiling chamber, $H = 300\ \text{mm}$

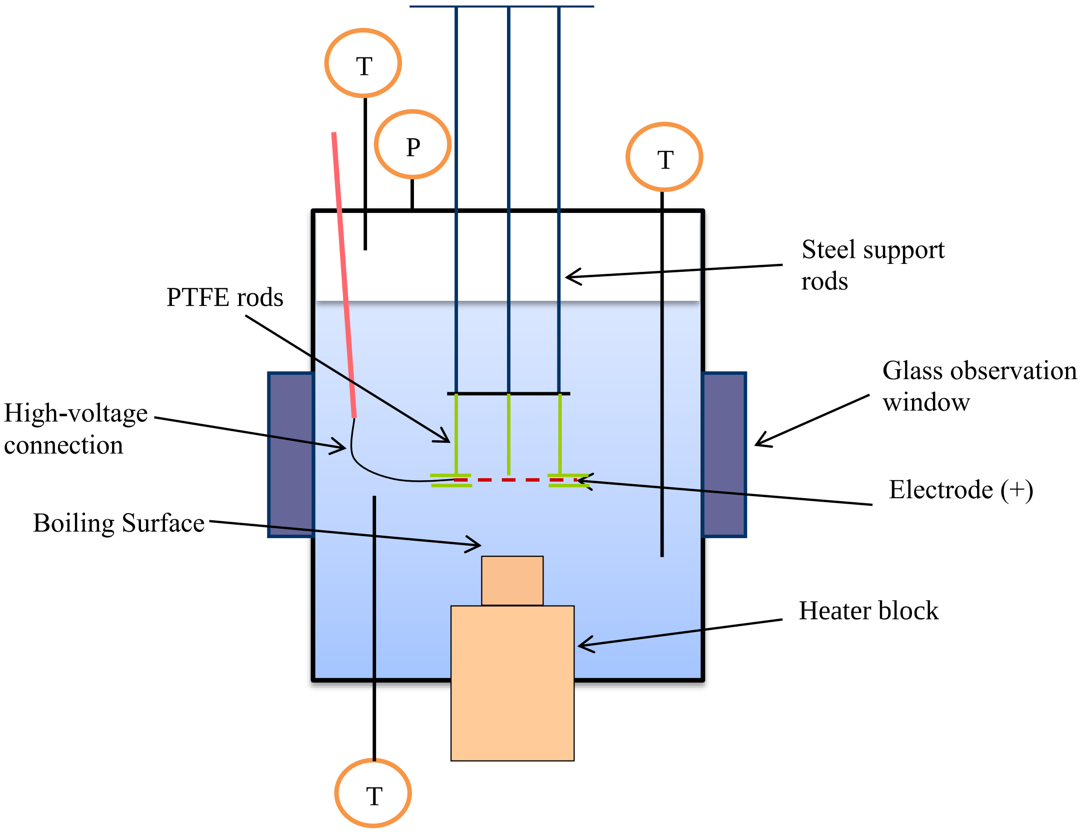

Figure 4.4 Schematic diagram of boiling chamber.

The boiling process was visualized using two glass windows of 140 mm diameter. The glass windows can withstand a pressure of 10 bar according to the supplier. To maintain saturated conditions within the chamber and to reduce heat loss an electric heater tape was wrapped around the chamber and nitrile foam rubber insulation was applied to a thickness of approximately 25 mm, see Figure 4.2. The saturation temperature within the boiling chamber was monitored using three Type K thermocouples; two were placed in liquid region and one was placed in the vapour region, see Figure 4.4. A pressure gauge and an absolute pressure transducer were connected at the top of the chamber to monitor the pressure.

4.1.2 Electrode system

For the experiments with EHD enhancement, the electric field was generated using a high-voltage DC power supply (Model AU 30P, Matsusoda Precision Inc) capable of providing voltages up to 30 kV. Three types of electrode, namely: a mesh electrode, a rod electrode with 5 mm a rod spacing and rod electrode with 8 mm rod spacing, were used to apply either a uniform or a non – uniform electric field. With this arrangement, the electric field strength could be varied from 0 to 3 MV/m. Note that the nominal magnitude of electric field strength is calculated as $E = V/d$, where V is the electric potential applied and d is the electrode spacing. The electrodes were sandwiched between PTFE washers to provide electrical isolation from the rest of the chamber. The inner diameter of the PTFE washers was 40 mm, corresponding to the boiling surface diameter. The material of all electrodes used was stainless steel (grade 304). The electrode assemblies were attached with PTFE rods to a support system that allowed the position of the electrode above the boiling surface to be adjusted from outside the boiling chamber, see Figure 4.3 and Figure 4.4. Uniform electric fields were generated using the mesh electrode which had a square aperture size of 5.1 mm × 5.1 mm and 64 % open area, see Figure 4.5 (a). Non – uniform electric fields were generated using the two rod electrodes, i.e. one with a 5 mm rod spacing and the second with a 8 mm rod spacing, see Figure 4.5 (b) and (c). The rod diameter was 1.56 mm in both cases.

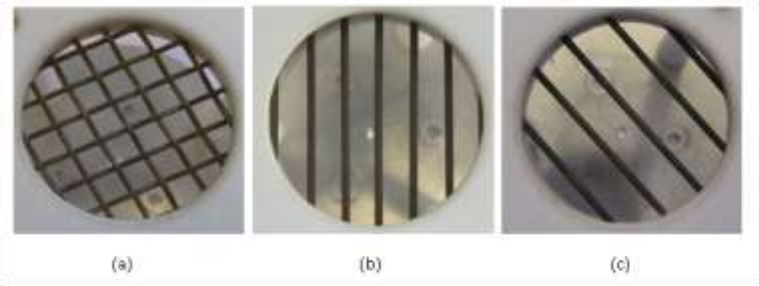

Figure 4.5 Photographs of electrodes (a) Mesh electrode with 5.1 mm square aperture, (b) Rod electrode with 5 mm rod spacing, (c) Rod electrode with 8 mm rod spacing. The inner diameter of all the electrodes was 40 mm. The diameter of the rods in (b) and (c) was 1.56 mm.

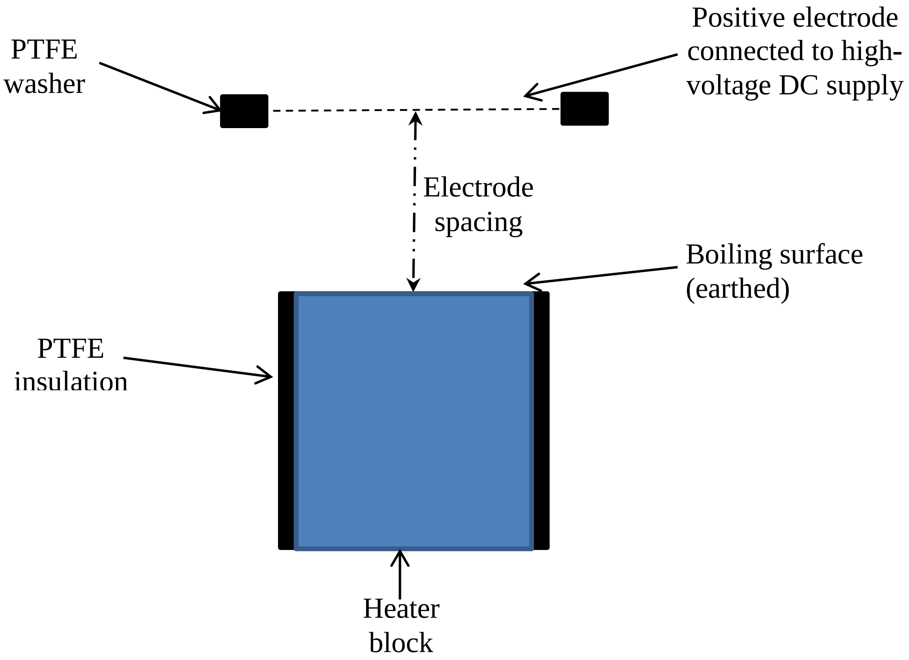

Figure 4.6 Electrode arrangement.

In the EHD experiments the electrode spacing distance above the boiling surface was set at 10 mm, 20 mm or 40 mm using the adjustable electrode arrangement. The positive electrode, see Figure 4.6, was connected to the high-voltage power supply. The boiling surface was earthed and served as a second electrode, see Figure 4.6.

4.1.3 Heater block

As previously mentioned, each of the different boiling surfaces tested in this study was formed by the upper face of an electrically heated copper block. Separate heater blocks were manufactured for each type of boiling surface. Figure 4.7 shows dimensioned drawings of the cylindrical heater block which was manufactured from oxygen-free copper. The block was heated by six 250 W cartridge heaters inserted into the base of the block in holes of 6 mm diameter and 40 mm depth. The power supplied to the cartridge heaters was regulated using a variable transformer and measured by a power meter. Temperatures in the heater block were measured using six Type K sheathed thermocouples of 0.5 mm diameter located 5 mm, 10 mm, 15 mm, 20 mm, 25 mm and 30 mm below the boiling surface in radial holes 1 mm diameter and 10 mm deep. The thermocouple holes were filled with thermal paste to ensure good contact. These thermocouple measurements were used to determine the axial temperature gradient in the heater block and the temperature at the boiling surface. The circumferential temperature uniformity in the heater block was assessed by inserting additional Type K thermocouples 5 mm below the surface at angles of 0º, 60º, 120º, 180º, 240º and 300º. Thermocouples were also inserted 10 mm below the boiling surface at angles of 0º, 120º and 240º, see Figure 4.7. The heating block was heavily insulated by a thick PTFE sleeve to help achieve one-dimensional axial heat conduction to the boiling surface, see Figure 4.8.

It was concluded from thermocouple readings that radial heat flow in the upper section of the heater block was negligible. Therefore, it was assumed that heat conduction upward through the copper block was one-directional and the temperature was uniform along the radius at any axial location.

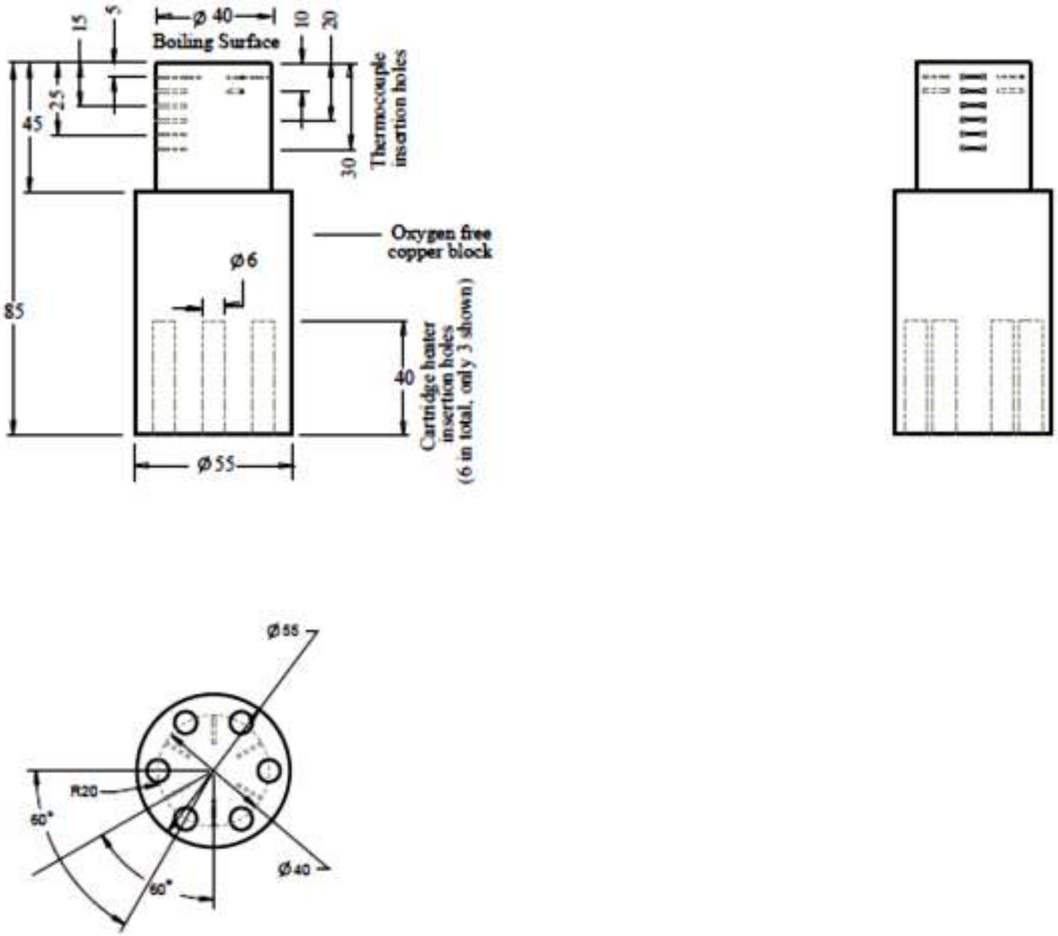

Figure 4.7 Detail drawing of heater block, all dimensions are in millimetres.

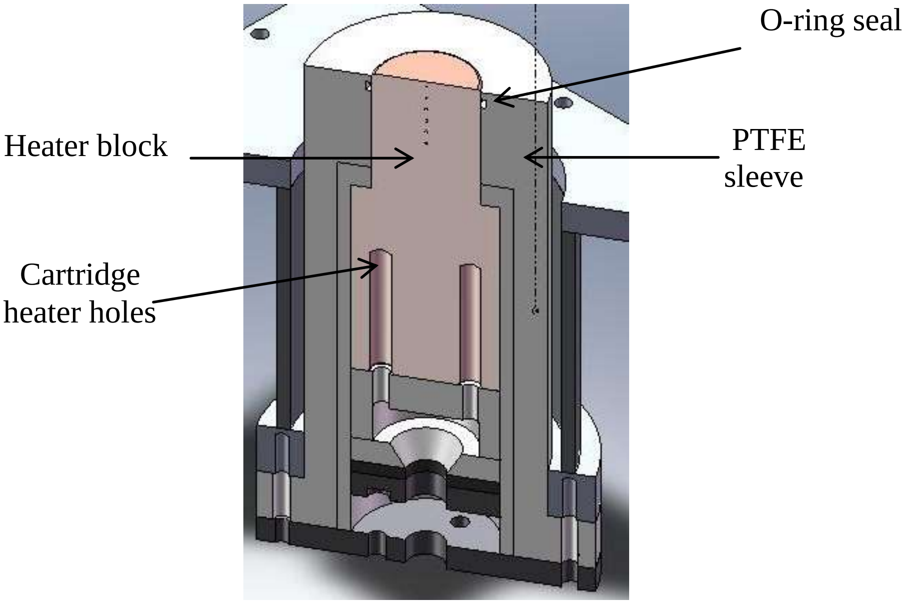

Figure 4.8 Heater block housing with PTFE sleeve.

4.2 Boiling surface preparation and characterization

Five boiling surfaces, modified by different treatments, were prepared for testing under saturated pool boiling conditions, namely: an emery polished surface, a fine sandblasted surface, a rough sandblasted surface, an EB enhanced surface and a sintered surface. The procedures used to prepare the test surfaces are outlined below. The boiling surfaces were characterized using an ultrasonic stylus instrument at Kassel University, see Luke (2006). The ultrasonic stylus method is contactless and employs a quartz tuning fork with an attached diamond having a defined tip radius. A change in the resonance characteristics of this oscillator occurs when the diamond tip is moved towards the sample surface due to hydrodynamic friction. The movements of the stylus in the normal z-direction represent the measured surface profile.

Values of the surface parameter, P_a, defined as the arithmetic mean deviation of the surface profile from the mean line, are given for each surface in the appropriate sections below. A two-dimensional surface profile was obtained for each surface (see Figures 4.10 to 4.13 and Figure 4.16).

4.2.1 Emery polished surface

The surface was polished with emery paper P1200. It was placed on the emery paper under its own weight of 24.5 N. The block was moved on the emery paper from front to back and then sideways, 50 times in each direction. After every 50 movements the emery paper was renewed. Compressed nitrogen was then blown over the surface to remove any fine particles. A value P_a = 0.044 µm was reported for the emery polished surface.

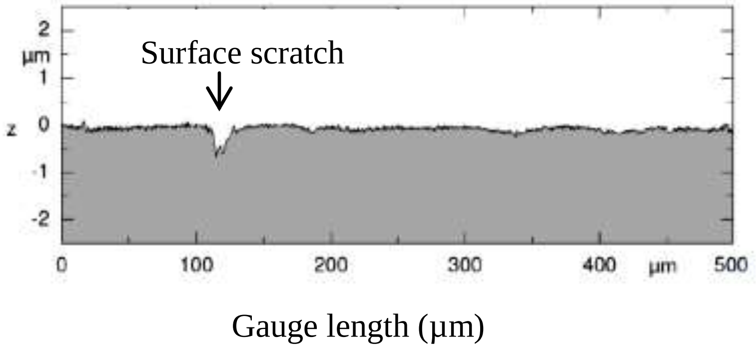

Figure 4.9 2-D profile for emery polished surface

The two-dimensional surface profile shown in Figure 4.9 was obtained by a single scan of the ultrasonic stylus along gauge length of 500 µm. Multiple scans along parallel gauge lengths, covering a sample area of 0.5 × 0.5 mm^2, were used to construct the three-dimensional isometric representation of the emery polished surface shown in Figure 4.10

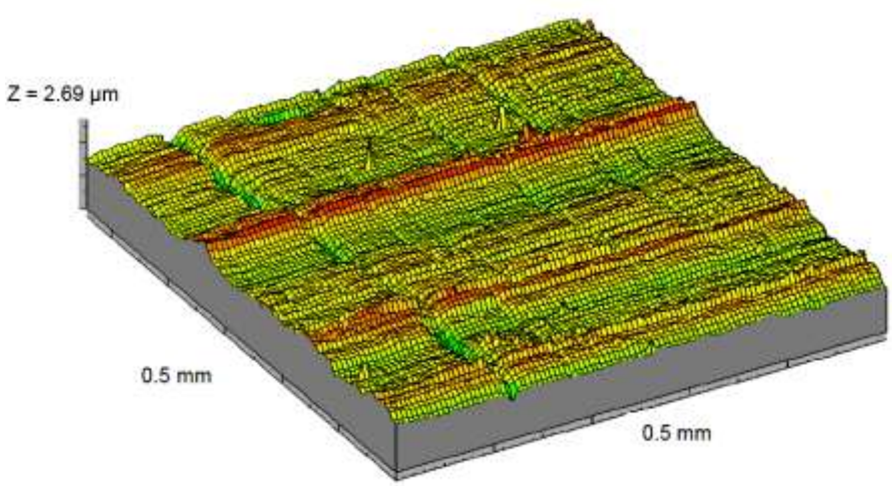

Figure 4.10 3-D topography of sample of the emery polished test surface.

4.2.2 Fine sandblasted surface

The surface was first carefully polished and then sandblasted with brown aluminum oxide (grit size 120-220 µm) in a standard sandblasting cabinet, as discussed by Luke (2006). During sandblasting the nozzle-to-surface distance was kept at 60 mm and the operating pressure was 3 bar. The P_a value was 0.0997 µm for the fine sandblasted surface.

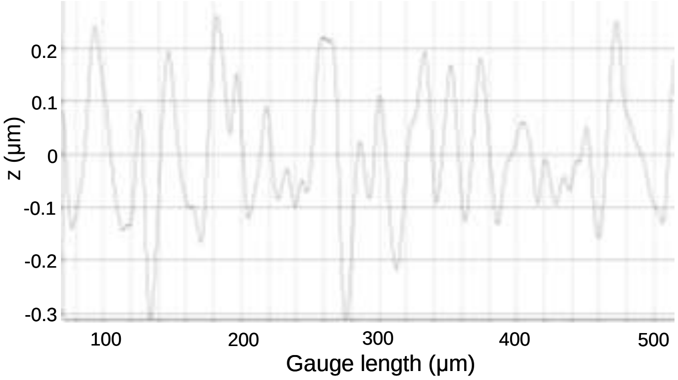

Figure 4.11 2-D profile for fine sandblasted surface.

4.2.3 Rough sandblasted surface

The surface was prepared using the same procedure as used for the fine sandblasted surface, but with a coarser abrasive blasting material. Brown aluminum oxide (grit size 300-425 µm) was employed. The rough sandblasted surface was found to have a surface parameter value P_a = 3.5 µm.

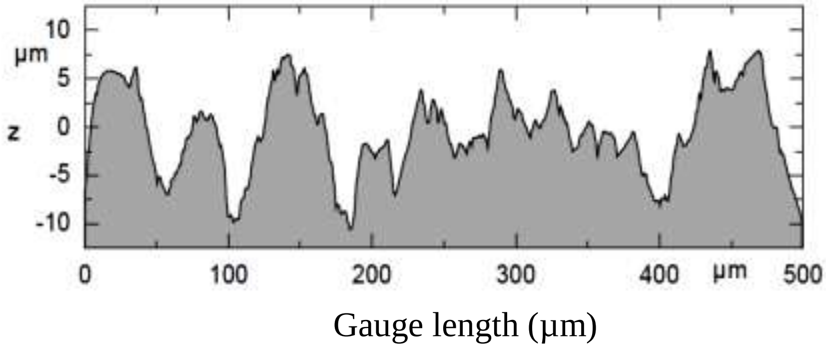

Figure 4.12 2-D profile for rough sandblasted surface.

4.2.4 EB enhanced surface

The enhanced surface was prepared at TWI Cambridge using an electron beam surface modification technology known as *Surfi-Sculpt*. In this process the electron beam is moved across the surface by a programmable system causing melting and displacement of surface material to form an array of protrusions, see Figure 4.14 and Figure 4.15.

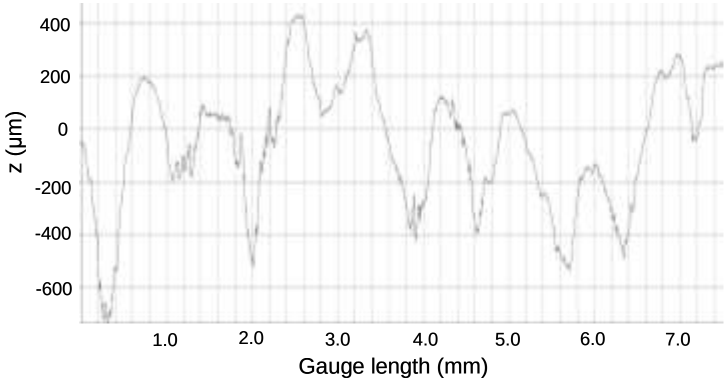

Figure 4.13 2-D profile for EB enhanced surface.

The process is discussed in detail by Buxton et al. (2009). A value P_a = 200 µm was determined for the EB enhanced surface.

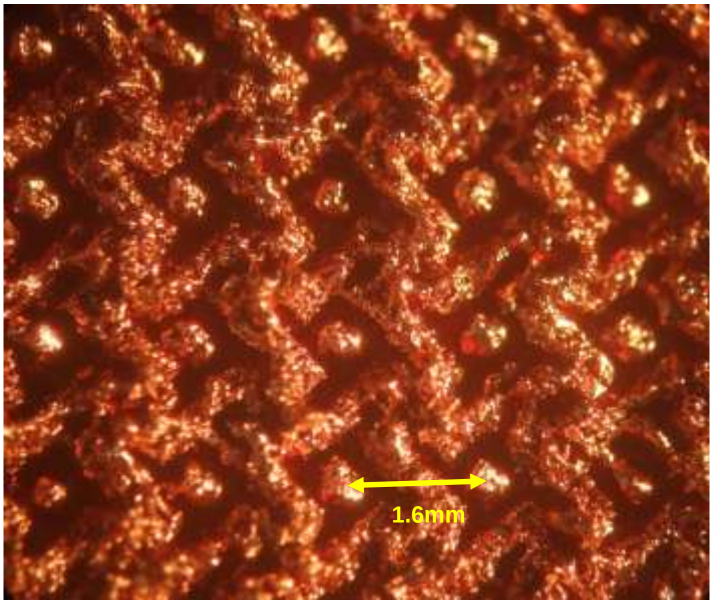

Figure 4.14 Photograph of EB enhanced surface.

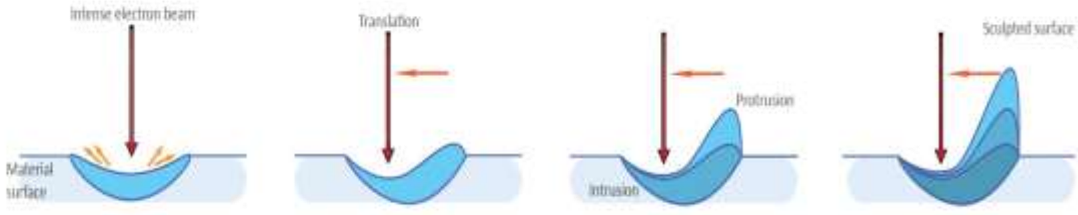

Figure 4.15 Illustration of *Surfi-Sculpt* process.

4.2.5 Sintered surface

The sintering procedure was carried out at Thermacore Europe. The sintered surface was created by sintering copper particles directly onto the upper face of the heater block. To produce the required thickness of particles a custom designed mandrel was clamped to the block, forming a chamber with a uniform depth of 0.5mm.

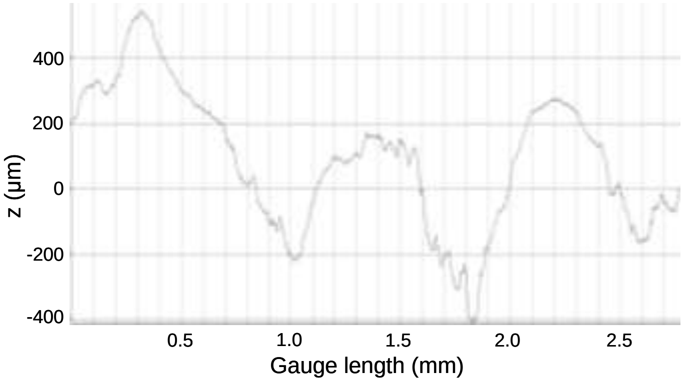

Figure 4.16 2-D profile for sintered surface.

Copper powder was inserted into the chamber and vibrated to ensure the particles were close packed. The assembly was heated in an inert atmosphere to just below the melting point of copper, allowing the particles to fuse together and to the surface of the heater block as a porous metal layer. To enable the material to fuse a secondary gas was used that fluxes with the powder to remove the oxide layer. A value P_a = 144 µm was found for the sintered surface.

4.2.6 Definition of surface profile parameters

As stated in the introduction in the Section 4.2, each of the boiling surfaces tested was characterized by determining the value of the surface profile parameter, P_a, using an ultrasonic stylus technique. Definitions of surface profile parameters are given in BS EN ISO 4287:1998. The following amplitude parameters are evaluated on the basis of a defined assessed two-dimensional profile.

Primary profile parameter, P_a

The primary profile parameter, P_a, is defined as the arithmetic mean deviation of the unfiltered primary profile (i.e. the surface profile without cut-off) from its mean line, see Figure 4.17 (a). The primary profile parameter, P_a, is evaluated over a length l_p in the x-direaction and given by

$$P_a = \frac{1}{l_p}\int_0^{l_p}|z(x)|dx \qquad (for\ primary\ profile) \tag{4.1}$$

The primary profile may include shortwave (surface roughness) and longwave (surface waviness) components.

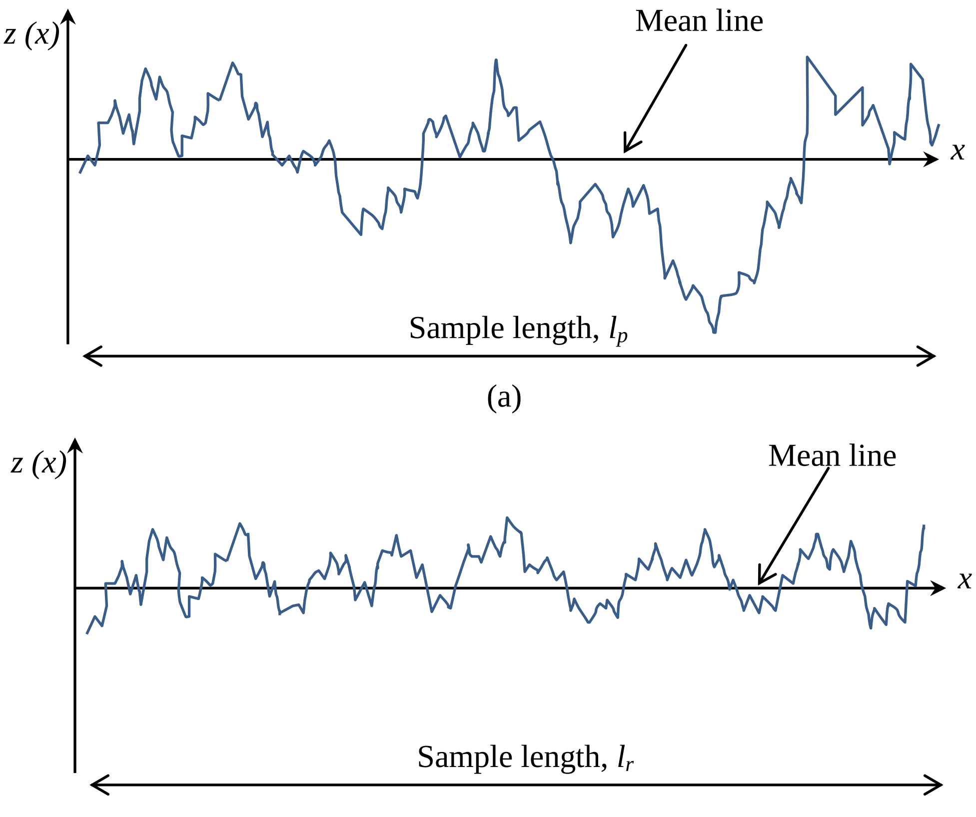

(a)

(b)

Figure 4.17 Illustrative 2D (a) primary profile (b) roughness profile

Roughness profile parameter, *Ra*

The roughness profile parameter, R_a, is defined as the arithmetic mean deviation of the roughness profile (i.e. the profile obtained by suppressing the longwave component of the primary profile using a filter with a cut-off wavelength, λ_c) from the its mean line , see Figure 4.17 (b). The roughness profile parameter, R_a, is evaluated over a length l_r in the x-direction and is given by

$$R_a = \frac{1}{l_r}\int_0^{l_r}|z(x)|dx \qquad (for\ roughness\ profile) \qquad (4.2)$$

The cut-off wavelength λ_c is the wavelength of a sinusoidal profile based on a Gaussian filters (for further details see BS EN ISO 16610-21). Furthermore, in the comparisons of the data from this study with published nucleate boiling correlations presented in Section 6.1.2 P_a values have been substituted for R_a.

4.3 Experimental methodology

4.3.1 Preparatory checks

Following assembly of the test rig the boiling chamber, condenser and interconnecting pipes were pressurized with nitrogen at a pressure of approximately 2.5 bar for a leakage test. A soapy water solution was used to detect leaks. The system was then put under vacuum to evacuate the system down to 0.5 bar absolute pressure. This pressure was observed for two hours. If the pressure did not increase noticeably, the system was considered to be leak proof. On the other hand, if the pressure increased significantly then the system was re-pressurized to 2.5 bar in order to identify and eliminate any leaks. This procedure was repeated until the system became leak proof.

For all the experiments the boiling chamber was charged with R-123 to 80 mm above the boiling surface. It was noted that low boiling point refrigerants, such as R-123, exhibit a tendency to absorb moisture and environmental impurities. Impurities in the liquid can result in the breakdown of the refrigerant molecules when they are subjected to an intense electric field. In addition, results of the boiling experiments will be affected by changes in the fluid properties due to the presence of impurities. In order to ensure the purity, the R-123 was boiled in a separate container and charged into the boiling chamber in vapour form. Furthermore, the deviation of the saturation temperature measured in the boiling chamber from the saturation temperature of pure R123 corresponding to the chamber pressure, defined by equation 4.3, was monitored.

$$\Delta T_{sat} = T_{sat,meas} - T_{sat,P} \tag{4.3}$$

If ΔT_{sat} was greater than ±0.2K, the fluid was drained from the boiling chamber and recharged in vapour form, as described above. This procedure was repeated until $\Delta T_{sat} \leq \pm 0.2$ K. After charging the working fluid into the boiling chamber, the refrigerant was boiled at a moderate heat flux for 30 minutes and any non – condensable gases released were vented through a valve fitted at the top of the condenser.

4.3.2 Test procedure

Test measurements were recorded at saturated pool boiling conditions when the system reached steady state. This was deemed to be when the chamber pressure remained stable for 10 minutes and corresponding saturation temperature remained constant within ±0.2K during this period. The saturation temperature within the chamber was monitored using three Type K thermocouples as discussed above and in section 4.1.1. The pressure in the boiling chamber was controlled by adjusting the cooling water flow rate recirculating through the R-123 condenser. Moreover, the cooling water was chilled using a R-134a refrigeration cycle, as described earlier in Section 4.1.

The following procedures were followed for all the experiments:

1. The rig was allowed to cool down overnight.
2. All test runs were performed for both increasing and decreasing heat flux.
3. The heat flux was increased gradually and incrementally by regulating the voltage supplied to the cartridge heaters.

4. The heat flux, at which the temperature of heater block suddenly increased, was considered to be critical heat flux. Special safety cut-out arrangements were installed to avoid burnout of the copper heater block.
5. The heat flux was decreased gradually and incrementally by reducing the voltage supplied to the cartridge heaters.
6. For each EHD test, the electrode type, the electrode spacing and the magnitude of high-voltage DC electric potential applied were fixed and only the heat flux was varied.

4.3.3 Test programme

Saturated pool boiling experiments without EHD were performed with the five different boiling surfaces, namely: the emery polished, fine sandblasted, rough sandblasted, EB enhanced and sintered surfaces. The emery polished surface was examined at pressures of 1.01, 2 and 4 bar, whereas the other surfaces were tested at 1.01 bar only.

Experiments with EHD were conducted for the emery polished, fine sandblasted, EB enhanced and sintered using all three electrodes, i.e. the mesh electrode, the rod electrode with 5 mm rod spacing and the rod electrode with 8 mm rod spacing. The electrode potential was varied from 0 to 30 kV and the electrode spacing was fixed at 10 mm. All these EHD tests were performed at 1.01 bar saturation pressure.

A second set of EHD experiments was performed to investigate the effect of saturation pressure on pool boiling for the emery polished surface. In these tests, the electrode spacing and the electrode potential were kept constant at 10 mm and 20 kV respectively. Tests were conducted at saturation pressures of 1.01 bar, 2 bar and 4 bar.

A third set of EHD experiments was performing with the rough sandblasted surface and the mesh electrode at a pressure of 1.01 bar. The electrode spacing was initially kept at 20 mm, while the electrode potential was varied from zero to 25 kV in 5kV steps. The effect of electrode spacing was then examined by keeping the electrode potential at 20 kV while the electrode spacing was changed from 20 mm to 40 mm. A detailed list of the experiments conducted in this work is shown in Appendix B.

4.4 Instrumentation and calibration

The instrumentation employed for the measurements required to determine the experimental conditions and to evaluate the boiling surface superheat, heat flux and heat transfer coefficient included several thermocouples and a pressure transducer. A full list of the temperature and pressure measurement sensors and their rig locations is given in Table 4.2.

Table 4.2 Details of temperature and pressure measurement instrumentation.

Location	Sensors	Number
Heater block		
5 mm below boiling surface	Type K thermocouple	6
10 mm below boiling surface	Type K thermocouple	3
15 mm below boiling surface	Type K thermocouple	1
20 mm below boiling surface	Type K thermocouple	1
25 mm below boiling surface	Type K thermocouple	1
30 mm below boiling surface	Type K thermocouple	1
Boiling chamber		
Liquid region	Type K thermocouple	2
Vapour region	Type K thermocouple	1
Vapour region	Absolute pressure transducer	1
Vapour region	Pressure gauge	1
Other rig locations		
Cooling water loop	Type K thermocouple	1
Refrigeration cycle	Type K thermocouple	1

A data acquisition system comprising a 20-channel Solartron IMP (isolated measurement pod) interfaced to a personal computer with National Instrument LabView software was used to handle the measurement, display and logging of the electrical sensor outputs. Readings were acquired at 0.5 s intervals for a period of 10 minutes. For each test condition, a sample of 100 consecutive readings was averaged and the standard deviation was calculated to assess the precision of the measurement. Type K thermocouples (NiCr-NiAl) were selected to measure all temperatures during the experiments on the basis of their thermoelectric characteristics and wide range of application. Each of the separate thermocouple circuits included a cold junction immersed in a Dewar flask filled with melting ice to produce a fixed reference temperature of 0 °C. The emf outputs of the thermocouples were connected to the data logger for signal conditioning, analogue-to-digital conversion and conversion to temperature units.

Calibration of the thermocouples was carried out in an Omega constant-temperature circulating liquid bath. The bath was fitted with a thermo regulator (Model HCTB-3030) consisting of an immersion heater, a circulating pump and a temperature controller. Diphyl THT liquid was used which was circulated by the pump to achieve a uniform temperature within the bath. Calibration was carried out at temperatures between 10 ºC and 120 ºC. All the thermocouples were placed into the bath together with a platinum resistance probe coupled to a precision thermometer (Automatic System Laboratories, F 250MLII). The combined accuracy of this instrument and probe was ±0.025 ºC, as reported by the manufacturer. The required temperature was set on the temperature controller and the calibration bath was allowed to achieve the set temperature. The readings of the thermocouples were recorded when a steady-state condition was achieved, taken to be when the temperature indicated by the precision thermometer did not change for five minutes. Note that the thermocouple calibrations were performed with the thermocouples connected to be data logger. Thus, the calibration process was used to eliminate systematic error sources associated with the thermocouple sensor, the reference junction and the data acquisition system.

The recorded temperatures for each thermocouple were then plotted against the temperatures indicated by the precision thermometer, see

Figure 4.18. The calibration data for each thermocouple was fitted by a best straight line equation using linear regression. For example, the data plotted in

Figure 4.18 for one sample thermocouple were fitted by the following equation:

$$y_1 = 1.0092x_1 + 0.3208 \tag{4.4}$$

where y_1 is the precision thermometer reading (in °C) and x_1 is the thermocouple reading (in °C) indicated by the data logger.

The thermocouple calibration equations, for example equation (4.4), were applied in the LabView programming to correct the temperatures obtained using the standard Type K millivolt-temperature conversion performed by the data logger.

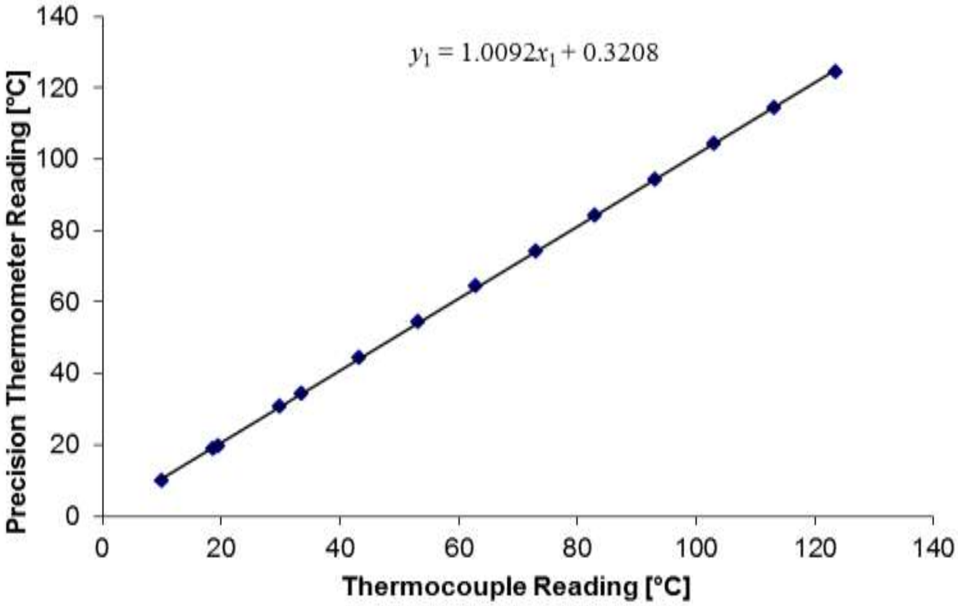

Figure 4.18 Sample thermocouple calibration.

As mentioned in Table 4.2, an absolute pressure transducer (Omega, Model: PX02C1-100A5T) was used to measure the pressure within the boiling chamber. This high-accuracy pressure transducer was quoted as having a linearity of 0.15 % of full-scale output by the manufacturer. The range of the transducer was 0 – 100 psi.

The pressure transducer was calibrated against a dead weight tester. The transducer was supplied with a 24 V DC supply for excitation. The lowest pressure setting available with the dead weight tester was 10 psi. Calibration was carried out over the range from 10 psi to 22 psi in 1 psi increments. Local atmospheric pressure was determined using a mercury barometer and added to the dead weight tester reading to convert the gauge pressure to absolute pressure.

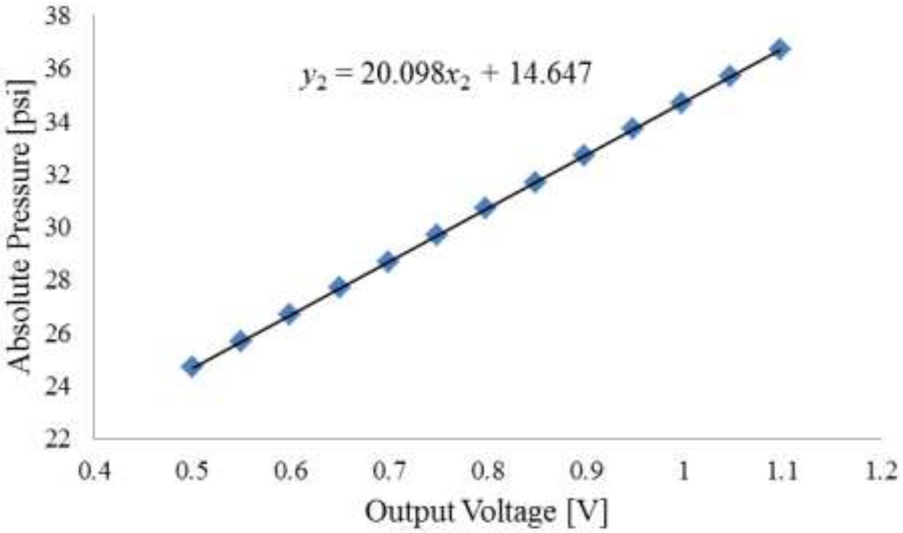

Figure 4.19 Pressure transducer calibration.

The output voltage of the pressure transducer was recorded using the data logger and the data was plotted against the absolute pressure (gauge pressure setting of the dead weight + local atmospheric pressure), see Figure 4.19. The following best straight line was fitted to the calibration data using linear regression:

$$y_2 = 20.098x_2 + 14.647 \tag{4.5}$$

where y_2 is the absolute pressure (psi) and x_2 is the transducer output voltage (V).The pressure transducer calibration equation, equation 4.5, was implemented in the LabView data acquisition programme.

4.5 Summary

This chapter describes the pool boiling facility developed at Brunel University to investigate the effects of surface modification and electrohydrodynamic (EHD) enhancement on pool boiling of R-123. The experimental rig incorporated a completely new boiling chamber that was designed and fabricated during this study. Detailed drawings of the boiling chamber and the heater block incorporating the test boiling surface are shown in Figure 4.3 and Figure 4.7. For the EHD tests, high-voltage uniform and non – uniform electric fields of up to 3 MV/m were generated using one mesh and two rod electrodes. The electrodes and associated adjustable support system are described in section 4.1.2.

Saturated pool boiling conditions were maintained within the boiling chamber using cooling water and R-134a refrigeration cycle. The temperature and pressure conditions in the chamber were monitored using Type K thermocouples and an absolute pressure transducer respectively. The outputs of all the thermocouples and the pressure transducer were recorded by a data acquisition system comprising a data logger unit interfaced to a computer using LabView software. All the sensors were calibrated to minimize systematic errors in the experimental measurements.

Experiments were performed using five different boiling surfaces; an emery polished surface, a fine sandblasted surface, a rough sandblasted surface, an EB enhanced surface and a sintered surface. The preparation and characterization of the boiling surfaces is discussed in section 4.2. The results of the experiments will be discussed in Chapter 6.

Chapter 5 Data Reduction & Validation

This chapter describes in Section 5.1 the data reduction calculation method used to obtain the heat flux and heat transfer coefficient from the experimental measurements. The associated analysis performed to estimate the uncertainties in these derived values is set out in Section 5.2. Furthermore, the experimental method and results were validated using repeatability tests for each of the five surfaces tested, which are represented in Section 5.3. Additional validation of the results by comparisons with published pool boiling data and nucleate boiling correlations is deferred to Section 6.1.

5.1 Data reduction

As described in Chapter 4, each test boiling surface was formed by the horizontal upper face of an electrically heated, cylindrical copper block. The heat flux and heat transfer coefficient at the boiling surface were determined using temperature measurements obtained from a vertical array of thermocouples inserted into the block at regular 5 mm intervals below the boiling surface.

The heater block was heavily insulted insulated by a PTFE sleeve to minimize the radial heat loss. Five additional thermocouples were inserted into the heater block 5 mm below the boiling surface to monitor the circumferential temperature uniformity.

It was observed that the variation in the readings obtained from these extra thermocouples was less than 0.1 K, which is within the uncertainty range of the thermocouple measurements. Moreover, the rate of heat loss from the heater block is discussed in Section 5.5. The heat loss was found to be approximately 5 % of the electrical power supplied to the cartridge heaters in the block when the test rig was operating in the nucleate boiling regime. It was assumed that most of this loss occurred in the lower part of the block and that heat flow in the upper part of the block was one-dimensional and axially upward.

The energy balance across the boiling surface was can be depicted as shown in Figure 5.1.

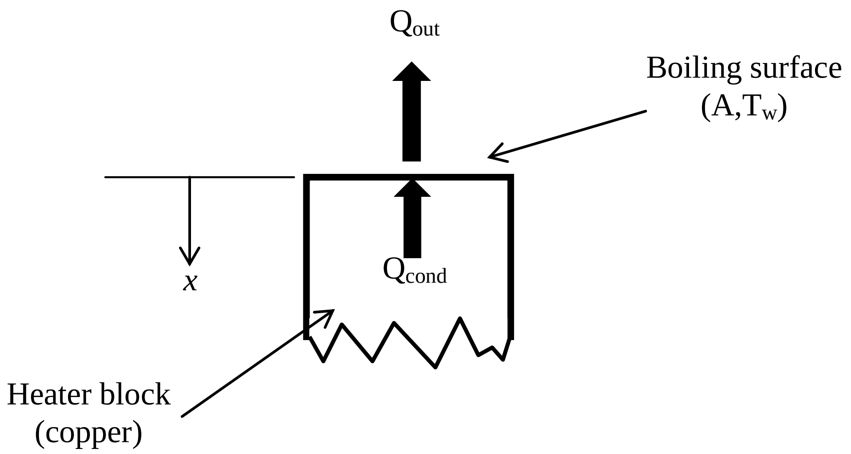

Figure 5.1 Energy balance across the boiling surface.

According to the one-dimensional form of Fourier's law of conduction in copper heater block at the boiling surface (*x*=0) is given by

$$Q_{cond} = k_{copper} A_s \left(\frac{\mathrm{d}T}{\mathrm{d}x}\right)_{x=0} \tag{5.1}$$

where A_s is the area of the boiling surface.

The vertical temperature gradient (dT/dx) in equation (5.1) was found using the readings obtained from thermocouples in the heater block at distances x = 5 mm, 10 mm, 15 mm, 20 mm, 25 mm and 30 mm below the boiling surface. A sample set of temperature measurements is plotted against the distance x below the boiling surface, in Figure 5.2 .

For each test, the temperature distribution in the upper section of the heater block was fitted by a linear regression line of the general form $y = mx+c$. The slope m of the line determined the required temperature gradient in the heater block. That is

$$m = \frac{dT}{dx} \tag{5.2}$$

Furthermore, the intercept value c gave the temperature at the boiling surface.

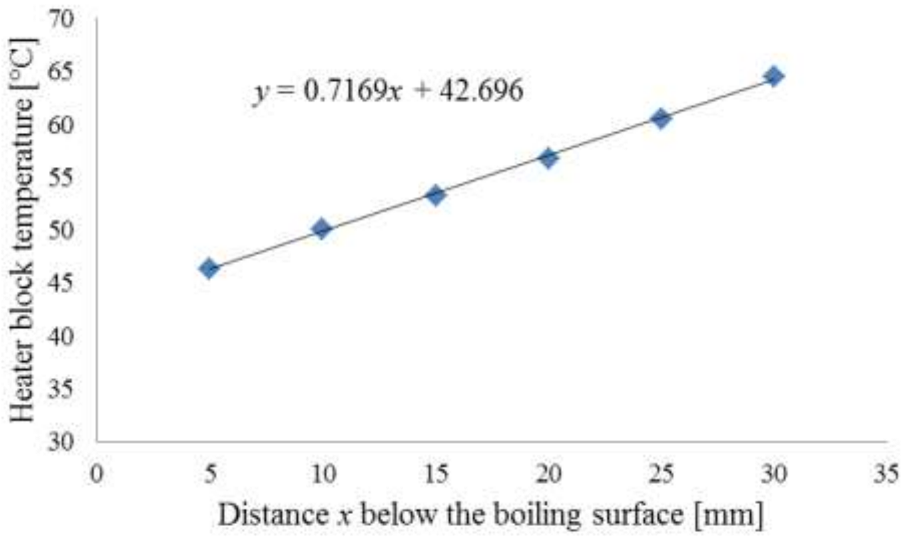

Figure 5.2 Sample temperature variation in the heater block.

The rate of heat transfer from the boiling surface of the heater block to the refrigerant can be expressed as

$$Q_{out} = hA_s(T_w - T_{sat}) \tag{5.3}$$

where h and T_w denote the heat transfer coefficient and the temperature at the boiling surface, respectively, and T_{sat} is the saturation temperature of the boiling refrigerant, which was measured by a thermocouple immersed in the liquid region of the boiling chamber, as discussed in Section 4.1.1.

Applying the principle of conservation of energy to the boiling surface (see Figure 5.1) for steady-state conditions we must have

$$Q_{in} = Q_{out} \tag{5.4}$$

By substituting equations (5.1) and (5.3) into equation (5.4) we obtain

$$k_{copper} A_s \frac{dT}{dx} = h A_s (T_w - T_{sat}) \tag{5.5}$$

After cancellation of A_s from the both sides, equation (5.5) can be rearranged for the heat transfer coefficient, *h*, as follows:

$$h = \frac{k_{copper}}{(T_w - T_{sat})} \left(\frac{dT}{dx}\right)_{x=0} \tag{5.6}$$

The corresponding expression for the heat flux, q, can be obtained directlyfrom equation (5.1), as follow:

$$q = \frac{Q}{A} = k_{copper} \left(\frac{dT}{dx}\right)_{x=0} \tag{5.7}$$

5.2 Uncertainty analysis

Equations (5.6) and (5.7), derived in Section 5.1, are the main data reduction equations used for calculating h and q, respectively. Both of these equations require the temperature gradient (d*T*/d*x*) in the heater block to found. This section explains how in the thermocouple measurements were used to calculate the uncertainties for *h* and *q*.

The uncertainties in the values of the heat transfer coefficient and heat flux were calculated using equations (5.8) and (5.9) respectively, see Coleman and Steele (1989).

$$\left(\frac{U_h}{h}\right)^2 = \left(\frac{U_m}{m}\right)^2 + \left(\frac{U_k}{k}\right)^2 + \left(\frac{U_{Tw}}{T_w - T_{sat}}\right)^2 + \left(\frac{U_{Tsat}}{T_w - T_{sat}}\right)^2 \tag{5.8}$$

$$\left(\frac{U_q}{q}\right)^2 = \left(\frac{U_m}{m}\right)^2 + \left(\frac{U_k}{k}\right)^2 \tag{5.9}$$

where U_i represents each of the uncertainties associated with the variable appearing in equations (5.8) and (5.9).

The uncertainty in k was considered to be negligible compared to the other sources of uncertainty and was therefore ignored. The other variable include the saturation temperature of the boiling refrigerant (T_{sat}), the temperature at the boiling surface (T_w) which is equal to the intercept c of the temperature variation in the heater block and m is equal to the temperature gradient within the heater block, i.e. $m = dT/dx$

According to Coleman and Steele (1989) measurement errors can be divided into two categories, namely; bias or systematic error, B_i , and precision or random error, P_i, which can be combined to give the uncertainty U_i as follows:

$$U_i = \sqrt{(B_i)^2 + (P_i)^2} \tag{5.10}$$

Bias error is the fixed error in a measurement and can be reduced using calibration. For the thermocouples, the remaining bias error was taken as quoted for the precision thermometer used as a calibration standard.

The precision error of an experimental measurement can be estimated by taking a sample of N readings and is given by

$$P_i = t_s S_i \tag{5.11}$$

where t_s is a factor dependent on the size of the sample. $N \geq 30$ then it can be assumed that

$t_s = 1.96$ with a confidence level of 95 %, see Coleman and Steele (1989). In equation (5.11), S_i is the standard deviation of the sample, defined as

$$S_i = \sqrt{\frac{1}{N-1}\sum_{j=1}^{N}(T_j - \bar{T})^2} \tag{5.12}$$

where $\bar{T}$ is the mean value given by

$$\bar{T} = \frac{1}{N}\sum_{j=1}^{N} T_j \tag{5.13}$$

5.2.1 Uncertainty in thermocouple readings

The readings of six thermocouples were used in order to calculate the heat flux and heat transfer coefficient, as discussed earlier in Section 5.1. These thermocouples were located at distances of 5 mm, 10 mm, 15 mm, 20 mm, 25 mm and 30 mm below the boiling surface.

Table 5.1 shows sample calculation to estimate the combined uncertainty U_i for each thermocouple. The bias error B_i is fixed and taken as the error contributed by the precision thermocouples calibration. Table 5.1 also lists the mean value $\bar{T}$ and the standard deviation S_i of the sample of readings taken for each thermocouple.

Table 5.1Sample calculations for estimation of error in the value of thermocouple.

Thermocouple number	Xi (m)	T_{avg} [°C]	Bi[K]	Pi[K]	U_{Ti}[K]
1	0.005	45.163	0.025	0.0266	0.03650
2	0.010	47.862	0.025	0.0183	0.03098
3	0.015	50.172	0.025	0.0112	0.02739
4	0.020	52.707	0.025	0.0217	0.03310
5	0.025	55.512	0.025	0.0195	0.03171
6	0.030	58.477	0.025	0.0177	0.03063

5.2.2 Uncertainty in the heater block temperature gradient and surface temperature

As discussed in section 5.1, both the heat flux and the heat transfer coefficient involved calculation of the temperature gradient within the copper block, see Figure 5.2. This is done by fitting a linear regression equation through the N (X_i,T_i) data pairs of thermocouple locations (X_i) and associated temperature measurement (T_i) of the form.

According to the equation of the line

$$T = mX + c \tag{5.14}$$

The linear regression finds the values of the slope m and intercepts c that minimizes the sum of the squares of the derivations of the data points from the regression line. It can be shown, see Coleman and Steele (1989),

$$m = \frac{dT}{dX} = \frac{B}{A} \tag{5.15}$$

and

$$c = \frac{C}{A} \tag{5.16}$$

where

$$A = N \sum_{i=1}^{N} X_i^2 - \left[\sum_{i=1}^{N} X_i\right]^2 \tag{5.17}$$

$$B = N \sum_{i=1}^{N} (X_i T_i) - \sum_{i=1}^{N} X_i \sum_{i=1}^{N} T_i \tag{5.18}$$

and

$$C = \sum_{i=1}^{N} X_i^2 \sum_{i=1}^{N} T_i - \sum_{i=1}^{N} X_i \sum_{i=1}^{N} X_i T_i \tag{5.19}$$

Thus, both the slope *m* and the intercept c depend on all values of X_i and T_i. In function from this is written as follows:

$$m = f(X_1, X_2 - - - X_N, T_1, T_2 - - - - T_N)$$

$$c = f(X_1, X_2 - - - X_N, T_1, T_2 - - - - T_N)$$

The uncertainty in the slope m is given by

$$\begin{gathered}\frac{U_m^2}{m^2} = \\ \left[\frac{T_1}{m}\frac{\partial m}{\partial T_1}\right]^2\left[\frac{U_{T1}}{T_1}\right]^2 + \left[\frac{T_2}{m}\frac{\partial m}{\partial T_2}\right]^2\left[\frac{U_{T2}}{T_2}\right]^2 + ---+ \\ \left[\frac{T_N}{m}\frac{\partial m}{\partial T_N}\right]^2\left[\frac{U_{TN}}{T_N}\right]^2 + \left[\frac{X_1}{m}\frac{\partial m}{\partial X_1}\right]^2\left[\frac{U_{X1}}{X_1}\right]^2 + \left[\frac{X_2}{m}\frac{\partial m}{\partial X_2}\right]^2\left[\frac{U_{X2}}{X_2}\right]^2 + ---+ \\ \left[\frac{X_N}{m}\frac{\partial m}{\partial X_N}\right]^2\left[\frac{U_{XN}}{X_N}\right]^2\end{gathered} \tag{5.20}$$

where

$$\frac{\partial m}{\partial T_i} = \frac{NX_i - \sum_{i=0}^{N} X_i}{A} \tag{5.21}$$

and

$$\frac{\partial m}{\partial X_i} = \frac{\left[NT_i - \sum_{i=0}^{N} T_i\right]A - 2\left[NX_i - \sum_{i=0}^{N} X_i\right]B}{A^2} \tag{5.22}$$

Similarly, the uncertainty in the intercept value c is given by the following expression:

$$\begin{gathered}\frac{U_c^2}{c^2} = \\ \left[\frac{T_1}{c}\frac{\partial c}{\partial T_1}\right]^2\left[\frac{U_{T1}}{T_1}\right]^2 + \left[\frac{T_2}{c}\frac{\partial c}{\partial T_2}\right]^2\left[\frac{U_{T2}}{T_2}\right]^2 + ---+ \\ \left[\frac{T_N}{c}\frac{\partial c}{\partial T_N}\right]^2\left[\frac{U_{TN}}{T_N}\right]^2 + \left[\frac{X_1}{c}\frac{\partial c}{\partial X_1}\right]^2\left[\frac{U_{X1}}{X_1}\right]^2 + \left[\frac{X_2}{c}\frac{\partial c}{\partial X_2}\right]^2\left[\frac{U_{X2}}{X_2}\right]^2 + ---+ \\ \left[\frac{X_N}{c}\frac{\partial c}{\partial X_N}\right]^2\left[\frac{U_{XN}}{X_N}\right]^2\end{gathered} \tag{5.23}$$

where

$$\frac{\partial c}{\partial T_i} = \frac{\sum_{i=0}^{N} X_i^2 - X_i \sum_{i=0}^{N} X_i}{A} \tag{5.24}$$

and

$$\frac{\partial c}{\partial X_i} = \frac{\left[2X_i \sum_{i=0}^{N} T_i - \sum_{i=0}^{N} T_i X_i - T_i \sum_{i=0}^{N} X_i\right]A - 2\left[NX_i - \sum_{i=0}^{N} X_i\right]C}{A^2} \tag{5.25}$$

Tables 5.2 and 5.3 show sample calculations of the uncertainties in heat flux and heat transfer coefficient for high and low values of heat transfer, 207.3 kW/m^2 and 4,68 kW/m^2 respectively. The variations with heat flux of the uncertainty in h and q are shown in Figures 5.3 and 5.4 respectively. It should be noted that the uncertainty in the thermocouple locations was estimated to be U_{xi} = 0.0004 m.

Table 5.2 Sample calculation of uncertainties in heat flux and heat transfer coefficient (207.25 kW/m^2).

Thermocouple number	X_i (m)	U_{Xi} (m)	T_i (K)	U_{Ti}(K)
1	0.005	0.0004	315.6157	0.033961
2	0.01	0.0004	319.2592	0.034186
3	0.015	0.0004	319.3501	0.030292
4	0.02	0.0004	323.153	0.028851
5	0.025	0.0004	326.2981	0.038247
6	0.03	0.0004	329.2015	0.042734
			U_q (%)	U_h (%)
			1.045374	2.585328765

Table 5.3 Sample calculations of uncertainties in heat flux and heat transfer coefficient (4.68 kW/m^2).

Thermocouple number	X_i (m)	U_{Xi} (m)	T_i (K)	U_{Ti}(K)
1	0.005	0.0004	304.127	0.03192
2	0.01	0.0004	304.174	0.03230
3	0.015	0.0004	304.163	0.03165
4	0.02	0.0004	304.246	0.03113
5	0.025	0.0004	304.317	0.03175
6	0.03	0.0004	304.39	0.03332
			U_q (%)	U_h (%)
			11.646	11.868

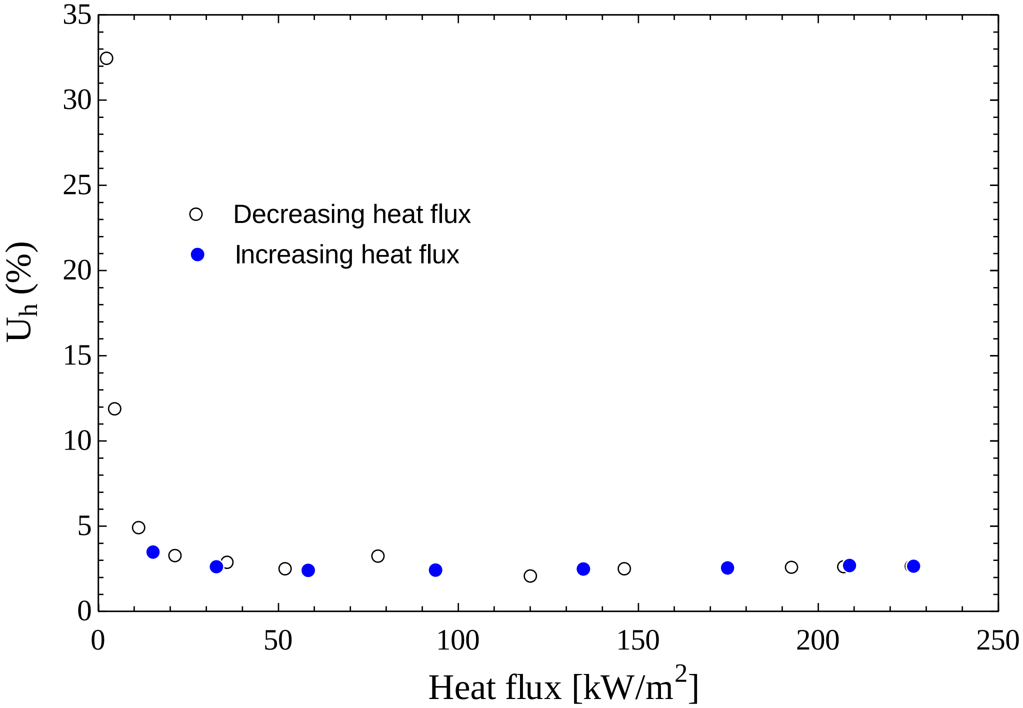

Figure 5.3 Variations of percentage uncertainty in the heat transfer coefficient.

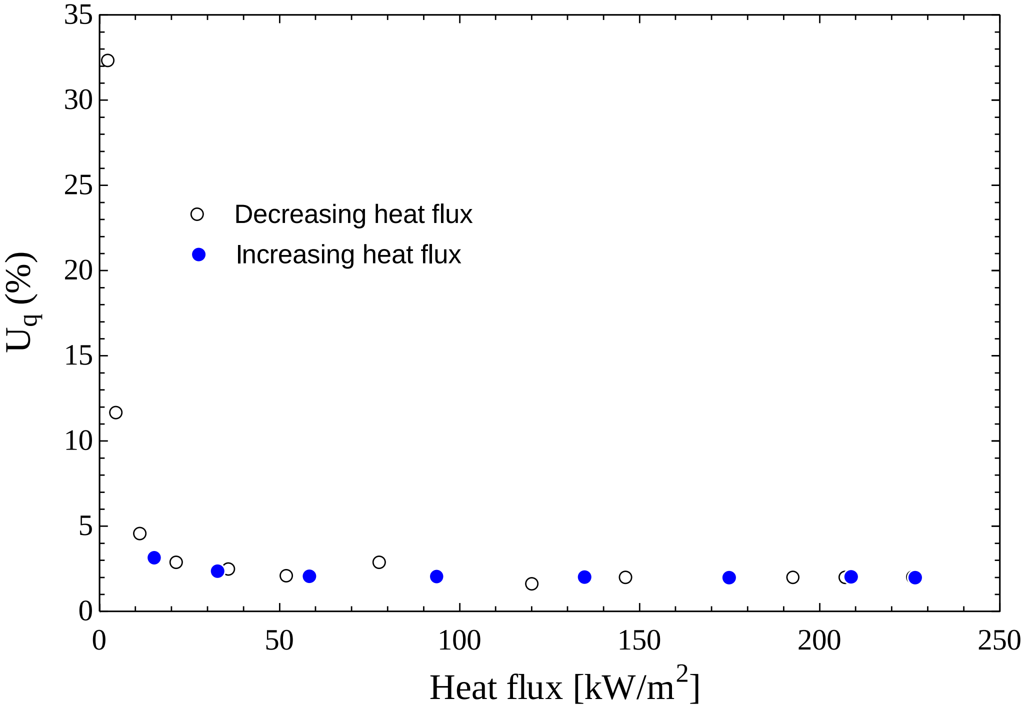

Figure 5.4 Variations of percentage uncertainty in the heat flux.

5.3 Data validation

The experimental methods used in this work were validated by examining the variability of the measurements. This was done by conducting repeatability tests. Tests runs were repeated for all five boiling surfaces, namely the emery polished, fine sandblasted, rough sandblasted, EB enhanced and sintered surfaces. The results of the original and repeat test runs are shown in Figure 5.5 to 5.9, respectively. Only small changes can be seen between the two runs, demonstrating that the demonstrating experiments were repeatable. In addition, the experimental results collected in this study have been compared with predictions made using published nucleate boiling correlations, as described in Section 6.1.2.

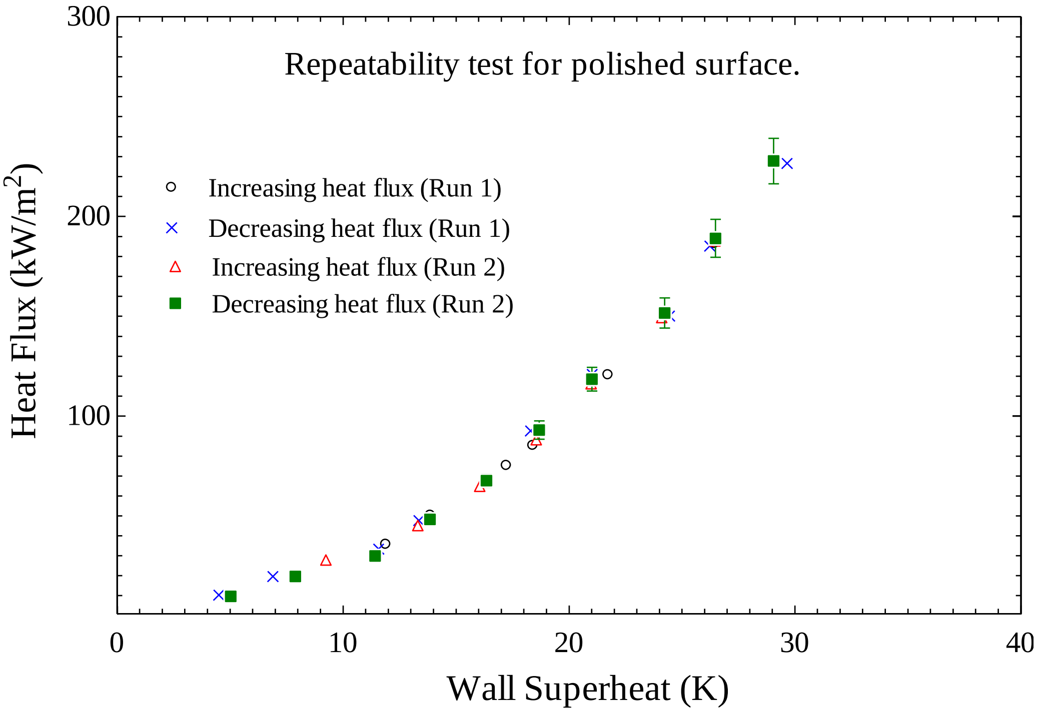

Figure 5.5 Repeatability tests for emery polished surface at 1.01 bar saturation pressure, without EHD.

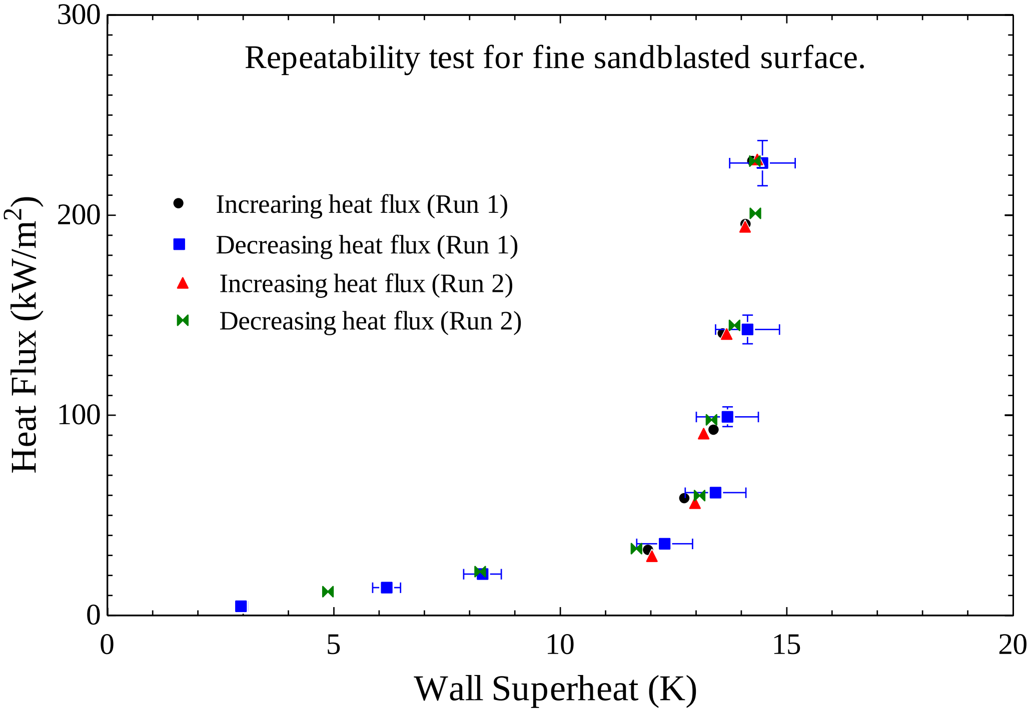

Figure 5.6 Repeatability tests for fine sandblasted surface at 1.01 bar saturation pressure, without EHD.

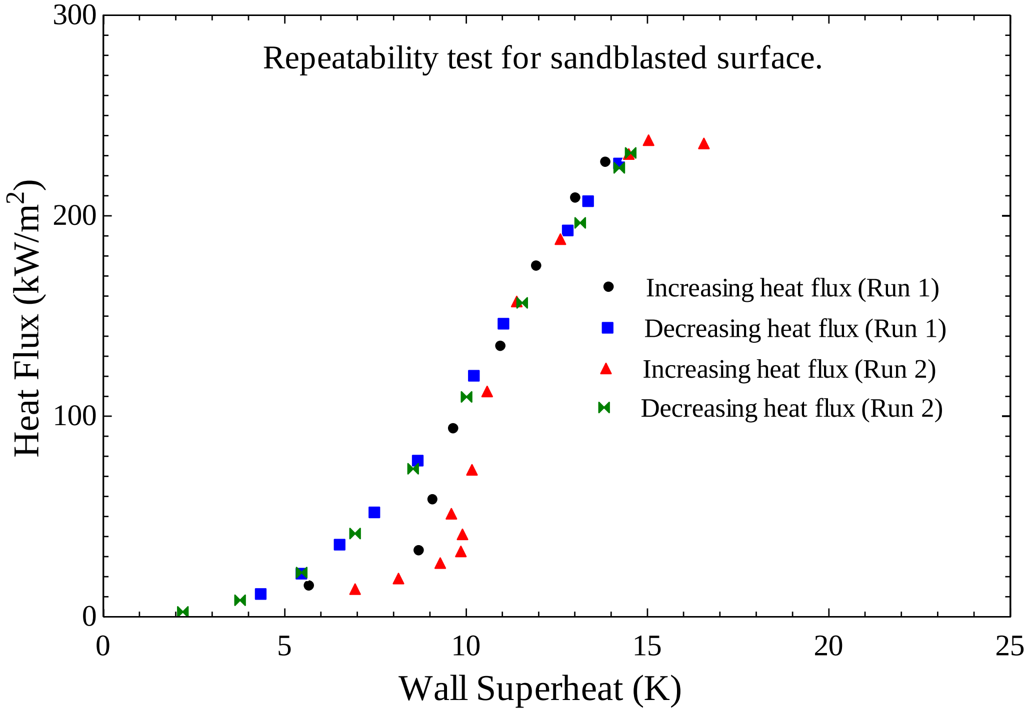

Figure 5.7 Repeatability tests for rough sandblasted surface at 1.01 bar saturation pressure, without EHD.

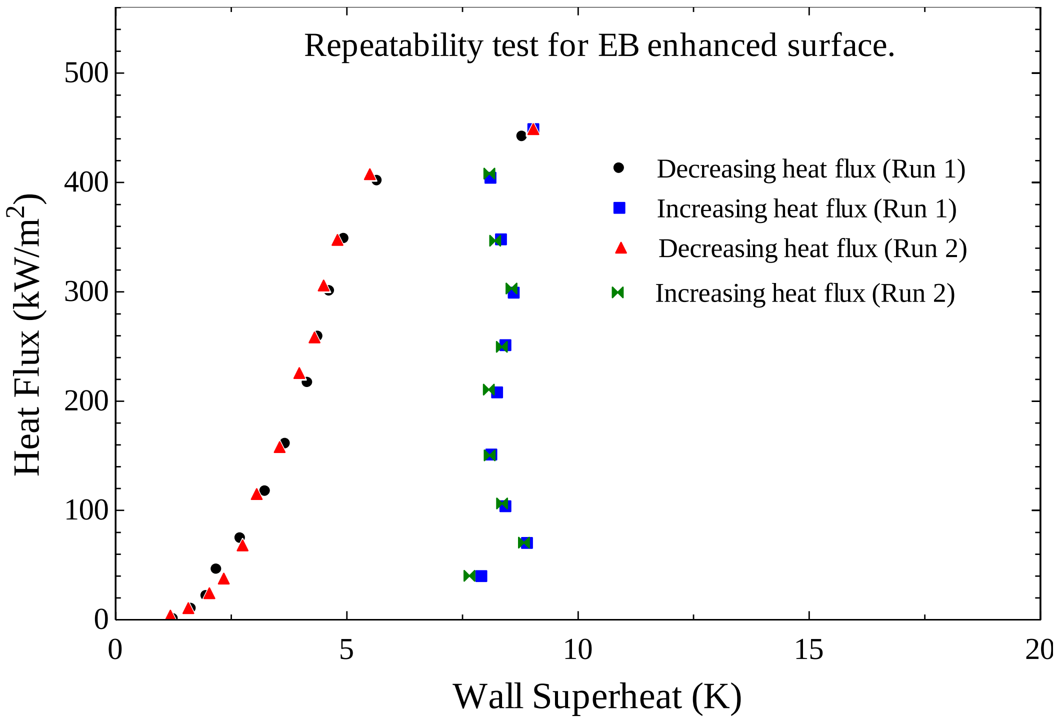

Figure 5.8 Repeatability tests for EB enhanced surface at 1.01 bar saturation pressure, without EHD.

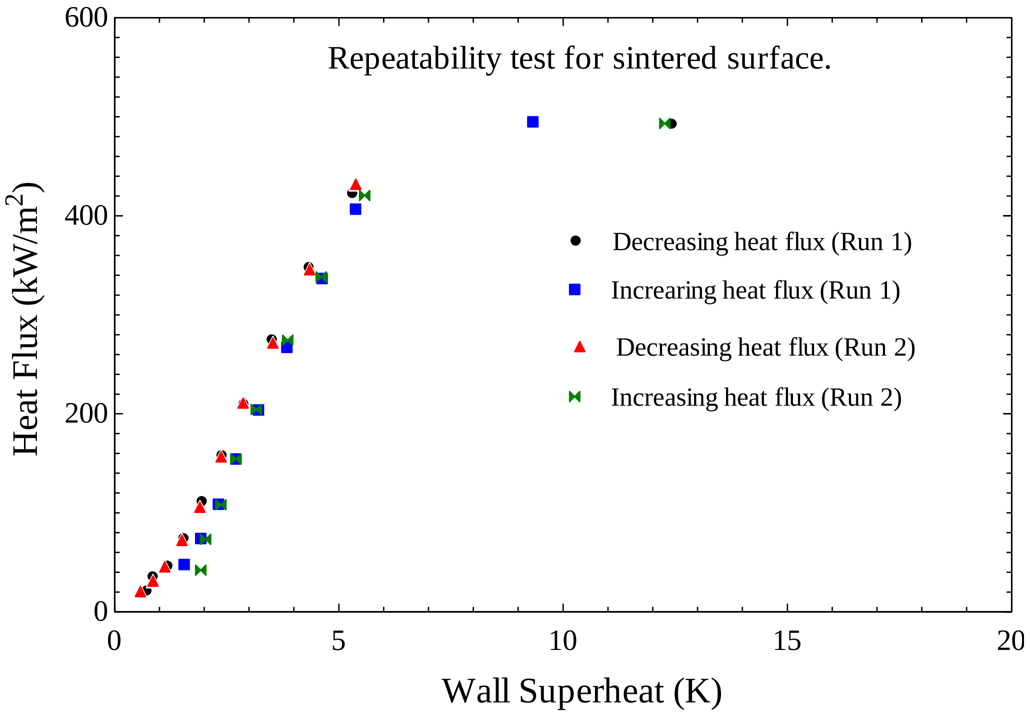

Figure 5.9 Repeatability tests for sintered surface at 1.01 bar saturation pressure, without EHD.

5.4 Power consumption due to application of electric field

The power consumption due to the application of a high-intensity electric field in the EHD tests can be compared with the rate of heat transfer at the boiling. The maximum current flow measured between the electrode and boiling surface was 0.06 mA when a 30 kV electric potential was imposed, as shown in Figure 5.10. The corresponding power dissipation was 1.8 W maximum. It can be deduced that the maximum power consumed in generating the electric field was small compared with the heat transfer rate at boiling surface, except at low heat flux values.

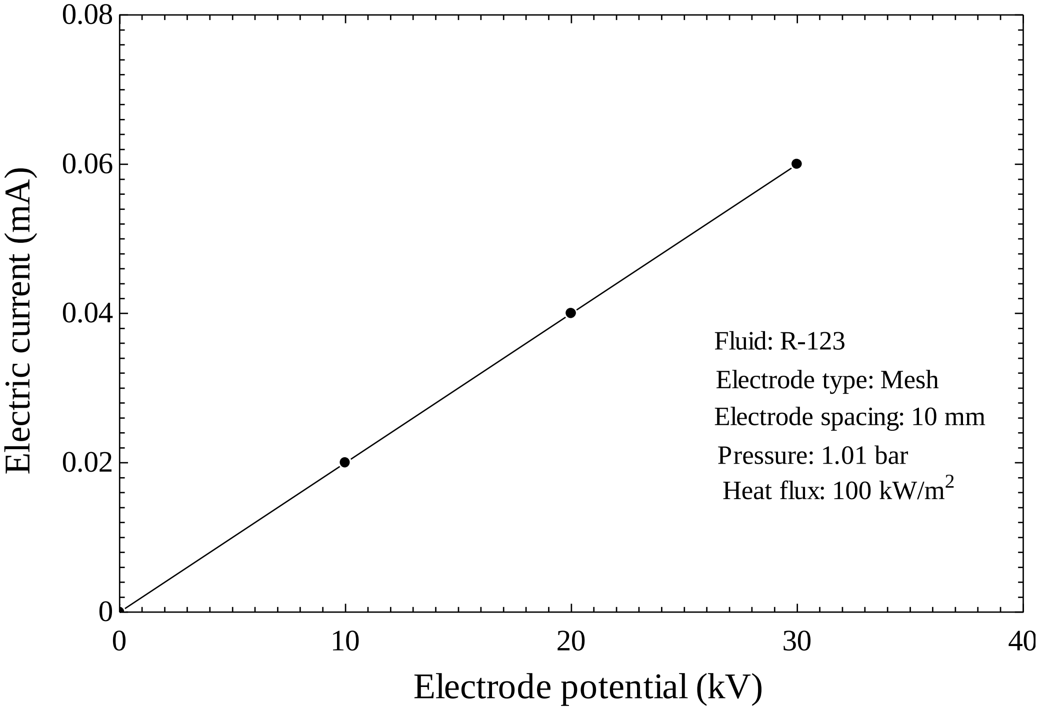

Figure 5.10 Electric current versus electrode potential due to application of high-intensity electric field.

5.5 Heat loss in heater block

The steady-state energy balance model for the heater block is illustrated in

Figure 5.11 . The rate of heat input to the heater block from the electrical cartridge heater is given by

$$Q_{input} = V_{input} I \tag{5.26}$$

The rate of heat output from the boiling surface of the heater block is equal to the product of the surface area and heat flux, assumed to be uniform and unidirectional that is

$$Q_{output} = q A_s \tag{5.27}$$

where the heat flux *q* is given by the equation (5.7)

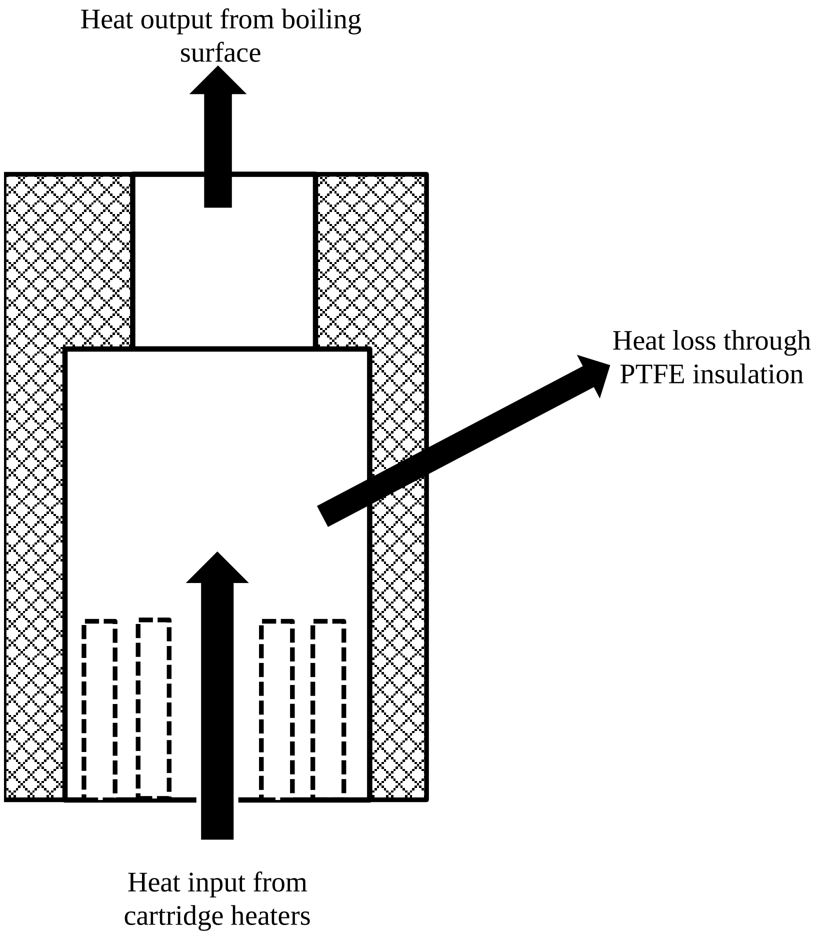

Figure 5.11 Heat balance around the heater block.

If follows that the rate of heat loss from the heater block through the surrounding PTFE insulation sleeve is given by

$$Q_{loss} = Q_{input} - Q_{output} \tag{5.28}$$

The heat loss can be expressed in percentage terms as follows:

$$\%\ Heat\ loss = \frac{Q_{input} - Q_{output}}{Q_{input}} \times 100 \tag{5.29}$$

The energy balance for the heater block was evaluated for all the experiments conducted in this study. The maximum heat loss in the nucleate boiling region was found to be approximately 5%. The heat loss data for tests performed with the emery polished surface without EHD is presented in Figure 5.12. At low heat flux, when temperature difference were small and natural convection was the principle heat transfer mode, the % heat loss increased significantly as shown in Figure 5.12.

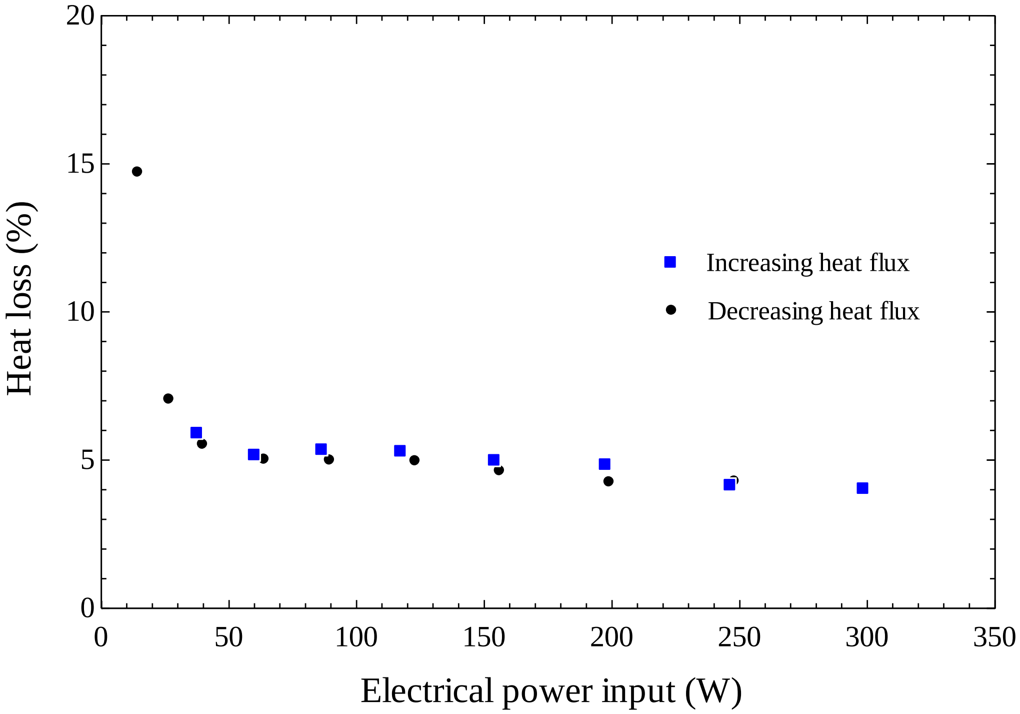

Figure 5.12 Heat loss from the heater block.

5.6 Summary

The work presented in this chapter can be summarized as follows:

- Data reduction equations were derived for calculating the heat flux and heat transfer coefficient from the experimental measurements.
- The uncertainty associated with the results for heat transfer coefficient and heat flux were analyzed and found to be 5 % and 4 % (maximum), respectively, in the nucleate boiling regime.
- Validation of the experimental data was demonstrated by repeatability tests; the experiments were shown to be repeatable.
- The electrical power dissipated in generating the high-intensity electric field form the EHD tests was shown to be small compared to the heat transfer rate; around 1.8 W maximum.
- Heat loss from the heater block was examined and found to be approximately 5 % of the heating power input for operation within nucleate boiling regime.

Chapter 6 Results and discussion

The experimental results will be presented and discussed in this Chapter following after the experimental procedure and data validation in Chapter 4 and 5. The first objective was the experimental work was to investigate the effect of surface modification on the pool boiling using a flat horizontal upward faced copper surface. As discussed in the Chapter 4, five different types of modified surfaces were examined during present studies namely; emery polished, fine sandblasted, rough sandblasted, EB (abbreviated for electron beam) enhanced and sintered surfaces. The emery polished surface was considered as the bench mark to calculate the enhancement in the value of the heat transfer coefficient for the other four modified surfaces. The 2 D profiles (discussed in Section 4.2) of all five modified surfaces were used to relate the pool boiling results with surface microstructures.

The second objective was to study the effect of high intensity electric field (uniform and non- uniform) in pool boiling. It can be observed from the Chapter 3 that the electrode geometry and the magnitude of the high intensity electric field have strong influence on the two phase heat transfer. As discussed earlier in Chapter 4, three kinds of electrodes were used to provide the high intensity electric field, namely; mesh electrode, rod electrode with 5 mm rod spacing and rod electrode with 8 mm rod spacing. The electric field was varied either by regulating the electric potential value at the power supply or by changing the electrode spacing (i.e. the distance between the electrode and the boiling surface). In the majority of the experiments, the electric potential was varied from 0 to 30 kV while the electrode spacing was kept constant at 10 mm. In order to observe the effect of electrode spacing on EHD (abbreviation for electrohydrodynamics) pool boiling, the distance between the electrode and the boiling surface was set at 20 mm and 40 mm while the electric potential was kept constant at 20 kV.

The third objective of the experiments was to assess the effect of saturation pressure on pool boiling with and without EHD. The saturation pressure was varied from 1.01 to 2 and 4 bar. During EHD experiments at the high saturation pressure, the electric field was provide using the mesh electrode and the electric potential was kept constant at 20 kV. As discussed earlier in Chapter 5, the saturation pressure within the boiling rig was monitored using a pressure transducer which was mounted in the vapour space and three Type K thermocouples were used to monitor the saturation temperature of the boiling fluid. Of these three thermocouples, one was placed in the vapour region and other two were placed in the liquid region. Furthermore, the combined effect of the surface modification and uniform electric field, surface modification and non – uniform electric field and uniform electric field and saturation pressure were also presented. Finally, the bubble growth pattern was monitored using high speed camera (800 frames per second).

All the experiments were performed from the convective heat transfer regime to the critical heat flux for both increasing and decreasing heat flux. The results for decreasing heat flux were used in the calculation in order to avoid any hysteresis (except in the hysteresis Sections 6.1.3 and 6.4.4). As discussed earlier in Section 3.5.3 the electrical properties of the boiling fluid also play an important role in the pool boiling enhancement under high intensity electric field conditions especially electric permittivity and the charge relaxation time. R – 123 was selected as the working fluid due to its electrical properties, i.e. the relative electric permittivity is 3.42 and charge relaxation time was 0.9×10^{-3} sec reported by Zaghdoudi and Lallemand (2005), as discussed in Section 3.2.

6.1 Pool boiling and surface modification

6.1.1 Effect of surface modification on pool boiling

In this section the effect of surface modification on pool boiling of R-123 is presented. The experimental data obtained in this study and earlier work for pool boiling of R-123 at 1.01 bar pressure on copper surfaces prepared using different methods, namely, emery polishing, fine and rough sandblasting, electron beam surface enhancement and sintering. The spread of the boiling curves in Figure 6.1 demonstrates that surface modification has an appreciable effect on the variation of heat flux with wall superheat. Experimental results reported by Zaghdoudi and Lallemand (2005) and Hristov et al. (2009) for pool boiling of R-123 at 1.01 bar on emery treated copper surfaces are also plotted in Figure 6.1 for comparison.

The results obtained for the emery polished surface with P_a = 0.044 μm are in reasonably good agreement with the measurements of Hristov et al. (2009) who utilized an earlier version of the apparatus shown in Figure 4.2 at Brunel University and a boiling surface polished using P1200 emery paper followed by an ultra-fine abrasive paper. In contrast, the results of Zaghdoudi and Lallemand (2005) exhibit an earlier rise of heat flux with wall superheat for a surface prepared using No. 600 emery paper. It should be noted that No. 600 emery paper is much coarser than grade P1200 and, therefore, would be expected to produce larger cavities and deeper peak-to-valley roughness in the surface, with greater potential for bubble formation at lower wall superheats. Beyond this, it is difficult to compare the emery polished surface results obtained by the present authors and Hristov et al. (2009) and those of Zaghdoudi and Lallemand (2005) because surface roughness was not quantified in the latter two studies.

The experimental results shown in Figure 6.1 for the two sandblasted boiling surfaces are characterized by different values of the primary profile parameter: P_a = 0.099 μm for the fine sandblasted surface and P_a = 3.5 μm for the rough sandblasted surface. As heat flux and wall superheat increase, the fine sandblasted surface data are initially in-line with the curve for the emery polished surface when natural convection is the principal heat transfer mode. At a wall superheat slightly above 12 K the fine sandblasted results diverge sharply upwards with the onset of nucleate boiling. This enhancement of boiling heat transfer is consistent with the presence of larger cavities on the rougher surface, i.e. P_a = 0.099 µm compared to 0.044 µm for the polished surface. It should be mentioned that the roughness value reported here for the emery polished surface may be slightly high due to surface scratches within the gauge length over which P_a was evaluated, as indicated in Figure 4.9.

In the case of the rough sandblasted surface (P_a = 3.5 µm) the boiling curve is further shifted to the left in Figure 6.1, compared with the curves for the fine sandblasted and emery polished surfaces. This pattern illustrates a progressive decrease, with increase of the surface roughness, of the wall superheat needed to dissipate a given heat flux by nucleate pool boiling on these surfaces. Inspection of the two-dimensional surface profiles, in Figures 4.11 and 4.12, show that the microstructure of the rough sandblasted test surface had much deeper valleys, higher peaks and a wider distribution of cavity sizes than the fine sandblasted test surface. Hence, the rough sandblasted surface microstructure would be more effective, both in a vapour trapping role and in promoting bubble formation over a range of wall superheats.

The EB enhanced surface and the sintered surface both achieved a large improvement in heat transfer compared to the conventional emery polished and sandblasted surfaces, as evidenced by their much steeper boiling curves in Figure 6.1. Application of the EB surface modification process causes the growth of a pattern of protrusions above the original surface level, accompanied by associated cavities in the substrate. This macrostructure is reflected by the large value of the primary profile parameter, P_a = 200 µm, measured for the EB enhanced surface, significantly larger than the P_a values determined for the other surfaces tested. The effectiveness of the cavities formed by the EB surface enhancement technique in trapping vapour is believed to be the primary reason for the large observed augmentation of heat transfer in nucleate boiling.

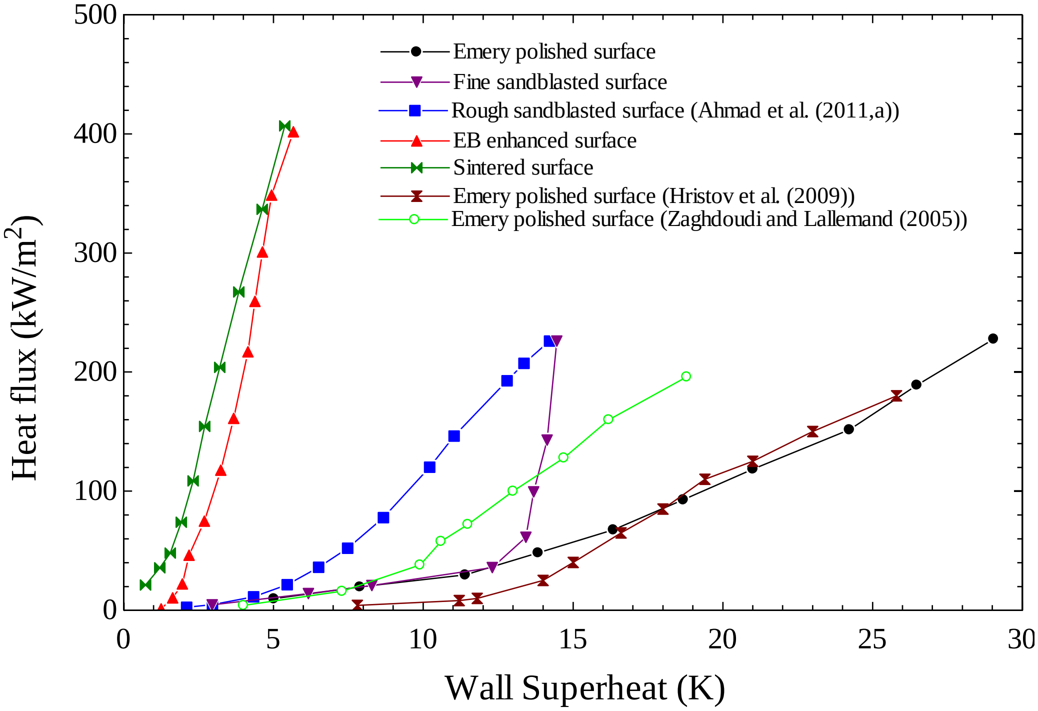

Figure 6.1 Boiling curves for modified surfaces, at *P* = 1.01 bar.

In addition, the increase in the heat transfer surface area provided by the protrusions may be a secondary factor contributing to an increase in the base heat flux. The strongest influence of surface modification on pool boiling heat transfer is displayed by the sintered surface results shown in Figure 6.1, albeit the surface (P_a = 144 μm) was smaller than for the EB enhanced surface. The sintering process forms a porous metallic (copper) structure on the heater block surface of assumed uniform porosity and cavity distribution, providing vapour entrapment a volume and a large number of active nucleation sites.

As discussed earlier in Chapter 2, that Kim et al. (2008) performed pool boiling experiments on finned surface using PF5060 as a working fluid. They reported the value of heat transfer coefficient as 11.26 kW/m^{2}K at 200 kW/m^2. Similar observations were reported by Yu and Lu (2007), when they performed pool boiling experiments using FC-72 as a working fluid on finned boiling surface and they reported the heat transfer coefficient as 14.8 kW/m^{2}K at 200 kW/m^2. In the present case, the EB enhance surface showed higher heat transfer coefficient, i.e. 50 kW/m^{2}K at 200 kW/m^2. In other words, the present EB enhanced surface showed higher heat transfer results as compared to previously used finned surfaces. Furthermore, the manufacturing traditional method for the finned structure is a costly and time consuming process while using the *Surfi-Sculpt* method is much less time consuming.

The heat transfer coefficient augmentation can be expressed as the ratio $h_{\text{modified surface}}/h_{\text{polished surface}}$. Trend lines of this factor are compared in Figure 6.2 for heat fluxes up to 220 kW/m^2. For the sintered, EB enhanced, rough sandblasted and fine sandblasted test surfaces the heat transfer coefficients were found to increase by around 9, 6.5, 2 and 1.5 times the value for the emery polished surface, respectively.

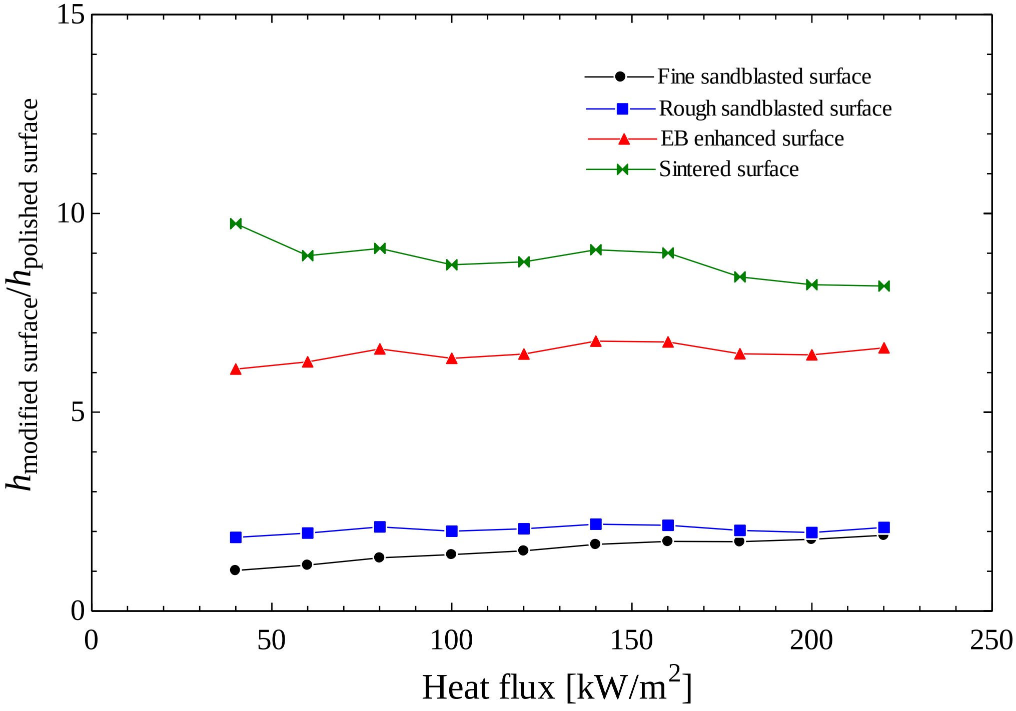

Figure 6.2 Augmentation of heat transfer coefficient due to surface modification

6.1.2 Comparison of pool boiling results with correlations

Experimental heat transfer coefficients obtained in this study for pool boiling of R-123 on the emery polished surface, at pressures of 1.01 bar, 2 bar and 4 bar, are compared with predictions based on published nucleate boiling correlations in

Figures 6.3, 6.4 and 6.5, respectively. Similar comparisons are presented in Figure 6.6 and 6.7 for the results obtained at 1.01 bar with the fine sandblasted surface and the rough sandblasted surface, respectively. These surfaces cover a range of roughness with primary profile parameter values P_a = 0.044 μm (emery polished), P_a = 0.099 μm (fine sandblasted) and P_a = 3.5 μm (rough sandblasted). As previously mentioned, P_a values were substituted for the average surface roughness R_a in the prediction calculations, although it is noted that the roughness of the heater surface is not used in all of the correlation equations considered here, i.e. the correlations predicted by Jung et al. (2003),Yagov (2009) and Shekriladze (2008).

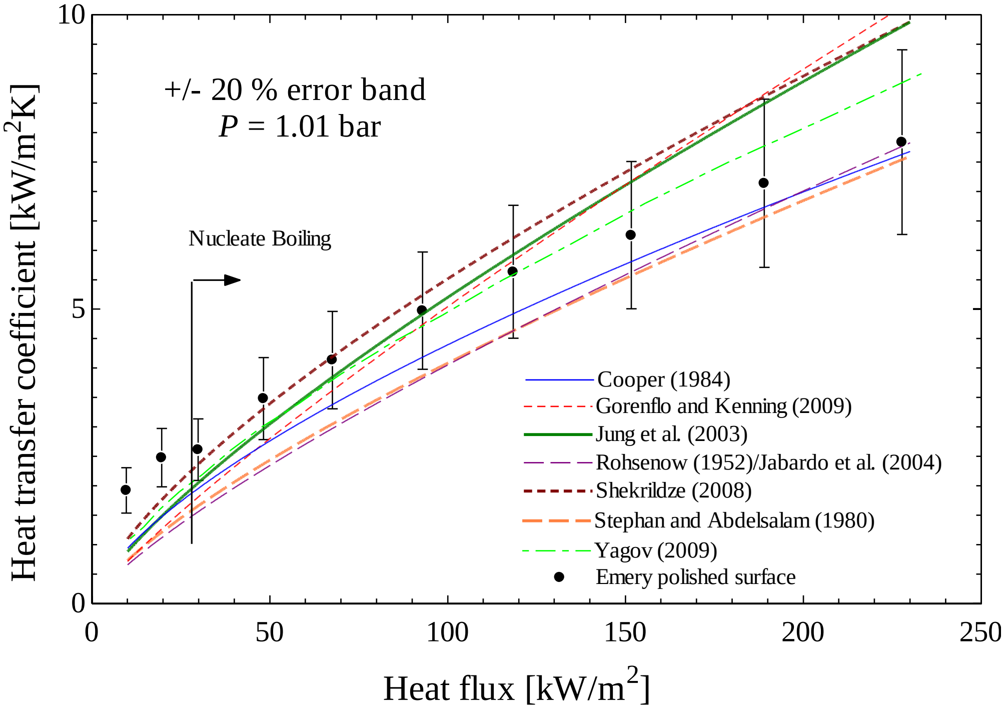

Figure 6.3 Comparison of pool boiling results of emery polished surface with published correlations, at P = 1.01 bar

The correlation proposed by Stephan and Abdelsalam (1980) for refrigerants, given by equation (2.6), is based on a regression analysis of published data covering a wide range of reduced pressure and includes thermal, transport and wetting properties of the fluid. An average surface roughness $R_{p,\text{old}}$ = 1 μm (as discussed in Section 2.9) was assumed in the development of this correlation. It was suggested that equation (2.6) should be multiplied by $R_{p,\text{old}}^{0.133}$ to account for the influence of surface roughness values other than 1 μm. When this factor is applied with the Stephan-Abdelsalam correlation, as plotted in Figure 6.4, the calculated heat transfer coefficients under predict the experimental results for the emery polished surface at P = 1.01 bar, only falling within the ±20% error band at higher heat fluxes. If the surface roughness factor is not included, the predictions (not shown) are within ±20% of the experimental data in the mid-to-low heat flux range, but are too high at high heat fluxes and too low at low heat fluxes. In the simple correlation developed by Cooper (1984) , the properties of the boiling fluid are represented in terms of the reduced pressure P_r and the molecular mass M only. The heater surface roughness measure $R_{p,\mathrm{old}}$ is included in the exponent on P_r. The Cooper correlation predicted line in Figure 6.4, calculated using equation (2.8) with C = 95, exhibits slightly closer agreement with the P = 1.01 bar experimental results than that of the Stephan-Abdelsalam correlation and remains within the ±20% error band apart from at the lowest heat flux values. The Jung et al. (2003) correlation for halogenated refrigerants is a modified form of the Stephan and Abdelsalam (1980) correlation and, following Cooper (1984) , introduces the reduced properties P_r and T_r. However, their equation does not include any term to account for the heater surface condition. Predicted values calculated with the Jung et al. correlation are within ±20% of the polished surface experimental data for P = 1.01 bar, except at the extremes of the heat flux range, i.e. they are lower than the experimental values at low heat flux region and higher at the high heat flux region

Heat transfer coefficients predicted from the correlations and the experimental results for the emery polished surface, at test pressures of 2 bar and 4 bar, are compared in Figure 6.4 and 6.5 respectively. It is immediately evident that the correlations discussed above, due to Stephan and Abdelsalam (1980), Cooper (1984) and Jung et al. (2003), show better agreement with the higher pressure data, particularly at P = 2 bar, than was obtained for the 1.01 bar condition.

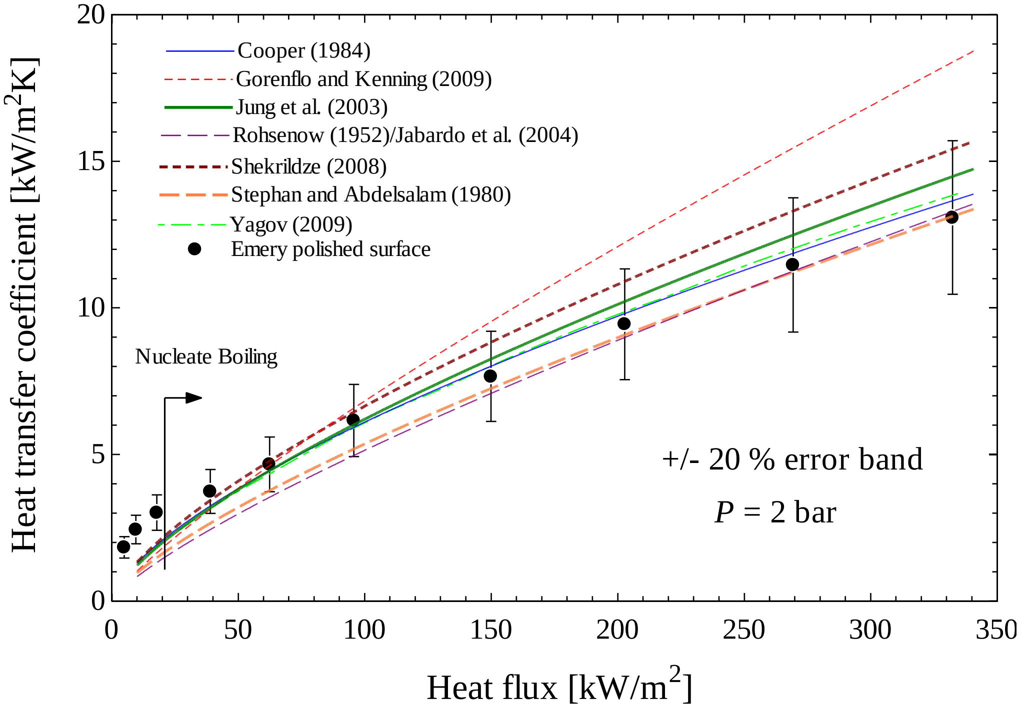

Figure 6.4 Comparison of pool boiling results of emery polished surface with published correlations, at *P* = 2 bar.

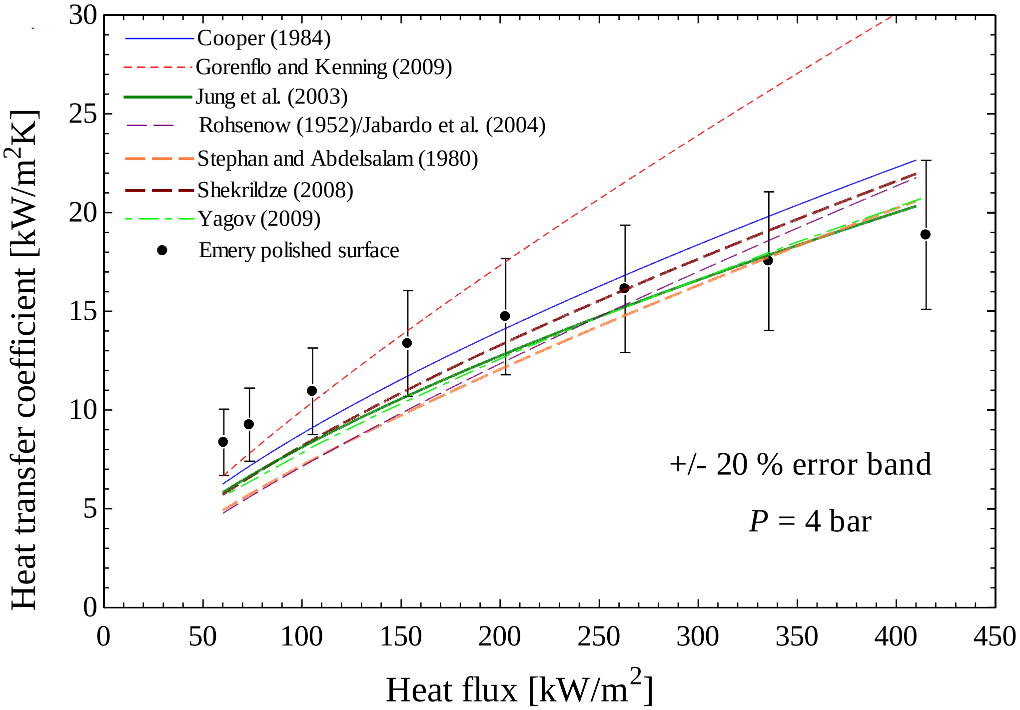

Figure 6.5 Comparison of pool boiling results of emery polished surface with published correlations, at *P* = 4 bar.

The heat transfer prediction equation developed by Yagov (2009) is based on an approximate theoretical model of nucleate boiling and includes empirically determined constants and the boiling fluid properties. Predictions made with this equation show close agreement with the experimental data for the emery polished surface for 1.01 bar and 2 bar, but slightly less good agreement at 4 bar; see Figures 6.3, 6.4 and 6.5.

The calculation method of Gorenflo and Kenning (2009) involves non-dimensional functions representing the relative influences of heat flux, reduced pressure, fluid properties and heating surface roughness and material properties on the heat transfer coefficient relative to that for a fictitious reference fluid. For P = 1.01 bar, the predicted coefficients are within the range of values given by the other correlations, as shown in Figure 6.3. However, at 2 bar and 4 bar, the predicted values only agree at low heat fluxes, but then deviate increasingly as the heat flux increases, as can be seen in Figures 6.4 and 6.5. This behaviour is presently unexplained and requires further investigation.

Shekriladze (2008) developed a nucleate boiling correlation with the average effective radius at the mouth of nucleation cavities as the characteristic linear size. As mentioned earlier, Shekriladze (2008) suggested using a value r_o = 5 μm as typical of commercial surfaces. Since r_o was unknown for the emery polished and sandblasted surfaces tested in this work, a constant value of 5 μm was used in order to evaluate equation (2.22). Nevertheless, the predicted heat transfer coefficients are mostly within ±20% of the experimental results for the emery polished surface at all pressures, except at low heat fluxes.

Jabardo et al. (2004) employed curve fits of experimental data for refrigerants (including R-123) to modify the exponents and the surface-fluid coefficient C_{sf} in the original Rohsenow (1952) nucleate boiling correlation. An expression, equation (2.28), was developed for calculating C_{sf} as a function of surface roughness and reduced pressure. Predictions made using the modified correlation are comparable with those of the Stephan and Abdelsalam (1980) correlation (including the surface roughness factor).

It has been already been discussed in Section 2.9 that Cooper (1984) proposed nucleate boiling correlation on the basis of reduced pressure, i.e. he converted the physical properties as a function of reduced pressure, P_r. Moreover, the power of reduced properties in equation (2.8), i.e. n is the function of heater surface properties. It can be noted that as the pressure increases the physical of the boiling liquid changes. These changes in physical properties appear as the reduced pressure in the correlation, which incorporate with the average surface roughness. Due to the approximations in the conversion of physical properties into reduced pressure, the deviation in the predicted data from the experimental results can be noticed, see Figures 6.3 to 6.5.

The correlation predicted by Stephan and Abdelsalam (1980) was basis on regression analysis of published experimental data. It can be noticed that the predicted correlation, see equation (2.6), consisted of the pressure dependent physical properties of boiling liquid and vapour. It has been analyzed that the ratio of vapour and liquid density one of the most pressure sensitive terms. It is shown in the Appendix A that when the pressure increases from 1.01 to 2 bar, the vapour density increased by the factor of 1.9 while the liquid density decreased by a factor of 0.96 (i.e. remains almost constant). The second term which is sensitive towards the pressure change is the bubble diameter, D_b see equation (2.7). Moreover, the bubble diameter is the function of vapour and liquid densities, surface tension and liquid contact angle. Stephan and Abdelsalam (1980) proposed the liquid contact angle as 35°. It can be concluded by the above discussion that vapour properties are more pressure sensitive than the liquid properties. Similar observation can be noticed in the correlation predicted by Jung et al. (2003), who modified the correlation of Stephan and Abdelsalam (1980). They introduced reduced pressure and temperature to in the proposed correlation, see equation (2.20). Furthermore, the heat flux is powered by the c_1, which is the function of vapour and liquid densities and reduced pressure. Due to introduction of reduced pressure, reduced temperature and c_1, the predicted boiling curve of Jung et al. (2003) moves up as compared to that of Stephan and Abdelsalam (1980), see Figure 6.4. Whereas, Yagov (2009) and Shekriladze (2008) introduced the physical properties of the both boiling liquid and vapour to predict the heat transfer coefficient in their correlations, see Section 2.9. The most pressure sensitive properties are reduced temperature, liquid density, specific enthalpy of vaporization and surface tension. As discussed earlier, Yagov (2009) did not introduce the heater surface condition in his proposed correlation but Shekriladze (2008) suggested that the radius of the mouth of boiling cavity contribute towards the heat transfer coefficient during nucleate boiling. Rohsenow (1952) correlation basically composed of physical properties and surface fluid factor C_{sf} which is the function of reduced pressure and average surface roughness. It can be noticed from the Figures 6.3 to 6.5 that the predicted data of Jung et al. (2003),Yagov (2009), Rohsenow (1952) and Shekriladze (2008) remained within 20 % error range when the heat flux as compared to experimental results at high heat flux, but found under predicted at low heat flux. As discussed earlier in Section 2.9 that Gorenflo and Kenning (2009) proposed nucleate boiling correlation on the basis of reduced pressure, fluid properties, heat flux and heater surface properties. It can be noticed that the data obtained from Gorenflo and Kenning (2009) correlation deviates largely from the experimental results, see Figures 6.3 to 6.5. It may be due the assumptions used to develop correlation, i.e. they use reference fluid to make the quantities dimensionless see equations (2.11 to 2.19). They assumed that value of heat flux and reduced pressure as 20 kW/m^2 and 0.1 respectively, for reference fluid. While, the reference average surface roughness was 0.4 µm. These assumptions may lead to large deviation in the predicted and experimental results.

Figures 6.3 to 6.5, and the discussion above, relate to the emery polished surface characterized by the single P_a value of 0.044 µm. It is of interest to examine how the same correlations perform in predicting heat transfer coefficients for the fine and rough sandblasted surfaces. The predictions from the Jung et al. (2003), Yagov

(2009) and Shekriladze (2008) correlations for the sandblasted surfaces shown in Figures 6.6 and 6.7are identical to those for the emery polished surface shown in Figure 6.3. This is because the conditions (saturated, P = 1.01 bar), and hence fluid properties, were the same in all cases and because surface roughness does not appear in these correlations. Also, a constant value of r_o was assumed in the Shekriladze correlation. In the case of the fine sandblasted surface (see

Figure 6.6), all the predictions fall below the experimental data. In Figure 6.2, the heat transfer coefficient augmentation for the fine sandblasted surface was around 1.5 times that of the emery polished surface, for an increase in P_a from 0.044 µm to 0.099 µm, whereas the dependence of h on surface roughness in the Stephan-Abdelsalam and Gorenflo-Kenning equations follows a weaker $h \propto R_a^{4/15}$ relationship.

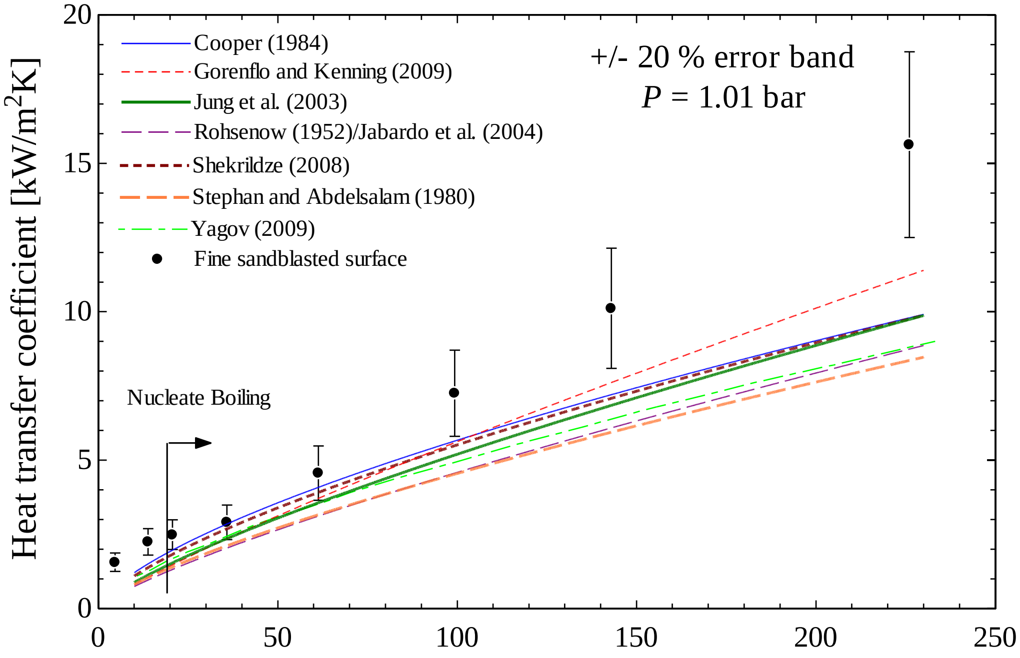

Figure 6.6 Comparison of pool boiling results of fine sandblasted surface with published correlations, at P = 1.01 bar.

Furthermore, it is known that sandblasted surfaces have a uniform granular microstructure with a larger size distribution of cavities, or roughness range, than produced by emery grinding, see Luke (2009). Consequently, the use of R_a alone may not be adequate to fully represent the surface condition.

The comparison for the rough sandblasted surface (P_a = 3.5 µm) in Figure 6.7 shows large deviations between the predictions and the experimental data, except for the Jabardo et al. (2004) modification of the Rohsenow (1952) correlation and the Gorenflo and Kenning (2009) correlation.

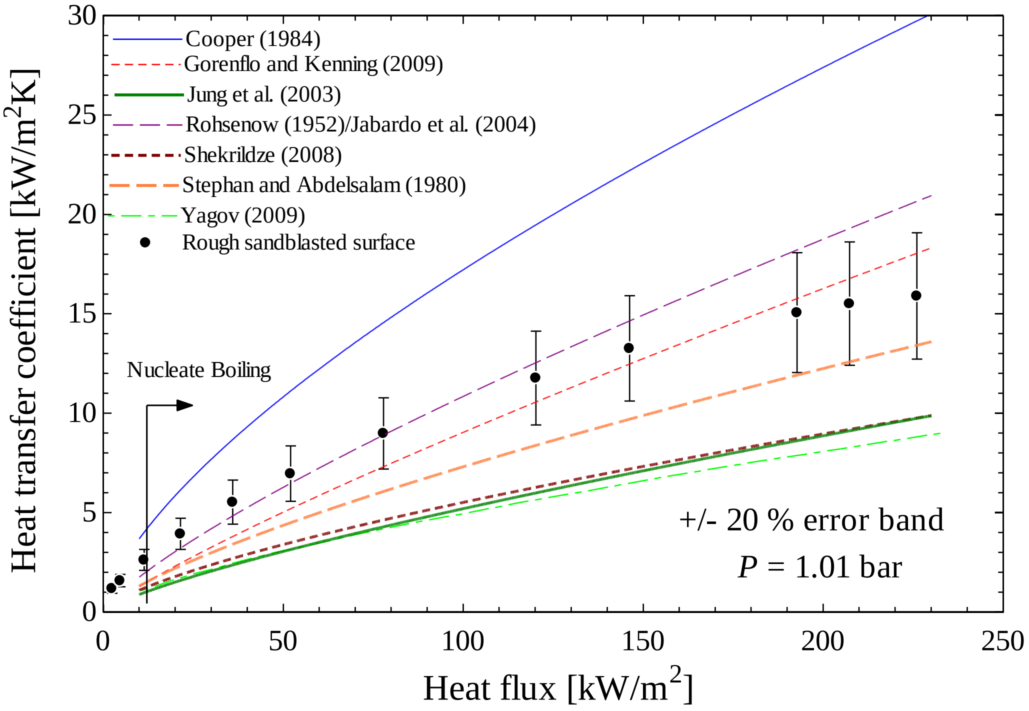

Figure 6.7 Comparison of pool boiling results of rough sandblasted surface with published correlations, P = 1.01 bar.

6.1.3 Effect of surface modification on boiling hysteresis

In this section, the effect of surface conditions on pool boiling hysteresis is presented, this was also discussed earlier in Chapter 2 where it was noted that the boiling hysteresis depends upon the characteristics of boiling liquid and shape of cavities located at the heater surface. It means that the deactivation of surface cavities (explained in Section 2.7) is responsible for boiling hysteresis. To investigate this phenomenon, the boiling surface kept overnight in boiling chamber, in order to cool the boiling surface, (see Figure 4.1) and pool boiling tests were performed for both increasing and decreasing heat flux. These tests were carried out for all five modified surfaces, i.e. emery polished, fine sandblasted, rough sandblasted, EB enhanced and sintered surfaces, at 1.01 bar saturation pressure.

The emery polished and fine sandblasted surfaces had no indication of boiling hysteresis, as shown in Figures 6.8 and 6.9, while the rough sandblasted and the EB enhanced surfaces showed boiling hysteresis, see Figures 6.10 and 6.11 . Zhou et al. (2004) explained (as discussed in Section 2.7) this fact on the basis of active and inactive nucleation sites. There are two factors which are responsible for boiling hysteresis. Firstly, the characteristic of the heating surface, i.e. the heating surface contains the cavities which have large wedge angles and as a result of this the boiling liquid replaces the vapour or gas phase from these cavities. This process makes these cavities inactive for boiling and large wall superheat is required to make them active. A second important factor is the liquid contact angle, which affects activation and deactivation of the surface cavities during boiling process. It has already been discussed earlier in Section 2.7 that a highly wetting liquid has a small contact angle, which results in the depletion of vapours or gas phase from the surface cavities. Furthermore, due to removal of the vapours or gas phase, these cavities do not remain active for nucleation.

On the emery polished and fine sandblasted surfaces, there are large number of small active cavities (also have small wedge angles), which behave in similar way during increasing and decreasing heat flux. While, the EB enhanced and rough sandblasted surfaces contain deeper cavities with large wedge angles as a result of this, most of the cavities are flooded by the liquid and become inactive for boiling. A large superheat is required for their activation. On the other hand, during decreasing heat flux, these cavities remain active and wall superheat can be low for a specific value of heat flux as compared to increasing heat flux. Similar observations were reported by Hristov et al. (2009), as discussed earlier in Section 3.5. They performed pool boiling experiments on R-123 using emery polished surface, which was similar to the emery polished surface used in present study. No hysteresis was reported by Hristov et al. (2009).

The observations of Figure 6.12 indicated that the sintered surface showed TD (temperature deviation) hysteresis (discussed earlier in Section 2.7) due to the large number of cavities present. The distribution of these cavities is more uniform as compared to conventional surfaces (i.e. emery polished and sandblasted) and most of them are active for nucleation during increasing heat flux. The cavities, which are not active for nucleation become active according to the vapour propagation phenomenon (see Figure 2.13 (a)). In the vapour propagation phenomenon, the vapour grows from the active nucleation site and the front of this growing vapour also covers the adjacent cavities and makes them active for nucleation. With decreasing heat flux, all these surface cavities remain active at low heat flux and result in deviation of boiling curves of increasing and decreasing heat flux, see Figure 6.12.

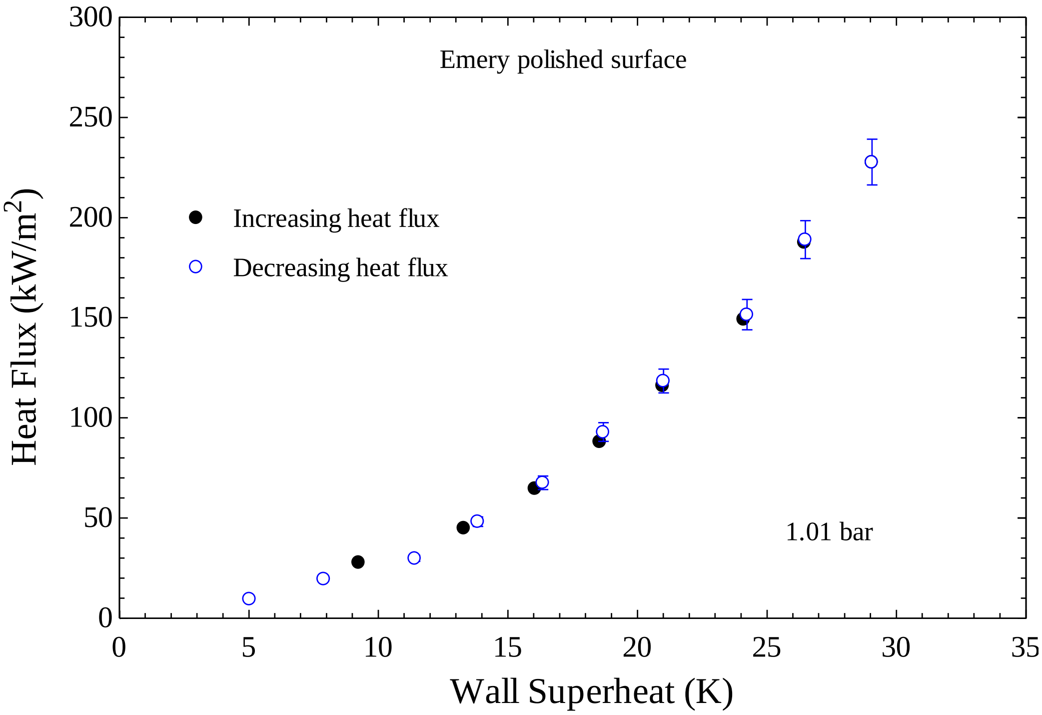

Figure 6.8 Hysteresis test for emery polished surface without EHD.

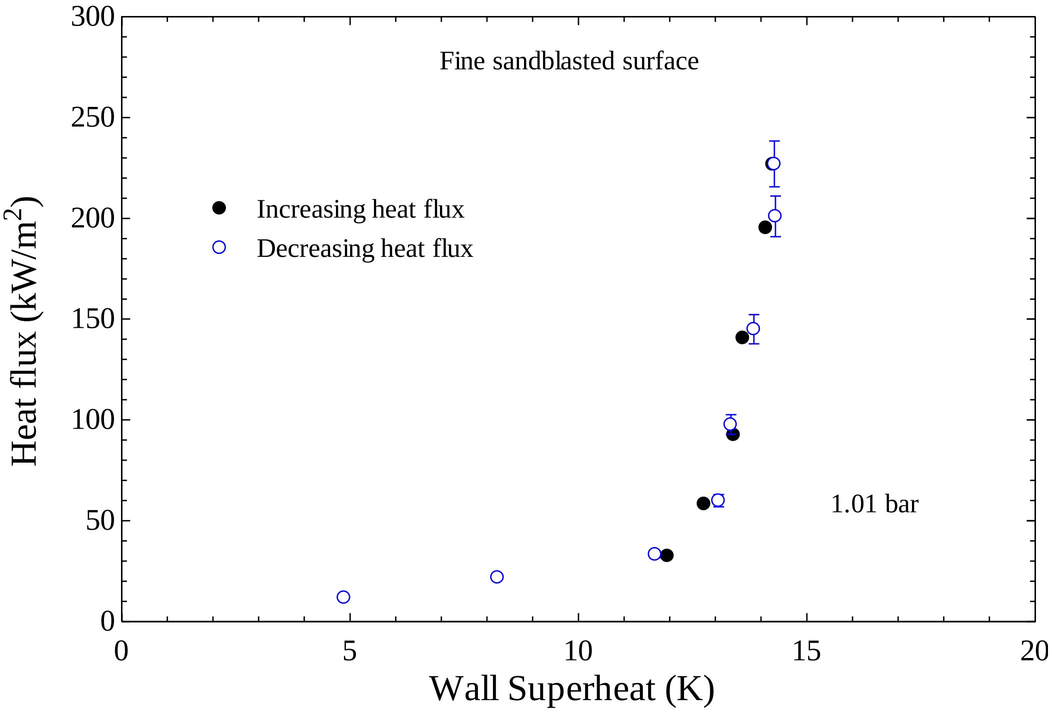

Figure 6.9 Hysteresis test for fine sandblasted surface, without EHD

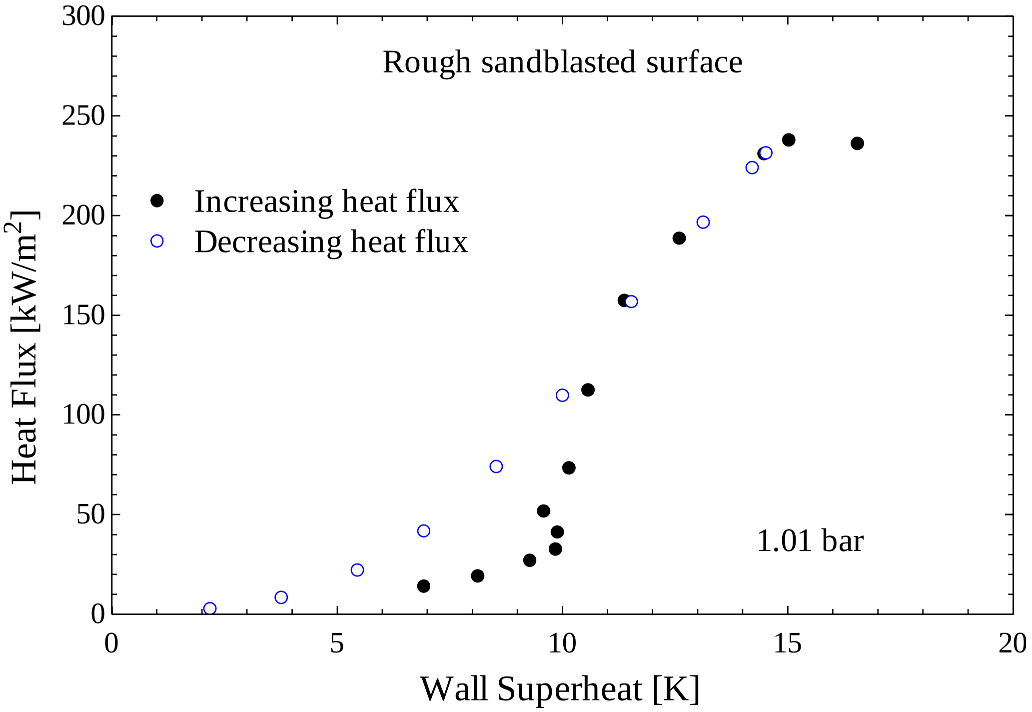

Figure 6.10 Hysteresis test for rough sandblasted surface, without EHD.

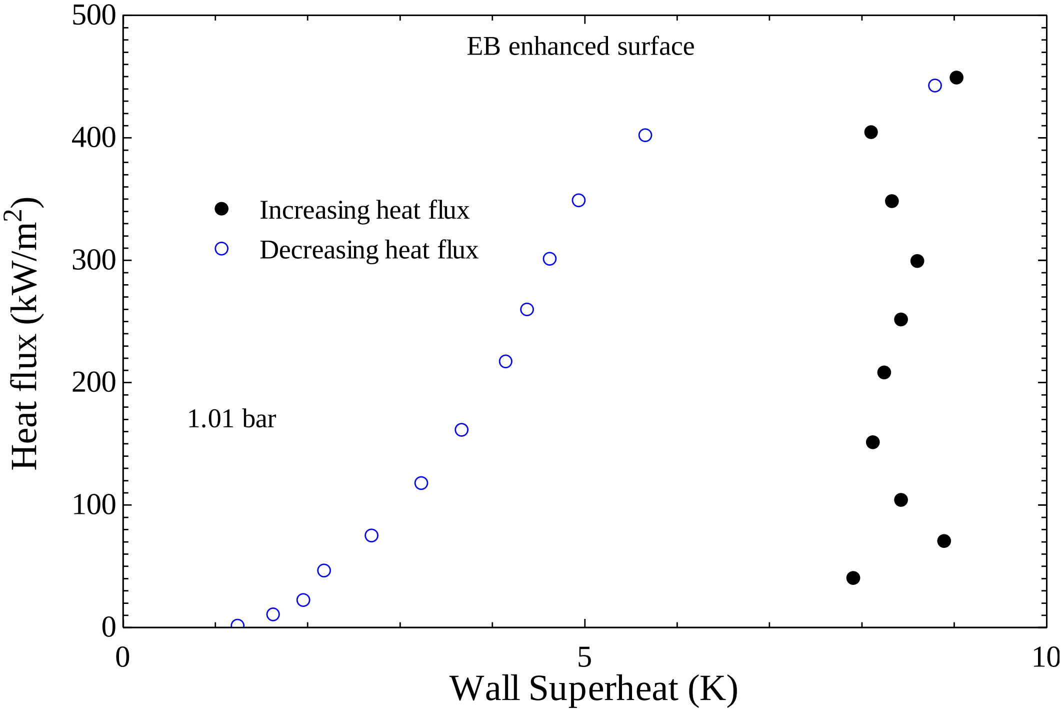

Figure 6.11 Hysteresis test for EB enhanced surface, without EHD

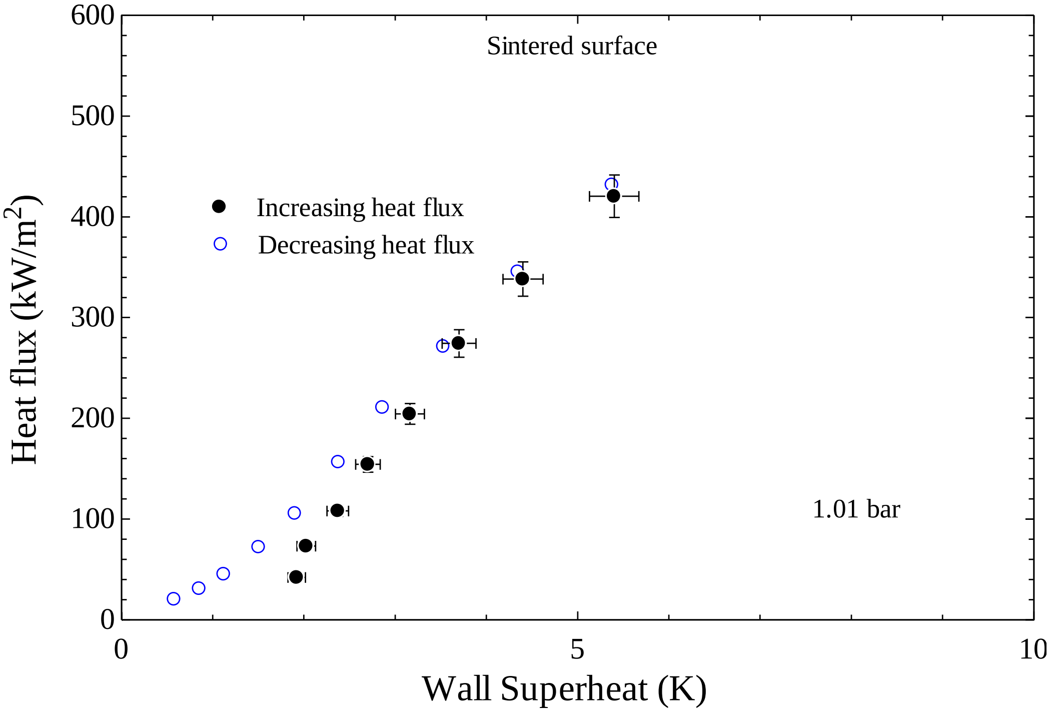

Figure 6.12 Hysteresis test for sintered surface without EHD.

6.1.4 Effect of surface modification on critical heat flux

The critical heat flux (abbreviated as CHF) is an important phenomenon, which can be helpful in the equipment design. The possible mechanisms of critical heat flux have already been reviewed in Section 2.10. In the present experiments, the critical heat flux value was determined by increasing the heater power supply gradually and at critical point the temperature of the copper block suddenly increased. At this point, a programmable switch was installed to turn off the heater power supply in order to prevent melting of the copper block. The heat flux was calculated, as mentioned in Chapter 5, and plotted against the wall superheat, i.e. the temperature difference between the heating surface and the boiling liquid. The point at which the boiling curve changes its slope (from nucleate to film boiling) is considered as the critical heat flux.

During present studies, the critical heat flux was determined using the five modified surfaces, i.e. emery polished, fine sandblasted, rough sandblasted, EB enhanced and sintered surfaces at 1.01 bar saturation pressure. The results of the critical heat flux are presented and discussed in this section. The value of critical heat flux for rough sandblasted, emery polished and fine sandblasted surfaces were 227 kW/m^2. At critical heat flux, vapour blanket forms on the heating surface, which blocks the cold liquid rewetting to the heater surface. This vapour blanket acts as an insulator for heat, this situation leads to sudden increase in the wall superheat and the heat flux corresponding to this point is known as critical heat flux.

These experimental results agreed with the hydrodynamic theory, i.e. there is no effect of surface conditions on the critical heat flux. The visual observations of bubbles near critical heat flux and also been presented late Figure 6.51 (a) which shows that near the critical heat flux, the rising bubbles from the heater surface coalesce and produce bubble columns. It is believed that, at this stage, the vapours are produced by the evaporation of liquid underneath these bubble columns. This results in the formation of a continuous vapour film on the heating surface, which doesn't allow liquid rewetting. Now at this stage, the vapours start to grow from the vapour film rather than from the nucleation sites. As the heater power supply is turned off, the vapour film slowly diminishes and boiling shifts again towards the nucleate boiling region. These observations are similar to visual observations reported by Gaertner (1965). He observed that the heater surface was covered by vapour mushrooms and the liquid cannot reach to the boiling surface and this situation led to critical heat flux. Similar visual observations were also reported by Wang et al. (2009) who observed big bubble columns near the critical heat flux during pool boiling experiments using liquid nitrogen. The present results contradict the experimental results of Ferjancic and Golobic (2002), where they reported that the critical heat flux is a function of average surface roughness, according to equation (2.26).

For the EB enhanced surface, the critical heat flux is found to be 447 kw/m^2, which is higher as compared to fine sandblasted, emery polished and rough sandblasted surfaces. This higher value of CHF is due to the special spike structure on the boiling surface, which forced the vapour liquid interface to become closely spaced and as a result of this, the interface remains stable for even higher heat flux values.

The value of CHF for the sintered surface was also determined and is equal to 440 kW/m^2. This increase in the CHF value can be attributed to its porous structure. It has been visually observed during the experiments that the diameter of the bubbles detached from the sintered surface was almost equal to the surface even at high heat flux. It can be deduced that the boiling takes place within the porous layer and then the bubbles pass through the pores before breaking into the bulk of the liquid. As the heat flux increases, the number of bubbles coming from the pores increases. The bubbles coalesce after passing through the pores while high heat flux is required to form bubble blanket on the heater surface, which hinders cold liquid rewetting. In the case of emery polished surface, there was no hindrance on the boiling surface and bubbles can coalesce during their growth and CHF takes place at low value of heat flux compared to the sintered surface. It can be concluded that the porous structure on the sintered surface changes the bubble dynamics which is responsible for the high value of critical heat flux.

6.2 Effect of saturation pressure on pool boiling

This section presents the effect of saturation pressure on pool boiling. Various experiments were performed to determine the effect of saturation pressure on pool boiling by using emery polished surface and saturation pressure of 1.01 bar, 2 bar and 4 bar. The results are shown in Figure 6.13, which shows the general boiling curve for emery polished surface at 1.01 bar saturation pressure. But as the saturation pressure increased to 2 bar, the heat transfer is found to be increased at a specific value of wall superheat. It can be noted, from Figure 6.13, that at low heat flux, i.e. convective boiling regime, the heat transfer augmentation is low. Whereas in the nucleate boiling regime the heat transfer enhancement increases. Similar trend of heat transfer augmentation can be observed for higher saturation pressure, i.e. at 4 bar.

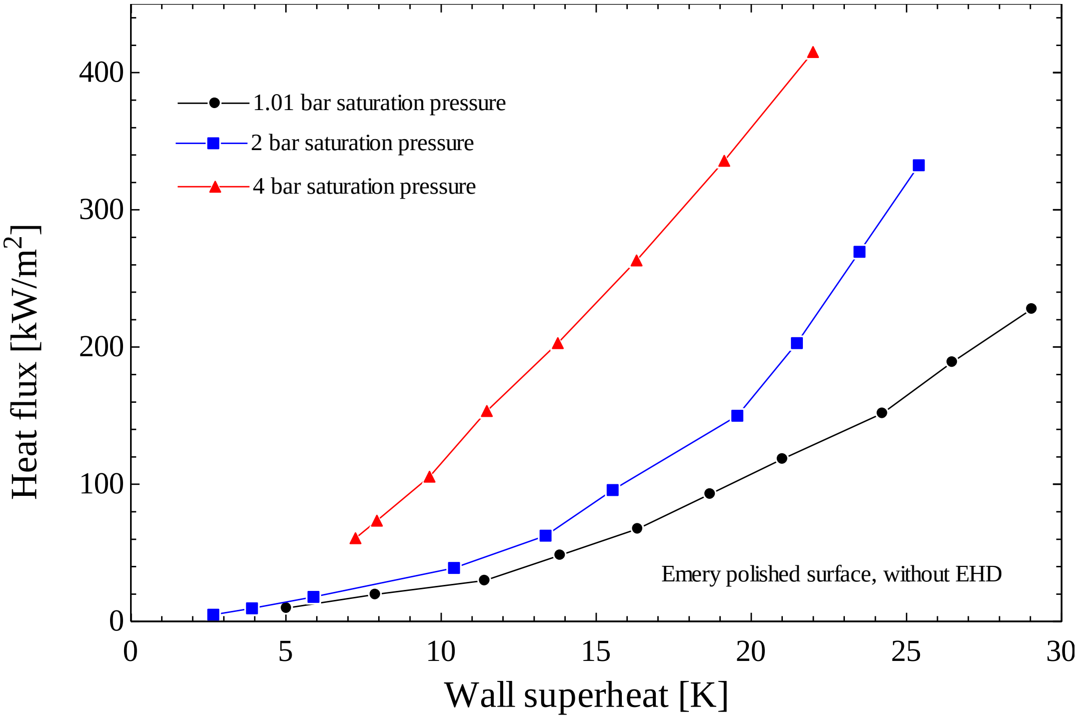

Figure 6.13 Boiling curves for emery polished surface at higher saturation pressure.

It is found that increase in saturation pressure results in enhancement of heat flux at the specific value of wall superheat during nucleate boiling regime. This enhancement of heat flux has been explained on the basis of Thomson equation (discussed earlier, see equation 2.1) which relates the equilibrium conditions between pressure gradient (inside and outside) of vapour and the radius of vapour (see Section 2.6).

At constant boiling pressure, an increase in the wall superheat is responsible for increasing pressure inside the vapour and makes the nucleation site active for bubble growth. Increasing the saturation pressure makes these cavities active for nucleation at lower value of the wall superheat. This activation of the cavity at low heat flux is due to decrease in surface tension of boiling liquid as boiling pressure increases. As a result of this, the equilibrium radius for the bubble decreases (see equation (2.1)). It means that small nucleation sites become active at low value of wall superheat. It is also worth noting that as the saturation pressure increase from 1 to 4 bar, the surface tension decrease by a factor of almost ‘10’, see Gorenflo et al. (2010). It can be concluded from the above discussion that altering the saturation pressure will change the physical properties of the boiling fluid, especially the surface tension. This change in the value of surface tension is responsible for the increase in the heat flux value at the specific value of wall superheat. This discussion can be validated using flow visualization; it can be observed from Figure 6.14 that at 1.01 bar saturation pressure the number of bubbles at specific location is less than that of 2 bar saturation pressure. It can be deduced that as the boiling pressure increases the number of bubbles as well as nucleation sites also increase, which results in augmentation of heat transfer at the specific value of wall superheat.

Furthermore, it was also observed during the flow visualization that the size of bubble decreases at detachment from the boiling surface. These visual observations were in accordance to equation (2.1), which shows that the equilibrium radius of the vapour decreases with the increase in saturation pressure.

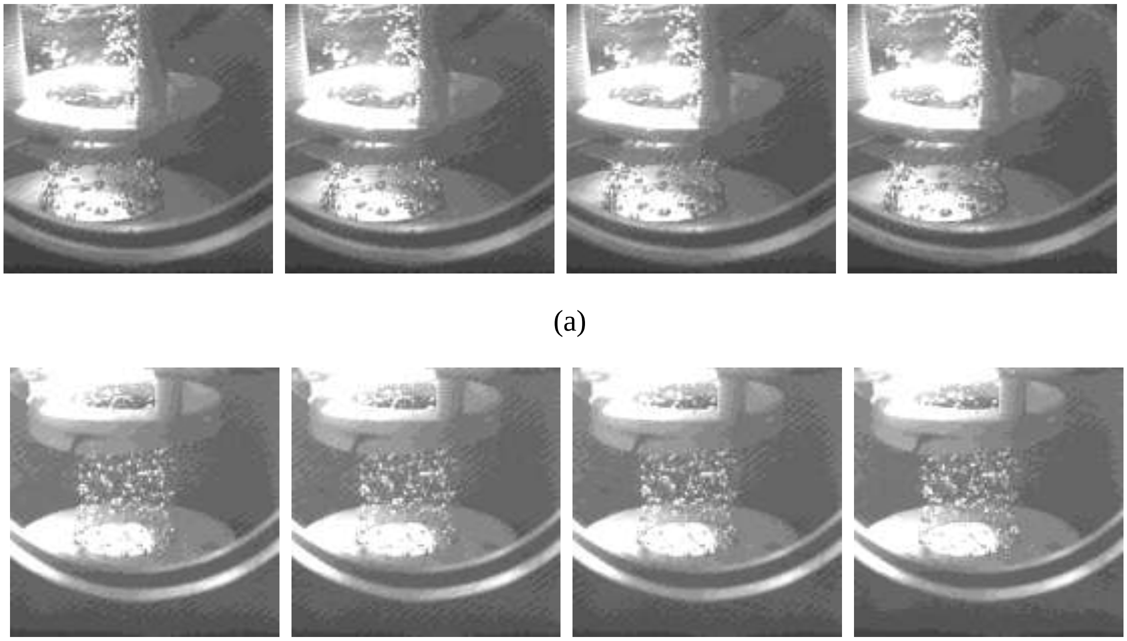

(a)

(b)

Figure 6.14 Flow visualization without EHD (10 kW/m^2), time elapsed between two frames is 1.25 msec (a) at P = 1 .01 bar (b) at P = 2 bar.

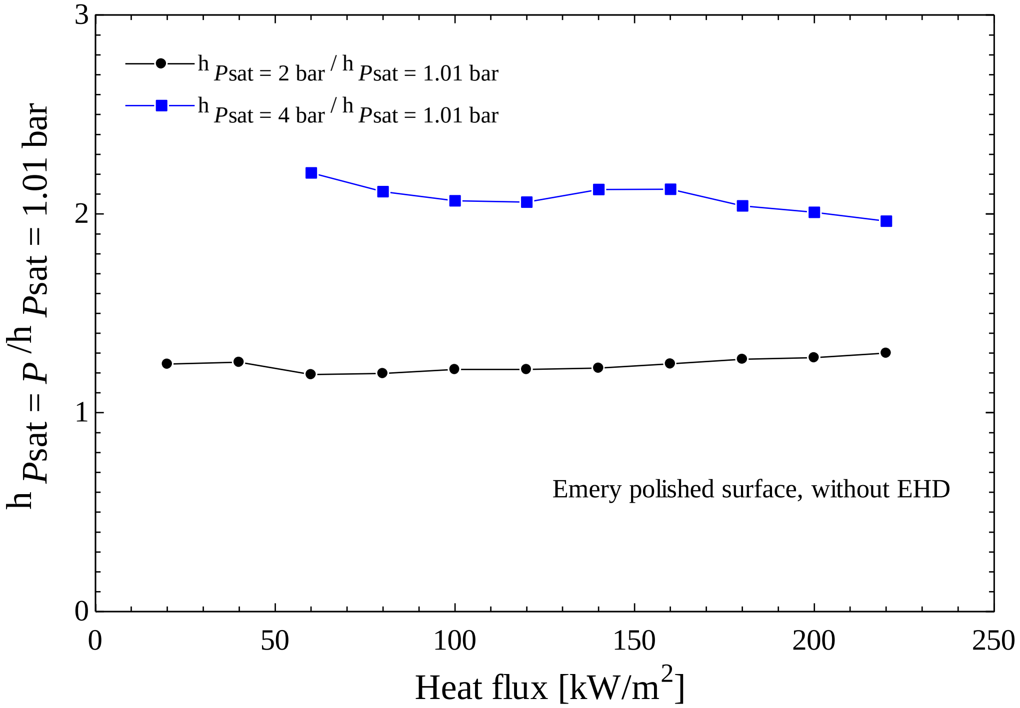

Figure 6.15 Augmentation ratio at higher saturation pressure for emery polished surface.

Similar observations were also reported experimentally by Gorenflo et al. (2010), when working with R-125 as a boiling fluid. The value of heat transfer coefficient augmented by a factor of ‘2’ at 4 bar saturation pressure as compared to 1.01 bar saturation pressure, see Figure 6.15.

6.3 Bubble dynamics

This section of thesis presents the results on bubble behaviour as recorded using the high speed camera (i.e. 800 frames per second). The bubble dynamics are presented in Figures 6.16 to 6.28. In these analyses, the heat flux was kept at 10 kW/m^2, so that isolated bubble growth could be monitored with and without EHD.

The bubble growth, without EHD, is depicted in the Figure 6.16 at 1.01 bar saturation pressure, which shows that the bubble grows approximately spherical under the effect of inertial and buoyancy forces. Then a thin neck appears at the bottom of the bubble, which detaches from the heating surface as the bubble breaks into the bulk of the liquid. Similar trend of bubble growth was also reported by Dong et al. (2006) and Chen et al. (2007 a), who injected air and nitrogen bubbles into a dielectric fluid respectively. Siedel et al. (2011) reported that the growth of thermally produced carbon tetra chloride bubbles is similar to the present study. The bubble detachment time (i.e. the time elapsed between bubble first appeared on the heating surface and the bubble detached into the bulk of the liquid) was 25 msec, see Figure 6.16. The impact of uniform electric field on bubble growth is presented in Figure 6.17 to Figure 6.18 , where the electric field was 0.5 MV/m and 1 MV/m respectively at 1.01 bar saturation pressure. It can be observed from the video and the photographs in the figure that when 0.5 MV/m uniform electric field is applied the bubble remains spherical similar to EHD = 0 condition, see Figure 6.16. However, the bubble detachment time increased as 27.5 msec, see Figure 6.17 . Furthermore, the bubble shape change from spherical to mushroom structure as the electric field increases to 1 MV/m and the bubble detachment time also increased to 30 msec, see Figure 6.18 .

The visual observations of present study are found to be similar to the mathematical findings of Karayiannis and Xu (1998) and Dong et al. (2006).

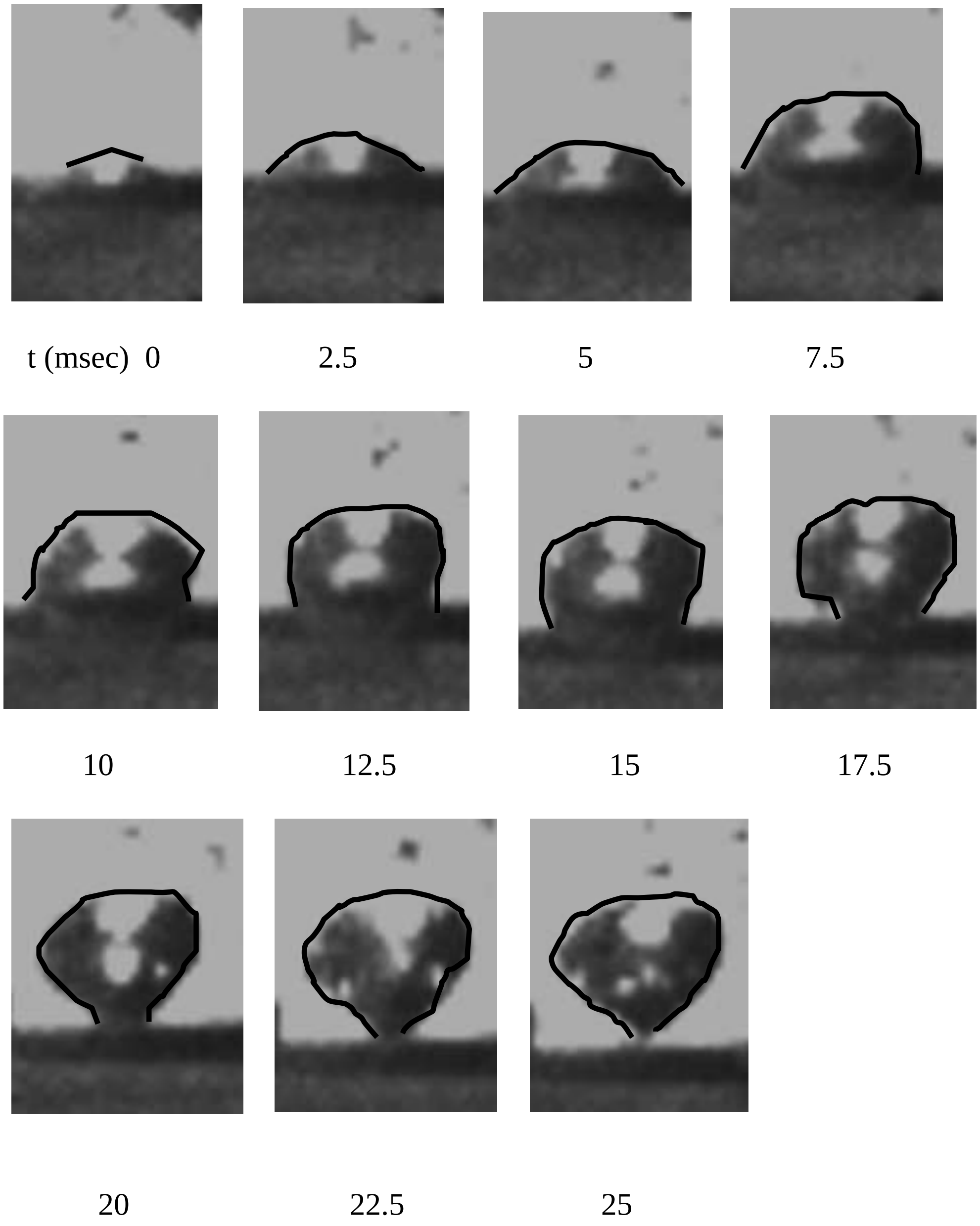

Figure 6.16 Bubble dynamics without EHD at 1.01 bar saturation pressure

As discussed earlier in Section 3.6, Karayiannis and Xu (1998) mathematically reported that the uniform electric field was distorted as bubble appeared. The value of electric field increases at the sides of bubble and decreases at the top of bubble. It can be deduced from the findings of Karayiannis and Xu (1998) that when bubble appears, the electric field did not remain uniform in the vicinity of vapour. According to Pohl (1978) the component of the fluid which has higher electric permittivity is attracted towards the region of high electric field intensity in non-uniform electric field, as discussed earlier in Section 6.3.1. Karayiannis and Xu (1998) reported that as the electric field increases at the sides of bubbles, the liquid molecules (having higher electric permittivity than vapours) are attracted towards the sides of these bubble. This process presses the bubble inwards. Moreover, the electric field decreases at the top of bubble (Karayiannis and Xu (1998)) while Pohl (1978) stated that the component of the fluid which has low electric permittivity is attracted towards the region of low electric field intensity. This means that the vapor was pulled upwards with the application of uniform electric field. Similar observations were reported by Siedel et al. (2011) (as discussed earlier in Section 3.6) who applied uniform electric field on thermally induced n – pentane bubbles. They reported that the bubble elongated in the direction of electric field as well as bubble detachment diameter increased as compared to no field conditions.

The effect of bubble growth under non – uniform electric field was depicted in Figures 6.19 to 6.22 at 1.01 bar saturation pressure. It can be deduced from the visual observations of Figures 6.19 to 6.21 that, with the application of 0.5 MV/m, the electric field (both uniform and non-uniform) a marginal change in bubble growth pattern has been seen as compared to no electric field conditions. While the bubble detachment time increases as 30 msec and 32.5 msec with rod electrodes having 5 mm and 8 mm rod spacing respectively, as in the Figures 6.19 and 6.21. When the electric field increased up to 1 MV/m the bubble shape at detachment changed from spherical to thin elongated shape with irregular edges as compared to no field conditions and the bubble detachment time also increased.

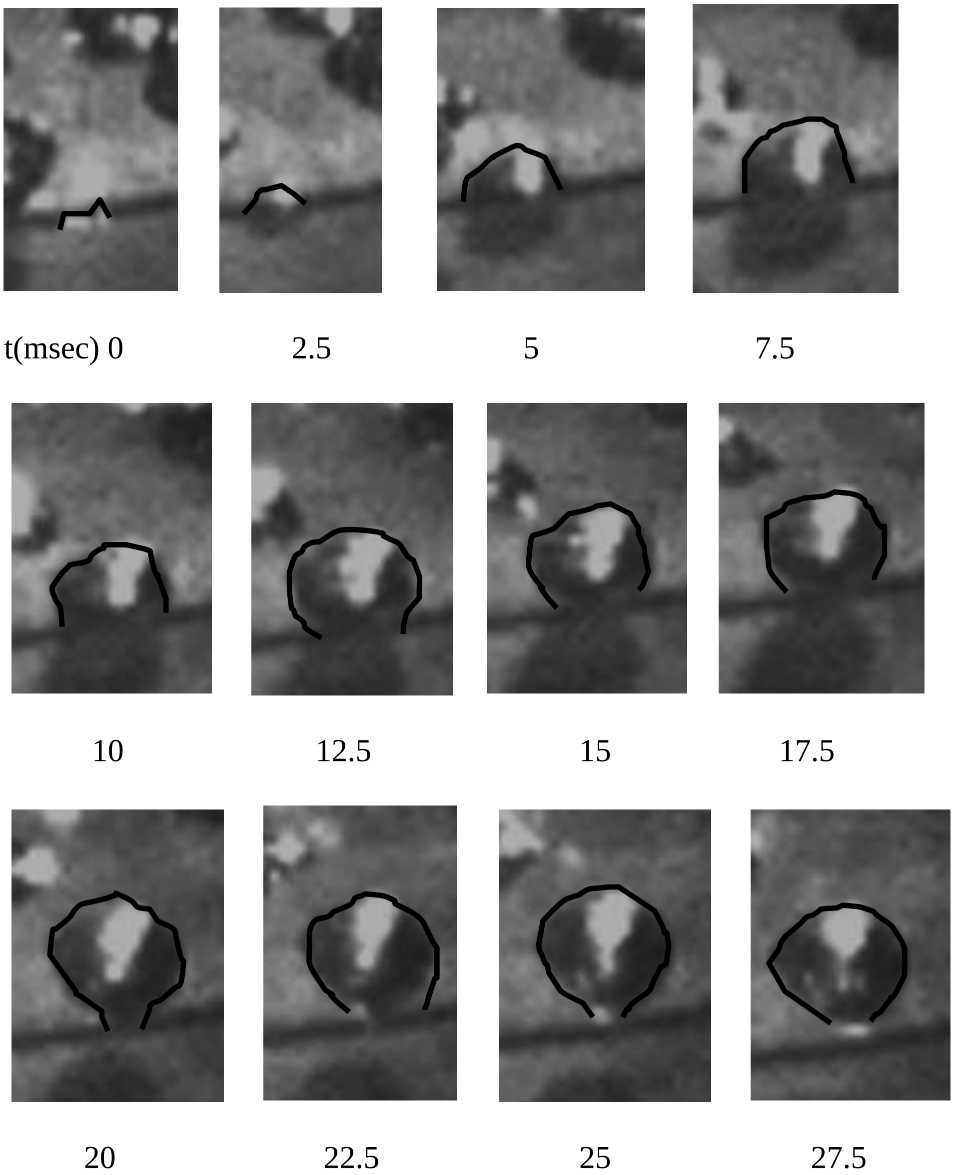

t(msec) 0 2.5 5 7.5

10 12.5 15 17.5

20 22.5 25 27.5

Figure 6.17 Bubble dynamics at E = 0.5 MV/m using mesh electrode.

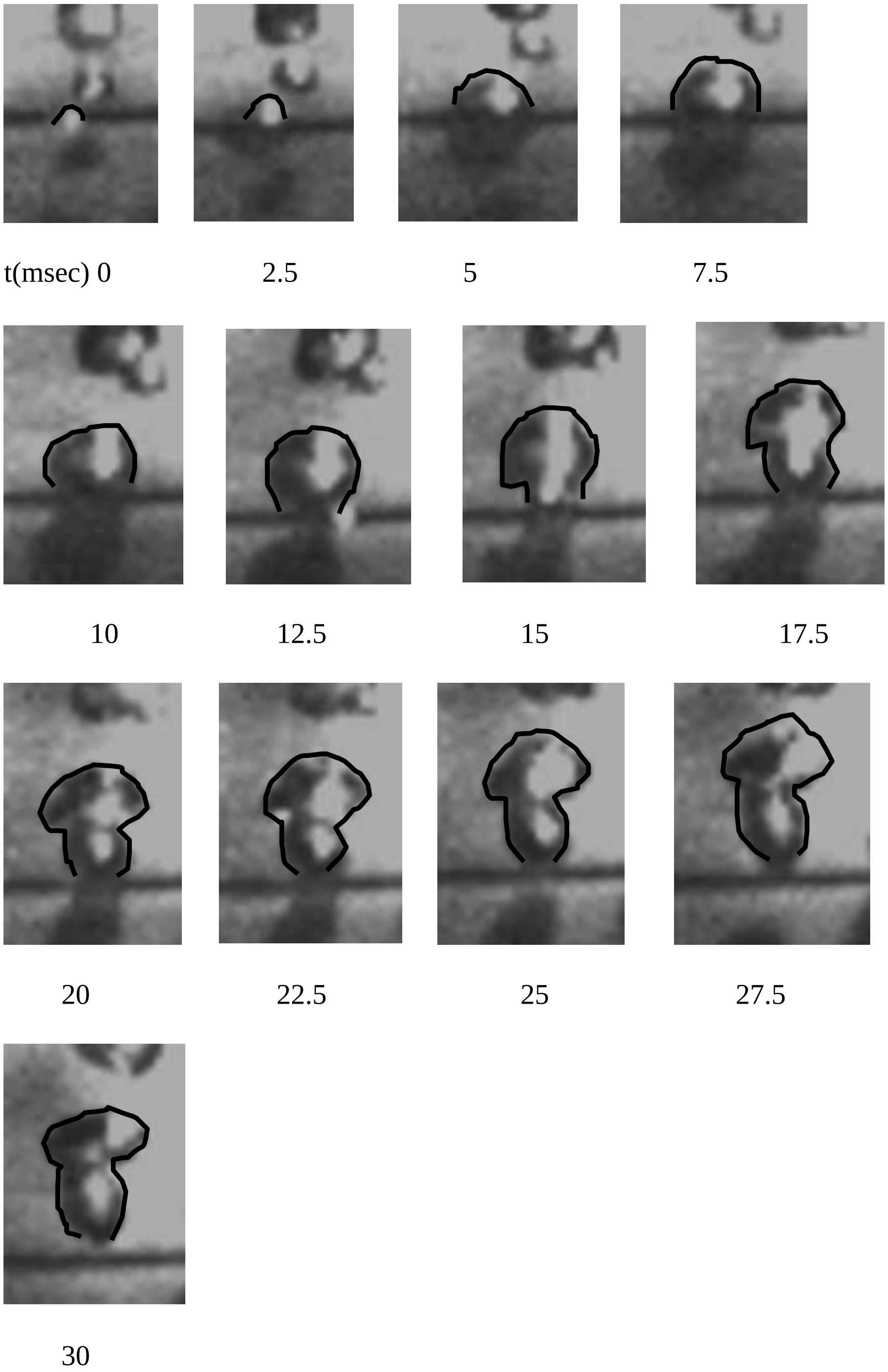

Figure 6.18 Bubble dynamics at E = 1 MV/m using mesh electrode.

The bubble behavior under the application of non – uniform electric field can be explained on the basis of the arguments reported by Pohl (1978), i.e. bubbles were pushed against the heating surface. Moreover, the alteration, due to the application of electric field, in the bubble shape during its growth is shown Figure 6.23, which depicts that due to the application of uniform electric field the bubble shape changes and the size of the bubble increases. While on the application of non – uniform electric field the alteration in the detachment shape as well as the size has also been found, see Figure 6.23 (c) and (d). Furthermore, it has also been noted from the videos and pictures that the bubble detaches upwards (i.e. at normal to the heating surface) during no field and under uniform field conditions, see Figure 6.23 (a) and (b). But as non – uniform electric field is applied, the bubble detaches diagonally and found titled towards right or left, (i.e. at some angle from the boiling surface). This change in pattern detachment pattern also evidence that the electrode push the bubble against the boiling surface. While, at high heat flux (100 kW/m^2), without EHD, bubbles with large diameter and moving up in disordered columns were observed, see Figure 6.51 (a). It was also observed that the bubbles follow their path, starting from the heating surface and pass through the mesh. But with the application of uniform electric field E = 1 MV/m, the bubble columns were found to be more ordered and the size of the bubbles smaller, as compared to field free case.

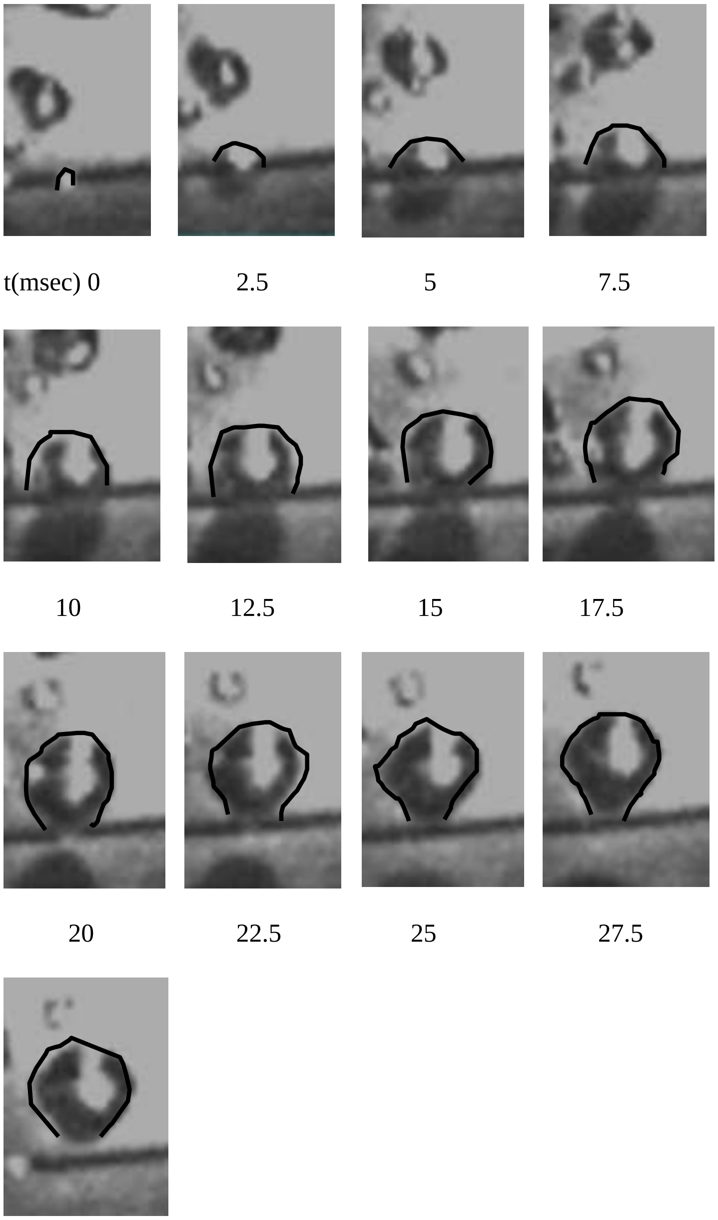

t(msec) 0 2.5 5 7.5

10 12.5 15 17.5

20 22.5 25 27.5

30

Figure 6.19 Bubble dynamics at E = 0.5 MV/m using rod electrode (5 mm rod spacing)

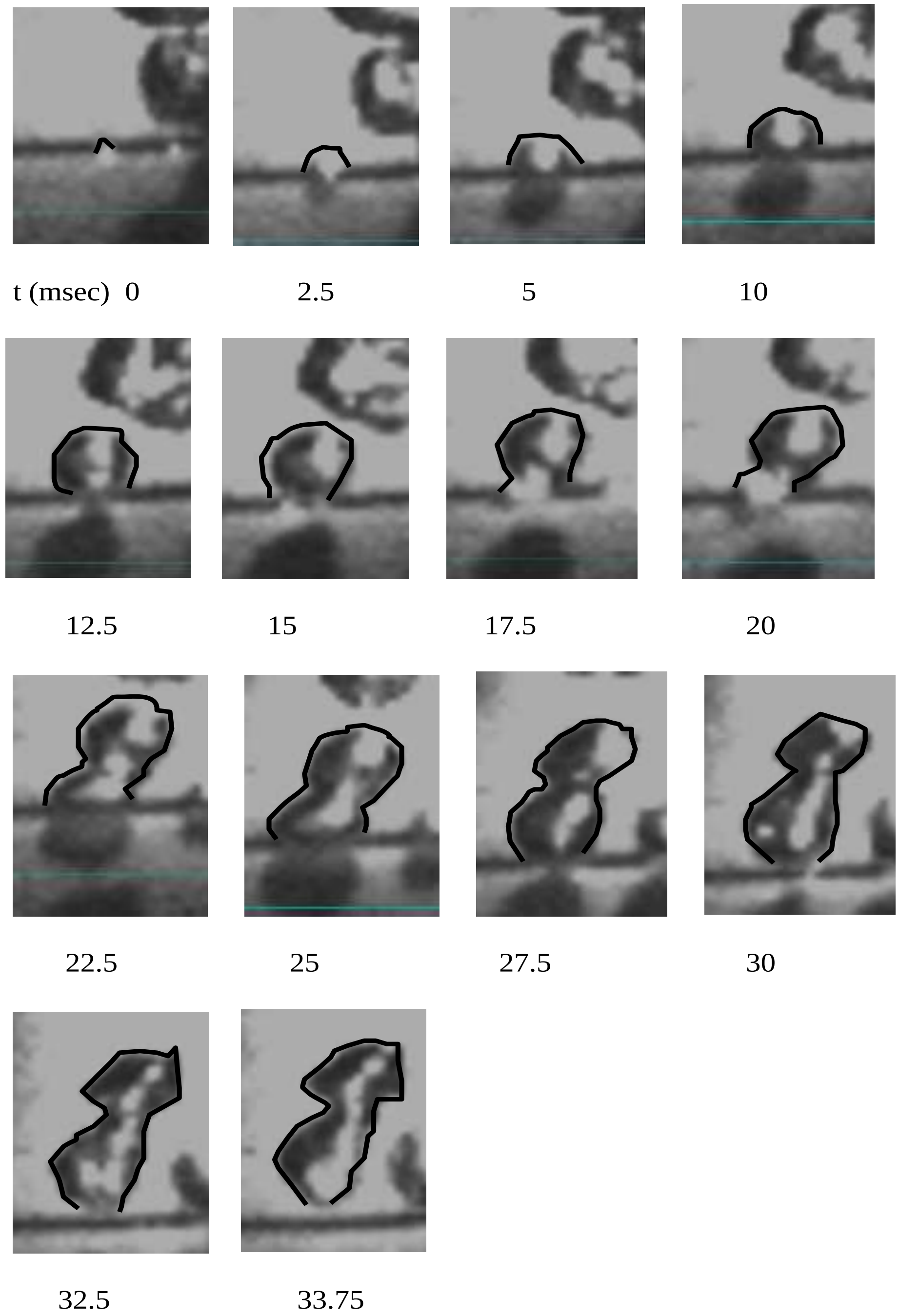

Figure 6.20 Bubble dynamics at E = 1 MV/m using rod electrode (5 mm rod spacing)

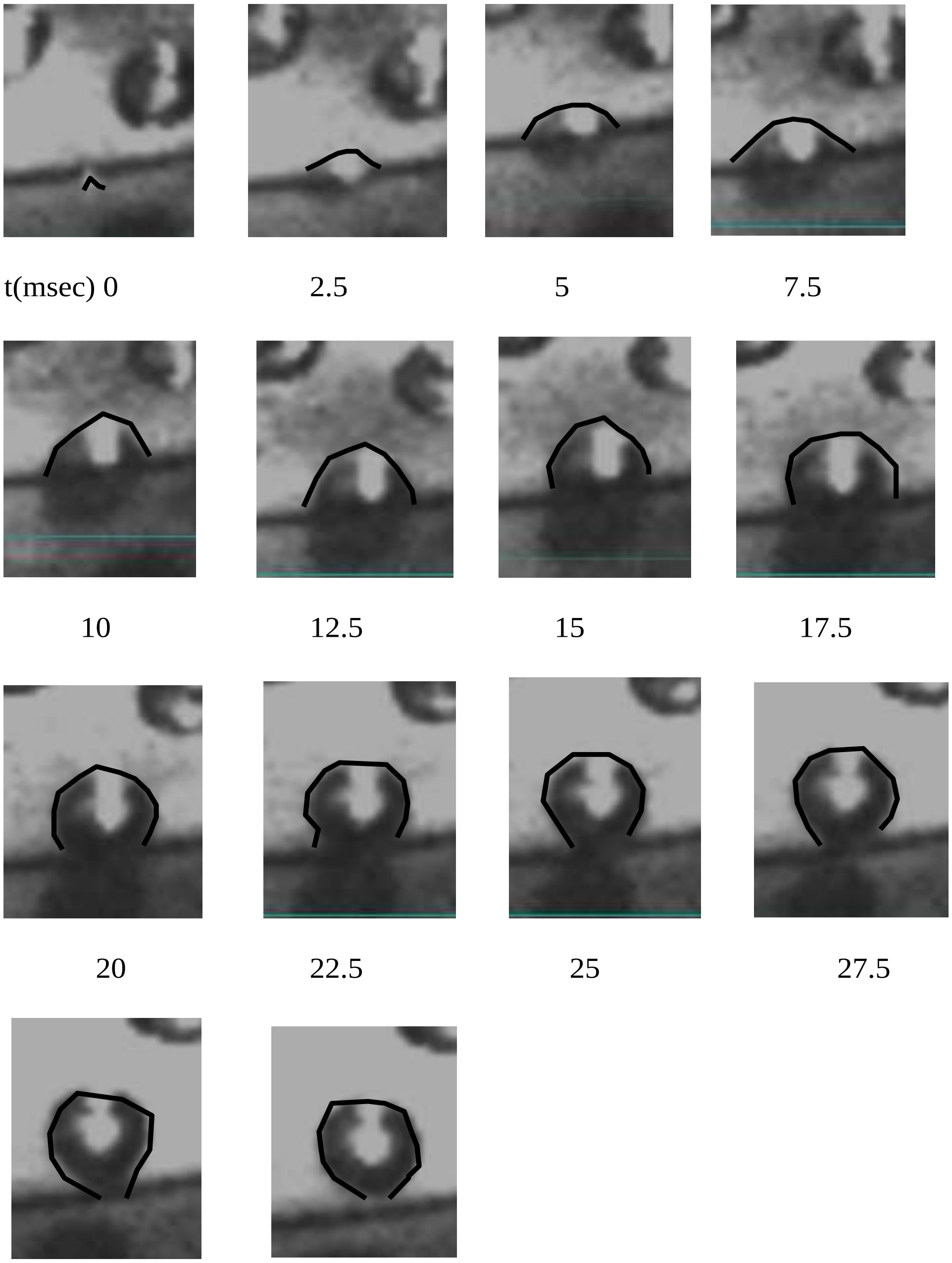

t(msec) 0 2.5 5 7.5

10 12.5 15 17.5

20 22.5 25 27.5

30 32.5

Figure 6.21 Bubble dynamics at E = 0.5 MV/m using rod electrode (8 mm rod spacing).

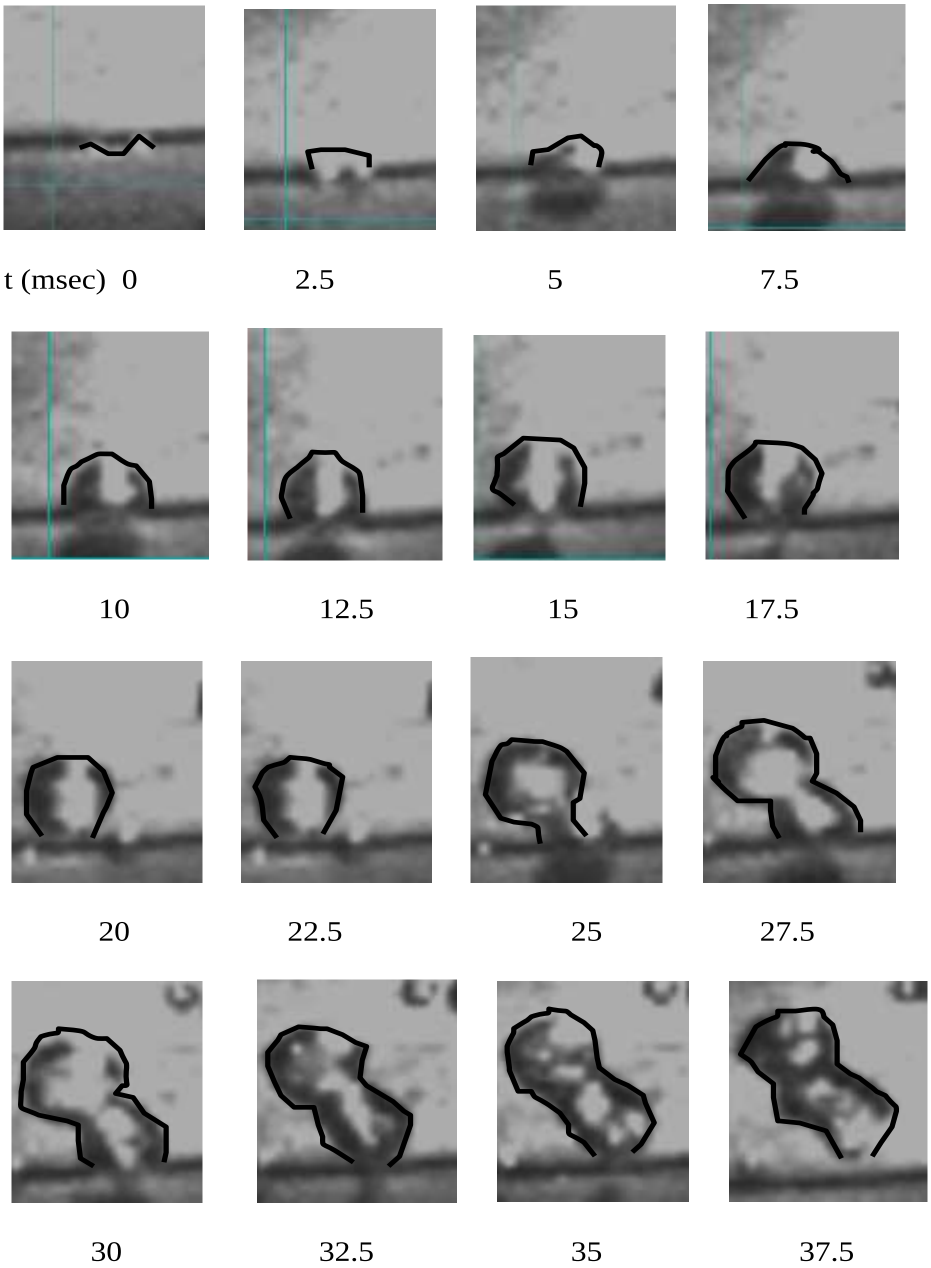

Figure 6.22 Bubble dynamics at E = 1 MV/m using rod electrode (8 mm rod spacing).

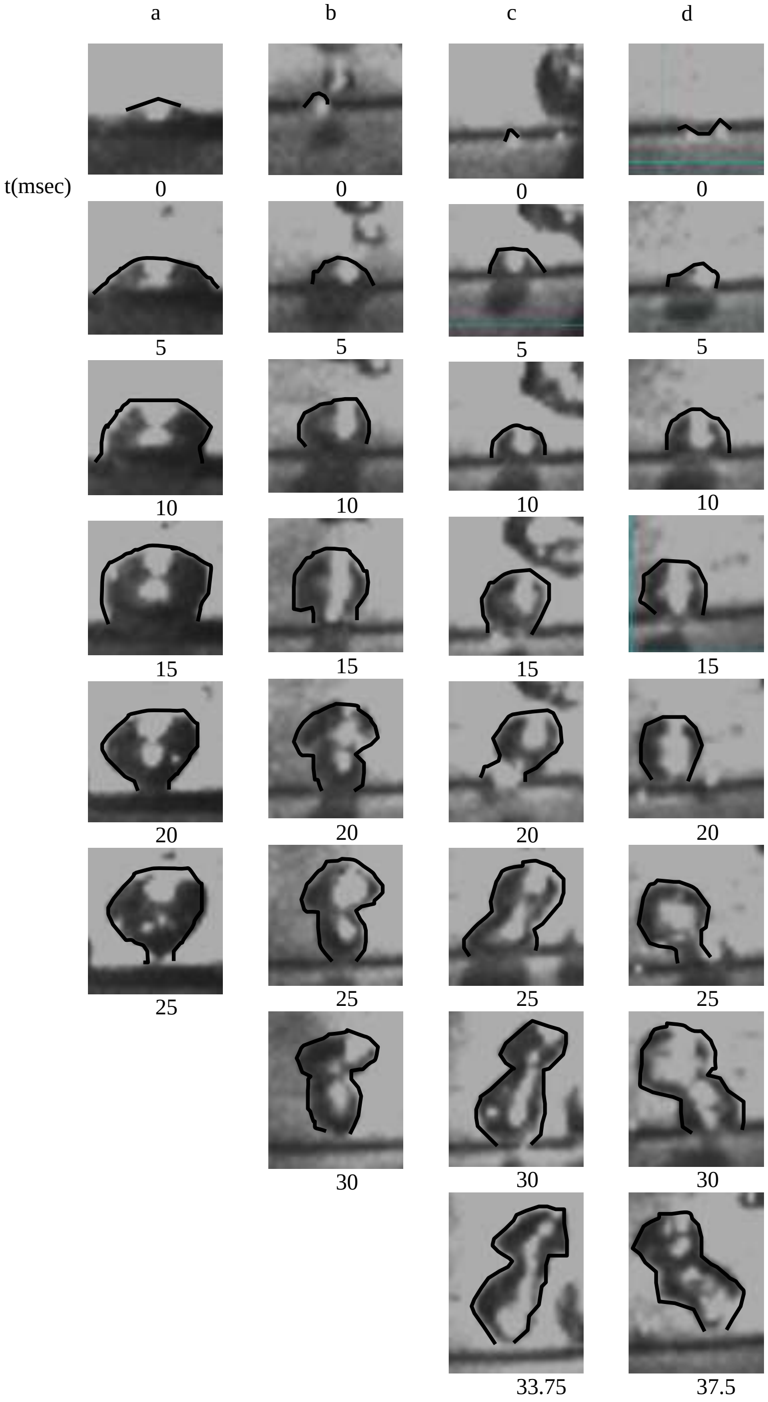

Figure 6.23 Comparison of bubble dynamics at (a) E=0 (b) E=1MV/m, mesh electrode (c) E = 1MV/m, rod electrode with 5mm rod spacing (d) E = 1MV/m rod, electrode with 8 mm rod spacing

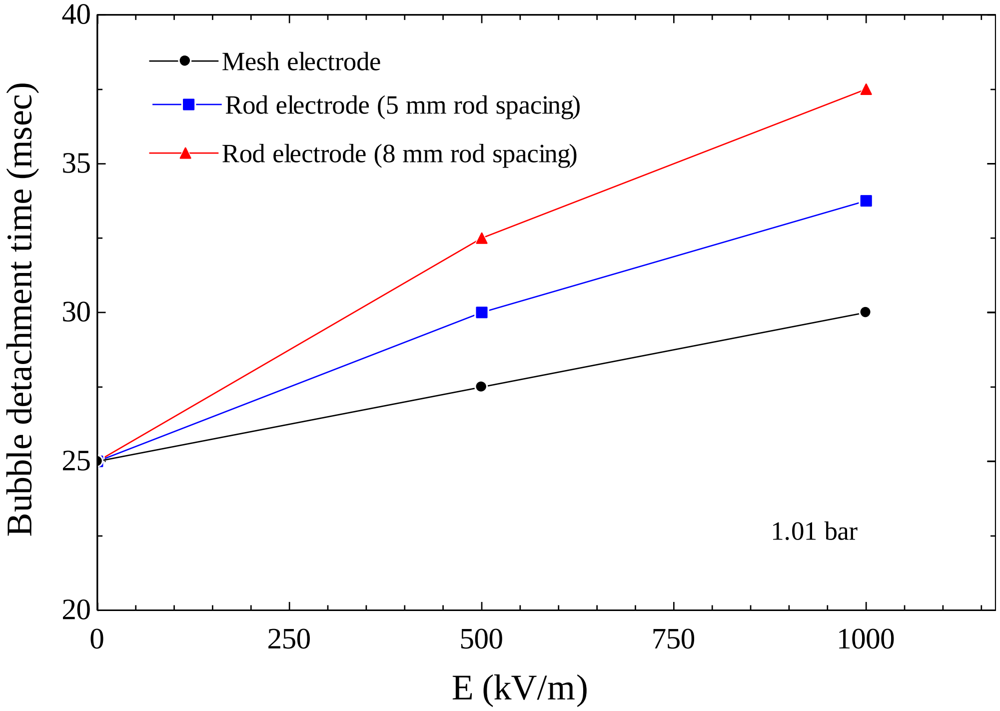

Figure 6.24 Effect of electric field on bubble detachment time.

Moreover, the density of the bubbles between the mesh electrode and the heating surface was also increased as shown in Figure 6.51 (b) and some of bubbles were found to escape from the other edge of the PTFE washers, which were used to support the electrode. This bubble movement behaviour, i.e. bubbles leaving from the edge of the PTFE washers was observed to increase when the non–uniform electric field was applied, i.e. E = 1 MV/m, see Figure 6.51 (c). This behaviour of the bubbles is, we believe, the result of pushing the bubbles against the heating surface, Pohl (1978), which then direct themselves to regions of weaker field at the outer edges of the heating surface-electrode and escape upwards under the influence of buoyancy.

The effect of electric field (uniform and non - uniform) on bubble detachment time has been shown in Figure 6.24, which depicts the bubble detachment time when the electric changes from 0 to 1 MV/m using all three electrode, discussed in section 4.2. It has been observed that the bubble detachment time increases due to increase in the magnitude of both electric filed and non – uniformity of electric field. As discussed above, that due to application of electric field, the bubble dynamics changes. Due to the application of electric field, an additional force (defined by the equation 3.6) acts on the bubble in combination with inertial and buoyancy forces. The force induced by the electric field pushes the bubble towards the heating surface, as a result of this the bubble detachment time increases.

It can be observed from the Figure 6.25 that as the boiling pressure increased from 1.01 bar to 2 bar the bubble detachment time decreased from 25 msec to 17.5 msec. These observation were similar to the experimental results of Bobrovich and Mamontova (1965), for pool boiling experiments using water as the working fluid. They reported that the bubble detachment time decreased from 0.029 s to 0.022 s as the boiling pressure increased from 10.8 bar to 52 bar at 9.6 ºC wall superheat. While on examining the Figures 6.16 and 6.26, it has been observed that the bubble growth pattern did not change with the increase in the pressure, i.e. it remained spherical at detachment.

On investigating Figures 6.26 and 6.27, it has been observed that the bubble detachment time doesn’t increase with the application of 0.5 MV/m and 1 MV/m uniform electric field. But the bubble growth pattern changed from spherical to mushroom with the application of 1 MV/m as compared to no field conditions (these observations are similar to the bubble growth under the action of uniform electric field at 1.01 bar pressure, see Figure 6.18). It has already been discussed that with the increase in boiling pressure the number of bubbles produced from the heating surface increased at the specific value of heat flux. This may reduce the effective electric field acting on the bubble (due to shielding effect of the bubbles, discussed in section 6.2.1). Therefore, the bubble detachment time didn’t change with the application of the electric field.

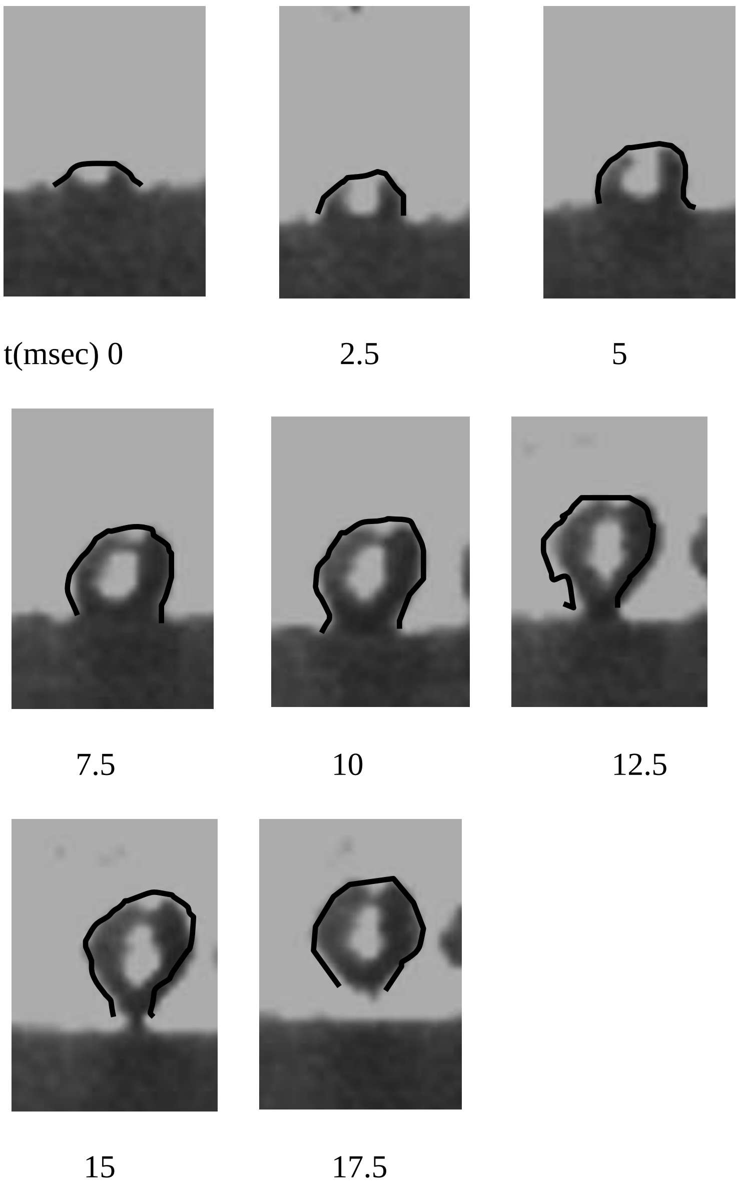

Figure 6.25 Bubble dynamics without EHD at 2 bar saturation pressure.

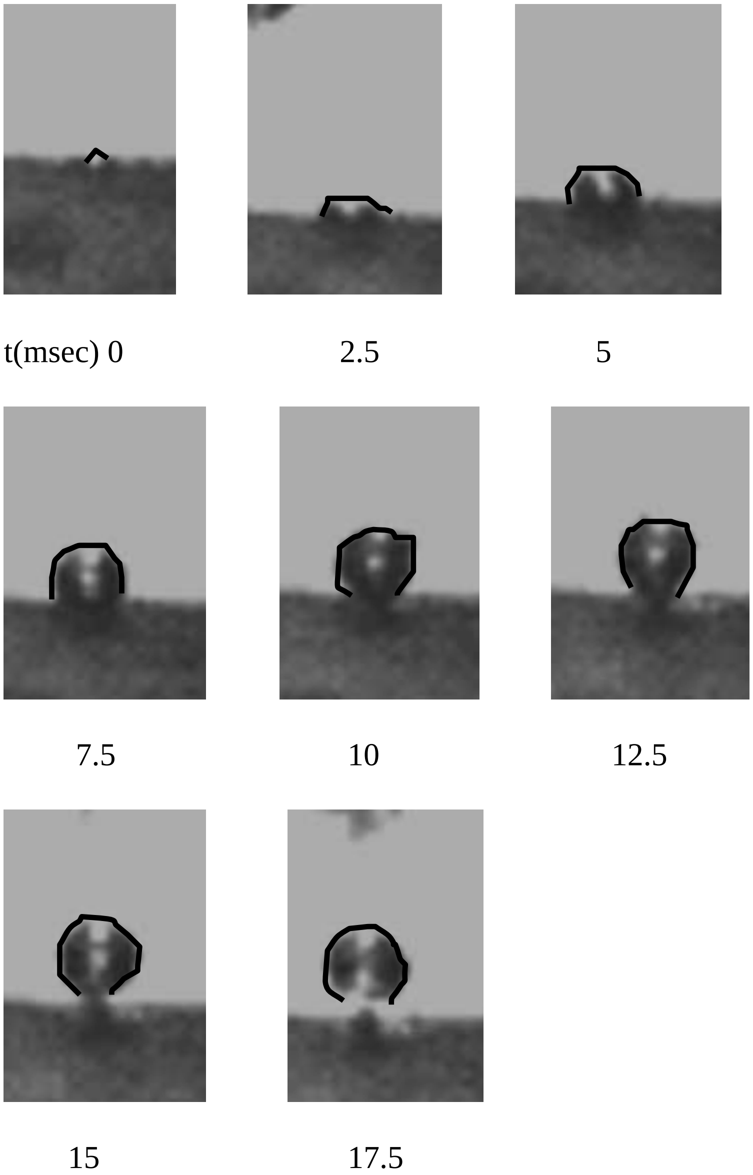

Figure 6.26 Bubble dynamics at E = 0.5 MV/m using mesh electrode, $P = 2$ bar

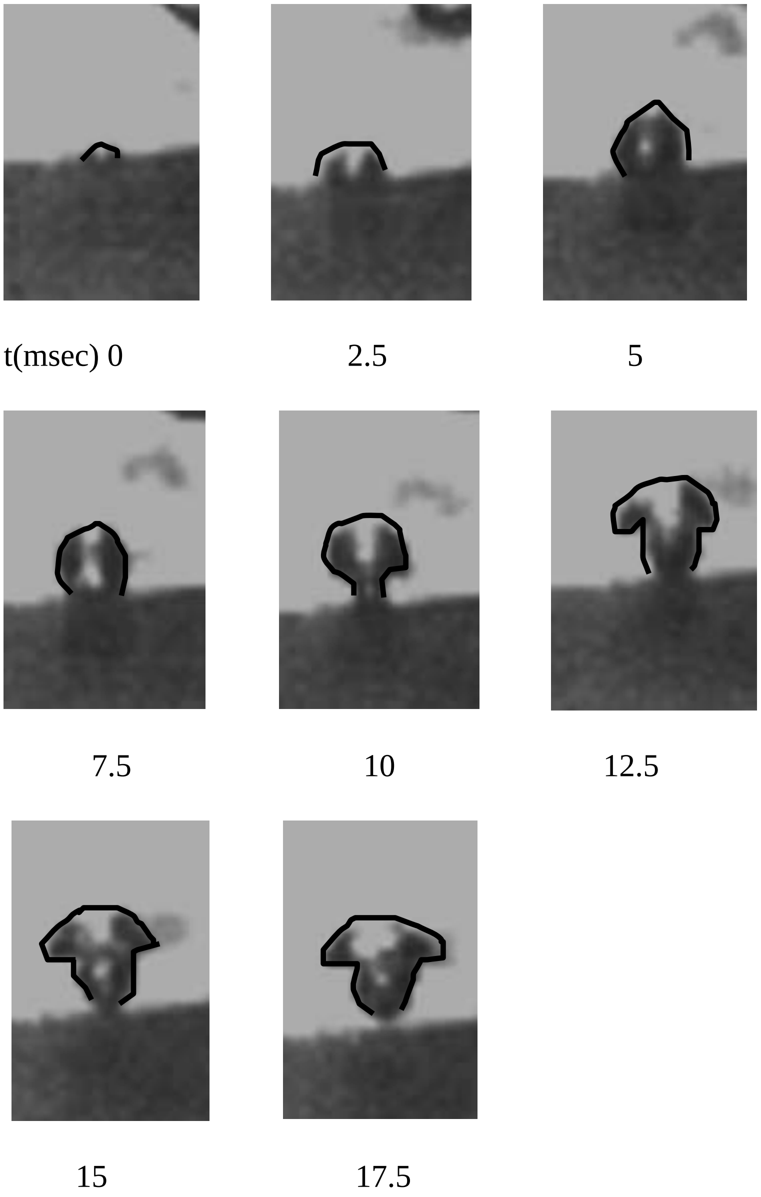

Figure 6.27 Bubble dynamics at E = 1 MV/m using mesh electrode, P = 2 bar

6.4 Effect of electric field on pool boiling

6.4.1 Uniform electric field

The effect of the uniform electric field is discussed in this section on five modified surfaces, i.e. emery polished, fine sandblasted, rough sandblasted, EB enhanced and sintered surface at 1.01 bar saturation pressure. The uniform electric field was provided using the mesh electrode and the bubble dynamics were observed the using high speed camera (i.e. 800 frames per second discussed in Section 4.1).

The boiling curves for emery polished, fine sandblasted, rough sandblasted, EB enhanced and sintered surfaces are presented in the Figures 6.28 - 6.32.

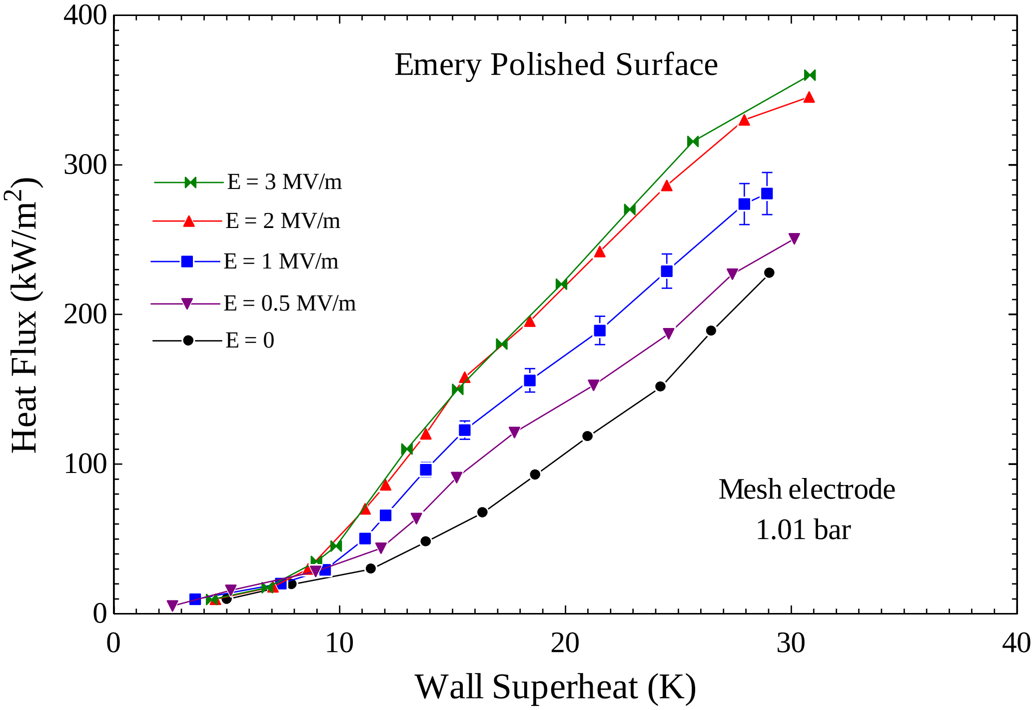

Figure 6.28 Boiling curves for emery polished surface with EHD

The results are shown in this section related to decreasing heat flux in order to avoid hysteresis. The effect of uniform electric field on the pool boiling using emery polished surface is shown in Figure 6.28. It can be deduced that, at E = 0, the ONB was at 12 K wall superheat. While, at E = 1 MV/m, the ONB was observed at 9 K wall superheat. This decreasing trend of wall superheat continues as the magnitude of electric field increases. Furthermore, as electric field increases the heat flux also increases at a specific value of wall superheat. Similar, observations have been noticed in Figure 6.29, which depict pool boiling results using the fine sandblasted surface both with and without electric field. It can be observed that the ONB was at

12.2 K (approximately) when E = 0. But at E =1, ONB was observed at lower value of wall superheat, i.e. 9 K, further increase in electric field results in the decreasing the value of wall superheat corresponding to ONB, see Figure 6.29. Moreover, with the application of uniform electric field the boiling curve move towards the left, i.e. the heat transfer enhancement was observed.

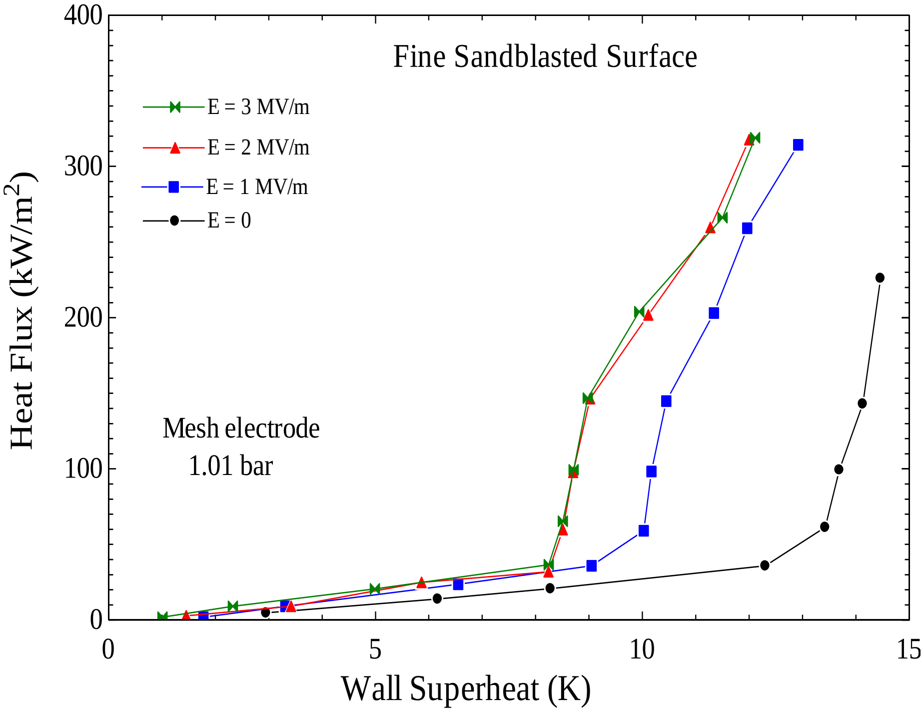

Figure 6.29 Boiling curves for fine sandblasted surface with EHD.

In Figure 6.30, the effect of uniform electric field on pool boiling using rough sandblasted surface is presented. The value of applied electric field was increased in smaller steps, i.e. 0.25 MV/m, by regulating the electric potential. Similar to the observations of emery polished and fine sandblasted surfaces, the magnitude of heat transfer increases at a specific value of wall superheat as the electric field increases. Same trend can be seen in Figure 6.31, which represents the effect of high intensity uniform electric field on pool boiling using special spike structure made by using electron beam, i.e. EB enhanced surface, see Section 4.2.

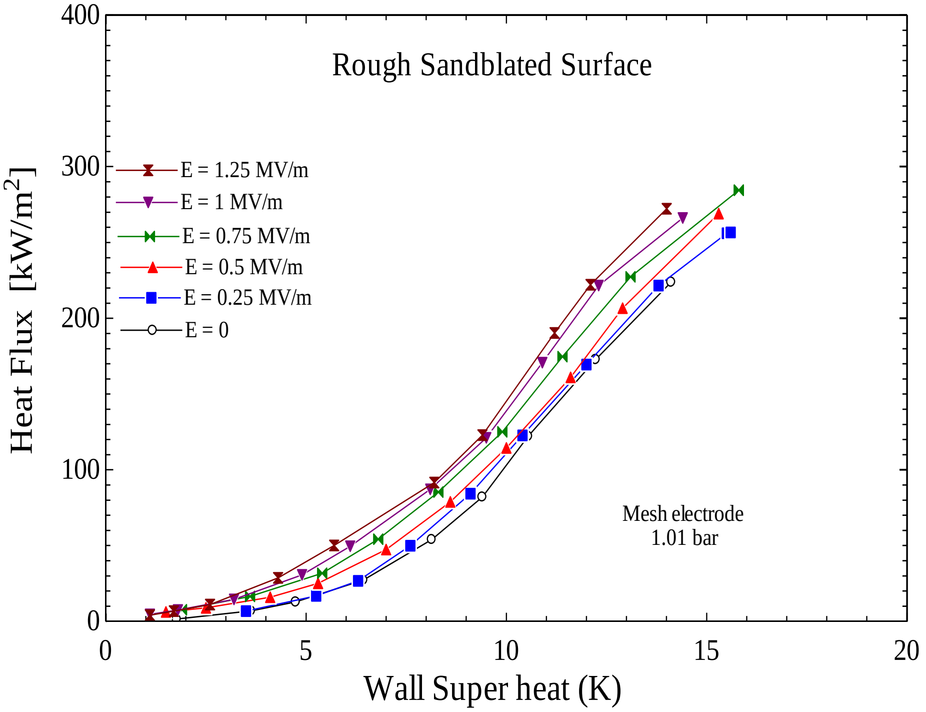

Figure 6.30 Boiling curves for rough sandblasted surface with EHD

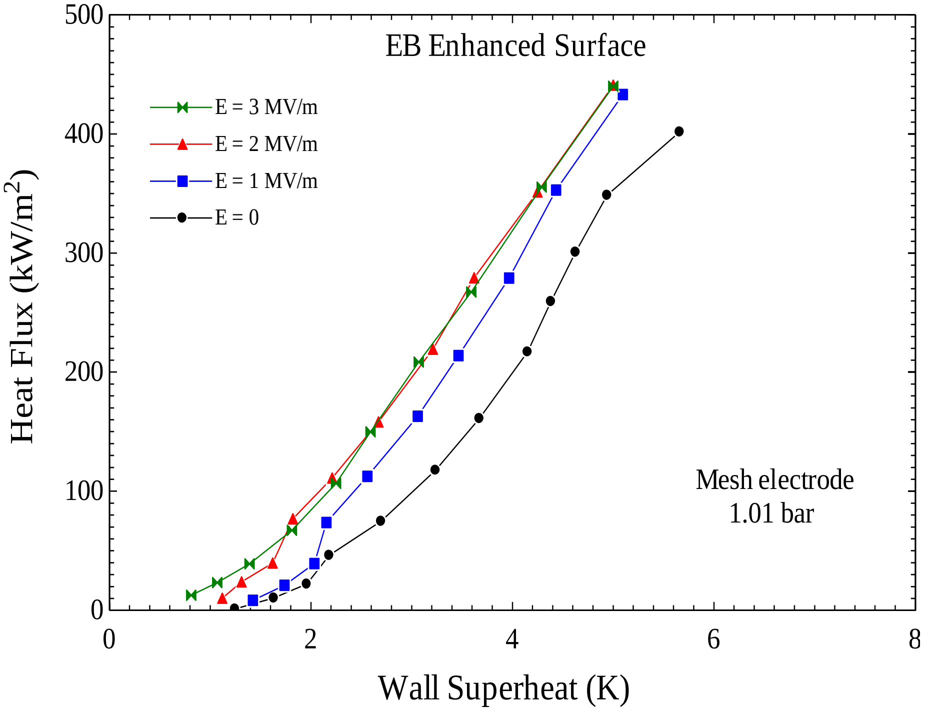

Figure 6.31 Boiling curves for EB enhanced surface with EHD

Similar to the emery polished, fine sandblasted and rough sandblasted surface, as the electric field increases the heat transfer also increases at a specific value of wall superheat as compared to no field conditions.

In Figure 6.32, the pool boiling under the application of high intensity uniform electric field is shown using sintered surface. On contrary to the observation mentioned for emery polished, fine sandblasted, rough sandblasted and EB enhanced surfaces, there is marginal effect of uniform electric field on the pool boiling using sintered surface.

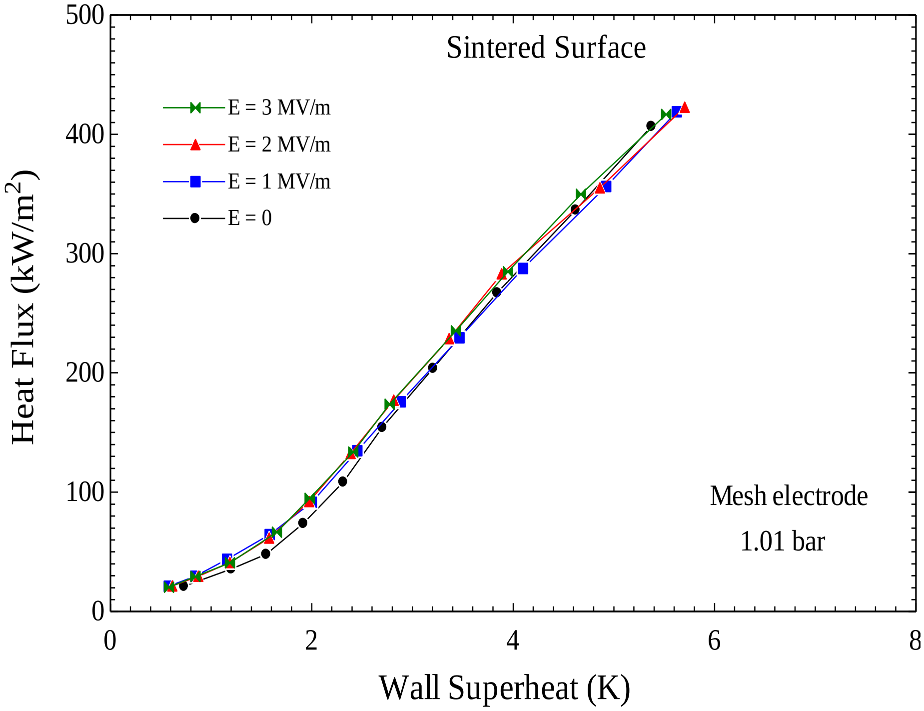

Figure 6.32 Boiling curves for sintered surface with EHD

The enhancement in the value of heat flux at specific value of wall superheat is due to following reasons:

- At low heat flux, when there are no bubbles on the heating surface, the application of electric field induces liquid convective currents. It was seen during the visual observations of present experiments that the application of the electric field is responsible for the liquid movement at low heat flux, i.e. within the convective heat transfer regime as shown in Figure 6.33. The liquid movement due to the application of electric field is known as electroconvection, also discussed in Section 3.5. These visual observation results are similar to that reported by Wang et al. (2009). The application of heat results in the formation of thermal boundary layer and the induction of thermal convection within the boiling liquid. Due to the induction of both electroconvection and thermal convection, the liquid movement increases towards the boiling surface, which results in enhancement of heat transfer rates from the boiling surface.

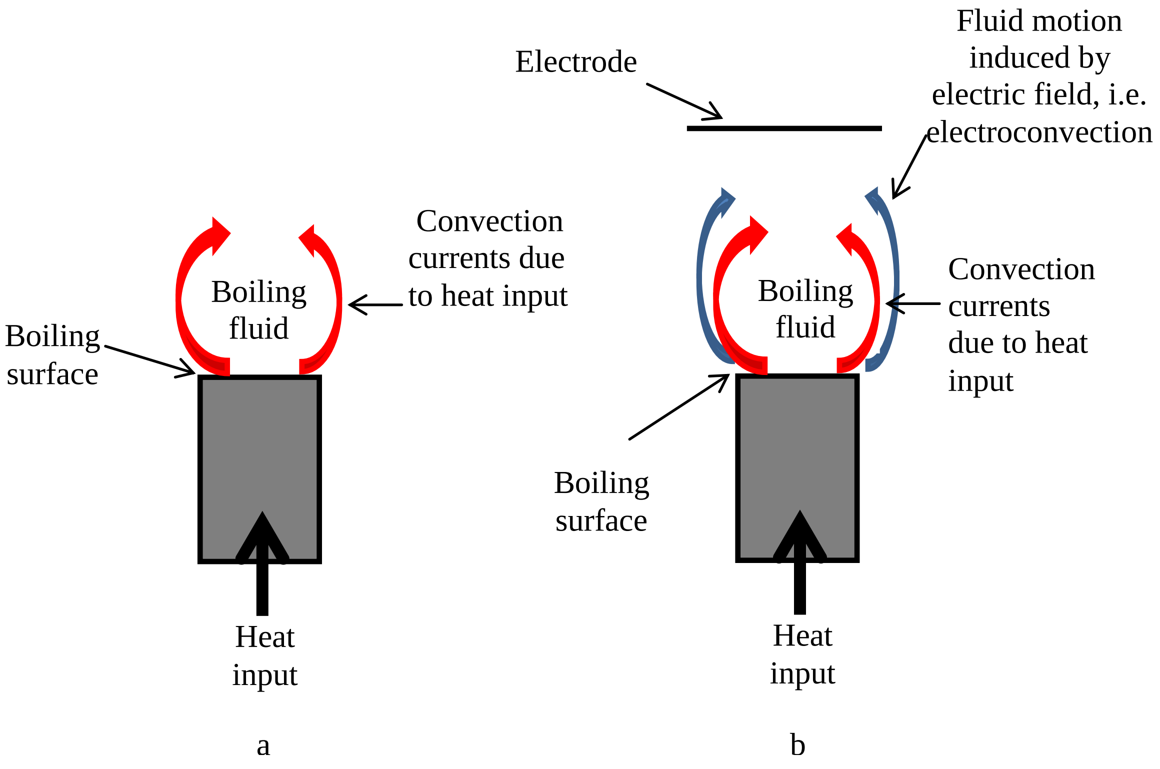

Figure 6.33 Demonstration of fluid motion (a) without EHD (b) with EHD

- There is a temperature gradient within the thermal boundary layer and the bulk of the liquid at the saturation temperature. The electric permittivity is the function of a temperature gradient, which remains constant in the bulk of the liquid. But within the thermal boundary layer, there is a gradient in the value electric permittivity due to the thermal gradient. The high intensity electric field acts on fluid due to the sparial changes in the electric permittivity within the thermal boundary layer, this induces a force on the liquid body, which leads to the augmentation in the value of heat flux at the specific value of wall superheat within the convective heat transfer regime. It can be concluded from above discussion that the application of EHD affects the thermal boundary layer and boost up the liquid circulation rate towards the heating surface which is responsible for increase in the heat flux within convective boiling regime. When bubbles appear in the nucleate boiling region electroconvection continues to play a role but is now complemented by the effect of the electric field on the bubbles. Allen and Karayiannis (1995) reviewed the EHD effect during two–phase heat transfer and reported that the enhancement could be attributed to the action of electric field on three factors namely: vapour – liquid interface, vapour bubble and change in the contact angle and surface tension. The EHD acts to destabilize the vapour – liquid interface and this destabilizing effect tend to reduce the thermal resistance. Furthermore, Karayiannis and Xu (1998) mathematically calculated the distortion in the uniform electric field with the formation of bubble. They reported a 30 % increase in electric field on the sides of the bubble and slight decrease in electric field at the top of the bubble. Later, similar mathematical observations were reported by Dong et al. (2006). With bubbles present, they found an increase in the electric field on the sides of the bubbles. They also reported a decrease in the magnitude of electric field at the top of the bubble. In two phase heat transfer systems, the presence of bubbles causes a local reduction in the electric field strength, which leads to non–uniformity of the field with how the possible effect of increasing the heat transfer rates. The stresses on the bubble under a uniform electric field were calculated by Chen et al. (2007 a), who found that the amount of the compressive stresses were more than the expanding stresses. This mathematical calculations presented by Karayiannis and Xu (1998) are similar to the visual observations during the present studies and has been discussed in Section 6.1. It can be observed from the Figure 6.16 that the vapours were nearly spherical in the absence of the electric field. But with the application of electric field, the bubble change to mushroom structure, see Figure 6.18. According to Karayiannis and Xu (1998) the local value of the electric filed is increased at the sides of the bubble and Pohl (1978) explained that if the electric field is non – uniform then the component of the fluid having higher electric permittivity is attracted towards the region of high electric field intensity. Using the Pohl (1978) statement, the liquid is attracted towards the sides of the bubble where the value of electric field intensity is high. The presence of liquid on the sides of the bubble pushes the interface inwards. On the other hand, according to Karayiannis and Xu (1998) the electric field decreases at the top of the bubble and using the Pohl (1978) statement, the top region of the bubble is favourable for bubble attraction (because the bubble have low permittivity and should be attracted towards the region of low electric field intensity). This will leads to the elongation of the bubble and typical mushroom structure, see Figure 6.18.

The effect of uniform electric field on pool boiling using sintered surface is presented in Figure 6.32. It can be observed from the Figure 6.32 that there is no effect of the electric field on boiling when the sintered surface was used for heating. This is due to the special structure of the sintered surface. As mentioned earlier in Chapter 4, a porous copper powder was fused on the surface, which gave a porous network on the heating surface. The bubbles are produced within the sintered layer and equally distributed through the pores of the layer. As mentioned above, EHD interacts with the vapor –liquid interface, vapour and alters the properties of the boiling liquid during bubble growth (Allen and Karayiannis (1995)) to enhance the boiling heat transfer. But in the case of sintered surface, the bubble growth takes place within the porous network and there is no direct interaction between vapour – liquid interface and vapour bubble with the applied electric. Therefore, there is no effect of electric filed on the boiling heat transfer with sintered surface.

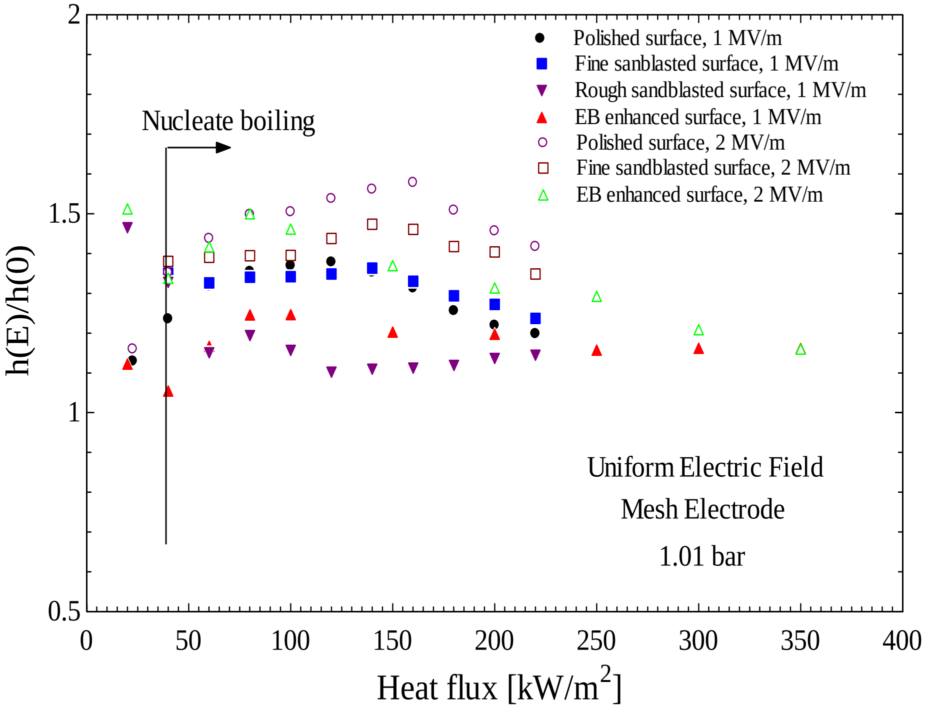

Figure 6.34 Enhancement in heat transfer coefficient due to application of uniform electric field.

The enhancement in the value of the heat transfer coefficient is presented in the Figure 6.34. It can be observed that at low heat flux the enhancement value, i.e. h(E)/h(0), is high but as the heat flux increases the augmentation in the value of heat transfer coefficient decreases, see Figure 6.34. This effect was also reported by Zaghdoudi and Lallemand (2005), Hristov et al. (2009) and Wang et al. (2009). Zaghdoudi and Lallemand (2005) argued that this is due to the shielding effect of the vapours, i.e. as heat flux increases the number vapour on the heating surface increases. These vapours hinder in the interaction of electric filed and the growing bubble. This fact is mathematically simulated by Karayiannis and Xu (1998) as shown in the

Figure 6.35. According to Karayiannis and Xu (1998), the bubbles in the can be divided into two categories, i.e. departing bubbles and growing bubbles, see

Figure 6.35. There was a reduction in the electric field strength to 6 MV/m in the middle layer and at the top of the growing bubble. This decrease in the value of the electric field is due to the shielding effect of the departing bubbles, which are responsible for decreasing the heat transfer enhancement at higher heat flux.

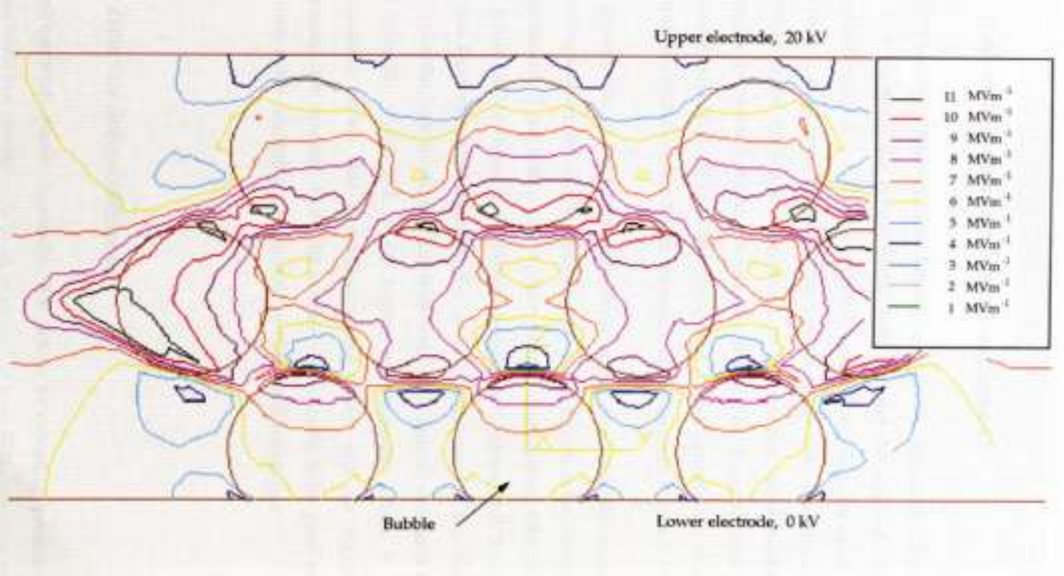

Figure 6.35 Electric field within the multiple vapour layers Karayiannis and Xu (1998).

6.4.2 Non – uniform electric field

The effect of a non – uniform electric field on pool boiling heat transfer is presented in this section. The results of decreasing heat flux obtained for emery polished, fine sandblasted, EB enhanced and sintered surface are depicted in the figure. As discussed earlier in Chapter 4, the non – uniform electric field was provided using two rod electrodes, i.e. one with 5 mm rod spacing and second with 8 mm rod spacing. The electric filed calculated is a nominal value defined simply as the electric potential divided by the electrode spacing, i.e E = V/d. Figures 6.36 to 6.43 depict the boiling curves with the application of non – uniform electric field at 1.01 bar saturation pressure.

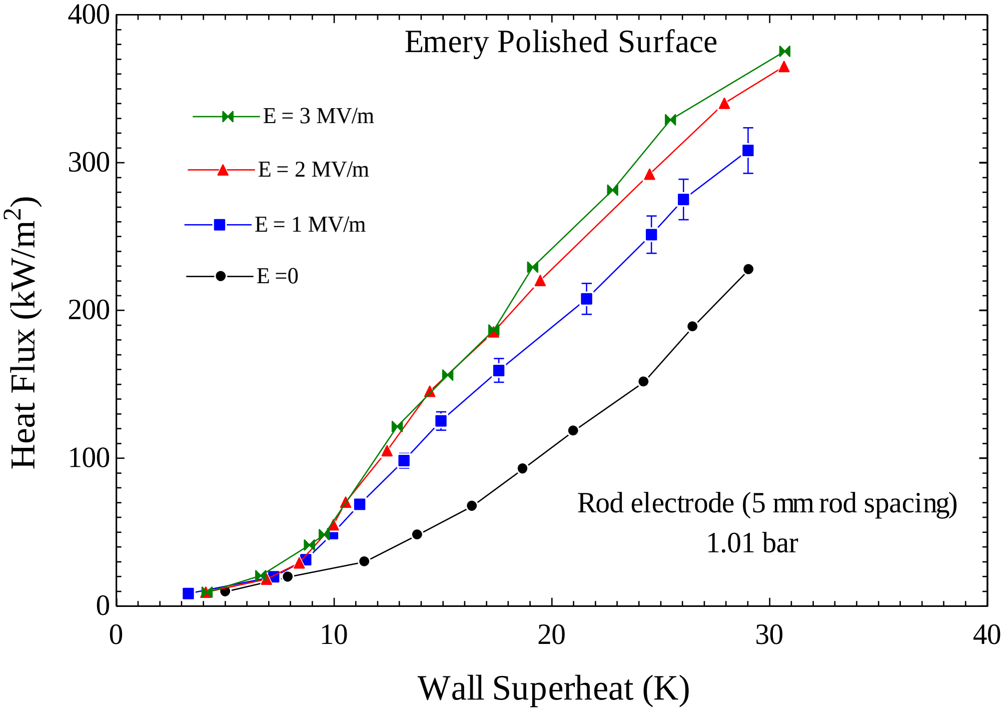

Figure 6.36 Effect of non- uniform electric field on pool boiling of emery polished surface using rod electrode (rod spacing 5 mm).

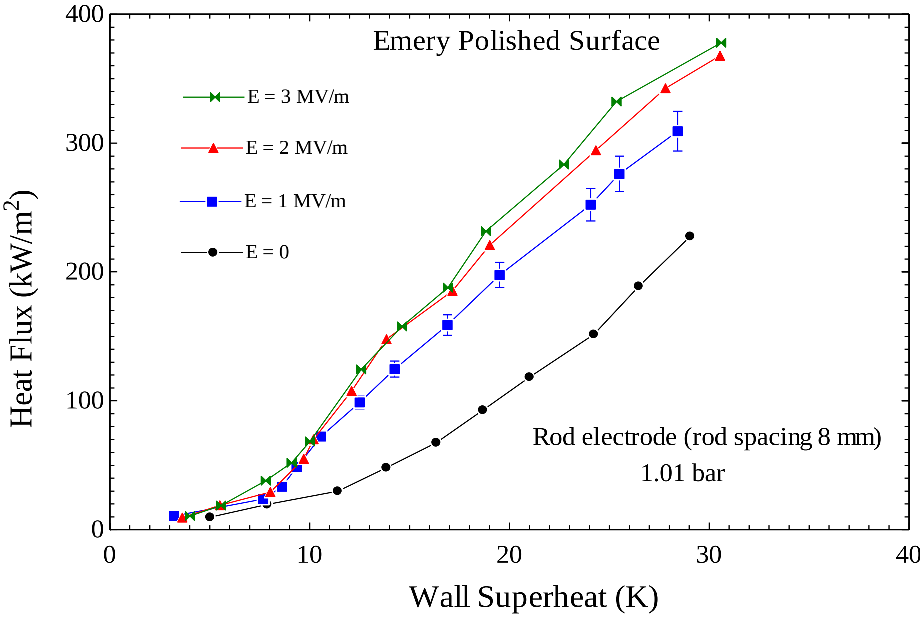

Figure 6.37 Effect of non- uniform electric field on pool boiling of emery polished surface using rod electrode (rod spacing 8 mm)

The effect of high intensity non- uniform electric field using emery polished surface has been shown in Figure 6.36 and Figure 6.37 with 5 mm rod spacing and 8 mm rod spacing respectively. It can be deduced from these figures that with the application of the electric field the heat transfer also increases at a specific value of wall superheat. Furthermore, as the magnitude of degree of non – uniformity increases, the heat transfer also increase, i.e. rod electrode with 8 mm rod spacing shows better heat transfer results as compared to rod electrode with 5 mm rod spacing. It can also been noted that with the application of high intensity non – uniform electric field ONB occurs at lower value of wall superheat.

In Figure 6.38 and Figure 6.39 the effect of high intensity non – uniform electric field has been depicted using rod electrode with 5 mm rod spacing and with 8 mm rod spacing respectively, when pool boiling was performed on fine sandblasted surface. Similar to the observation for emery polished surface, it can be noted that as the magnitude of electric field increases the boiling curve moves towards the left, i.e. heat transfer augments.

Furthermore, as the magnitude of non – uniformity increases the heat transfer also increases, i.e. rod electrode with 8 mm shows better heat transfer results as compared to rod electrode with 5 mm rod spacing. Moreover, with the application of electric field the ONB occurs at low value of wall superheat.

The application of non – uniform electric fields on pool boiling using EB enhanced surface has been shown in Figure 6.40 and Figure 6.41. It can be noted from these figures that, similar to the pool boiling results using emery polished and fine sandblasted surfaces, the heat transfer increases as the electric field increase. Furthermore, the EHD pool boiling results with 8 mm rod spacing is better as compared to 5 mm rod spacing.

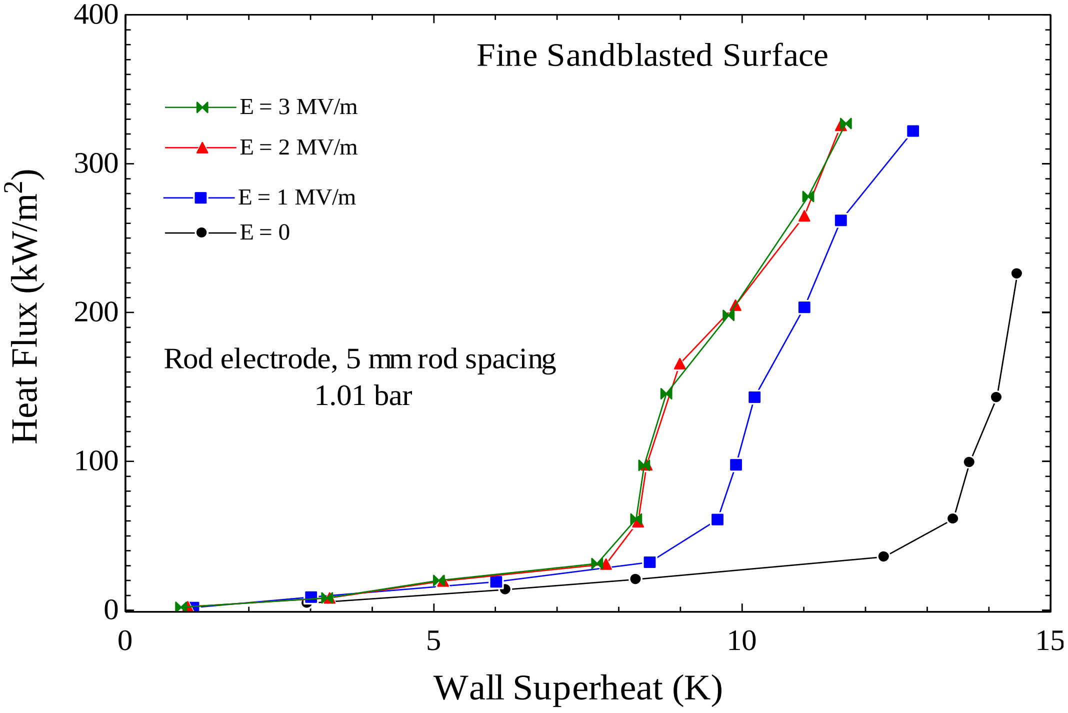

Figure 6.38 Effect of non- uniform electric field on pool boiling of fine sandblasted surface using rod electrode (rod spacing 5 mm).

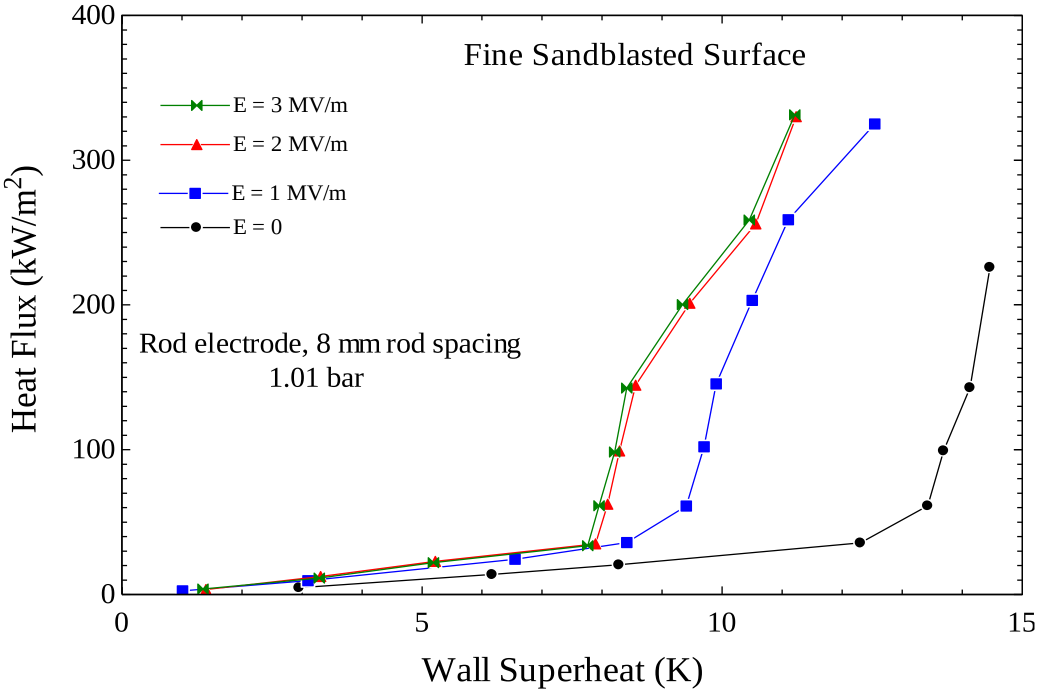

Figure 6.39 Effect of non- uniform electric field on pool boiling of fine sandblasted surface using rod electrode (rod spacing 8 mm)

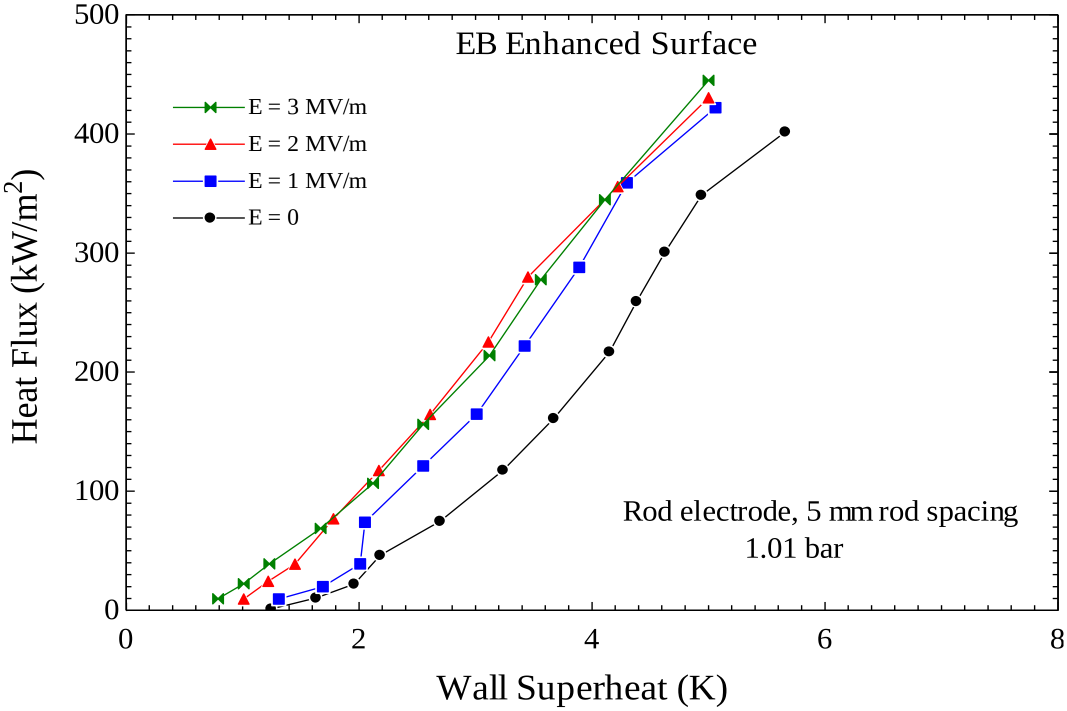

Figure 6.40 Effect of non- uniform electric field on pool boiling of EB enhanced surface using rod electrode (rod spacing 5 mm).

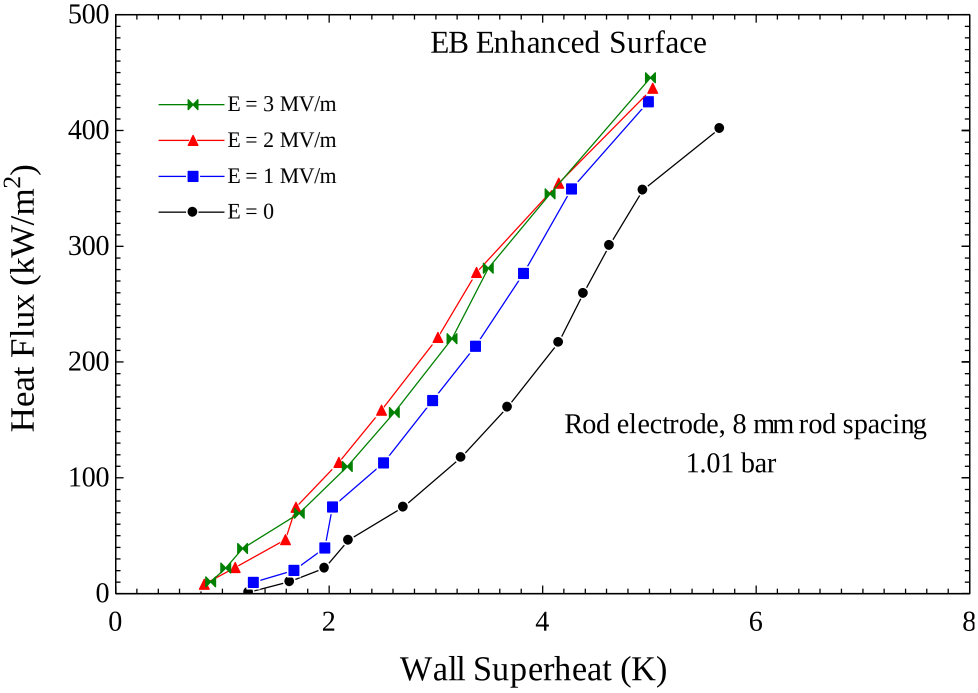

Figure 6.41 Effect of non- uniform electric field on pool boiling of EB enhanced surface using rod electrode (rod spacing 8 mm).

On contrary to the pool boiling results using emery polished, fine sandblasted and EB enhanced surfaces, there is no effect of the non – uniform electric field on pool boiling using the sintered surface, see Figures 6.42 and 6.43.

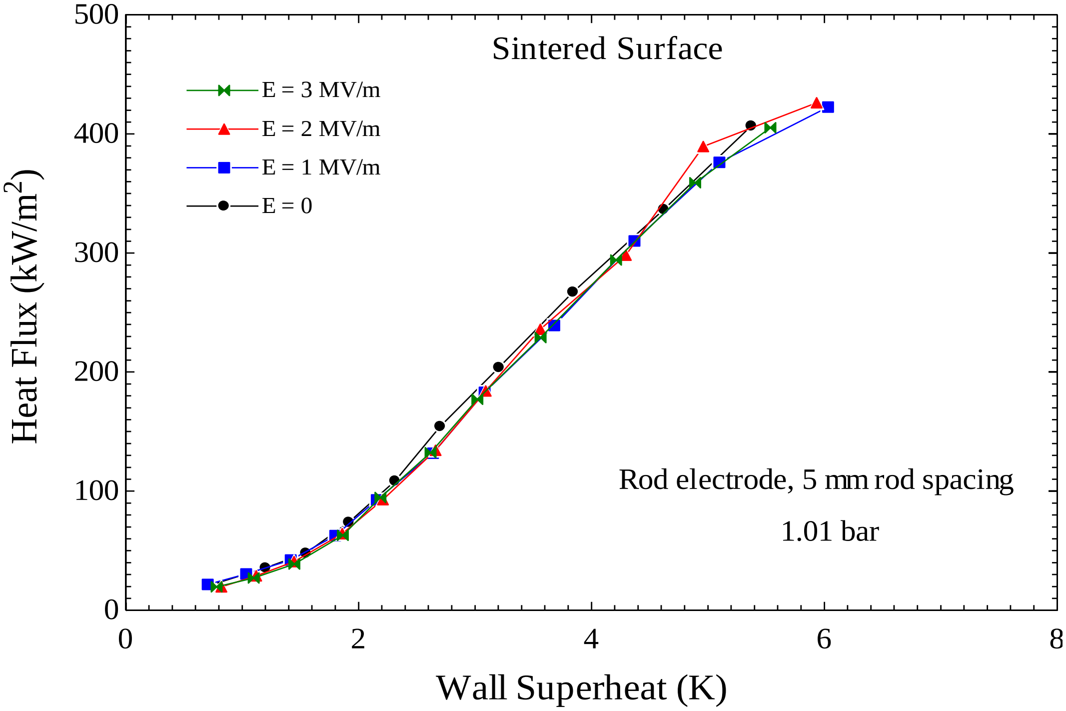

Figure 6.42 Effect of non- uniform electric field on pool boiling of sintered surface using rod electrode (rod spacing 5 mm).

The increase in the value of heat transfer coefficient at specific value of wall superheat is due to the behaviour of a dielectric molecule in a non-uniform electric field, which was discussed by Pohl (1978), see Section 3.2. As discussed earlier, under the application of non- uniform electric field the molecules become polarized and the part of the fluid with the higher electric permittivity is attracted towards the region of high electric field intensity.

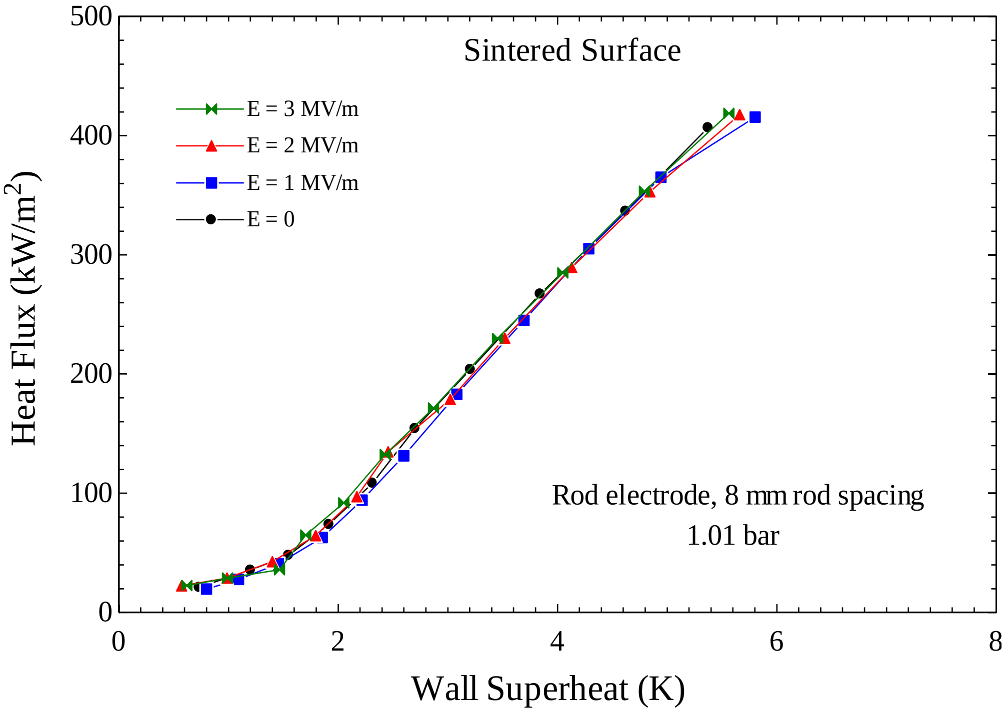

Figure 6.43 Effect of non- uniform electric field on pool boiling of sintered surface using rod electrode (rod spacing 8 mm)

For R-123, liquid has a relative electric permittivity of 3.42 (compared to the dielectric constant of the air) Hristov et al. (2009), whereas the value for vapour is very close to 1. Under the action of electric field molecules of the liquid are attracted towards the region of high electric field intensity, i.e. the rod electrode. On the other hand, the component having low relative electric permittivity is attracted towards the region of low electric intensity. It can be deduced from the argument of Pohl (1978) that the bubbles (which have low electric permittivity) should be pushed away from the rod electrode (i.e. the region of high electric intensity). It can be summarised, the motion which was induced on the dielectric molecule due to the application of non – uniform electric field is responsible for the heat transfer augmentation during pool boiling process.

The visual observations of growing and departing bubbles were similar to the theoretical explanation given by Pohl (1978). It can be observed that with a non-uniform electric field of 1 MV/m the departing bubble had a thin elongated shape with irregular edges, see in Figures 6.20 and 6.22. In addition on detachment from the boiling surface, bubbles deviated from their normal path (i.e. that without EHD) and were pushed away from the rod electrode.

The effect of the electric field on the pool boiling using sintered surface has already been discussed in Section 6.4.1. The porous structure on the sintered surface is responsible for bit of heat transfer augmentation. The enhancement ratio of heat transfer coefficient is presented in Figures 6.44 and 6.45 for the rod electrode where the 5 mm spacing and the rod electrode with the 8 mm rod spacing respectively. The enhancement value is found to decrease at high heat flux, which is due to the shielding effects of the (as mentioned above).

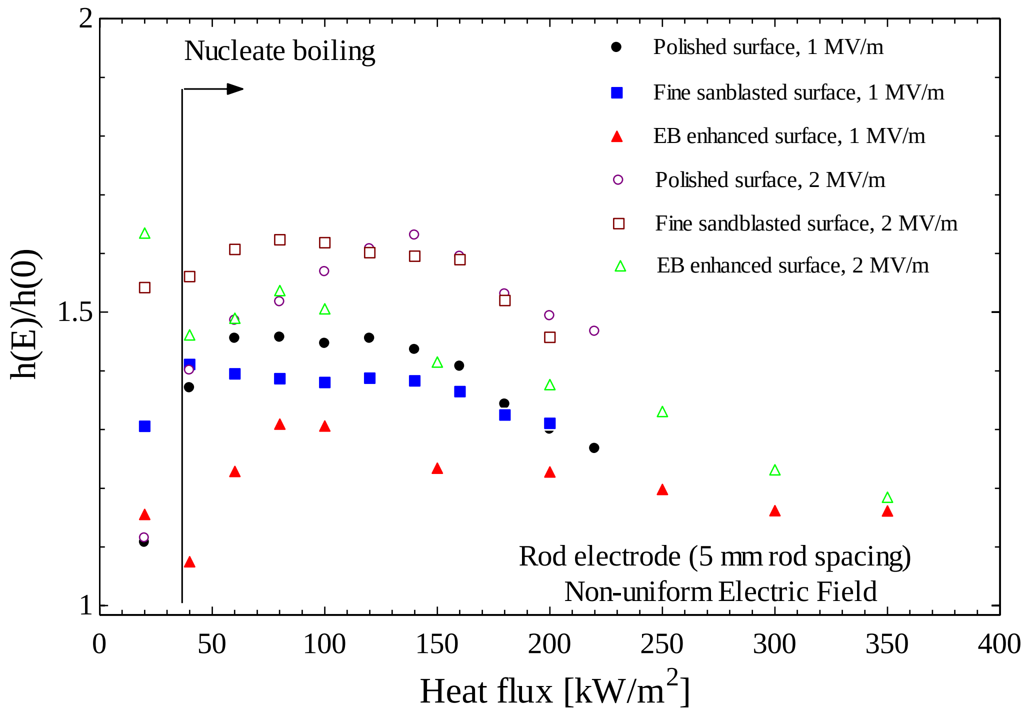

Figure 6.44 Enhancement in heat transfer coefficient due to application of non – uniform electric field (rod electrode with 5 mm rod spacing).

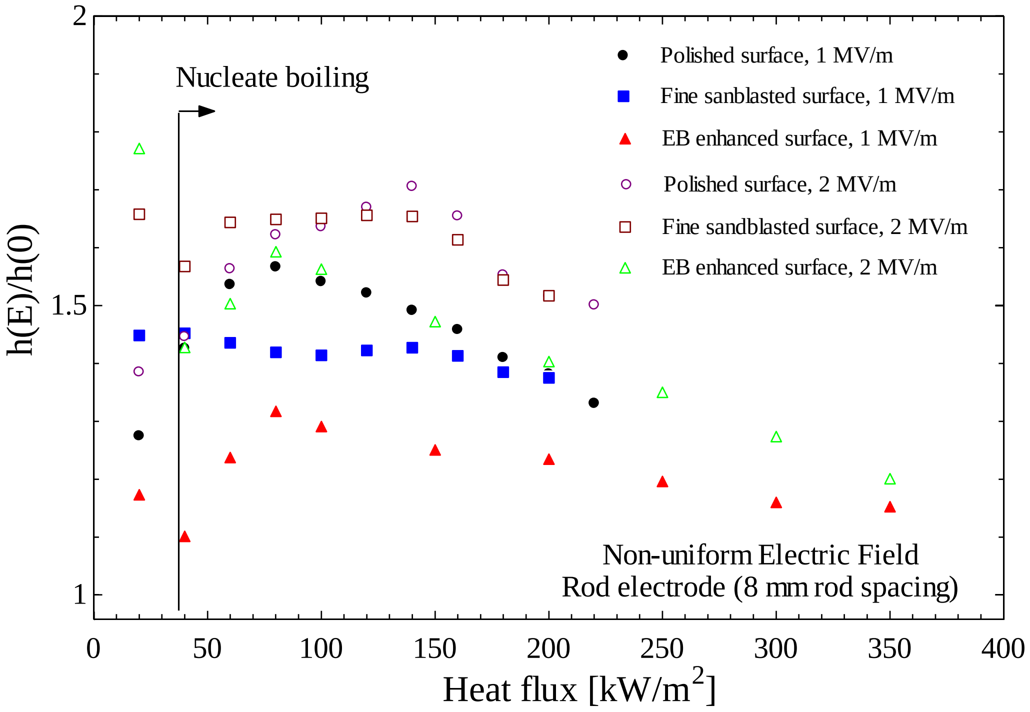

Figure 6.45 Enhancement in heat transfer coefficient due to application of non – uniform electric field (rod electrode with 8 mm rod spacing).

6.4.3 Comparison of EHD results

The EHD results of emery polished surface is compared with the experimental results reported by Zaghdoudi and Lallemand (2005) and Hristov et al. (2009), see Figure 6.46 (a) and (b) respectively. It should be noted that only the results of emery polished surface are compared because both Zaghdoudi and Lallemand (2005) and Hristov et al. (2009) used emery polished surface to perform their pool boiling experiments. For detailed comparison, the results of emery polished surface without EHD have also been plotted in Figure 6.46. It can be deduced from the Figure 6.46 (a) that the results of Zaghdoudi and Lallemand (2005) shows higher values of heat flux at specific value of the wall superheat. As discussed earlier in Section 6.1 that Zaghdoudi and Lallemand (2005) polished their boiling surface with emery paper No 600, while in present experiments smoother emery paper, i.e. P 1200, was used for polishing the surface. Polishing with a coarser emery paper, resulted in the boiling surface used by Zaghdoudi and Lallemand (2005) to be rougher than the present emery polished surface. The difference in the surface condition is responsible for higher value of heat flux at specific value of wall superheat. It can also be observed from the experimental results of Zaghdoudi and Lallemand (2005) that the augmentation in the value of heat transfer with the application of 1 MV/m electric is smaller as compared to presents results, see Figure 6.46 (a). The low enhancement was due the factor that Zaghdoudi and Lallemand (2005) used fine mesh for providing uniform electric field (i.e. 54 %free area) while in present case the mesh electrode was coarser (i.e. 64 % free area). The degree of non – uniformity of electric field is more with the coarser mesh and this can lead to high heat transfer augmentation.

On the other hand, Hristov et al. (2009) used a similar experimental facility as the current one at Brunel University and they polished the surface with the same emery paper (i.e. P 1200), which was used during the present experiments. The results reported by Hristov et al. (2009) was in good agreement with the present experimental results of emery polished surface without EHD, see Figure 6.46 (b). But the augmentation in heat transfer due to the application of 2MV/m electric field was low as compared to the present results for emery polished surface. It was due to two factors, firstly Hristov et al. (2009) used fine mesh (54 % free area) (as mentioned above) which may result in low heat transfer augmentation. Second factor was electrode spacing, i.e. the distance between the mesh electrode and heating surface. The electrode spacing was 5 mm in the experiments performed by Hristov et al. (2009), while in present case it was 10 mm. It will be discussed late in Section 6.4.6, it can be stated that if the electrode spacing increases the augmentation in the value of heat flux at specific value of wall superheat and the electric filed strength also increases.

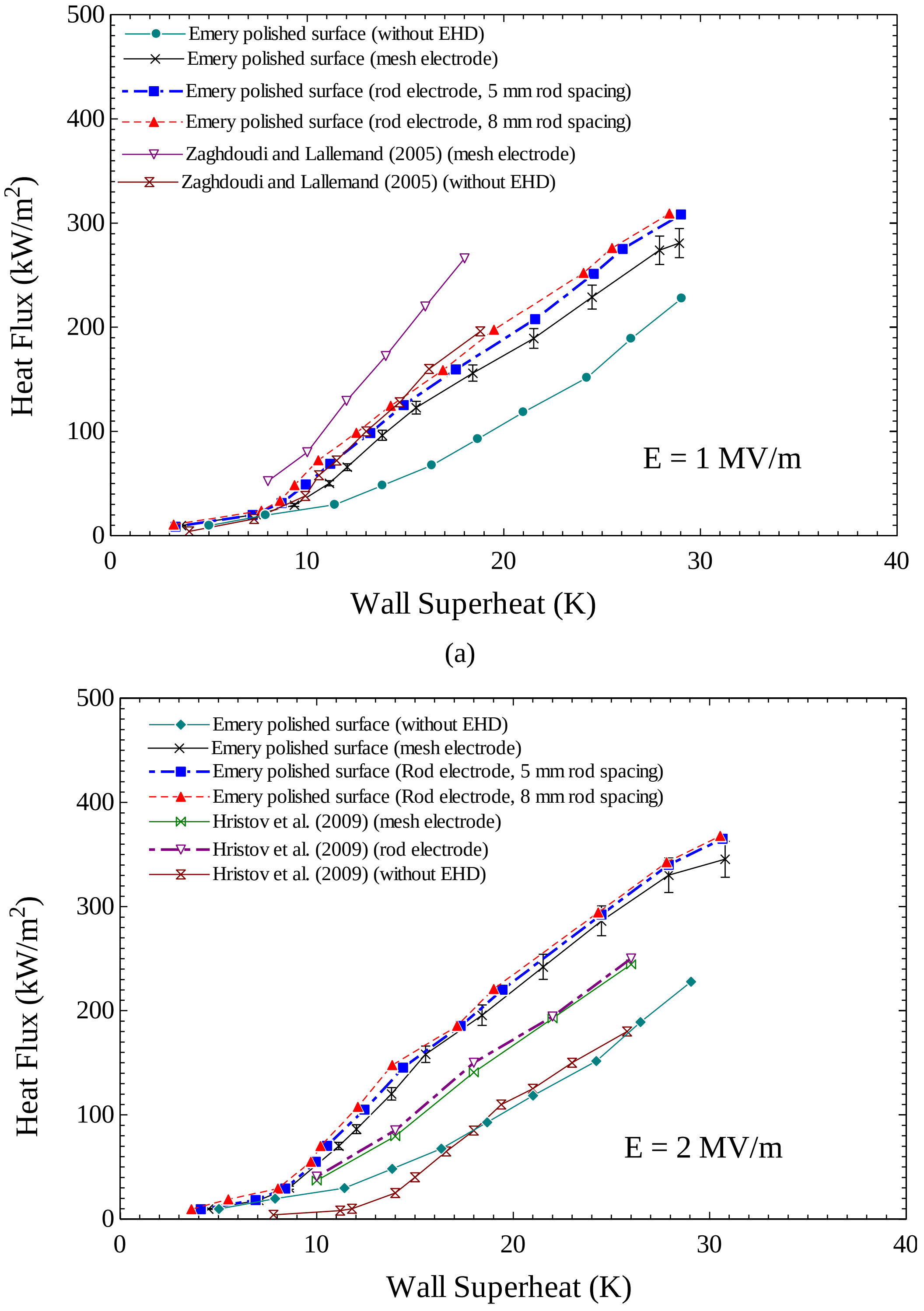

(a)

(b)

Figure 6.46 Comparison of EHD results of emery polished surface with past researchers (a) at E = 1 MV/m (b) at E = 2 MV/m.

6.4.4 Effect of EHD on boiling hysteresis

Pool boiling hysteresis has already been reviewed in Section 2.7 and the effect of surface modification on the boiling hysteresis is presented in Section 6.1.3. The effect of a high intensity electric field on boiling hysteresis is discussed in this section. As mentioned in section 6.1.3 the emery polished and the fine sandblasted surfaces did not show any hysteresis. Therefore, the hysteresis tests for the emery polished and fine sandblasted surface are not presented here. Also discussed in Section 6.4.1, there is no effect of the EHD on pool boiling using the sintered surface. The rough sandblasted and the EB enhanced surfaces exhibit boiling hysteresis and there results are discussed here.

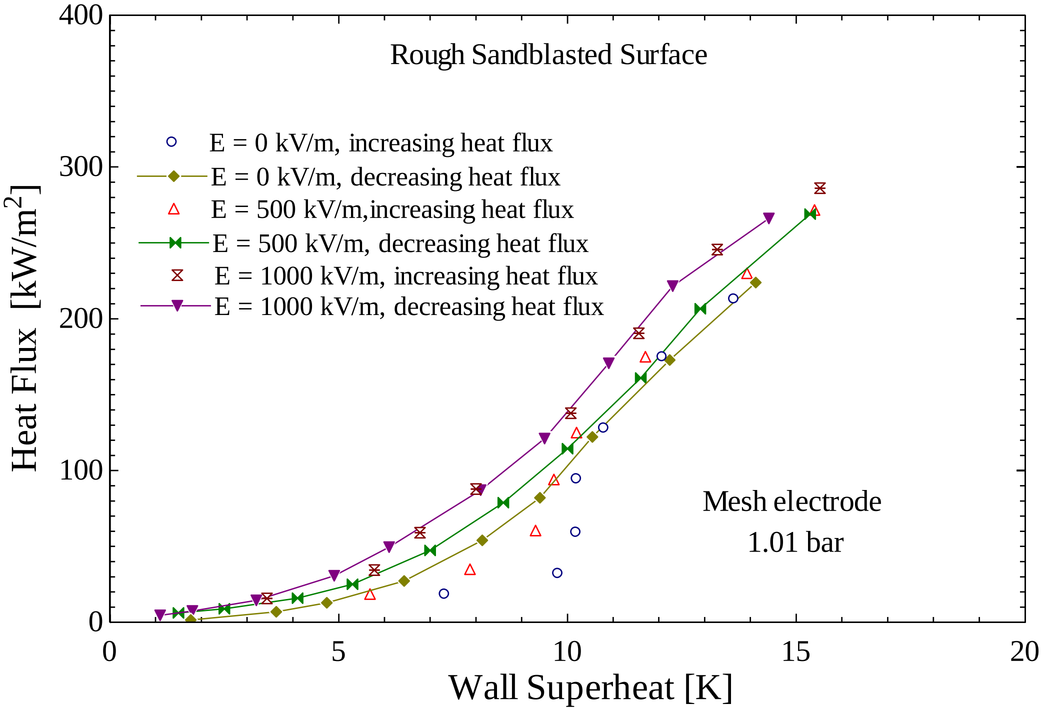

Figure 6.47 Effect of uniform electric filed on boiling hysteresis using rough sandblasted surface

The effect of the high intensity electric filed on the pool boiling hysteresis is presented in Figure 6.47. All the tests represented in this figure were carried out on rough sandblasted surface, while the electric filed was provided using the mesh electrode at 1.01 bar saturation pressure. It can be observed from the results that as the electric field increased from 0 kV/m to 1000 kV/m the boiling hysteresis was progressively eliminated and at 1000 kV/m the hysteresis was fully eliminated.

It has already been discussed in Section 2.7 that the boiling hysteresis depends on fluid properties and the characteristics of the heater surface. It has also been mentioned in Section 6.1.3 that boiling hysteresis was due to the deactivation of surface cavities, which depends upon the wedge and contact angles of the cavities and boiling liquid respectively. Allen and Karayiannis (1995) summarized this fact, i.e. with the application of electric field the liquid contact angle changes. They presented in their review that the liquid contact angle is a function of surface tension as follows:

$$\cos\theta = \frac{\sigma_{wl} - \sigma_{gw}}{\sigma_{lg}} \tag{6.1}$$

It was reported that with the application of electric field the surface tension and liquid contact angle changes. Due to alteration in the surface tension and liquid contact angle, the surface cavities become active and responsible for ebullition of nucleate boiling at low value of wall superheat. Furthermore, Cooper (1990) explained that this electrical activation is identical to the thermal activation and the cavities remained active when the electric field was removed. As mentioned earlier, Zaghdoudi and Lallemand (2005) explained the effect of electric field on the pressure difference within the cavity, see equation 3.8. It can be deduced from the mathematical expression presented by Zaghdoudi and Lallemand (2005) that the surface tension of the liquid changes due to application of electric field. This mathematical evidence is similar to the findings of Allen and Karayiannis (1995).

Moreover, similar experimental results were reported by Zaghdoudi and Lallemand (2005). As discussed earlier, during their experiments with R-123, the hysteresis was eliminated with the application of 2000 kV/m uniform electric field.

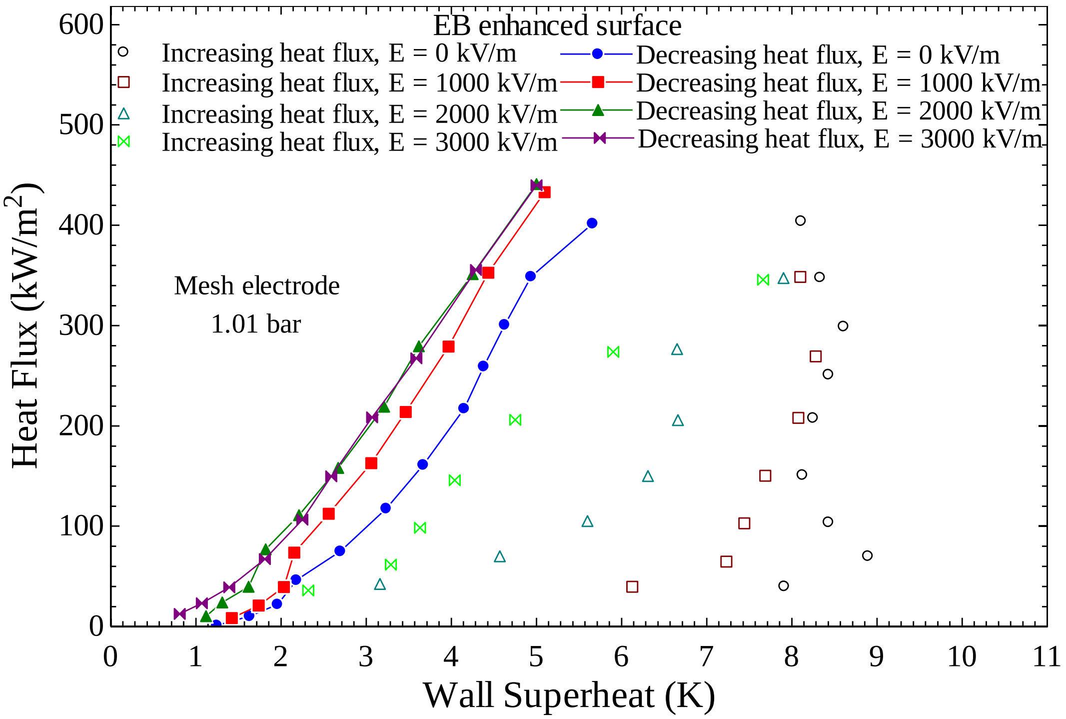

Figure 6.48 Effect of uniform electric field on pool boiling using EB enhanced surface

Furthermore, the hysteresis results for the EB enhanced surface are depicted in Figures 6.48 and 6.49 for uniform and non – uniform electric field respectively. During these experiments, the saturation pressure was maintained at 1.01 bar. It can be observed from Figure 6.48 that as the electric field increases the boiling hysteresis gradually reduces but is not fully eliminated at the maximum electric potential that can be applied up to 30 kV, which can generate 3000 kV/m electric field. Similar observations can be deduced from Figure 6.49, where the non – uniform electric field was provided using the rod electrodes. Due to the degree of non - uniformity of the electric field, the removal of boiling hysteresis with the application of non – uniform electric field is slightly better than that with uniform electric field. The same observation was reported by Wang et al. (2009), as discussed earlier in Section 2.7 with the tests they performed using highly wetting liquid nitrogen. They reported that as uniform electric potential was increased from 0 to 40 kV the boiling hysteresis was reduced but not fully eliminated.

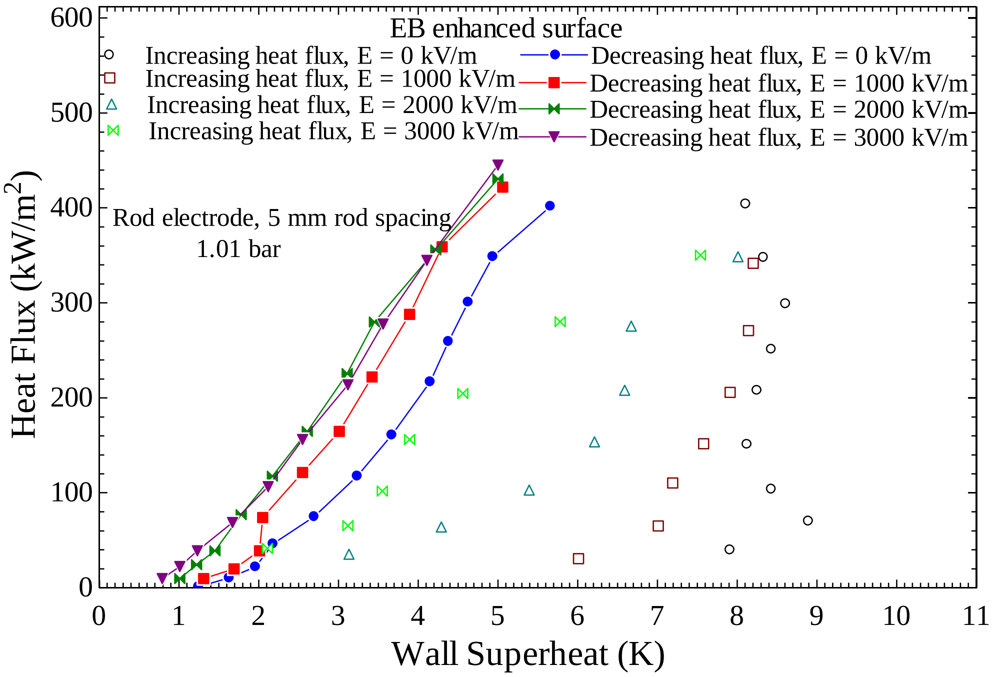

(a)

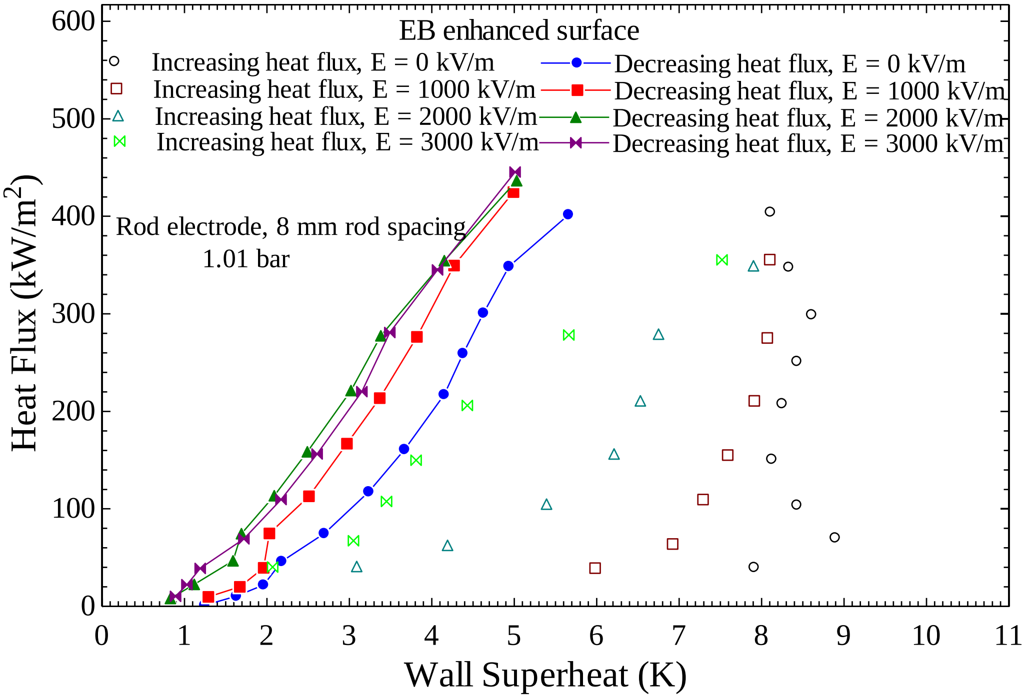

(b)

Figure 6.49 Effect of non – uniform electric field on pool boiling using EB enhanced surface with (a) rod spacing 5 mm (b) rod spacing 8 mm.

6.4.5 Effect of EHD on critical heat flux

The effect of high intensity electric field on critical heat flux is discussed in this section. The mechanism of critical heat flux and method of determining the value of critical heat flux has already been discussed in Section 2.10 and Section 3.7 respectively. The value of critical heat flux is an important parameter in equipment design and enhancing the value of CHF can lead to improve equipment design.

Figure 6.50 shows the effect of electric field on the critical heat flux when emery polished, fine sandblasted surface (uniform and non – uniform) and rough sandblasted surface (uniform only) are used. The comparison of present results with a published correlations and past experimental studies are also shown in Figure 6.50. As discussed earlier in Section 6.4.1 that there is no effect of EHD on pool boiling with sintered surface and the similar observations were found in the critical heat flux value. In the case of the EB enhanced surface, due to limitation of the heater power supply, the effect of EHD on critical heat flux value could not be measured.

It can be deduced from the Figure 6.50 that the value of this critical heat flux increases as the electric field increases. Furthermore, there is better enhancement in the value of critical heat flux when non – uniform electric field is applied. The maximum enhancement in the value of critical heat flux is by a factor of 1.75 (approximately) at 3000 kV/m. The present critical heat flux results are in good agreement with Hristov et al. (2009), who used a similar facility to the present one(see Section 6.1).

It was observed during this study that near the critical heat flux small bubbles from the heating surface tend to coalesce, eventually forming larger bubbles, see Figure 6.51. The heating surface was covered by these bubbles, which were observed to swirl in the pool. It is suggested that these bubbles obstruct bulk liquid from reaching the heating surface, promoting the formation of vapour patches and eventually leading to rapid temperature rise and dryout.

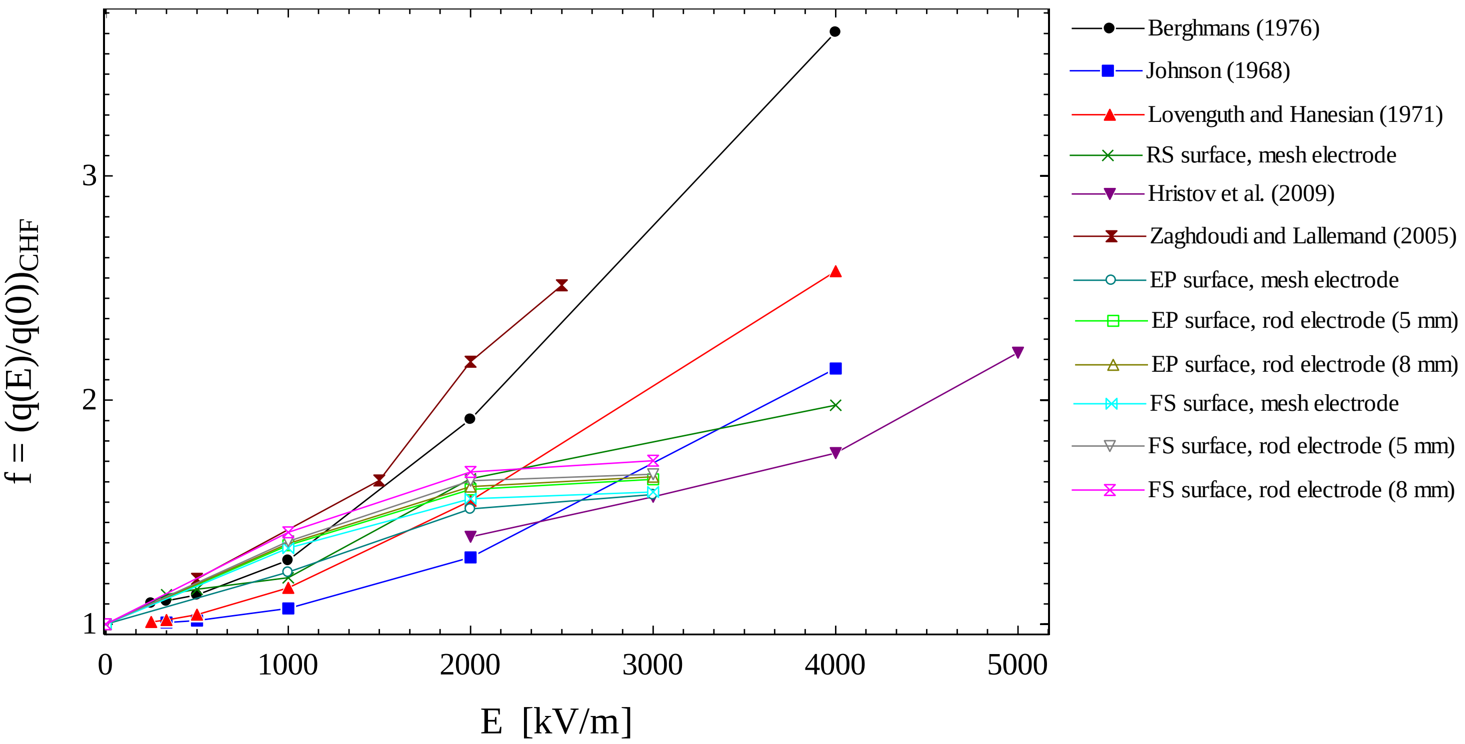

Figure 6.50 Enhancement in the value of CHF due to application of electric field, EP = emery polished, FS = fine sandblasted and RS = rough sandblasted.

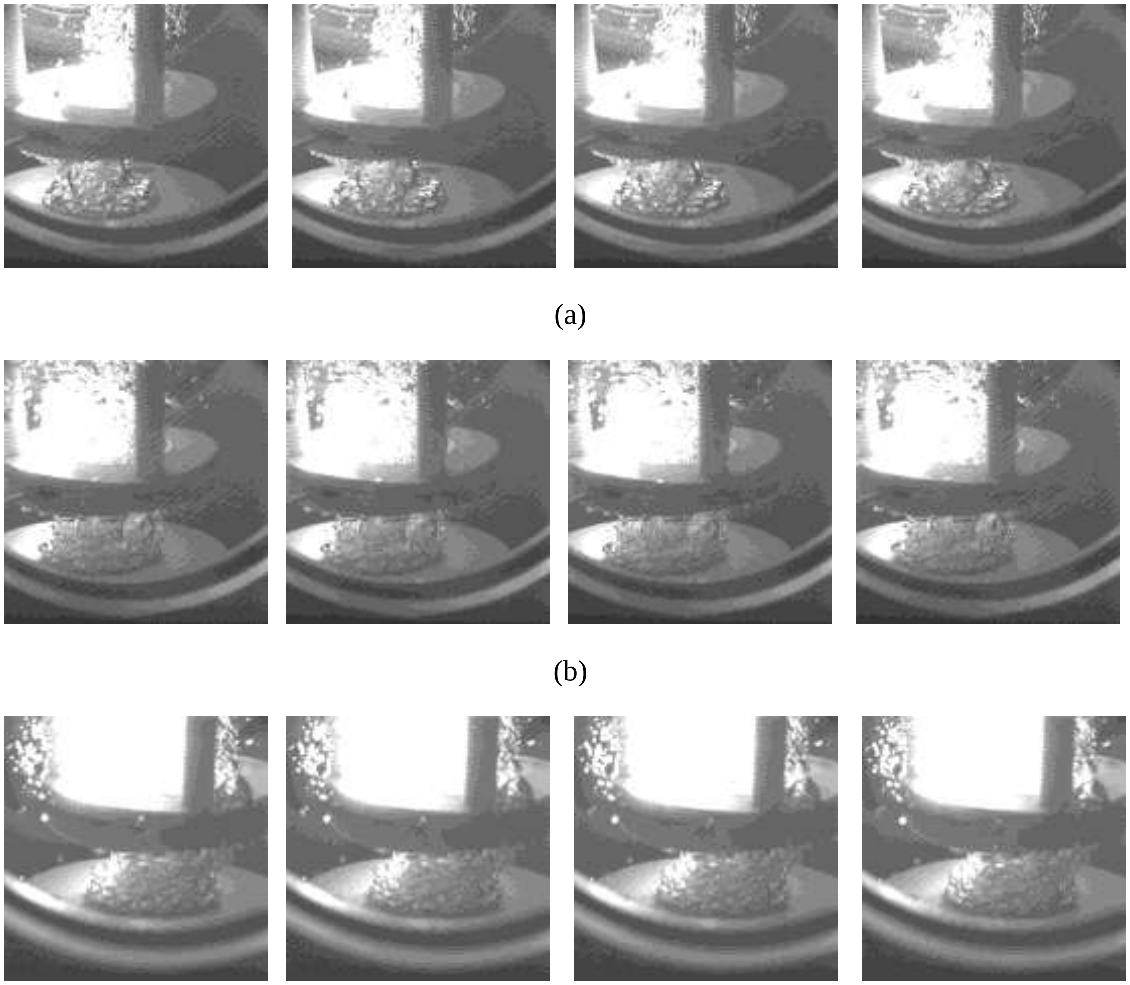

(a)

(b)

(c)

Figure 6.51 Bubble dynamics near critical heat flux (time elapse between two frames is 1.25 msec)(a) without EHD (b) with EHD using mesh electrode at 1MV/m (c) with EHD using rod electrode (5 mm rod spacing) at 1MV/m.

With the application of the electric field a change in the bubble dynamics takes place. This fact was mathematically determined by Karayiannis and Xu (1998), See . Under the application of the electric field, it was observed visually during the present experiments, that the big bubbles were pushed against the heating surface and they were converted into smaller columns, see Figure 6.51. This suppression may be responsible for changes in the bubble dynamics and more liquid may be available for the heating surface even at higher heat flux values, which may give rise to as increase in the CHF.

Similar bubble behavior was observed by Wang et al. (2009) during the pool boiling experiments with liquid nitrogen. They reported that the rise in critical heat flux was by a factor of 1.4 at 4000 kV/m. This increase is lower than the present study, which might be due to the difference in electrical properties of the liquid nitrogen and R123, i.e. the relative electrical permittivities of liquid nitrogen and R123 are 1.42 Wang et al. (2009) and 3.42 Zaghdoudi and Lallemand (2005) respectively.

6.4.6 Effect of variable electrode spacing

As shown in the preceding section, the enhancement of heat transfer increases as the electric potential is increased at fixed electrode spacing. The experiments were performed on rough sandblasted surface at 1.01 bar saturation pressure. The electric field was provided using the mesh electrode. The effect of changing the electrode spacing at fixed electric potential is shown in Figure 6.52 for decreasing heat flux. According to equation (3.6), the electrohydrodynamic forces depend on the field strength, the nominal value of which is given by E = V/d. Hence, as expected, the highest enhancement, at constant voltage, is obtained with the electrode closest to the heating surface (highest E). Two combinations of V and d that give the same field strength E = 500 kV/m are compared in Figure 6.52 for 20 mm, 10 kV and 40 mm, 20 kV. The effectiveness of the electric field in promoting heat transfer is reduced slightly as the electrode is moved towards the wall. The difference increases with heat flux, corresponding to increased rate of generation of vapour. Further research will be necessary to determine the cause, which might depend simply on obstruction of the bubble motion or the change of the electric field by the presence of bubbles.

This fact was reported by Zaghdoudi and Lallemand (2005), where they described the numerical simulation results. They performed the simulation using the electrode spacing as the function of degree of non – uniformity of electric field. According to Zaghdoudi and Lallemand (2005), as the electrode spacing was increased the degree of non – uniformity of electric field also increased, which leaded to increase in heat flux at a specific value of wall superheat. This mathematical findings of Zaghdoudi and Lallemand (2005) is similar to the present experimental results, see Figure 6.52.

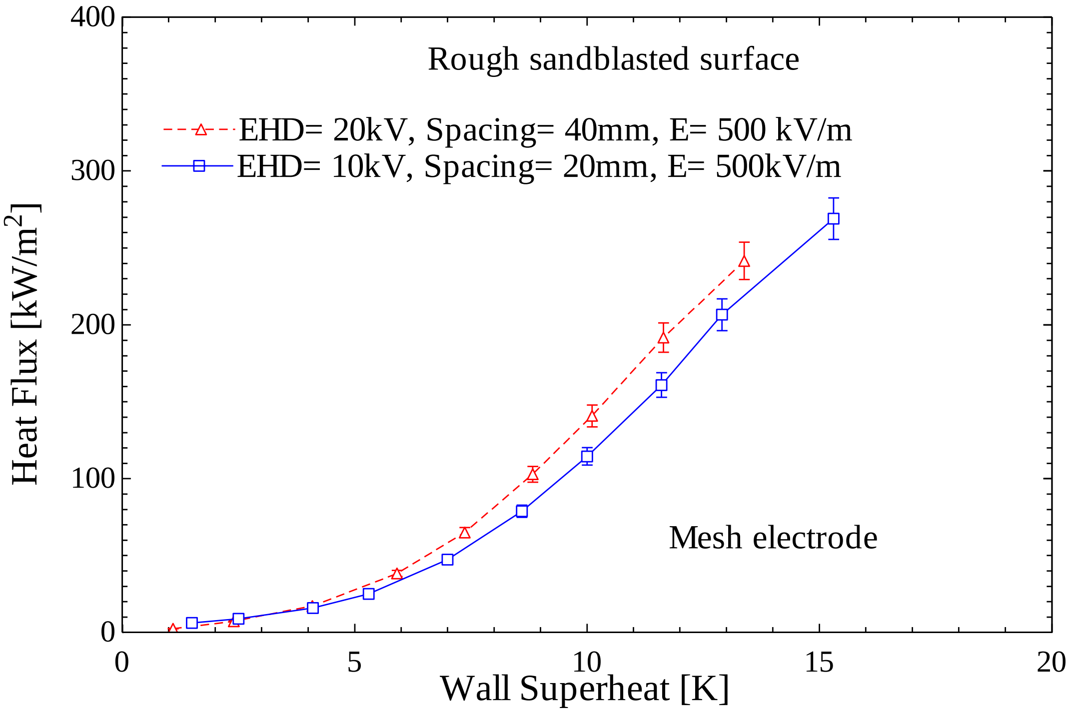

Figure 6.52 Effect of electrode spacing on EHD pool boiling

6.5 Compound effect of Electric field and surface modification

The compound effect of high intensity electric field (uniform and non – uniform) and the surface modification are presented in Figures 6.53 and 6.54. It has already been mentioned that the uniform electric was provided using a mesh electrode while non – uniform electric field was employed using two rod electrodes (with 5 mm and 8 mm rod spacing). It can be observed from the Figures 6.53 and 6.54 that with the application of the electric field, the boiling curves move towards the left. The non – uniform electric field shows slightly better heat transfer enhancement at specific value of superheat. Moreover, surface modification moves the boiling curve significantly towards the left (i.e. increasing heat flux at specific value of wall superheat). It can be deduced from these facts that the surface modification is better technique (i.e. maximum heat transfer enhancement was achieved by the factor of approximately 8, see Figure 6.2) for heat transfer enhancement as compared to EHD (i.e. maximum heat transfer enhancement was achieved by the factor of approximately 1.7, see Figure 6.44).

The magnitude of the compound enhancement due to the application of the electric field and surface modification is presented in Figures 6.55 and 6.56. It can be observed that with conventional surface preparation methods (i.e. emery polishing and sandblasting) the maximum compound enhancement achieved was approximately 2.7 and 3 with the application of 1 MV/m and 2 MV/m respectively. On the other hand, the EB enhanced surface produced the best results (i.e. heat transfer was augmented by approximately a factor of 10 (approximately, see Figure 6.56)), when a 2 MV/m electric field was applied.

The sintering process itself makes an efficient technique of modifying the surface for boiling enhancement. But the effect of electric field on the pool boiling in the presence of sintered surface was marginal. It can be concluded from the above discussion that for compound enhancement, the EB enhanced surface was out performing the rest. Moreover, it is easy to manufacture different array of structures on the heating surface in a short time.

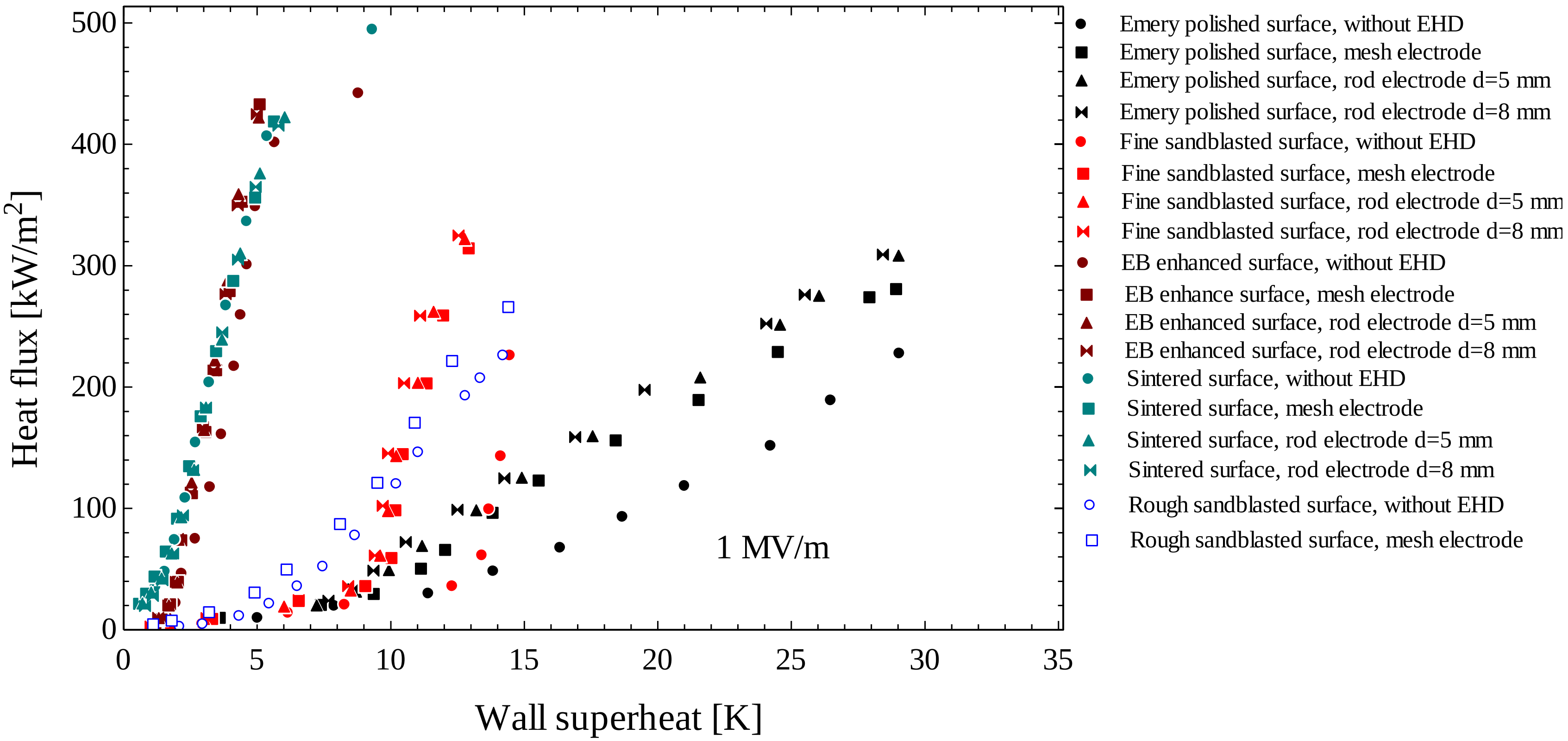

Figure 6.53 Effect of surface modification and electric field on pool boiling at 1 MV/m

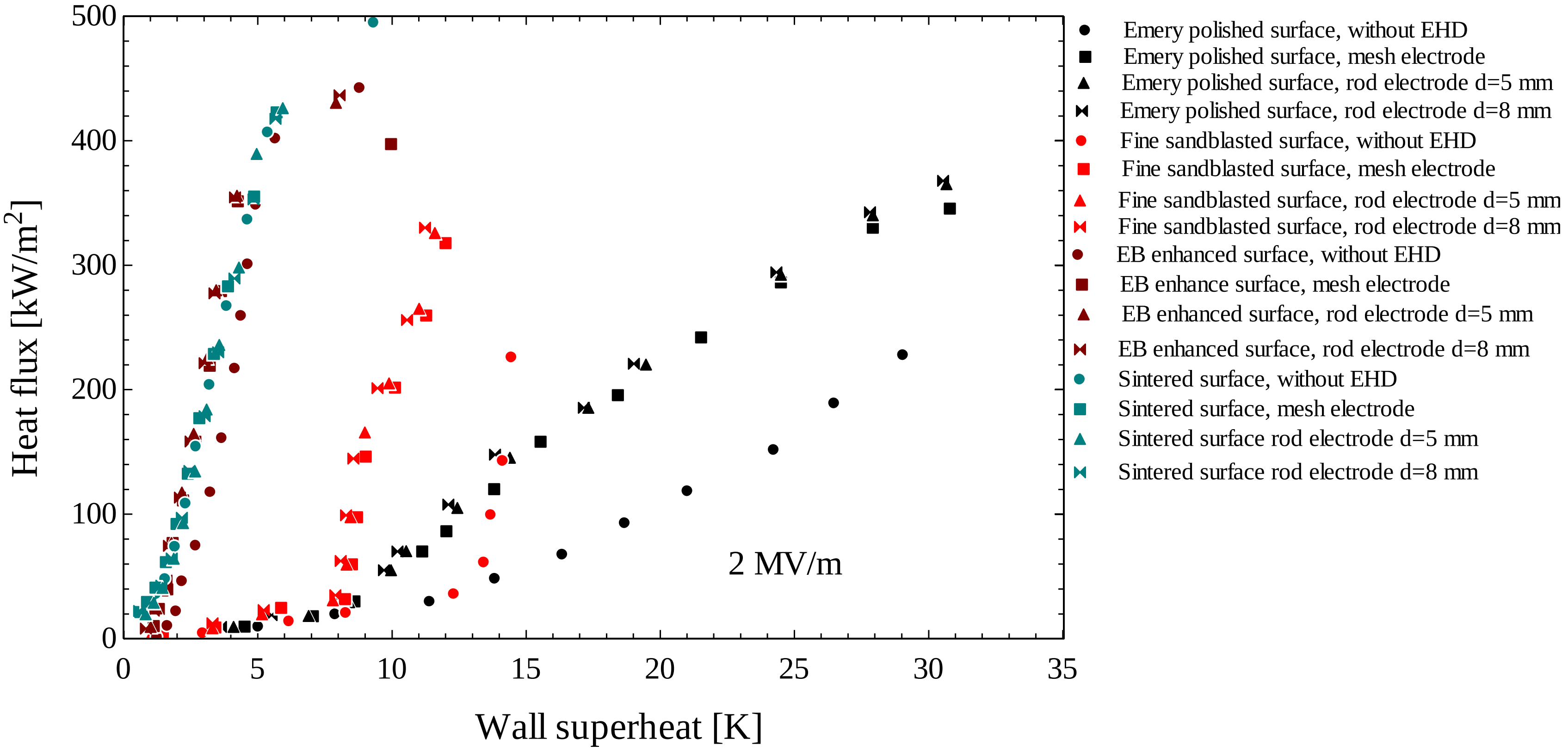

Figure 6.54 Effect of surface modification and electric field on pool boiling at 1 MV/m at 2 MV/m

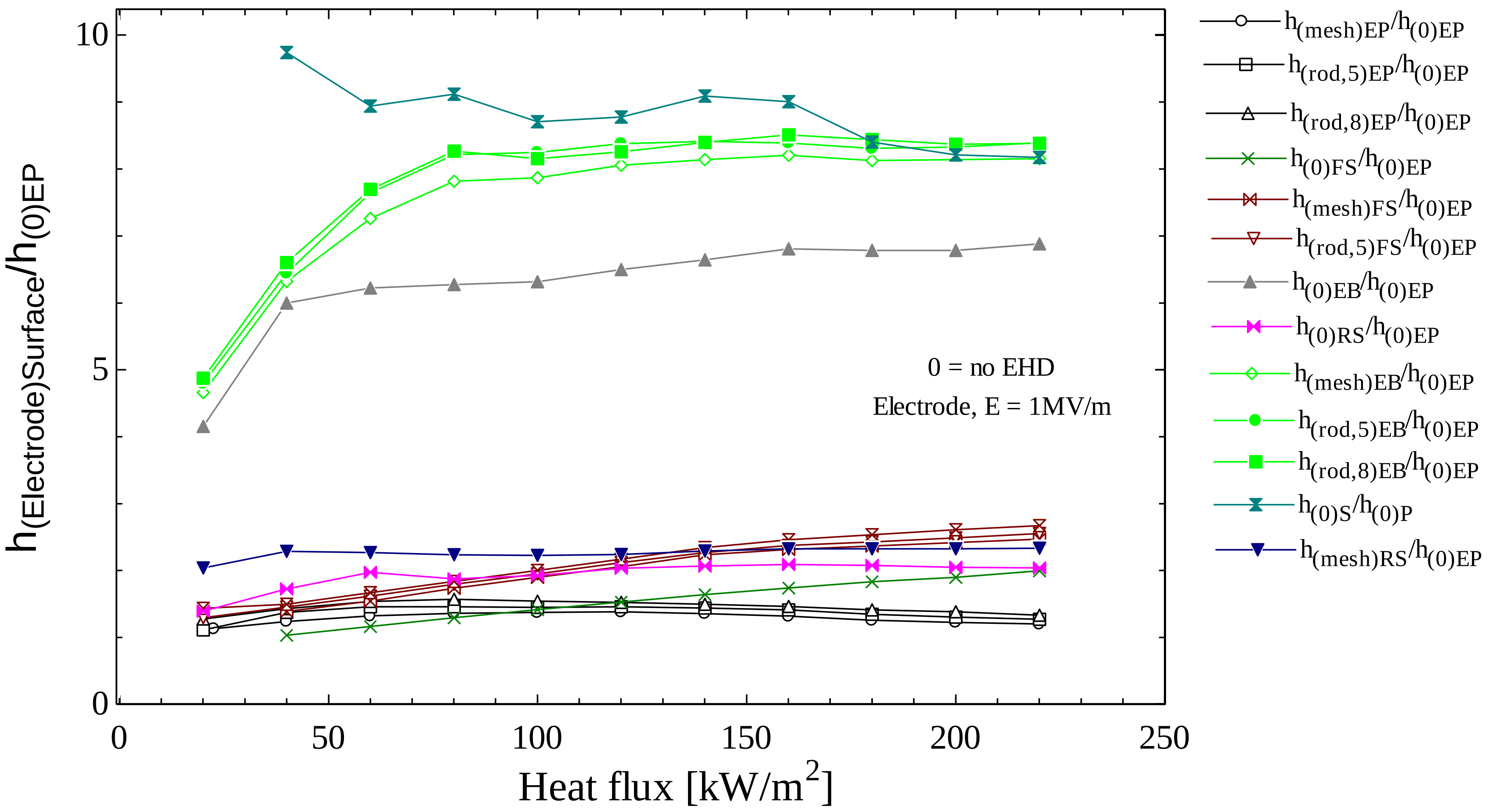

Figure 6.55 Compound enhancement at 1 MV/m, EP = emery polished, FS = fine sandblasted, RS = rough sandblasted, EB = EB enhanced, S = sintered, rod 5 = rod electrode 5 mm rod spacing and rod 8 = rod electrode 8 mm rod spacing

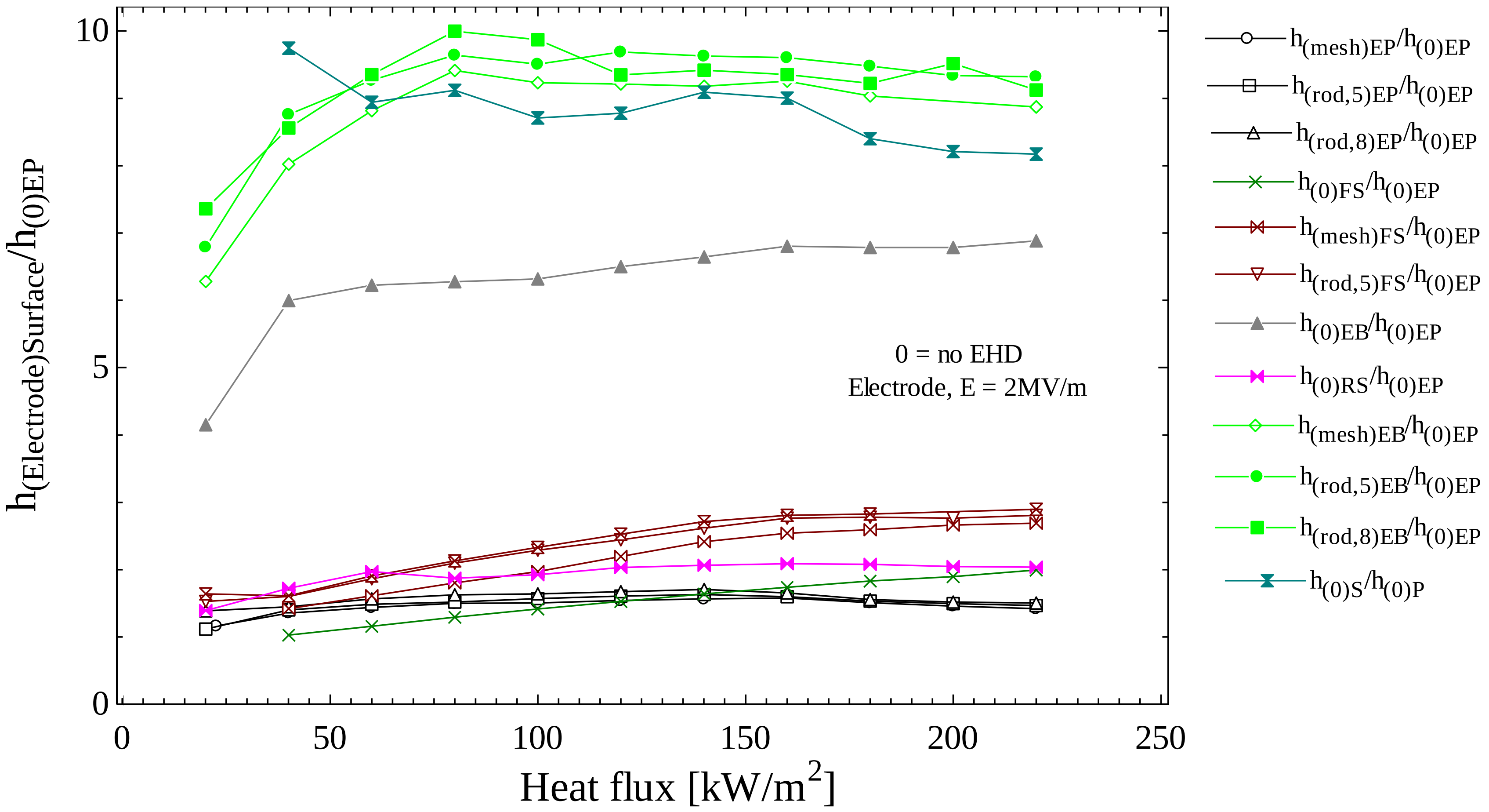

Figure 6.56 Compound enhancement at 1 MV/m, EP = emery polished, FS = fine sandblasted, RS = rough sandblasted, EB = EB enhanced, S = sintered, rod 5 = rod electrode 5 mm rod spacing and rod 8 = rod electrode 8 mm rod spacing.

6.6 Effect of boiling pressure on EHD pool boiling

The effect of saturation pressure on EHD pool boiling is represented using emery polished surface, see Figure 6.57. As discussed earlier, with the increase in saturation pressure the heat transfer also increases at a specific value of wall superheat with no field applied. It can also be observed that with the application of electric field the heat transfer augments at specific saturation pressure. Furthermore, it can be deduced from Figure 6.58 that as saturation pressure increases the augmentation effect of EHD decreases. This fact can be explained on the basis of flow visualization, as the saturation pressure increases the bubble size decreases (see Figure 6.27). According to Dong et al. (2006), as the bubble appeared the uniform electric field was distorted in the vicinity of the bubble, i.e. around the bubble the field becomes non – uniform. They also noted that higher the size of the bubble the higher would be the degree of non-uniformity of the local electric field. In case of 1.01 bar saturation pressure, the diameter of the bubble is bigger as compared to the higher saturation pressures (i.e. at 2 bar and 4 bar). The bigger bubble distorted the electric more, which leads to higher heat transfer augmentation.

As discussed earlier in section 6.2, the number of bubbles increases with the rise in boiling pressure. Due to increase in number of bubble the effective electric field acting on the bubbles decrease, which result in decrease in heat transfer enhancement. Similar observations were experimentally reported by Xu (1995), when he performed EHD experiments on pool boiling of R-123. He reported that as the boiling pressure increases the EHD enhancement decreases.

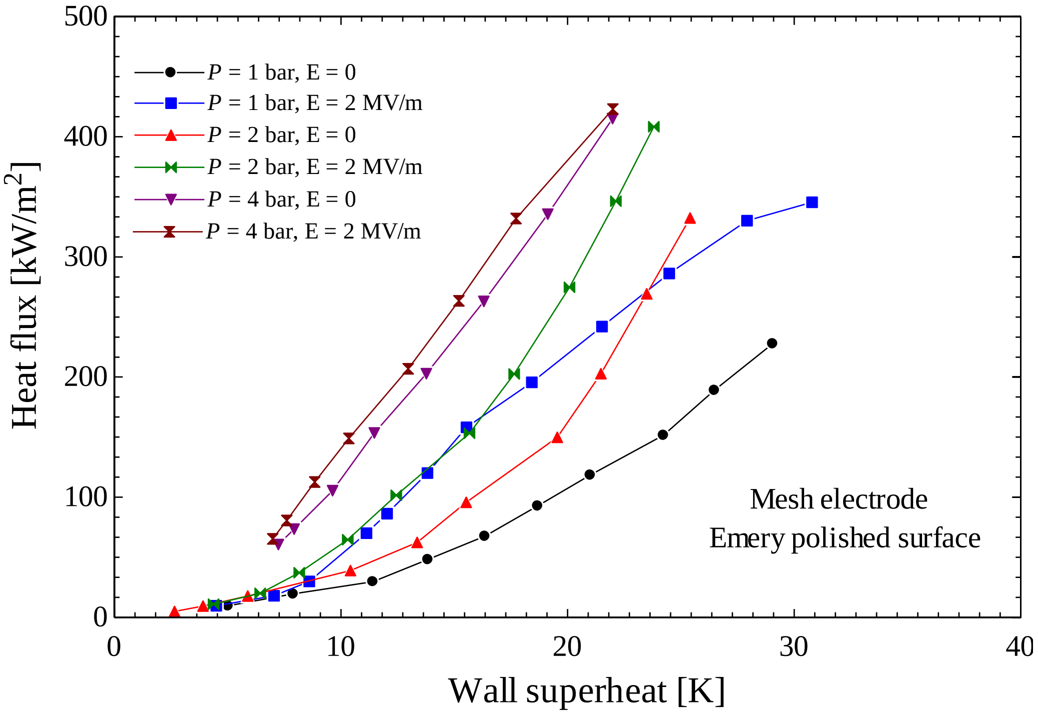

Figure 6.57 Effect of saturation pressure on EHD using emery polished surface.

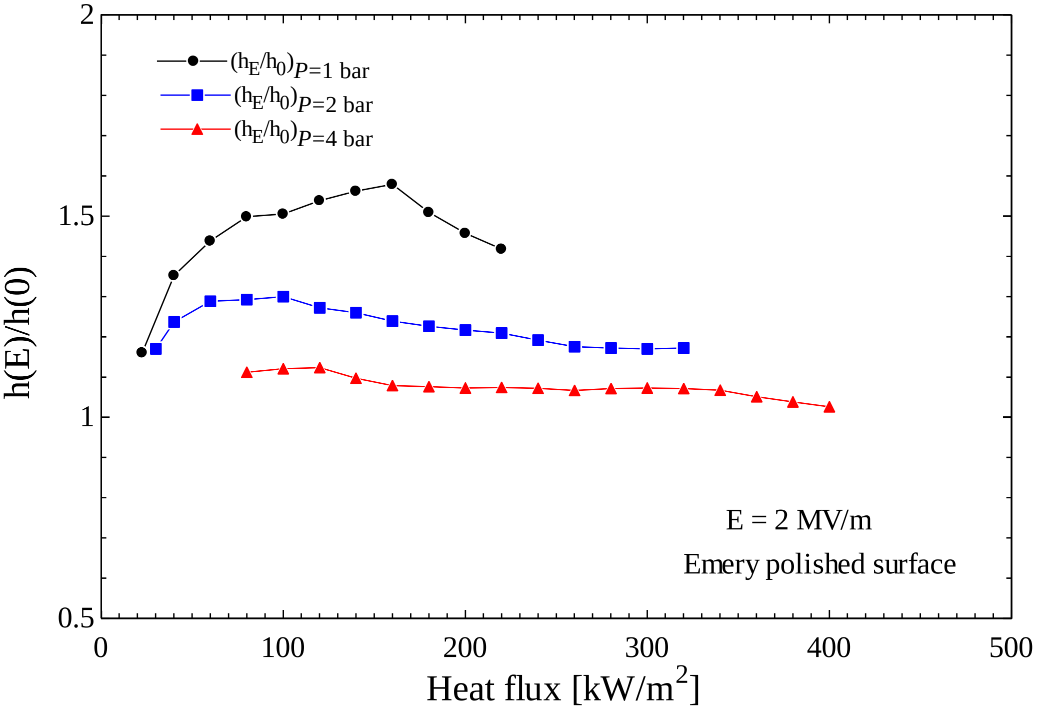

Figure 6.58 Augmentation in the value of heat transfer coefficient under the effect of saturation pressure and EHD.

6.7 Summary

The experimental results of pool boiling heat transfer using R-123 as working fluid were presented in this chapter. The experiments were performed with and without the application of an electric field. Furthermore, the impact of boiling pressure was also reported. The findings of this chapter can be summarized as follows:

- The surface modification technique proved to be very effective in enhancing pool boiling heat transfer. In the present studies, EB enhanced and sintered surface showed higher heat transfer results as compared to traditional surfaces (i.e. emery polished and sandblasted).
- The EB enhanced surface is better in enhancing heat transfer as compared to the finned surfaces presented by Yu and Lu (2007) and Kim et al. (2008). Further the manufacturing of EB enhanced surface is easy and time taken less as compared to that for finned surfaces.
- The data obtained for the emery polished, fine and rough sandblasted surfaces were compared to the published nucleate boiling correlations. The experimental results lie within 20 percent range with most of the correlations.
- Hysteresis has also been observed during the present experimental studies. It has been found that boiling hysteresis depends upon the fluid properties and surface characteristics. It occurs for rough sandblasted, EB enhanced and sintered surfaces but not for emery polished and fine sandblasted surfaces.
- The critical heat flux was found to be independent of the surface characteristics in the pool boiling of emery polished and sandblasted surfaces. But due to special spike and porous structure of the EB enhanced and sintered surfaces respectively, an increase in the value of critical heat flux (CHF) was observed.
- It has also been found that as boiling pressure increases the heat transfer at the specific value of wall superheat also increases.

- The impact of uniform and non – uniform electric field was also observed on pool boiling of R-123. It has been found that due to the application of electric field the heat transfer increases.
- Non – uniform electric field showed better heat transfer enhancement as compared to uniform electric field.
- It was found that with the application of an electric field boiling hysteresis can be eliminated.
- An enhancement in the value of the critical heat flux was also observed due to the application of electric field.
- The combined effect of surface modification and high intensity electric field moves the boiling curve towards the left, i.e. augmentation in heat transfer.
- The value of the enhancement ratio decreases as the system pressure increases.
- The bubble growth patterns are affected by the application of an electric field. The bubbles take longer to detach and can change the shape from spherical to a mushroom type shape.

Chapter 7 Conclusions and Recommendations

The enhancement in the pool boiling heat transfer has been investigated in this experimental study. For this purpose, a poorly electrically conductive refrigerant, R-123, was used as the working fluid and boiling was carried out on horizontal upward facing circular copper surface. The study covered following areas of research:

- Effect of surface modification on pool boiling.
- Effect of saturation pressure on pool boiling.
- Effect of high intensity electric field (uniform and non- uniform) on pool boiling.
- Combined effect of surface modification and high intensity electric field on pool boiling.
- Combined effect of saturation pressure and high intensity electric field on pool boiling.
- Effect of a high intensity electric field on bubble shape and dynamics.

The research conclusions are summarized in Section 7.1, while the recommendations for future work are mentioned in Section 7.2.

7.1 Conclusions

7.1.1 Effect of surface modification on pool boiling

The impact of surface modification on pool boiling has been investigated using five different surfaces, namely: emery polished, fine sandblasted, rough sandblasted, EB enhanced and sintered surfaces, as discussed earlier in Section 6.1.1. The effect of these surfaces on pool boiling can be concluded as follows:

1. Surface modification can yield significant enhancement of the heat transfer coefficient. The best performance was achieved by the sintered surface with a heat transfer coefficient approximately nine times that for the emery polished surface. The corresponding augmentation factors for the EB enhanced, fine sandblasted and rough sandblasted surfaces were around 6.5, 2 and 1.5 respectively.
2. The EB enhanced surface showed better heat transfer results as compared to finned surfaces (presented by past researchers) see Section 6.1.1. In addition, the preparation of the EB enhanced surface (using *Surfi-Sculpt* process) is easier and economical as compared to the finned structures, especially when the shape of the heating surface is difficult to modify (i.e. tubes).
3. The experimental values of the heat transfer coefficients for the emery polished surface (at 1.01 bar, 2 bar and 4 bar) were compared with predictions from seven different nucleate boiling correlations. Some correlations gave predictions within ±20% of the experimental results over a wide range of heat flux and pressures. Comparison of experimental and predicted coefficients for the sandblasted surfaces (at 1.01 bar) showed much greater disagreement, with general under-prediction for the fine sandblasted surface and some large deviations for the rough sandblasted surface.
4. The pool boiling results obtained for the emery polished surface and two sandblasted surfaces suggest that the effect of different heater surface conditions may not be adequately represented by the dependence of heat

transfer coefficient on average surface roughness R_a assumed in the nucleate boiling correlations.

5. The boiling hysteresis is a function of heating surface conditions and the boiling liquid properties. It has experimentally been observed that the emery polished and fine sandblasted surfaces didn't exhibit hysteresis. While the rough sandblasted, EB enhanced and sintered surfaces show boiling hysteresis due to their modified surface structures.
6. It has been found that the critical heat flux is independent of the heater surface conditions for traditionally modified surfaces (i.e. emery polished and fine and rough sandblasted). Higher values of CHF were observed with the EB enhanced and sintered surfaces due to their spike and porous structures respectively.

7.1.2 Effect of Saturation pressure on pool boiling

The effect of saturation pressure on pool boiling has been tested at 1.01 bar, 2 bar and 4 bar boiling pressure using the emery polished surface. It was concluded that as the saturation pressure increases, heat transfer rates also increase at specific values of wall superheat. It has also been visually observed that, at constant heat flux, the number of bubbles increases when the boiling pressure increases.

7.1.3 Effect of high intensity electric field on pool boiling

The effect of uniform and non – uniform electric fields on pool boiling of R-123 has also been experimented and presented in this study (see Section 6.4). The main findings of these experiments are summarized as follows:

1. The heat transfer augmentation due to the application of non – uniform electric field was found to be higher than with the uniform electric field. Furthermore, at low heat flux the heat transfer enhancement is better as compared to high heat flux. This is due to the shielding effect of the vapour bubbles at high heat flux, see Section 6.4.1.

2. It has also been observed that there was no effect of high intensity electric field (uniform or non – uniform) on the pool boiling using the sintered surface, which is attributed to porous structure of the surface.
3. The boiling hysteresis was gradually eliminated due to the application of high intensity electric field. This is probably due to change in the surface tension, and contact angle.
4. It has been detected from the experiments that the value of critical heat flux was increased due to the application of a high intensity electric field. At high heat flux, the alteration in bubble dynamics is responsible for the increase in critical heat flux value, see Section 6.4.5.
5. It is also found that, at constant electric field, as the electrode spacing increases the heat transfer also increases at a specific value of wall superheat.

7.1.4 Combined effect of surface modification and high intensity electric field on pool boiling

The combined effect of surface modification and high intensity electric field is calculated in this thesis and found that, with the application of electric field on a modified surface, the boiling curve moves further towards left, i.e. the value of heat transfer increases at specific value of wall superheat. Furthermore, the effect of non – uniform electric field provides comparatively better results than uniform electric field. The maximum enhancement in the value of heat transfer coefficient was by a factor of 10 as compared to emery polished surface, when a non – uniform electric field, E = 2 MV/m, was applied using EB enhanced surface.

7.1.5 Combined effect of saturation pressure and high intensity electric field on pool boiling

The combined effect of saturation pressure and high intensity electric field has also been examined during present pool boiling experiments, see Section 6.5. The experimental results show that the magnitude of EHD heat transfer augmentation decreases as a result of a rise in saturation pressure. It has visually been observed that, as saturation pressure increases, the number of bubbles also increases which results in higher shielding effect. This shielding effect of vapour bubbles can be attributed to a decrease in the heat transfer augmentation due to application of high intensity uniform electric field at high saturation pressure.

7.1.6 Alteration in bubble dynamics due to the application of a high intensity electric field

The alteration in the bubble dynamics has been visually monitored and presented. The findings of visual observations can be summarized as follows:

1. With the application of a uniform electric field, E = 0.5 MV/m, the shape of bubble growth remains same. Further increase in the electric field, up to 1 MV/m, alters the bubble detachment shape from spherical to mushroom as compared to no field conditions. This is the practical explanation of the mathematical findings of Karayiannis and Xu (1998).
2. Similarly, the bubble detachment shape remains unchanged with the application of non – uniform electric field up to 0.5 MV/m. But as the non – uniform electric increases up to 1 MV/m, the bubble shape changes from spherical to thin elongated shape with irregular edges as compared to no field conditions. It has also been noticed that the bubbles avoid the natural path after detachment from the heating surface when subjected to high intensity non – uniform electric field. It means that the rod electrodes push the bubbles towards the heating surface, which is the visual proof of Pohl (1978) statement, i.e. during the application of non – uniform electric field the component of the dielectric which has higher electric permittivity is attracted towards the region of high electric field intensity.
3. With the application of uniform and non – uniform electric field the bubble detachment time increases as compared to no field conditions. The increase in the magnitude of bubble detachment time is slightly higher when non – uniform electric field is applied. Further increase in bubble detachment period was also observed when the non – uniformity of electric field increases.

4. There is no effect of boiling pressure on bubble shape at detachment from the heating surface, but the bubble detachment time decrease as saturation pressure increases.
5. Due to the application of a uniform electric field up to 1 MV/m, at 2 bar saturation pressure, the bubble shape changes from spherical to mushroom shape. This bubble behaviour is similar as observed at 1.01 bar saturation pressure, see Section 6.3. The change in the bubble detachment time was marginal.

7.2 Recommendations

Further experimental and mathematical work is required to apply these findings to industrial level. The future work recommendations are summarized as follows:

1. EB enhanced surface is found to be efficient in heat transfer enhancement. More experiments are required with different surface textures manufacture using the electron beam technique in order to optimize the surface effects on pool boiling.
2. The sintered surface is relatively better in enhancing heat transfer as compared to EB enhanced surface. The same tests should be repeated using boiling tubes, which also have applications in boiling equipments.
3. The present experimental study should be repeated using different boiling fluids in order to investigate the effect of fluid properties, which may lead to develop an appropriate nucleate boiling correlation.
4. It has been found that the boiling surfaces are characterized in terms of roughness profile parameter, R_a or primary profile parameter, P_a. These terms correspond to the average height of the surface cavity, which can’t fully demonstrate the role of the surface cavity during boiling process. Some comprehensive parameters should be used to address this issue.
5. The effect of electrode spacing is not fully understood, more experimental and mathematical analysis should be required to optimize the effect of

electrode spacing on pool boiling heat transfer during the application of high intensity electric field.

6. The effect of non – uniform electric field has also investigated. Further experimental analysis is required with increased degree of non – uniformity of electric field to quantify the effect of field non – uniformity.
7. During visual observations, it has been noticed that the bubble dynamic are change due to the application of high intensity electric field. Mathematical studies are required to understand the interaction of inertial, buoyancy and electric forces on single and multi-bubbles under uniform and non – uniform electric fields.

Chapter 8 References

Abuaf N., Black S. H. and Staub F. W. (1985). "Pool boiling performance of finned surfaces in R-113." International Journal of Heat and Fluid Flow **6**: 23-30.

Allen P. H. G. and Karayiannis T. G. (1995). "Review paper: Electrohydrodynamics enhancement of heat transfer and fluid " Heat Recovery Systems & CHP **15**: 389-423.

Ayub Z. H. and Bergles A. B. (1987). "Pool boiling form GEWA surfaces in water and R-113." Wärme-Undstoffübertragung **21**: 209-219.

Babaoi N. F., Bologa M. K. and Klyukanov A. A. (1968). "Some features of ebullition in an electric field " Applied Electric Phenomenona (USSR) **20**: 57-60.

Bankoff S. G. (1958). "Entrapment of gas in the spreading of a liquid over a rough surface." AIChE Journal **4**: 24-26.

Bankoff S. G., Hajjar A. J. and McGlothein B. B. (1958). "On the nature and location of nuclei in boiling from surfaces." Journal of Applied Physics **29**: 1739-1741.

Basu D. K. (1973). " Effect of electric field on boiling hysteresis in carbon tetrachloride." International Journal of Heat and Mass Transfer **16**: 1322-1324.

Benjamin R. J. and Balakrishnan A. R. (1997). "Nucleation site density in pool boiling of saturated pure liquids : Effect of surface micro roughness and surface and liquid physical properties." Experimental Thermal & Fluid Sciences **15**: 32-42.

Berenson P. J. (1962). "Experiments on pool boiling heat transfer." International Journal of Heat and Mass Transfer **5**: 985-999.

Berghmans J. (1976). "Electrostatic fields and the maximum heat flux " International Journal of Heat and Mass Transfer **19**: 791-797.

Bobrovich G. I. and Mamontova N. N. (1965). "A study of the mechanism of nucleate boiling at higher heat fluxes." International Journal Heat and Mass Transfer **8**: 1421-1424.

Bonjour E., Verdier J. and Well L. (1962). "Electroconvection effect on heat transfer." Chemical Engineering Progress **58**: 63-66.

Buxton A. L., Ferhati A., Glen R. J. M., Dance B. G. I., Mullen D. and Karayiannis T. G. (2009). EB surface engineering for high performance heat exchangers. First International electron beam welding conference Chicago USA.

Chen C., He L., Li X. and Fu L. (2007 b). "Experimental investigation of nucleate boiling heat transfer enhancement by non – uniform electric field." Annual Report Conference on Electrical Insulation and Dielectric Phenomena.

Chen F., Peng Y., Song Y. Z. and Chen M. (2007 a). "EHD behavior of nitrogen bubbles in DC electric fields." Experimental Thermal and Fluid Sciences **32**: 174-181.

Chu C. R. and Morgan K. P. (1977). Method for customizing nucleate boiling heat transfer from electronic units immersed in dielectric coolant. US Patent 4050507.

Chung H. J. and No H. C. (2003). "Simultaneous visualization of dryspots and bubbles for pool boiling of R-113 on a horizontal heater." International Journal of Heat and Mass Transfer **46**(2239-2251).

Coleman W. H. and Steele G. W. (1989). Experimentation and Uncertainty Analysis for Engineers, John Wiley & Sons.

Cooke D. and Kandlikar S. G. (2011). "Pool boiling heat transfer and bubble dynamics over plain and enhanced microchannels." Journal of Heat Transfer: 129-138.

Cooper M. G. (1984). "Saturation nucleate pool boiling – a simple correlation." IChemE Symposium Series **86**: 786-793.

Cooper M. G. and Lloyd A. J. P. (1969). "The microlayer in nucleate pool boiling." International Journal of Heat and Mass Transfer **12**: 895-913.

Cooper P. (1990). "EHD enhancement of nucleate boiling." Jounal of Heat Transfer **112**: 458-464.

Corty C. and Foust A. S. (1955). "Surface variables in nucleate boiling." Chemical Engineering Progress Symposium Series **51**: 1-12.

Das A. K. and Das P. K. (2007). "Nucleate boiling of water from plain and structured surfaces." Experimental Thermal & Fluid Sciences **31**: 967-977.

Dong W., Li R. Y., Yu H. L. and Yan Y. Y. (2006). "An investigation of behavior of a single bubble in a uniform electric field." Experimental Thermal & Fluid Sciences **30**: 579-586.

Edminister J. A. (1993). Schaum's outlines: Electromagnetics, McGraw Hill.

Ferjancic K. and Golobic I. (2002). "Surface effects on pool boiling CHF." Experimental Thermal & Fluid Sciences **25**: 565-571.

Gaertner R. F. (1965). "Photographic study of nucleate pool boiling on a horizontal surface." Jounal of Heat Transfer **87**: 17-26.

Germant A. (1934). Liquid Dielectric NewYork, Wiley London, Chapman and Hall.

Gorenflo D., Baumhogger E., Windmann T. and Herres G. (2010). "Nucleate pool boiling, film boiling and single-phase free convection at pressure up to the critical state. Part I: integral heat transfer for horizontal copper cylinders." International Journal of Refrigeration **33**: 1239-1250.

Gorenflo D., Chandra U., Kottoff S. and Luke A. (2004). "Influence of thermophysical properties on pool boiling of refrigerants." International Journal of Refrigeration **27**: 492-502.

Gorenflo D. and Kenning D. B. R. (2009). H2 Pool boiling, VDI Heat Atlas Springler-Verlag.

Griffith P. (1965). "Nucleation and bubble formation in boiling." Proceeding Instn Mechanical Engineers **180**: 93-100.

Griffith P. and Wallis J. (1958). "The role of surface conditions in nucleate boiling." A Technical Report No.14 Massachusetts Institute of Technology (MIT).

Ha S. J. and No C. (1997). "A dryout model of critical heat flux in pool and forced convection boiling." International Journal of Heat and Mass Transfer **41**: 793-810.

Hahne E. (1983). "Pool boiling – And the effect of pool geometry." Warme-Stoffubertagung **17**: 155-159.

Han C. Y. and Griffith P. (1965). "The mechanism of heat transfer in nucleate pool boiling II." International Journal of Heat and Mass Transfer **8**: 905-914.

Haramura Y. and Katto Y. (1983). "A new hydrodynamic model of critical heat flux, applicable widely to both pool and forced convection boiling on submerged bodies in saturated liquids." International Journal of Heat and Mass Transfer **26**: 389-399.

Hippel A. V. (1954). Dielectric and Waves, John Wiley & Sons.

Hristov Y., Zhao D., Kenning D. B. R., Sefiane K. and Karayiannis T. G. (2009). "A study of nucleate boiling and critical heat flux with EHD enhancement." Heat Mass Transfer **45**: 999-1017.

Hsieh S. S. and Weng C. J. (1997). "Nucleate pool boiling from coated surfaces in saturated R-134(a) and R-407(c)." International Journal of Heat and Mass Transfer **40**: 519-532.

Hsu Y. Y. (1962). "On the size range of active nucleation cavities on the heating surface." Jounal of Heat Transfer **34**: 207-214.

Hübber P. and Künstler (1997). "Pool boiling heat transfer at finned tubes: influence of surface roughness and shape of fins." International Journal of Refrigeration **20**: 575-582.

Jabardo J. M. S., Silva E. F. D., Ribatski G. and Barros S. F. D. (2004). "Evaluation of the Rohsenow correlation through experimental pool boiling of halocarbon refrigerants on cylindrical surfaces." J Braz. Soc. of Mech Sci Eng **24**: 218-230.

Johnson R. L. (1968). "Effect of an electric field on boiling heat transfer." AIAA Journal **6**: 1456-1460.

Jones B. J., McHale J. P. and Garimella S. V. (2009). "The influence of surface roughness on nucleate pool boiling heat transfer." Journal of Heat Transfer **131**: 1-14.

Jones T. B. (1978). "Electrohydrodynamic enhanced heat transfer in liquids a review." Advances in Heat Transfer **14**: 107-148.

Joudi K. A. and James D. D. (1977). "Incipient boiling characteristics at atmospheric and subatmospheric pressures." Journal Heat Transfer **99**: 398-403.

Jung D., Kim Y., Ko Y. and Song K. (2003). "Nucleate boiling heat transfer coefficients of pure halogenated refrigerants." International Journal of Refrigeration **26**: 240-248.

Kang M. G. (2000). "Effect of surface roughness on pool boiling heat transfer." International Journal Heat and Mass Transfer **43**: 4073-4085.

Karayiannis T. G. (1998). "EHD boiling heat transfer enhancement of R-123 and R11 on a tube bundle." Applied Thermal Engineering **18**: 809-817.

Karayiannis T. G. and Xu Y. (1998). "Electric field effect in boiling heat transfer. Part A: Similation of the electric field and electric forces." Enhanced Heat Transfer **5**: 217-229.

Katto Y. and Yokoya S. (1968). "Principal mechanism of boiling crisis in pool boiling." International Journal of Heat and Mass Transfer **11**: 993-1002.

Kawahira H., Kubo Y., Yokoyama T. and Ogata J. (1990). "The effect of an electric field on boiling heat transfer of regrigerant -11 – boiling on a single tube." IEEE Transection on Industrial Application **26**: 359-365.

Kim N. H. and Choi K. K. (2001). "Nucleate pool boiling on structured enhanced tubes having pores with connecting gaps." International Journal of Heat and Mass Transfer **44**: 17-28.

Kim Y. H., Lee K. J. and Han D. (2008). "Pool boiling enhancement with surface treatments." Heat Mass Transfer **45**: 55-60.

Kottof S., Gorenflo D., Danger E. and Luke A. (2006). "Heat transfer and bubble formation in pool boiling: effect of basic surface modification for heat transfer enhancement." International Journal of Thermal Sciences **45**: 217-236.

Kweon Y. C. and Kim M. H. (2000). "Experimental study on nucleate boiling enhancement and bubble dynamic behavior in saturated pool boiling using a non – uniform dc electric field." International Journal Multiphase Flow **26**: 1351-1368.

Lee Y. C., Bhuiya M. M. H. and Kim K. J. (2010). "Pool boiling heat transfer with nano-porous surface." International Journal of Heat and Mass Transfer: 4274-4279.

Lienhard J. H. and Hasan M. M. (1979). "On prediction boiling burnout with the mechanical energy stability criterion." Journal Heat Transfer **101**: 276-279.

Liu Z., Herman C. and Mewes D. (2006). "Visualization of bubble detachment and coalescence under the influence of a non – uniform electric field." Experimental Thermal and Fluid Sciences **31**: 151-163.

Lorenz J. J., Mikic B. B. and Rohsenow W. M. (1972). The effects of surface conditions in boiling characteristics. Report No. DSR 73413-79 of Mechanical Engineering Department of the Massachusetts Institute of Technology.

Lovenguth R. F. and Hanesian D. (1971). "Boiling Heat transfer in the presence of non –uniform, direct current electric fields." International Engg. Chem. Fundam, **10**: 571-576.

Luke A. (2006). "Preparation, measurement and analysis of microstructure of evaporator surfaces." International Journal of Thermal Sciences **45**(237-256).

Luke A. (2006,a). "Pool boiling heat transfer from horizontal tubes with different surface roughness." International Journal of Refrigeration **20**: 561-574.

Luke A. (2009). "Preparation and analysis of different roughness structures for evaporator tubes." Heat Mass Transfer **45**: 909-917.

Luke A., and B. and Scheunemann P. (2000). "3-Dimensional description of the microstructure of heated surface in nucleate pool boiling." Multiphase Science and Technology **12**: 17-29.

Madadnia J. and Koosha H. (2003). "Electrohydrodynamics effects on characteristic of isolated bubbles in the nucleate pool boiling regime." Experimental Thermal and Fluid Sciences **27**: 145-150.

Mardarskii O. I. and Bologa M. K. (2009). "On the mechanism of heat transfer enhancement at boiling in an electric field." Surface Engineering and Applied Electrochemistry **45**: 42-48.

Markels M. and Durfee R. L. (1964). "The effect of applied voltage on boiling heat transfer." AIChE Journal **10**: 106-109.

McGillis W. R., Carey V. P., Fitch J. S. and Hamburgen W. R. (1991). "Pool boiling enhancement techniques for water at low pressure." Seventh IEEE Semi-Therm Symposium: 64-72.

Memory S. B., Sugiyama D. C. and Marto P. J. (1995). "Nucleate boiling of R-114 and R-114 oil mixtures from smooth and enhanced surfaces – I. Single tubes." International Journal of Heat and Mass Transfer **38**: 1347-1361.

Moissis R. and Berenson P. J. (1963). "On the hydrodynamics transitions in nucleate boiling." Journal Heat Transfer **85**: 221-226.

Nukiyama S. (1966). "The maximum and minimum values of the heat transmitted from metal to boiling water at atmospheric pressure." International Journal of Heat and Mass Transfer **9**: 1419-1433.

Ogata J., Iwafuji Y., Shimada Y. and Yamazaki T. (1992). "Boiling heat transfer enhancement in tube – bundle evaporator utilizing electric field effects." ASHRAE Transactions **98**: 435-444.

Oh S. D. and Kwak H. Y. (2000). "A study of bubble behavior and boiling heat transfer enhancement under electric field." Heat Transfer Engineering **21**: 33-45.

Ohadi M. M. and Paper R. A. (1992). "EHD Enhancement of shell-side boiling heat transfer coefficient of R-123/oil mixture." ASHRAE Transactions **90**: 427-434.

Pascual C. C., Jeter S. M. and Abdel – Khalik S. I. (2001). "A statistical analysis of EHD enhanced nucleate boiling along a heated wire." International Journal of Heat and Mass Transfer **44**: 1201-1212.

Pascual C. C., Stromberger J. H., Jeter S. M. and Abdel – Khalik S. I. (2000). "An empirical correlation for electrohydrodynamic enhancement of natural convection." International Journal of Heat and Mass Transfer **43**: 1965-1974.

Pioro I. L. and Rohsenow W. (2004). "Nucleate Pool- boiling heat transfer I: review of parametric effects of boiling surface." International Journal Heat and Mass Transfer **47**: 5033-5044.

Pohl H. A. (1978). Dielectrophoresis: The behavior of neutral matter in non-uniform electric field, Cambridge University Press.

Rainey K. N. and You S. M. (2001). "Effects of heater size and orientation in pool boiling heat transfer from micro porous coated surfaces." International Journal of Heat and Mass Transfer **44**: 2589-2599.

Reay D. A. (1991). "Review Paper Heat transfer enhancement – a review of techniques and their possible impact on energy efficiency in UK." Heat Recovery Sys & CHP **11**: 1-40.

Rohsenow W. M. (1952). "A method of correlating heat transfer data for surface boiling liquids " Journal of Heat Transfer **74**: 969-976.

Rutkowski (1977). "The influence of electric field on heat transfer in boiling cryogenic liquid." Cryogenic **17**: 242-243.

Saidi H. M., Ohadi M. and Souhar M. (1999). "Enhanced pool boiling of R-123 refrigerant on two selected tubes." Applied Thermal Engineering **19**: 885-895.

Schnurmann R. and Lardge M. G. C. (1973). "Enhanced heat flux in non – uniform electric fields." Proceeding R. Society London **334**: 71-82.

Scurlock R. G. (1995). "Enhanced boiling heat transfer surfaces." Cryogenics **35**: 233-237.

Sefiane K., Benielle D. and Steinchen A. (1998). "A new mechanism for pool boiling crisis recoil instability and contact angle influence." Colloids and Surfaces A: Physico Chemical and Engineering Aspects **142**: 361-373.

Shekriladze I. G. (2008). "Boiling Heat Transfer: Mechanisms, Models, Correlations and the lines of further research." The Open Mechanical Engineering Journal **2**: 104-127.

Shi M. H., Ma J. and Wang B. X. (1993). "Analysis on hysteresis in nucleate pool boiling heat transfer." International Journal of Heat and Mass Transfer **36**: 4461-4466.

Siedel S., Cioulachtjian S., Robinson A. j. and Bonjour J. (2011). "Electric field effects during nucleate boiling from an artificial nucleation site." Experimental Thermal and Fluid Sciences **35**: 762-771.

Snyder T. J., Schneider J. B. and Chung J. N. (1996). "A second look at electrokinetic phenomena in boiling." Journal of Applied Physics **79**: 6755-6760.

Stephan K. (1977). Bubble formation and heat transfer in natural convection boiling Heat Transfer in Boiling London, Hemisphere Publishing Corporation

Stephan K. and Abdelsalam M. (1980). "Heat transfer correlation for natural convection boiling." International Journal Heat and Mass Transfer **23**: 73-87.

Stutz B., Lallemand M., Raimbault F. and Passos J. (2007). "Nucleate and transition boiling in narrow horizontal spaces." Heat and Mass Transfer **45**: 929-935.

Tang Y., Tang B., Li Q., Qing J., Lu L. and Chen K. (2012). "Pool-boiling enhancement by novel metallic nanoporous surface " Experimental Thermal and Fluid Sciences.

Theofanous T. G., Dinh T. N., Tu J. P. and Dinh A. T. (2002). "The boiling crisis phenomenon part II: dryout dynamics and burnout." Experimental Thermal and Fluid Sciences **26**: 793-810.

Tong L. S. and Tang Y. S. (1997). Boiling heat transfer and two phase flow. Washington, Taylor & Francis.

Verplaetsen F. (1999). Film boiling in the presence of an electric field, PhD Thesis, Katholieke Universiteit Leuven. **Ph.D**.

Wang P., Lewis P. L., Swaffield D. J. and Chen G. (2009). "Electric field effects on boiling heat transfer of liquid nitrogen." Cryogenics **49**: 379-389.

Wang P., Swaffield D. J., Lewis P. L. and Chen G. (2008). The effect of an electric field on behaviour of thermally induced bubble in liquid nitrogen. Dielectric Liquids, IEEE International Conference.

Webb R. L. (1994). Principles of Enhanced Heat Transfer, John Wiley & Sons.

Webb R. L. and Bergles A. E. (1983). "Heat transfer enhancement: second generation technology." Mechanical Engineering **115**: 60-67.

Webb R. L. and Pais C. (1992). "Nucleate pool boiling data for five refrigerants on plain, integral fin and enhanced tube geometry." International Journal of Heat and Mass Transfer **35**: 1893-1904.

Winterton R. H. S. (1977). "Nucleation of boiling and cavitation." Journal Applied Physics **10**: 2041-2056.

Xu Y. (1995). "Effect of electric fields on pool boiling heat transfer." Ph.D. Thesis, South Bank University

Yabe A., Mori Y. and Hijikata K. (1985). Heat transfer enhancement techniques utilizing electric fields. Proceedings of United – Japan Joint Seminar on Heat Transfer Problems in High Technology ad Power Engineering. San DIEGO, USA.

Yabe A., Mori Y. and Hijikata K. (1996). "Active heat transfer enhancement by utilizing electric fields." Annual Review of Heat Transfer **7**: 191-244.

Yagov V. V. (2009). "Nucleate boiling heat transfer: possibilities and limitations of theoretical analysis " Heat Mass Transfer **45**: 881-892.

Yan Y. Y., Gao N. and Barthlott W. (2011). "Minicking natural superhydrophobic surfaces abd grasping the wetting process: A review on recent process in preparing superhydrophobic surfaces." Advances in Colloid and Interface Science: 80-105.

Yan Y. Y., Neve R. S., Karayiannis T. G., Collins M. W. and Allen P. H. G. (1996). "EHD effect on nucleate boiling at passively enhanced surfaces." Experimental Heat Transfer **9**: 195-211.

Yokoyama T., Yamazaki T., Kubo Y., Ogata J., Kawada A. and Ooki Y. (1986). The effect of an electric field on boiling heat transfer of fluorocarbon R-11. Proceedings of the XVIII International centre for Heat and Mass Transfer, Dubrobnik, Yugoslavia.

Yu C. K. and Lu D. C. (2007). "Pool boiling heat transfer on horizontal rectangular fin array in saturated FC–72." International Journal of Heat and Mass Transfer **50**: 3624-3637.

Yu C. K., Lu D. C. and Cheng T. C. (2006). "Pool boiling heat transfer on artificial micro – cavity surfaces in dielectric fluid FC-72." Journal of Micromechanics and Microengineering **16**: 2092-2099.

Zaghdoudi M. C. and Lallemand M. (2005). "Pool boiling heat transfer enhancement by means of high DC electric field." The Arabian Journal for Science and Engineering **30**: 189-212.

Zhao Y. H., Masuoka T. and Tsuruta T. (2002). "Unified theoretical prediction of fully developed nucleate boiling and critical heat flux based on a dynamic microlayer model." International Journal of Heat and Mass transfer **45**: 3189-3197.

Zhou D. W., Ma C. F. and Yu J. (2004). "Boiling hysteresis of imping circular submerged jets with highly wetting liquids." International Journal of Heat and Fluid Flow **25**: 81-90.

Zu Y. Q., Yan Y. Y. and Li J. Q. (2010). "Wetting behaviours of a single droplet biomimetic micro structure surfaces." Journal of Bionic Engineering.

Zuber N. (1958). "On stability of boiling heat transfer " Journal of Heat Transfer **80**: 711-720.

Appendix A Physical properties

Chemical name of R-123

2,2-Dicholoro-1,1,1-trifluoro ethane

Trade name

HCFC-123

Chemical formula

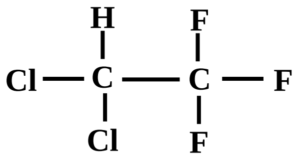

$$\mathrm{Cl{-}\overset{H}{\underset{Cl}{C}}{-}\overset{F}{\underset{F}{C}}{-}F}$$

Physical properties

It is a colourless liquid having ether like smell. The saturated properties of R-123 obtained using Engineering Equation Solver (EES) software.

A 1 Saturated properties of R-12 at 1.01 bar pressure

Properties of R-123 1.01 bar saturation pressure			
Property	Symbol	Value	Units
Molecular mass	M	152.93	kg/kmol
Critical pressure	P_c	36.68	bar
Critical temperature	T_c	456.83	K
Specific gas constant	R	54.368	
Reduced pressure	P_r	0.02754	
Saturated	T_{sat}	300.8	K

temperature			
Reduced temperature	T_r	0.65845	
Specific enthalpy of vaporization	h_{fg}	170600	J/kg
Vapour density	ρ_g	6.455	kg/m^3
Liquid density	ρ_l	1457.0	kg/m^3
Specific heat capacity of the liquid	c_{pl}	1039.0	J/kg K
Thermal conductivity of the liquid	k_l	0.07651	W/m K
Thermal diffusivity of the liquid	α_l	5.054E-08	m^2/s
Dynamic viscosity of the liquid	μ_l	4.100E-04	kg/m s
Kinematic viscosity of the liquid	ν_l	2.81E-07	m^2/s
Liquid Prandtl number	Pr_l	5.57	
Surface tension	σ	1.486E-02	N/m

A 2 Saturated properties of R-123 at 2 bar pressure

Properties of R-123 2 bar saturation pressure			
Property	Symbol	Value	Units
Molecular mass	M	152.93	kg/kmol
Critical pressure	P_c	36.68	bar
Critical temperature	T_c	456.83	K
Specific gas constant	R	54.368	
Reduced pressure	P_r	0.05453	
Saturated temperature	T_{sat}	321.2	K
Reduced temperature	T_r	0.70311	
Specific enthalpy of vaporization	h_{fg}	161600	J/kg
Vapour density	ρ_g	12.310	kg/m^3
Liquid density	ρ_l	1403.0	kg/m^3
Specific heat capacity of the liquid	c_{pl}	1070.0	J/kg K
Thermal conductivity of the liquid	k_l	0.0714	W/m K
Thermal diffusivity of the liquid	α_l	4.756E-08	m^2/s
Dynamic viscosity of the liquid	μ_l	3.230E-04	kg/m s
Kinematic viscosity of the liquid	ν_l	2.30E-07	m^2/s

Liquid Prandtl number	Pr_l	4.84	
Surface tension	σ	1.251E-02	N/m

A 3 Saturated properties of R-123 at 4 bar pressure

Properties of R-123 4 bar saturation pressure			
Property	Symbol	Value	Units
Molecular mass	M	152.93	kg/kmol
Critical pressure	P_c	36.68	bar
Critical temperature	T_c	456.83	K
Specific gas constant	R	54.368	
Reduced pressure	P_r	0.10905	
Saturated temperature	T_{sat}	345.3	K
Reduced temperature	T_r	0.75586	
Specific enthalpy of vaporization	h_{fg}	149700	J/kg
Vapour density	ρ_g	23.980	kg/m^3
Liquid density	ρ_l	1335.0	kg/m^3
Specific heat capacity of the liquid	c_{pl}	1112.0	J/kg K
Thermal conductivity of the liquid	k_l	0.0654	W/m K
Thermal diffusivity of the liquid	α_l	4.405E-08	m^2/s
Dynamic viscosity	μ_l	2.500E-04	kg/m s

of the liquid			
Kinematic viscosity of the liquid	ν_l	1.87E-07	m^2/s
Liquid Prandtl number	Pr_l	4.25	
Surface tension	σ	9.820E-03	N/m

Appendix B Experiments performed during present studies

B 1 List of performed experiments at 1.01 bar pressure

Sr no	Boiling surface	Applied electric potential (kV)	Electrode	Electrode spacing (mm)	Remarks
1	Emery polished surface	0			No EHD
2	Emery polished surface	10	Mesh	10	EHD
3	Emery polished surface	20	Mesh	10	EHD
4	Emery polished surface	30	Mesh	10	EHD
5	Emery polished surface	10	Rod (5 mm rod spacing)	10	EHD
6	Emery polished surface	20	Rod (5 mm rod spacing)	10	EHD
7	Emery polished surface	30	Rod (5 mm rod spacing)	10	EHD

8	Emery polished surface	10	Rod (8 mm rod spacing)	10	EHD
9	Emery polished surface	20	Rod (8 mm rod spacing)	10	EHD
10	Emery polished surface	30	Rod (8 mm rod spacing)	10	EHD
11	Fine sandblasted surface	0			No EHD
12	Fine sandblasted surface	10	Mesh	10	EHD
13	Fine sandblasted surface	20	Mesh	10	EHD
14	Fine sandblasted surface	30	Mesh	10	EHD
15	Fine sandblasted surface	10	Rod (5 mm rod spacing)	10	EHD
16	Fine sandblasted surface	20	Rod (5 mm rod spacing)	10	EHD
17	Fine sandblasted surface	30	Rod (5 mm rod spacing)	10	EHD

18	Fine sandblasted surface	10	Rod (8 mm rod spacing)	10	EHD
19	Fine sandblasted surface	20	Rod (8 mm rod spacing)	10	EHD
20	Fine sandblasted surface	30	Rod (8 mm rod spacing)	10	EHD
21	Rough sandblasted surface	0			No EHD
22	Rough sandblasted surface	5	Mesh	20	EHD
23	Rough sandblasted surface	10	Mesh	20	EHD
24	Rough sandblasted surface	15	Mesh	20	EHD
25	Rough sandblasted surface	20	Mesh	20	EHD
26	Rough sandblasted surface	25	Mesh	20	EHD
27	Rough sandblasted surface	20	Mesh	40	EHD

28	EB enhanced surface	0			No EHD
29	EB enhanced surface	10	Mesh	10	EHD
30	EB enhanced surface	20	Mesh	10	EHD
31	EB enhanced surface	30	Mesh	10	EHD
32	EB enhanced surface	10	Rod (5 mm rod spacing)	10	EHD
33	EB enhanced surface	20	Rod (5 mm rod spacing)	10	EHD
34	EB enhanced surface	30	Rod (5 mm rod spacing)	10	EHD
35	EB enhanced surface	10	Rod (8 mm rod spacing)	10	EHD
36	EB enhanced surface	20	Rod (8 mm rod spacing)	10	EHD
37	EB enhanced surface	30	Rod (8 mm rod spacing)	10	EHD

38	Sintered surface	0			No EHD
39	Sintered surface	10	Mesh	10	EHD
40	Sintered surface	20	Mesh	10	EHD
41	Sintered surface	30	Mesh	10	EHD
42	Sintered surface	10	Rod (5 mm rod spacing)	10	EHD
43	Sintered surface	20	Rod (5 mm rod spacing)	10	EHD
44	Sintered surface	30	Rod (5 mm rod spacing)	10	EHD
45	Sintered surface	10	Rod (8 mm rod spacing)	10	EHD
46	Sintered surface	20	Rod (8 mm rod spacing)	10	EHD
47	Sintered surface	30	Rod (8 mm rod spacing)	10	EHD

B 2 List of the experiments performed at higher pressures

Sr No	Boiling surface	Electric potential (kV)	Boiling pressure (bar)	Electrode/ Electrode spacing (mm)	remarks
1	Emery polished surface	0	2	-	No EHD
2	Emery polished surface	20	2	10	EHD
3	Emery polished surface	0	4	-	No EHD
4	Emery polished surface	20	4	10	EHD